6-9-2016

Optimizing Powder Metallurgy Methods: Carbon Nanotube Metal Composites

Ben Rael

Ben Jose Rael
Candidate

Mechanical Engineering
Department

This dissertation is approved, and it is acceptable in quality and form for publication:

Approved by the Dissertation Committee:

Tariq Khraishi, Chairperson

Yu-Lin Shen

Ying-Bing Jiang

Ganesh Balakrishnan

OPTIMIZING POWDER METALLURGY METHODS: CARBON NANOTUBE METAL COMPOSITES

by

BEN JOSE RAEL

B.S., Physics, University of New Mexico, 2009

DISSERTATION

Submitted in Partial Fulfillment of the
Requirements for the Degree of

Doctor of Philosophy
Engineering

The University of New Mexico
Albuquerque, New Mexico

May, 2016

DEDICATION

I would like to thank my loving family and friends for their moral support and patience. Finally, I would like to dedicate my work to my parents, for never giving up on me and who mean the world to me.

ACKNOWLEDGEMNTS

I would like to give a special thanks to Dr. Khraishi for his support and guidance from the onset of my doctoral studies. I am greatly indebted to Dr. Khraishi for his mentorship which allowed me to work on such exciting, interesting, and time challenging project. Additionally, I would like to extend my gratitude to Dr. Shen, for his wisdom, knowledge, and providing me with opportunities to broaden my horizons by working with composite materials outside my field of study. Moreover, I like to thank Dr. Jiang for his help to overcome experimental hurdles and imparting me with knowledge of various sample preparation and characterization techniques. I like to thank Dr. Tehrani for his help in carrying out thermal measurements, use of his lab, and help from his graduate students. Without their support, this study and important chapter of my academic career wouldn't have come to fruition.

Gratitude is extended to Dr. Yang at Sandia National Laboratories (Electronic, Optic and Nanomaterials Department) for help in characterizing mechanical properties using acoustic techniques. Much thanks to Dr. Guessasma at the French National Institute for Agricultural Research (Biopolymers, Interactions & Assemblies Research Unit) in Nantes, France for the invitation to learn valuable image analysis techniques during summer 2012.

Finally, this work would not be possible without crucial funding from The National Science Foundation, University of New Mexico School of Engineering and the New Mexico State Legislature.

OPTIMIZING POWDER METALLURGY METHODS: CARBON NANOTUBE METAL COMPOSITES

by

Ben Jose Rael

B.S. PHYSICS

Ph.D. ENGINEERING

ABSTRACT

Since their discovery in 1991, CNTs have revolutionized the composites industries and continue to show great promise as exotic reinforcers in a variety of materials. Extensive studies have been carried out by researchers to impart the unique physical properties of CNTs in metal systems and understand their interfacial interactions. However, the thermal, electrical and mechanical advantages of CNTs in metal systems are limited because of their tendency to aggregate together in rope-like bundles.

The objective of this research is two-fold: 1) optimize carbon nanotube (CNT) dispersal mechanisms in the fabrication of aluminum carbon nanotube metal-matrix composites (Al-CNT/MMCs) via the powder metallurgy method (PM), 2) characterize the effects of CNT morphology on the physical properties of Al-CNT/MMCs.

Powder processing techniques have been employed to successfully synthesize a wide range of particulate reinforced composite materials utilized in transportation industries and as structural materials. PM techniques have emerged as a highly effective and economic fabrication route for composite mixtures with constituents on the sub-micron to

nano scale, such as CNT reinforced aluminum matrix composites. At relatively low cost, PM is a very attractive forming technique because of its ability to form complex near net shapes with little secondary machining steps required. This lowers the fraction of starting material going to waste, lowers power requirements, and is environmentally favorable. However, the PM process poses some challenges that are not yet fully understood. There exist many works performed to address challenges such as analytical models for density predictions, sintering behavior, mixing of constituent phases prior to consolidation, and tool kinematics. In this work, the effectiveness of analytical models which attempt to predict the density of unsintered powder metallurgy (PM) compacts as a function of consolidation pressure is investigated. These models do not incorporate the non-uniform densification of powder compacts and may insufficiently describe the pressure/densification process. Also elucidated in this work are effects of particle size distribution parameters and particle morphology on material properties of metal powder compacts. One can intuitively conceive the important role particle size distribution and morphology plays in the densification behavior and flowability of metal powders into confined spaces. All of which can have implications on resulting microstructures and mechanical performance of PM components. Of central importance in the PM technique is optimal blending and mixing of constituent phases. This is especially critical when mixing high aspect ratio nano particles such as CNTs with micron sized metal granules. This study shows that the state and quality of CNT dispersion in the starting composite powder mixture is crucial to gain full advantage of subsequent consolidation/thermal processing phases in the PM fabrication route. In order to begin addressing the issue of a stable dispersion, a comprehensive study of dispersal mechanisms in CNT/MMCs that

are prepared via PM techniques must be conducted. A variety of techniques are used to obtain stable dispersions of individual CNTs including, but not limited to: mechanical mixing (high energy milling, ultra-sonication, etc.), wet-process (surfactant assisted), molecular level mixing, and functionalization of CNT surfaces through acid treatments. Each CNT dispersal mode offers its own unique advantages and disadvantages and some viable paths for obtaining dispersal may be limited by the complexity of the procedure. The results of this research signify that a synergistic effect of dispersal routes are needed to effectively dispersal CNTs in metal systems, which can depend on CNT morphology. Unlike traditional reinforcements such as brittle ceramics, CNTs have the added benefit of acting as highly functional materials in the surrounding metal matrix medium. Not only enhancing mechanical properties, but simultaneously improving thermal and electrical. In order to characterize the effects of CNT dispersal mechanisms and morphology on the physical properties and microstructures of Al-CNT/MMCs, thermal conductivity and mechanical measurements are employed in this study. Of equal importance in this study is delineating composite strengthening mechanisms due to fabrication processes from the incorporation of CNTs into the soft metal matrix. This is done through the aid of qualitative x-ray microanalysis, scanning electron microscopy and image analysis techniques.

TABLE OF CONTENTS

LIST OF FIGURES

LIST OF TABLES

Chapter 1

Introduction

1.1 Motivation

Powder metallurgy (PM) is a solid state processing route for a wide range of metallic, ceramic, and composite components. PM is characterized by being able to produce near-net shape components with lower fraction of starting material going to waste, lowered power requirements, and reduced environmental impact. As previously noted the attracting feature of near-net shaping has shown to bestow PM with 95% material utilization [1]. Unlike conventional machining methods, where "chips" of material are being removed and material utilization is significantly lower. Furthermore, machining is typically carried out in the presence of some type of cutting fluid to simultaneously cool and lubricate the tool/metal interface during the metal removing process. These cutting fluids may not be easily recycled and not only pose additional environmental risks in their disposal, but also health risks to workers. Scrap metal also produced in the machining process may be difficult to recycle depending on the chemical toxicity of the cutting fluid used. Metal powders widely used in industry such as iron/steel can be repetitively recycled (in the form of electrically melted steel scrap), this is due to the atomization method in which they are commonly produced. It has been estimated that up to 85% of metal powders produced for PM industry are produced from recycled material [1]. The near-net shape capability of PM also greatly influences the energy demand placed on producing an individual component. All manufacturing processes require energy in the form of electrical, thermal, or mechanical to achieve desired product shape from the raw materials. In the PM fabrication route, thermal processing is carried out

below the melting temperature of most metals. In forging and casting the metal liquid to solid phase transition must be carefully controlled as to avoid unwanted precipitation of incoherent phases which can lead to poor microstructure in the fully annealed metal. In these processes, raw ingots are typically further cold/hot worked to arrive at a desired microstructure for a specific application. These post-processing procedures act to further drive up power consumptions in the fabrication process. In a study performed by Dale, a side-by-side comparison of a truck-transmission notch segment manufactured using conventional means and the PM route, a 41% savings advantage in kilowatt-hour per work piece was shown using PM [1]. With U.S. manufacturing contributing more economic activity than any other sector, economic considerations of PMs cost competitiveness against other manufacturing routes offers greater design flexibility. The sum of the above mentioned, plus their impact on workers, suppliers, and customers demonstrates the inherent "sustainability" of the PM industry over more conventional manufacturing industries.

According to a new market study released by Materials Technology Publications, "The Powder Metallurgy Industry World- Wide 2007-2012," world-wide PM markets are projected to approach $30 billion by 2012. This figure is up $23 billion from 2007 at an annual growth rate of five percent. However, according to this report, PM markets of North America and Europe will slowly lose share to expanding Asian countries. This is partly due to cheaper man power and less stringent environmental regulations encountered in these geographic locations. From 2007-2012 the European PM market was expected to grow from $9.5 billion to $11.6 billion. During this same time period the North American market was projected to increase by $500 million, up from $5

billion. This slow growth in the North American PM market can be attributed to the 2008-2010 global financial "meltdown" and its resulting effects on the American automobile manufacturing industry. The high end users of powder components which dominate over all other industries are the automobile industry. As of 2007 a standard American car uses 19 kg of PM components [2]. Typical North American built engines contain up to 170 individual parts, with PM components accounting for about 30% [3]. With diminished growth experienced in both European and North American markets, this trend is expected to reverse with the adaptation of new eight-speed auto transmissions and resulting increased PM content [3]. Other potential inroads for PM components in the automobile industry are expected to arise in transfer-case and transmission applications. It is expected that luxury car brands in Europe and the US will make the shift from six-speed transmission designs to eight-speed designs in the 2014 model year [3]. In addition, as the US and European economies stabilize it is expected that consumers wallets will open up and more high-end purchases will be made further increasing the PM global market in automobile and consumer industries. However, as the PM industry rebounds, 20-30% reductions in staff during the 2009 recession may not be easy to reverse. Thus, one of the key issues facing growth here in North America and abroad is the serious need for highly skilled workers and PM engineering professionals.

Currently in the US and Europe, the PM industry is driven by automotive applications, prolonged growth and vitality must be found in other markets in order for the PM industry to survive. As the industry continues its focus on new technology, metal-powder producers have introduced new materials to meet performance demands of PM components. Properties of these materials can be custom tailored by powder producers to

take advantage of the elemental or alloying properties of a specific metal. These include nickel-free alloys; leaner alloys with reduced amounts of copper, molybdenum, and nickel. Technical improvements made in the PM industry and advancements made by powder suppliers have resulted in a significant increase in the number of industries/applications served. Certain high temperature alloys and materials can only be produced via PM methods. As an example, Hastelloy® produces a nickel-base alloy with an exceptional combination of oxidation resistance, fabricability and high-temperature strength. These materials are used as key components in jet engines increasing operating temperatures, promoting better performance and improved fuel economy. Boeing recently approved PM as a viable fabrication route to replace more common metallurgy routes (forging, casting, machining, etc.) in the production of titanium alloys used as structural components in their commercial aircraft. Beyond transportation industries, PM can take advantage of the emerging alternative-energies industries such as solar power, wind power, and fuel cells where lightweight and multi-functional materials are needed. For example, gears manufactured using PM techniques could be utilized in wind-motor design.

The need for lightweight and high strength materials has been recognized in transportation industries for quite some time. Given a particular structural application, as the strength and stiffness of the material increase, the resulting dimensions and mass typically decrease. This results in multiple advantages in automobile and aircraft design, such as an increase in payload and increased fuel efficiency. However, most metals and their alloys are inadequate in providing both strength and stiffness, which greatly limits their use in structural applications. It is commonly known that aluminum and its alloys

are widely used in aerospace design; this is due to its light weight, decent strength, and ductility. However, compared to high strength steels and titanium alloys, its strength are relatively low for applications that require high performance metals. This inability of most engineering metals to supply both stiffness and strength to a structure has led to the development of metal-matrix composites (MMCs). MMCs are characterized by stiff reinforcement particles homogeneously dispersed in a metal matrix which provides ductility and strength. Traditionally, metals are reinforced with tough ceramic particles or graphitic whiskers. Research in the 1960s and 1970s led to the large scale development of long carbon fibers which further increased technological advancements in aerospace and electronic packaging operations. These advanced carbon fiber reinforced composites with increased thermal management capabilities were widely used in re-entry heat shielding and missile applications. Today we see carbon reinforced composites in a wide variety of applications ranging from sporting goods to aircraft brakes.

In the past decade Nanotechnology has emerged as one of the most innovative fields in engineering and promising for manufacturing industries worldwide. Research in the field of carbon was revolutionized with the discovery of exotic allotropes of carbon such as carbon nanotubes, single graphitic sheets, "Buckey" balls and paper. Since their discovery in 1991 by Sumio Iijima [4], CNTs have emerged as the "darling" of material science and have revolutionized composite industries with their extraordinary mechanical properties; tensile strengths of SWNTs as high as 22 GPa [5], and an average Young's modulus of 1.25 TPa [6]. These mechanical properties make CNTs ideal candidates as reinforcement phases for a wide range of structural materials such as aluminum, titanium,

and magnesium used in transportation design. CNTs have been reported to be excellent thermal conductors which can be beneficial in thermal heat sink applications such as electronic packaging and automobile/aircraft disc break design. In a study carried out by Pop et. al the thermal conductivity of a single-walled carbon nanotube (SWCNT) was measured along the tube axis to be about 3500 W·m−1·K−1 [7]. Compared to copper which is considered to be a well-known metal for its thermal conductivity transmits 385 W·m−1·K−1 whereas aluminum transmits 205 W•m−1•K−1 [7]. Frank et al. [8] were able to reach a current density in a multi-walled carbon nanotube greater than 10^7 A/cm^2. Copper, generally speaking, half of the red metals applications are attributed to its electrical conductivity, not its mechanical or thermal properties. Why not reinforce this material further with CNTs obtaining a highly functional copper composite with enhanced thermal/mechanical properties?

In the past decade CNT reinforced MMCs have been fabricated using a variety of approaches: solid state processing routes such as PM, melting/solidification routes commonly known as casting and metal infiltration. Researchers have also recently developed novel fabrication techniques such as friction-stir processing, sandwich processing, nano-scale dispersion, and sputtering techniques to fabricate CNT/MMCs. PM has emerged as the most widely used fabrication route for reinforcing a broad range of metals and their alloys with CNTs. This is not only due to the attributes of PM itself, as discussed above, but also for its ability to effectively homogeneously disperse CNTs at or below the melting temperature of most metal matrices. This has important implications, as with melting and casting, at such elevated temperatures unwanted chemical reactions may occur at the CNT/metal interface severely degrading the

composite performances. Plus, during casting processes CNTs have been shown to re-agglomerate in the metal melt forming CNT clusters that can further degrade microstructure and or physical properties of MMCs. Of central importance in the PM technique is optimal blending and mixing of constituent phases. This is especially critical when mixing high aspect ratio nano particles such as CNTs with micron sized metal granules. Although recent technological advances now allow CNTs to be produced in bulk quantities, they are typically only available in powder form. CNTs tend to aggregate into rope-like structures when in powder form; such rope-like bundles may contain hundreds of close-packed CNTs that are tightly bound via Van der Waals attraction energies. The addition of small Van der Waals energies existing along the large surface areas of the CNTs produces a high affinity between the CNTs. This leads to rope-like CNT aggregates that are highly entangled. One of the main technical hurdles facing researchers in their physical manipulation is obtaining long stable dispersions. The state and quality of CNT dispersion in the starting composite powder mixture is crucial to gain full advantage of subsequent consolidation/thermal processing phases in the PM fabrication route and obtain CNT/MMCs with improved performances.

1.2 Research Objective

The first objective of this research is to investigate the effectiveness of analytical models which attempt to predict the density of unsintered PM compacts as a function of consolidation pressure. To achieve this goal, micro-indentation testing is used extensively to characterize density gradients and evaluate the degree of non-uniformity in fabricated PM tablets. Scanning electron microscopy (SEM) is also employed to verify tablet density by visual examination of surface porosity as compaction pressure is varied

and sintering is applied. The second objective, fabrication and testing is conducted to characterize the effect of Rosin-Rammler powder size distribution function parameters and particle morphology on material properties of PM compacts. The third objective in this work outlines recent developments carried out by researchers in the fabrication of carbon nanotube metal matrix composites (CNT/MMCs) and their resulting material properties. More specifically, this review focuses on various CNT dispersal mechanisms in the fabrication of CNT/MMCs via the PM method. The present review brings into focus the critical issues which affect the mechanical performances of CNT reinforced MMCs that include: CNT dispersal route, state and quality of nanotube dispersion, and the importance of the CNT/metal transition layer as an effective stress transfer medium. Also elucidated in this review are nanotube dispersal mechanisms, resultant material properties of CNT/MMCs, compatibility of CNTs in different metal systems, and CNT strengthening mechanisms. Finally, CNT dispersal mechanisms are optimized to insure homogenous distribution of different CNT morphologies (SWCNT, MWCNT-long, and MWCNT-short) in the surrounding metal matrix. With CNTs optimally dispersed mechanical, thermal, and electrical properties are characterized as a function of porosity content.

1.3 Organization by Chapter

The rest of this Ph.D. dissertation is organized in the following manner: Chapter 2 presents a brief overview of the PM process and the fabrication steps necessary to arrive at a spatially homogeneous PM compact. Importantly, elucidated in this chapter is an in depth look into the effectiveness of constitutive equations which attempt density predictions of PM components as a function of consolidation pressure. Chapter 3

explains the crucial role particle size distribution and morphology play in the densification process. In this chapter, the most widely used Rosin-Rammler size distribution function, and its adequacy in describing bimodal metal powder distributions which are ball milled is investigated. In addition, a relationship between Rosin-Rammler functional parameters and strength of PM compacts is attempted. Chapter 4 presents a systematic review of studies carried out on the fabrication and mechanical characterization of CNT/MMCs fabricated via PM techniques. This chapter provides an in depth look of recent developments by researchers in the dispersion of CNTs in metal powder systems and subsequent material properties of CNT/MMCs using dispersion-PM techniques. Chapter 5 discusses CNT dispersal mechanisms implemented in this study, their optimization, and effectiveness at homogeneously dispersing nanotubes in aluminum (Al) matrix. Also discussed in this chapter are resultant mechanical properties (Rockwell Superficial hardness) and microstructures of Al/CNT composites fabricated via PM techniques. Chapter 6 is a continuation of chapter 5 which further discusses the mechanical properties (elastic properties), microstructural characterization (SEM analysis, image analysis and x-ray microanalysis) and thermal properties of Al/CNT composites.

Chapter 2

Factors Effecting Analytical Powder Metallurgy Models for Density Predictions

2.1 Introduction

The effectiveness of analytical models which attempt to predict the density of unsintered powder metallurgy (PM) compacts as a function of consolidation pressure is investigated. These models do not incorporate the non-uniform densification of powder compacts and may insufficiently describe the pressure/densification process. Fabrication of uniform and non-uniform Zinc (Zn) tablets is conducted to assess the validity of the pressure/density model developed by Quadrini et al. [9]. Different tablet properties were obtained by varying the compaction pressure and fabrication protocol. Density gradients within Zn tablets result in a spatial dependence of Vickers microhardness (HV) throughout the fabricated specimen. As a result, micro-indentation testing is used extensively in this study as a characterization tool to evaluate the degree of non-uniformity in fabricated Zn tablets. Scanning electron microscopy (SEM) is also employed to verify tablet density by visual examination of surface porosity as compaction pressure is varied and sintering is applied.

Powder metallurgy is a very attractive forming and fabrication technique due to its relatively low costs and the ability to form complex near net shapes. The key to fabricating successful PM components are selection of the right material appropriate for a desired application and processing it under optimal processing conditions. Key processing variables include consolidation pressure, green density, and sintering conditions. Extensive work has been carried out by researchers to characterize

consolidation pressure to achieved green density of PM components. However, theoretical models, which relate the consolidation pressure to achieved green density, assume spatially uniform densification throughout the powder compact. For these reasons a more in-depth look, as achieved in this paper, is needed into the effectiveness of theoretical models which attempt density predictions of statistical materials such as PM compacts.

A plethora of studies have been carried out to understand the densification mechanism in the PM process as well as to determine the mechanical properties of the compacts. Researchers have primarily focused on density measurements and calculations. Quadrini et al. used small flat-surface indentations and an analytical model to try and predict the density of powder metal compacts [9]. Ludwig et al. proposed the use of electrical conductivity measurements as a means to measure the density of green-state metal compacts [10]. Dawson et al. used ultrasonic measurements to track density changes during compaction [11]. While many focused on measuring the density of the compactions, Fleck et al. showed that the yield stress, ultimate tensile stress, resistance to fatigue crack propagation, and fracture toughness of a compacted metal powder is directly related to the compaction density [12]. Carnavas et al. explored the effects that particle shape and size have on the physical properties of PM compacts [13]. All the above proposed methods may be effective in finding the overall density of the compacts but fail to address the issue that a completely uniform compaction is nearly impossible to achieve.

The primary focus of this paper is to show that models which describe the pressure/densification process, as in reference [9], are sensitive to fabrication procedures. If great care is not taken to homogenize PM components to the furthest extent possible poor correlation between data and theory can result. One method proposed by Quadrini et al. [9] to obtain compacted tablets with higher degrees of homogeneity (by first compacting one side, flipping the tablet over and then compacting the other side) is used in this study. The sensitivity of the Quadrini model to this uniforming procedure (flipping of the tablets) is characterized through hardness mapping and a least-squares analysis. Finally, visual confirmation of the density and porosity is achieved with the use of a scanning electron microscope (SEM) to illuminate the effects of compaction pressure magnitude and sintering.

Nomenclature and greek symbols:

F	compaction force
r_o	tablet radius
r	radial distance along tablet
H	tablet height
z	distance along height of tablet
p, $p(R_{\text{uniform}})$, $p(R_{\text{non-uniform}})$	compaction pressure for uniform and non-uniform zinc tablets
R, R_{uniform}, $R_{\text{non-uniform}}$,	relative density (compacted powder density/max theoretical density ρ_f) for uniform and non-uniform zinc tablets
R_o	relative density of zinc tablets at zero compaction
σ_s	maximum yielding stress of the compacted powder (at $R = 1$)
η^*	efficiency coefficient of a compaction test due to the die friction
n	hardening coefficient of the metal powder
S_r ,$(S_r)_{\text{non-uniform}}$ $(S_r)_{\text{non-uniform}}$	sum of the residuals squared for uniform and non-uniform test data
$p_{\text{i-measured}}$, $p_{\text{i-moodel}}$	measured and calculated pressures

r^2,$(r^2)_{\text{uniform}}$, ,$(r^2)_{\text{non-uniform}}$	correlation coefficients for uniform and non-uniform test data

2.2 Experimental Procedure

Metal tablets were fabricated by "cold" compaction of commercially available zinc powder (97.5% pure, median 6-9 micron, Alfa-Aesar Inc., Ward Hill, Massachusetts, USA) ,Fig.2-1(inset). Particle size distribution of the Zn powder was determined using a JEOL 5800LV Scanning Electron Microscope, where the diameters of 800 Zn particles were measured (Fig.2-1)

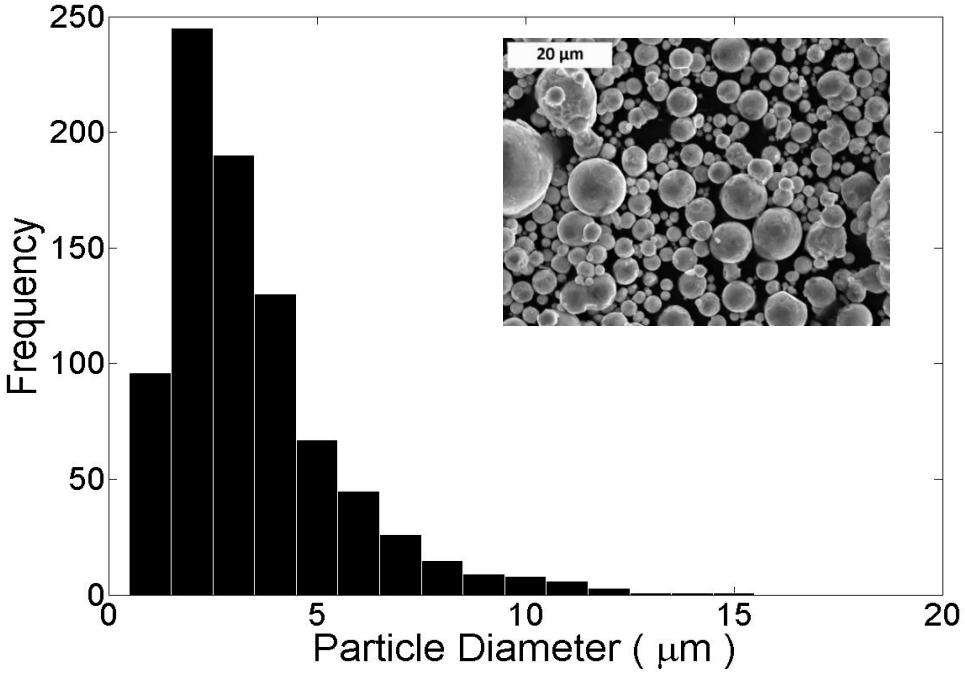

Figure 2-1: Particle size distribution for zinc powder (median 6-9 μm) used in this study, (inset) SEM micrograph of zinc powder.

The die and discs used in the compaction process were constructed of high-strength (HS) steel and produced cylindrical tablets with diameters of approximately 12.72 mm. A half-inch (12.7 mm) nominal diameter steel plunger was used to transfer the compaction force "F" from an Instron® 4400R tensile/compression testing machine to the upper disc and onto the powder during the compaction process (Fig.2-2).

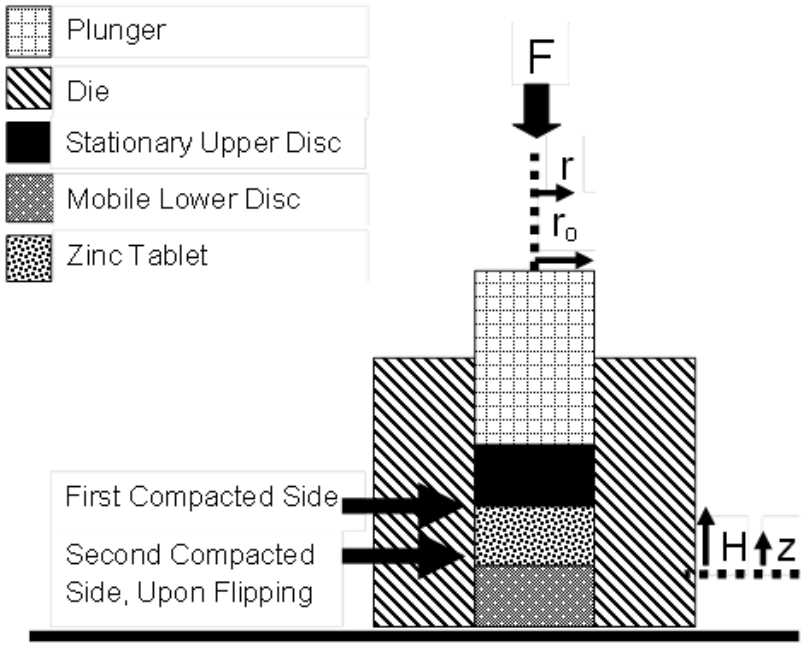

Figure 2-2: Experimental setup.

Approximately 5 grams of Zn powder was weighted to manufacture each tablet. Before consolidation of Zn tablets could commence, it was necessary to apply zinc stearate [14] to the inner die wall and disks. This is done to reduce wear and friction between moving components in Fig.2-2. In order to adequately lubricate the inner die surface, it is first swabbed with acetone, a mixture of shredded cork and zinc stearate is then consolidated at a pressure of 50 MPa, after which the mixture is ejected from the die. After this lubrication protocol is carefully implemented, Zn powder is carefully loaded into the die with the compaction pressure varying from 150 MPa to 450 MPa in 50 MPa increments.

The advancement rate of the Instron machine was held constant at 0.254 mm/minute until the desired compaction pressure was achieved at which point the unloading phase would commence at 0.254 mm/minute. This advancement rate was chosen as such to facilitate particle rearrangement/movement, and to help with minimizing density gradients in the green compact. The tablets were then ejected from the die, the density of the cylindrical tablets was then determined using a micrometer and electronic weight balance. These tablets were flipped and then reloaded into the die with the same lubrication and compaction protocol performed as outlined above. Upon completion of the second compaction cycle, the densities of the cylindrical tablets were determined. Multiple samples at each compaction pressure were fabricated in order to ensure accuracy and repeatability.

Half of the samples from each compaction pressure were sintered at 378 °C for 45 minutes with 60 standard cubic centimeters per minute (sccm) of nitrogen flowing to provide an inert environment for sintering. This is done to see the effect of sintering on the porosity of compacts compared to their green state.

Characterizing the material properties and microstructure of the fabricated tablets consisted of Vickers microhardness tests and SEM micrographs, in addition to the density measurements mentioned above. The microhardness tests were performed using a Buehler Micromet II Microhardness Tester with 50-300 gram loads which were held constant for 10 seconds. Hardness tests were performed on both green and sintered tablets, on both sides of the tablets, and across tablet diameters (indents spaced 400 μm apart). Hardness tests were also performed along the depth of the fabricated tablets, before and after the second compaction cycle (indents spaced 500 μm apart). SEM

micrographs (Fig.2-3) of the Vickers indents confirm that no surface preparation of green tablets is necessary since the indents are clearly visible and symmetric. If the surface was not completely flat then the shape of the indents would not be a perfect diamond. It should also be noted that the indent in Fig.2-3 encompasses a large number of Zn particles. This is indicative of adequate indentation loads used in this study. To perform indentations along the specimen depth a HARIG 618 Automatic precision grinder was utilized to create flat surfaces. The hardness values used in this study are the mean values from equally placed indentations on multiple samples.

Live images were taken using a JEOL 5800LV Scanning Electron Microscope which provided insight into surface porosity and morphology of zinc tablets consolidated at different pressures. SEM micrographs also give valuable insight into the increased bonding between zinc particles that is a result of the sintering process.

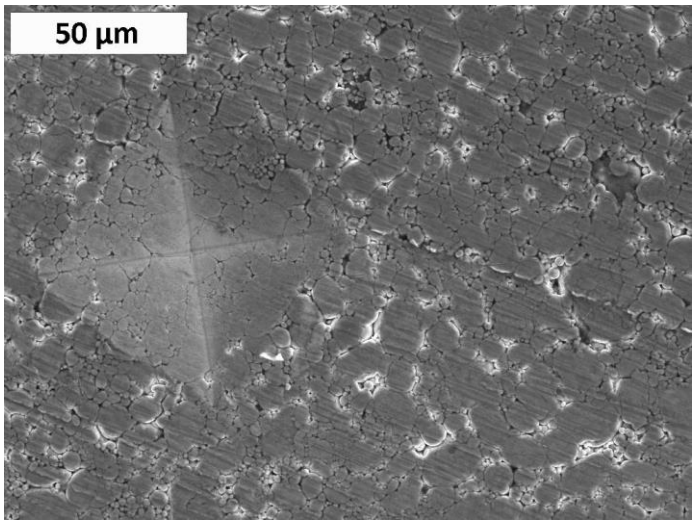

Figure 2-3: Scanning electron micrograph of Vickers indent of sample consolidated at 300MPa.

An analytical model for density prediction was proposed by Quadrini et al. [9] which relate the relative density "R" and compaction pressure "p" by:

$$p = \frac{\sigma_s}{\eta^*}\left(2 - R^2\right)\sqrt{\frac{\left[\frac{R - R_o}{1 - R_o}\right]^{n/R_o}}{\left(1 - R^2\right)\left(4 - R^4\right)}} \quad . \tag{2-1}$$

To assess the density prediction capability of Equation 1-1, a MATLAB® nonlinear least-Squares fitting routine was applied to the experimental data set [R_{uniform}, $p(R_{\text{uniform}})$] to fit the Quadrini model (determine the η^* and n parameters). The parameter, σ_s, is considered deterministic and has the value of 124 MPa for zinc [9]. This optimization procedure minimizes the sum of the squares of the residuals [15]:

$$S_r = \sum_{i=1}^{m}\left(p_{i,measured} - p_{i,model}\right)^2 , \tag{2-2}$$

where "m" is the total number of points. The MATLAB® "lsqcurvefit" routine (algorithm: 'large-scale, trust-region reflective Newton') performed repetitive fittings until the sum of the residuals squared $(S_r)_{\text{uniform}}$ is minimized. This provides us then with the correlation coefficient $(r^2)_{\text{uniform}}$. With the parameters η and n determined, S_r and r^2 are then determined for non-uniform tablets (single-sided compactions) using the [$R_{\text{non-uniform}}$, $p(R_{\text{non-uniform}})$] data set. Correlation coefficients r^2 and S_r values for uniform and non-uniform tablets are then compared.

2.3 Effectiveness of constitutive equations which attempt density predictions of PM components as a function of consolidation pressure

In the fabrication of each tablet, a loading and unloading curve was created for both the first and second compaction cycles. Figure 4 shows the typical loading and unloading curves for the first and second compaction cycles. During fabrication of the tablets, it can be seen from Fig.2-4 that flipping the tablet over after the initial compaction cycle

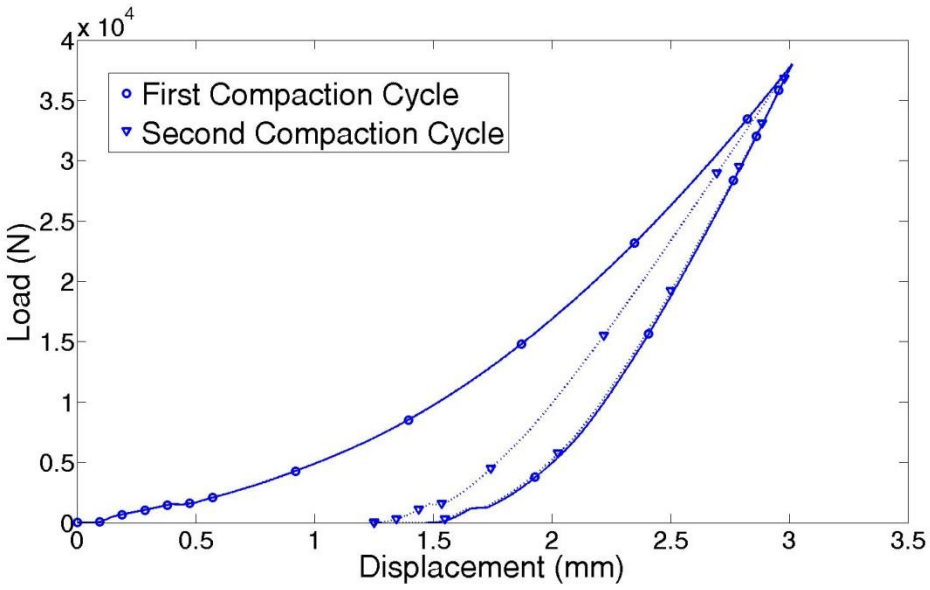

Figure 2-4: Superposed loading and unloading curves for a specimen consolidated at 450 MPa. 2 gm of Zn powder was used was used for each tablet.

does allow for further consolidation during the second loading and unloading phase. The idea set forth by Quadrini et al. was that this procedure would create tablets with a more uniform density [9]. However, [9] did not demonstrate this idea as herein using experimental load- and unload-displacement curves. The large net displacement of the first loading and unloading curves in Fig.2-4 shows majority of the consolidation occurring during this part of the procedure. The small net displacement seen in the second loading and unloading cycle shows that flipping the tablet over does indeed allow for further consolidation, though not nearly as much as the first loading and unloading cycle. Furthermore, the nearly collapsed loading and unloading curves for the second cycle in Fig. 2-4 is indication that the specimens were compacted to the furthest extent possible.

Further indication that Zn tablets are attaining a higher degree of uniformity due to the fabrication procedure adopted in this study is exemplified in Fig. 2-5. For the uniform tablet, HV as a function of depth remains constant throughout the depth of the tablet. For the non-uniform tablet, HV is highest on the compacted surface and overall is less than for the uniform tablet. This can be explained by deformation strengthening due to high compressive stresses at the upper disc/tablet interface (compacted surface). For the lower disc/tablet interface (non-compacted surface), compressive stresses due to the plunger are lower and grain size reduction drops. As a result, HV values are lowest for the non-compacted surface. This can be seen in Fig.2-5 where the double-compacted tablets were more densified throughout than the single-compacted ones resulting in a harder material response, i.e. less overall porosity. Note also in Fig.2-5 how at one depth point for the non-uniform tablets the HV values rapidly decline towards the non-

compacted side. This indicates a loss of compaction efficiency there and should be guarded against in the design of PM-manufactured parts intended to be load-bearing in service.

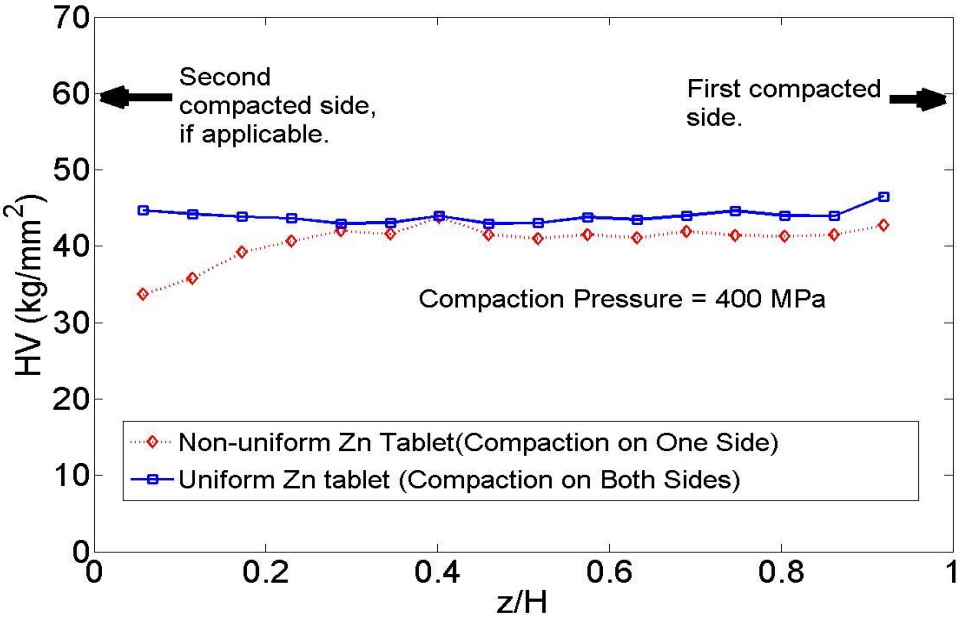

Figure 2-5: Microhardness as a function of specimen/tablet depth. Indent load = 300g. Each data point represents the average of 3 specimens tested. 8 gm of Zn powder was used for each tablet.

To further affirm that the fabrication technique adopted from Quadrini et al. [9] did indeed create a more uniformly dense tablet (i.e. with less porosity), Vickers microhardness tests were performed radially on both sides of uniform and non-uniform tablets. Figure 2-6 indicates higher overall HV values for double-compacted tablets compared to single-compacted ones. Furthermore, the single-compacted (non-uniform) tablets see an increase in HV near the tablet edges on the compacted side, and a decrease

in HV near tablet edges on the non-compacted side. The reason for this is due to machining tolerances between the two discs and the inner die cavity. Because of this tolerance, particles during pressurization are squeezed out the tolerance of the stationary disc forming a severly-deformed lip (an elephant foot shape) due to frictional and shearing effects. This is at the expense of losing particles from right below that region, i.e. a deficiency of particles at the other tablet-disc interface. This explains the disparate HV behavior of uniform and non-uniform tablets. These results for microhardness as a function of tablet radial distance agree in trend with results reported and explained elsewhere [16].

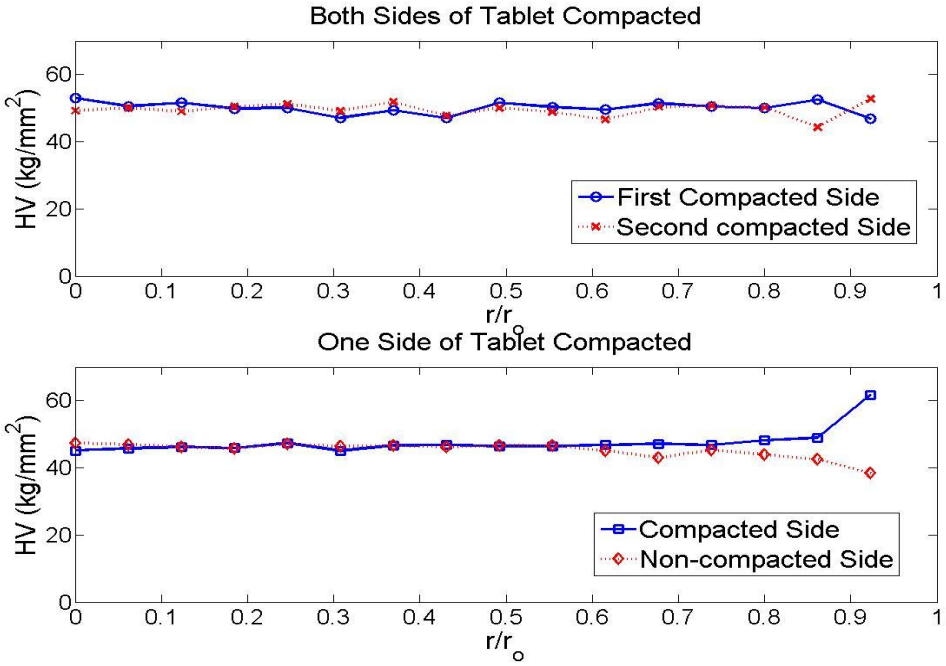

Figure 2-6: Hardness as a function of radial distance. Tablets consolidated at 400 MPa in the green state, 300 gram load. 2 gm Zinc powder was used for each tablet here.

The fitting parameters n and η^* from minimizing Equation (2-2) are listed in Table 2-1. Fig.2-7 shows optimized Equation 2-1 superposed on experimental data. It is seen in this

figure that computed *R* of both uniform and non-uniform tablets exhibit a greater sensitivity to compaction pressure in the lower pressure range. Also, as the compaction pressure increases, the rate of increase of densification falls off. At later stages of the compaction process Zn particles are work hardened, which consequently impedes densification [17]. This work hardening is related to dislocation density saturation [18].

Although equation (2-1), the Quadrini model, captures the trend of the experimental data it does not do as good a job capturing the values. There are multiple reasons for why this may have happened. First, the Quadrini model does not take into account particle rearrangement, rotation, and sliding [19]. This is active especially during the early phases of compaction, i.e. for the lower pressure region. Later in the compaction process, i.e. at higher pressure values, particle sliding, rearrangement, and rotation become less likely with plastic deformation being the responsible agent for densification. In fact, the Quadrini model, and similar such models [16-17,19-26], only take into account the densification of powder compacts as a result of plastic deformation and nothing else. Second, σ_s used in Equation 2-1 was considered a deterministic parameter with a value (provided in Table 2-1) that was assumed constant with deformation. However, according to Tszeng et al. [27] it was shown that the apparent yield stress of a powder compact increases with particle morphological index "M" (M=0 for spherical particles, M=1 for highly irregular particles). What this means is that σ_s is actually a function of M. Furthermore M is a function of compaction pressure *p* as the more the compaction the more M increases, especially starting out with spherical particles as in our case (Fig.2-1, inset). Furthermore, for this fit $(r^2)_{\text{uniform}}=0.9757$, which indicates a goodness of fit between the Quadrini model and $[R_{\text{uniform}}, p(R_{\text{uniform}})]$ data. However, for

$(r^2)_{\text{non-uniform}}$=0.8543 the Quadrini model does not describe well Zn tablets that have not undergone a homogenization/uniforming procedure. This is further evident in the higher value for $(S_r)_{\text{non-uniform}}$. This clearly shows that applying models such as the model in Equation (2-1) to double-sided compactions would give fitting parameters for the model that are not suitable for single-sided compactions of the same powder. In other words, the fitting parameters in models such as the Quadrini model are very sensitive to the degree of densification of produced PM parts.

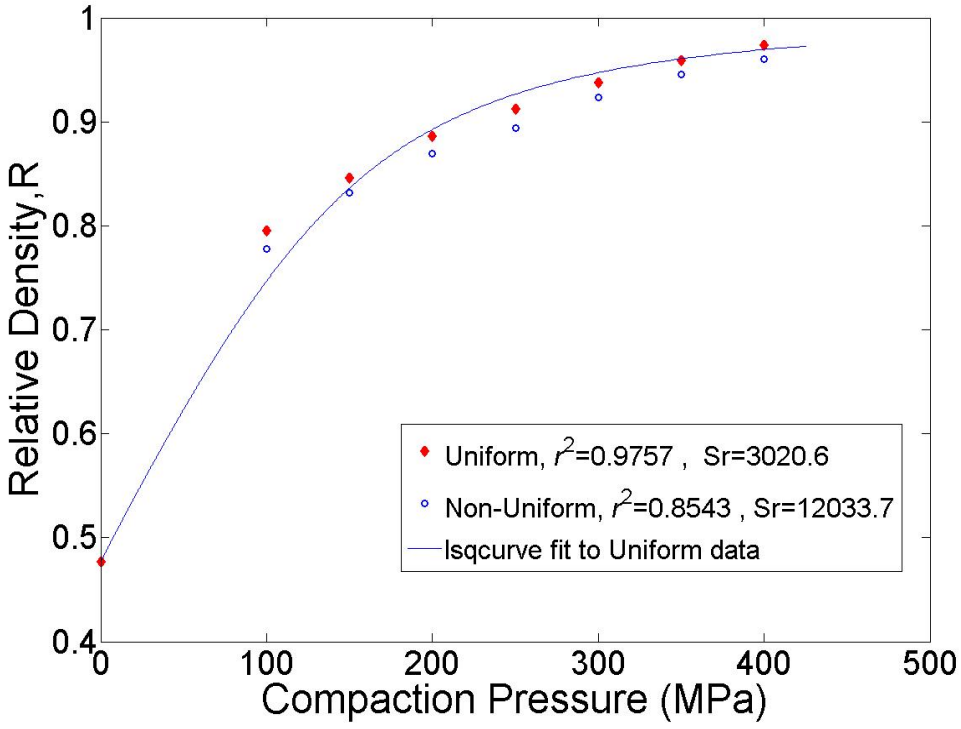

Figure 2-7: Numerical optimization of Equation 1 superposed on experimental data. Each data point represents the average of 3 specimens tested. 5gm of Zn powder was used for each tablet

σ_s [MPa]	η^*	ρ_f [g/cm^3]	R_o	n
124	0.7141	7.133	0.477	0.971

Table 2-1: Least-squares curve fitting of the parameters used in minimizing Equation 2-1.

Microhardness results for the sintered specimens are shown in Fig. 2-8. The hardness of the sintered samples was approximately 12-14% greater than that of the green tablets fabricated under the same compaction pressure. Solid-state diffusion bonding, facilitated by sintering, between adjacent particles at or near the melting point of zinc [28] accounts for this increase in hardness. Fig.2-8 also indicates that sintering plays a more meaningful role in the hardening of the compact under higher pressures. As compaction pressure increases the total contact area between Zn granules increases, which increases the amount of diffusing region availabl

SEM images (Fig.2-9–2-11) show the physical organization of the zinc particles after compaction and sintering. The higher density and lower porosity, due to the higher compaction pressures, can be clearly seen when comparing Fig.2-9 and Fig.2-10. The increased bonding between zinc particles due to the sintering process can be visually observed from the SEM micrographs presented in Fig.2-10 and Fig.2-11.

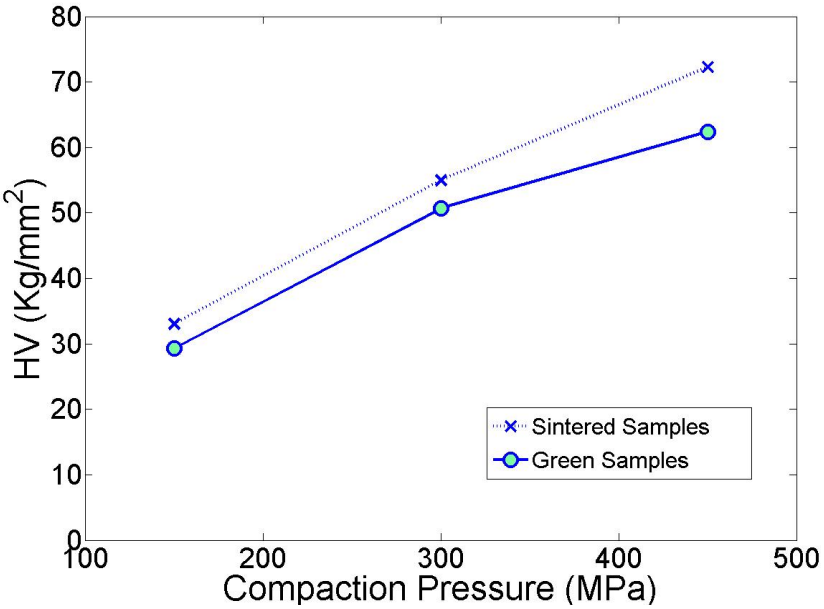

Figure 2-8: Hardness comparison for green and sintered tablets. All hardness indents were performed close to the center of the tablet using a 50 gram load. Each data point represents the average of five hardness measurements. 2 gm of Zinc powder was used for each tablet here.

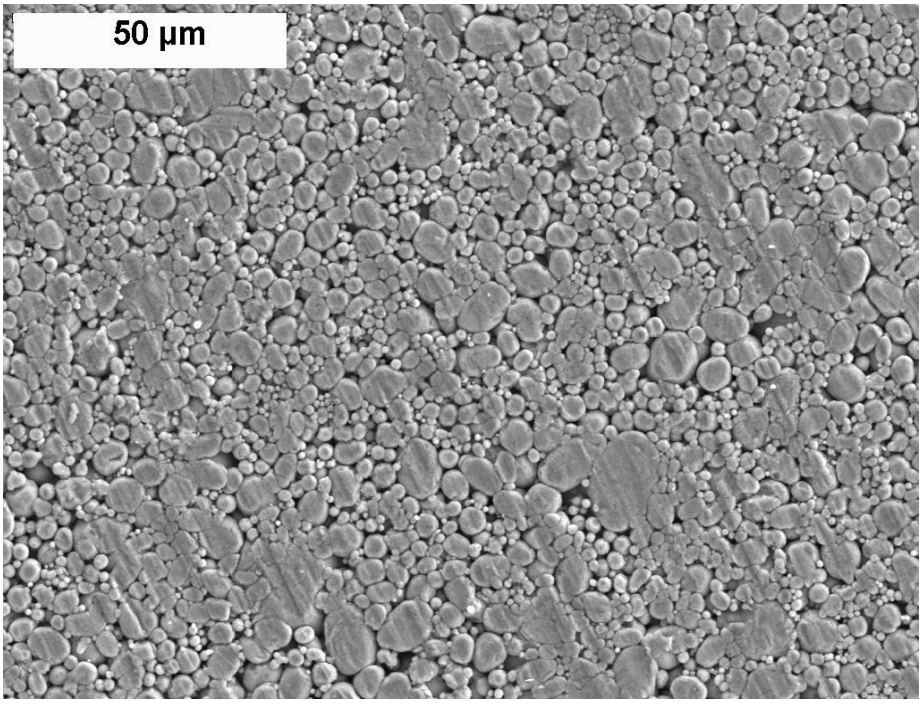

Figure 2-9: SEM image of zinc powder compacted at 200 MPa in green state.

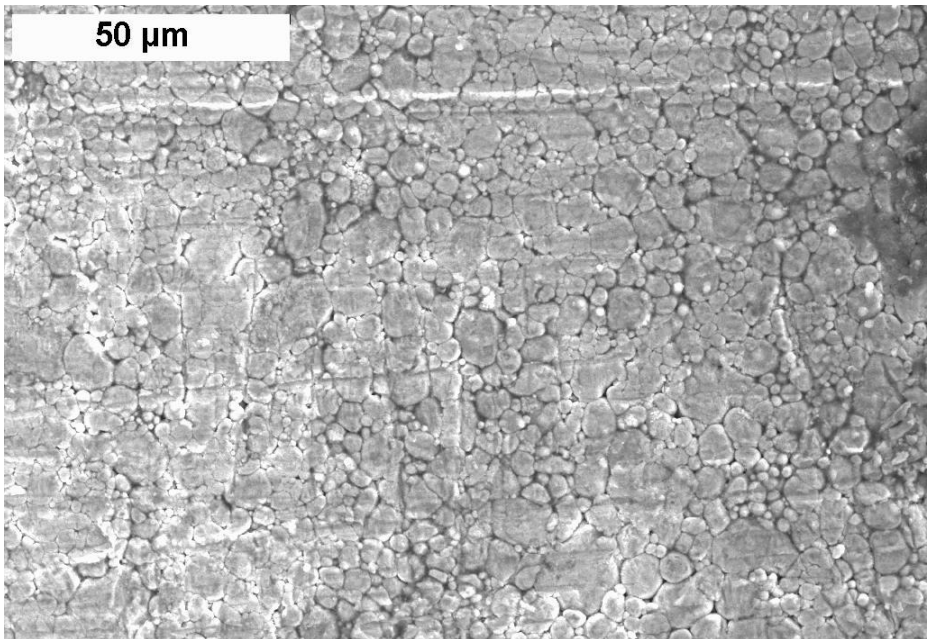

Figure 2-10: SEM image of zinc powder compacted at 400 MPa in green state

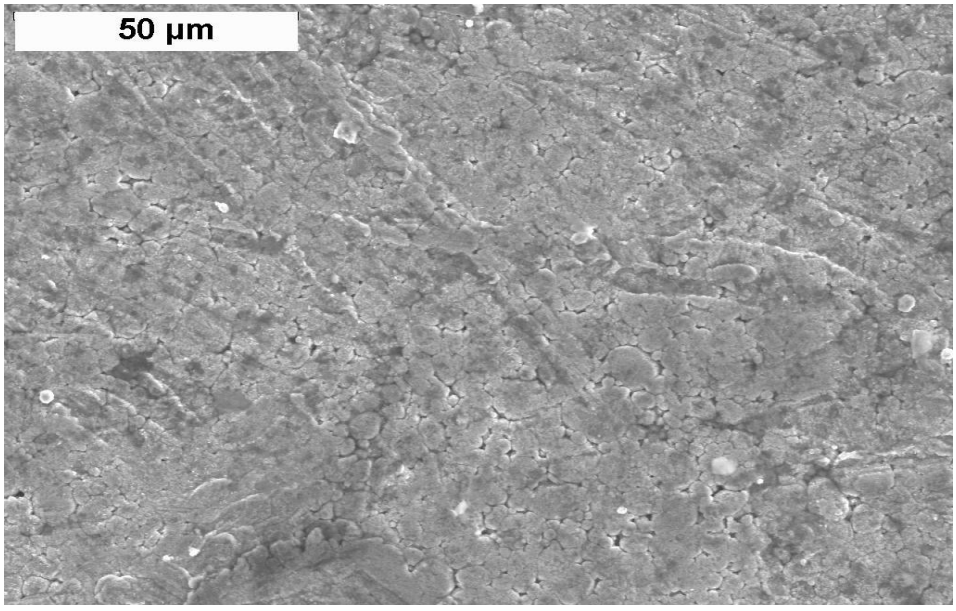

Figure 2-11: SEM image of zinc powder compacted at 400 MPa after sintering at 378˚C for 45 minutes with 60 sccm nitrogen flow.

2.4 Conclusion

The Quadrini model (Equation 2-1) developed for uniformly dense tablets is not an accurate description of the pressure-density relationship for Zn tablets that have not undergone a density-uniforming procedure. Furthermore, the Quadrini and such models [16-17,19-26] are based on densification stemming from plastic deformation only and thus do not take into account factors affecting the density such as particle sliding, movement, re-arrangement [18]. Also, such models [16-17,19-26] do not take into account the effect of particle morphological changes on the apparent yield stress of the powder material [27].

To improve the density prediction capabilities of Equation (2-1) the authors suggest including particle morphology in the constitutive model which this analytical model was derived from. This may be accomplished by introducing an appropriate state variable $\Lambda = \Lambda(M)$ into the modified yield criteria from which Equation (2-9) is based off ,where a morphology index, $M \in (0,1)$, is used to describe particle morphology.

Another lesson learned from this study is that sintering is more effective on mechanical properties at higher compaction pressure values compared to lower values. In addition, this study clearly shows the positive effect that double-sided compactions have on uniforming the material hardness throughout the PM product (both radially and axially) and increasing its value.

Chapter 3

Effects of Rosin-Rammler Parameters and Particle Morphology on Powder Metallurgy Compacts

3.1 Introduction

The extensive utilization of Powder Metallurgy (PM) products in industries has motivated the need to better understand manufacturing process parameters and their resulting effects on material properties of PM products. In the present study, fabrication and testing is conducted to characterize the effect of Rosin-Rammler parameters and particle morphology on material properties of zinc powder compacts. Using "cold" compaction techniques, zinc powders of varying size distributions are consolidated at a pressure of 450 MPa. The compacted "green" tablets were then tested using micro-indentation tests, micro-structural examinations, and dimension/weight measurements. The results of this study reveal the sensitivity of Vickers Microhardness (HV) to Rosin-Rammler function parameters η and *D*. The function parameters η and *D* describing particle distribution spread and average particle size. Scanning electron microscopy also affirms the sensitiveness of material properties of zinc compacts to particle morphology.

The aim of characterizing PM process parameters is to fabricate green compacts with minimal variation in density and reduced porosity [29, 30]. Process parameters that are not suitably optimized to minimize density gradients hinder diffusion processes during the sintering stage, which can lead to sintered components with reduced strength and poor microstructure [31]. In a variety of industries such as automobile and consumer products

it is considered more cost effective to utilize metal powders which are highly irregular and have a wide range of particle size distributions [32]. Particle size distribution plays an important role in the densification behavior of metal powder compactions. Particle size and morphology affect flowability of metal powders into confined spaces [33]. Poor flowability performance can result in inefficient powder packing in tap density, and hinder particle rearrangement during the consolidation phase. For these reasons, it is necessary that an adequate mathematical function be used to characterize size distribution. In the current study, the most widely used Rosin-Rammler size distribution function, and its adequacy in describing zinc powders which are ball milled is investigated. In addition, a relationship between Rosin-Rammler parameters and HV of zinc compactions is also investigated.

The mathematical function proposed by Rosin and Rammler is listed as follows [34]:

$$R(d) = 100e^{-\left(\frac{d}{D}\right)^{\eta}} \tag{3-1}$$

Where *R (d)* is the cumulative percentage oversize, *d* is the corresponding particle diameter (μm), *D* is the average particle size (μm), and η is a dimensionless parameter describing the distribution spread.

3.2 Experimental Procedure

Zinc tablets were formed via cold compaction techniques using an Instron 4400R tensile/compression machine. The die (cylindrical body with 12.78 mm hole) and discs (each 6.1 mm thick) used in the compaction process was constructed of A2-Air Hardened Tool Steel. A half inch (12.7mm) nominal diameter plunger constructed of A2-Air

Hardened Tool Steel was used to transfer the compaction force from the Instron. The tablets consisted of 97.5% pure zinc powder (Alfa-Aesar Inc., Ward Hill, Massachusetts, USA) in two size ranges (-100 mesh, median 9-6 microns), Fig 3.1-3.2. Where the convention "-100 mesh" denotes a mesh opening of 150 µm. In order to vary the size distribution of zinc powder, compositions of 5, 10, 15, 25, 35, 50 weight percent of Zn (median 9-6 µm) were combined with Zn (-100 mesh). Blending of the zinc mixtures was achieved through the use of a Ball Mill of Planetary Type (Torrey Hills Technologies.,LLC), as this was necessary to obtain as homogenous of a mixture as possible and break up any particle agglomerations. Mixtures at each composition were milled for 1 hour at 400 rpm.

Fig 3-1: Zn (-100 mesh)

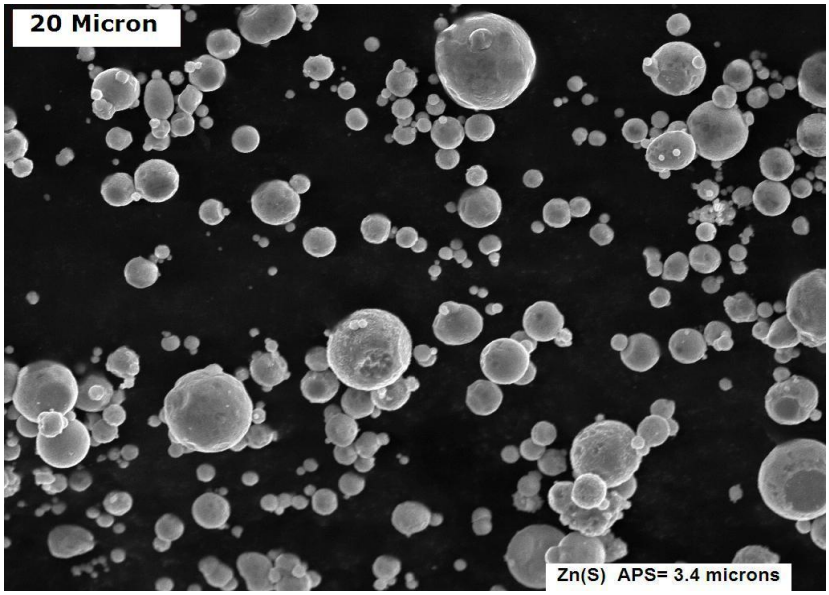

Fig.3-2: Zn (median 9-6 µm)

Once the ball milling procedure was completed approximately 2 grams of the combined zinc powders at each composition were weighted to manufacture each tablet. Before consolidation of zinc mixtures could commence, it was necessary to apply zinc stearate to the inner die wall and disks, this is done to reduce wear and friction between moving components in Fig.3-3. In order to adequately lubricate the inner die surface, it is first swabbed with acetone, a mixture of shredded cork and zinc stearate is then consolidated at a pressure of 50 MPa, after which the mixture is ejected from the die. Zinc mixtures at each composition were carefully loaded into the die setup (Fig. 3-3) ,and consolidated at a relatively high pressure of 450 MPa in order to maximize tablet density.

The advancement rate of the Instron was held constant at 0.254 mm/minute. This rate was chosen to facilitate particle movement and maximize densification of green

compacts. Once the prescribed pressure was met the unloading phase would commence at 0.254 mm/minute. Tablets were then removed from the die and flipped with the same lubrication and compaction protocol performed as outlined above. This idea set forth by Quadrini et al. was that this procedure creates tablets with more uniform density [35]. The tap densities of each zinc powder mixture and consolidated tablets were determined using standard techniques and presented in Fig.3-4.

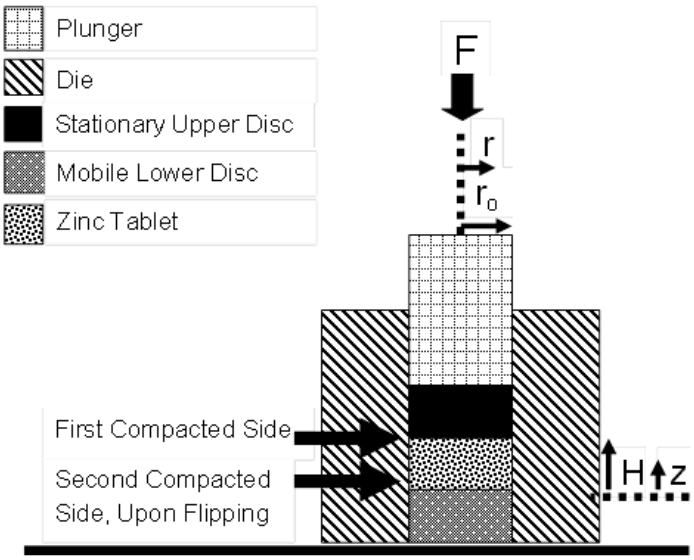

Fig.3-3: Experimental Setup

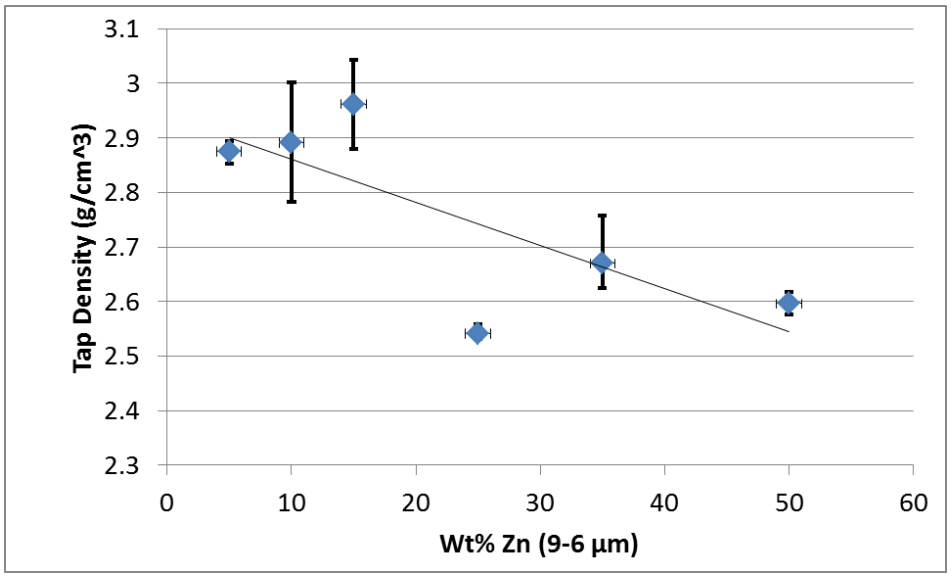

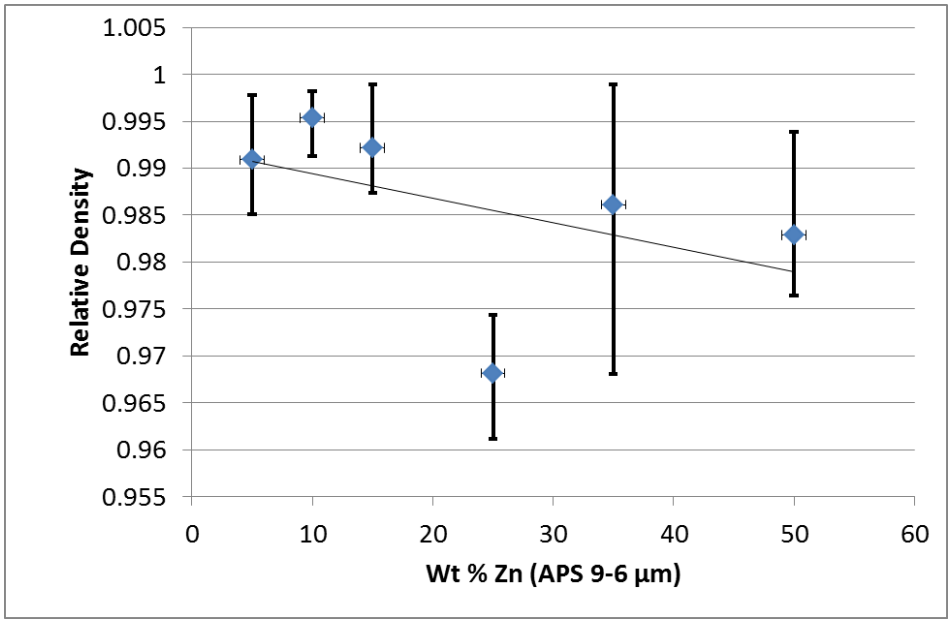

Fig.3-4: Tap (top) and tablet (bottom) densities vs. wt% Zn (median 9-6 µm)

Multiple samples at each compaction pressure were fabricated to ensure accuracy and repeatability. During the fabrication of each tablet, loading and unloading curves were created for both compaction cycles (flipping of the tablets). Fig. 3-5 shows typical loading and unloading curves for Zn (-100 mesh) and Zn (median 9-6 µm), separately. As can be seen from Fig.5, flipping the tablet over after the initial compaction cycle, does indeed allow for further densification during the second compaction cycle. This can be seen by the partially collapsed loading and unloading curves during the second compaction cycle in Fig.3-5.

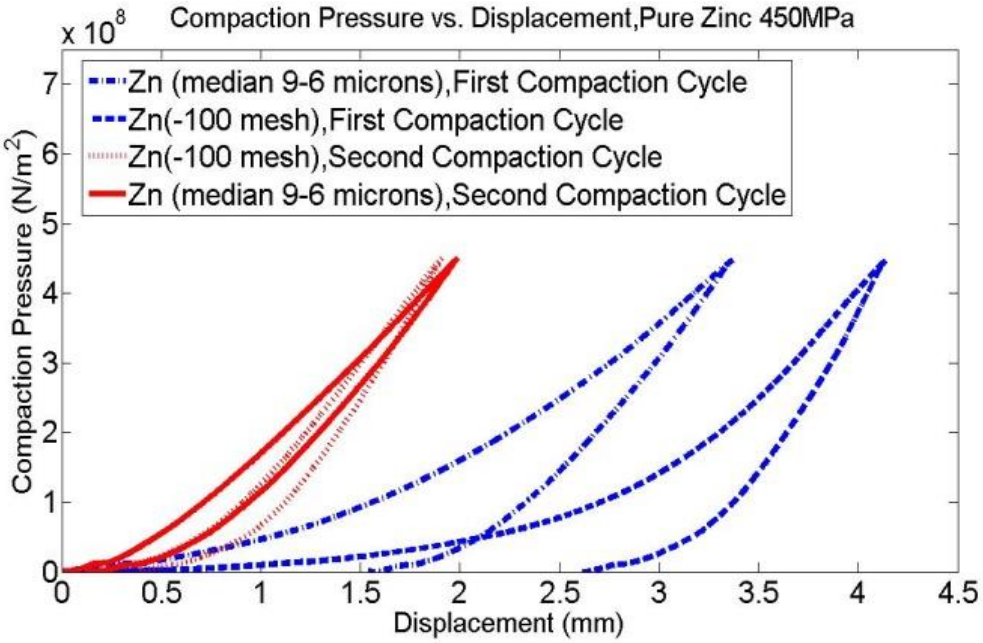

Fig.3-5: Compaction Pressure vs. Displacement, 450 MPa

Characterizing the effects of Rosin-Rammler parameters on the physical properties of the fabricated zinc tablets consisted of HV tests and Scanning Electron Microscope

(SEM) micrographs. Micro indentation testing is an important indicator of the degree of plastic deformation experienced by powder compacts and its overall strength [36]. Quadrini et al. used small indentation testing as a means to measure density of powder compacts [35]. SEM micrographs offer visual examination of surface morphology of tablets, visual confirmation of density and porosity, and facilitate the determination of particle size distributions. Due to the relatively large size (1-160 microns) of zinc particles used in this experiment, dynamic light scattering analysis was not a viable option to determine size distributions. As the size of the particles being studied must be small compared to the wavelength of light scattered off particles in liquid suspension, most typical wavelengths being on the order of 300 nm.

Hardness tests were performed using a Buehler Micromet II Micro hardness Tester (Buehler Corp., Lake Bluff, Illinois). Indents were made on the tablet surfaces with a pyramid shaped diamond indenter, with a 200 gram load being held for 10s. Hardness results of the samples are shown in Fig.3-6. To determine particle size distributions of the powders listed in Table 3-1, SEM micrographs were taken using a JEOL 5800LV Scanning Electron Microscope.

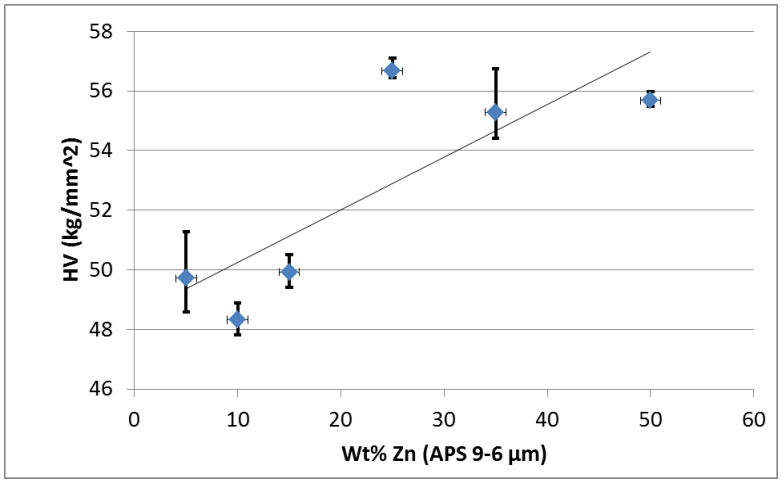

Fig.3-6: HV vs. wt% Zn (median 9-6

1. Zn (median 9-6 microns)
2. Zn (-100 mesh)
3. Zn (-100 mesh)5wt% Zn (median 9-6 microns)
4. Zn (-100 mesh)10wt% Zn (median 9-6 microns)
5. Zn (-100 mesh)15wt% Zn (median 9-6 microns)
6. Zn (-100 mesh)25wt% Zn (median 9-6 microns)
7. Zn (-100 mesh)35wt% Zn (median 9-6 microns)
8. Zn (-100 mesh)50wt% Zn (median 9-6 microns)

Table 3-1: Zn Powder Mixtures Used in Experiment

Multiple live images were taken at magnifications of 8000X and 4000X. The images were then imported into ImageJ imaging software and the long diameters of particles were counted. For each sample set in Table 1, the long diameters of 800 particles were measured and binned into histograms (Fig.3-7). Cumulative particle size distributions for each sample set were also determined and superimposed in Fig.3-8.

In order to determine if Equation 1 adequately describes the cumulative distribution data plotted in Fig.3-8 the two unknown parameters η and *D* must be determined. Taking logarithms of Equation 1 two times,

$$log\left\{log\left(\frac{100}{R(d)}\right)\right\} = \eta log(d) - \eta log(D) \qquad (3\text{-}2)$$

Equation 3-2 exhibits a linear relationship between the terms log{log(100/R(d))} and log(d). However, as shown in Fig.9, a linear relationship was not arrived at through the use of Equation 3-2. It was found that a linear least squares fit to the coordinates log{log(100/R(d))} and log(d) in Fig.3-9 result in inaccurate values for η and *D*. As a

result, to minimize errors, this experiment took on a MATLAB® nonlinear equation fitting routine (lsqcurvefit function) to fit the Rosin-Rammler distribution (equation 1) to the actual set of data [d, R(d)] in a least-squares sense. Here, η and *D* parameters and R(d) were selected as dependant variables for the independent variable particle diameter (d). The MATLAB® nonlinear equation fitting routine (lsqcurvefit function) performed repetitive fittings until the sum of the residuals squared (S_r) is minimized and correlation coefficient (r^2) indicates a goodness of fit. Table 2 lists the results of the nonlinear fitting routine. The results (fitting parameters) from Table 3-2 closely approach the actual data in Fig.3-8, individual plots of actual data and fits are shown in Fig.3-10.

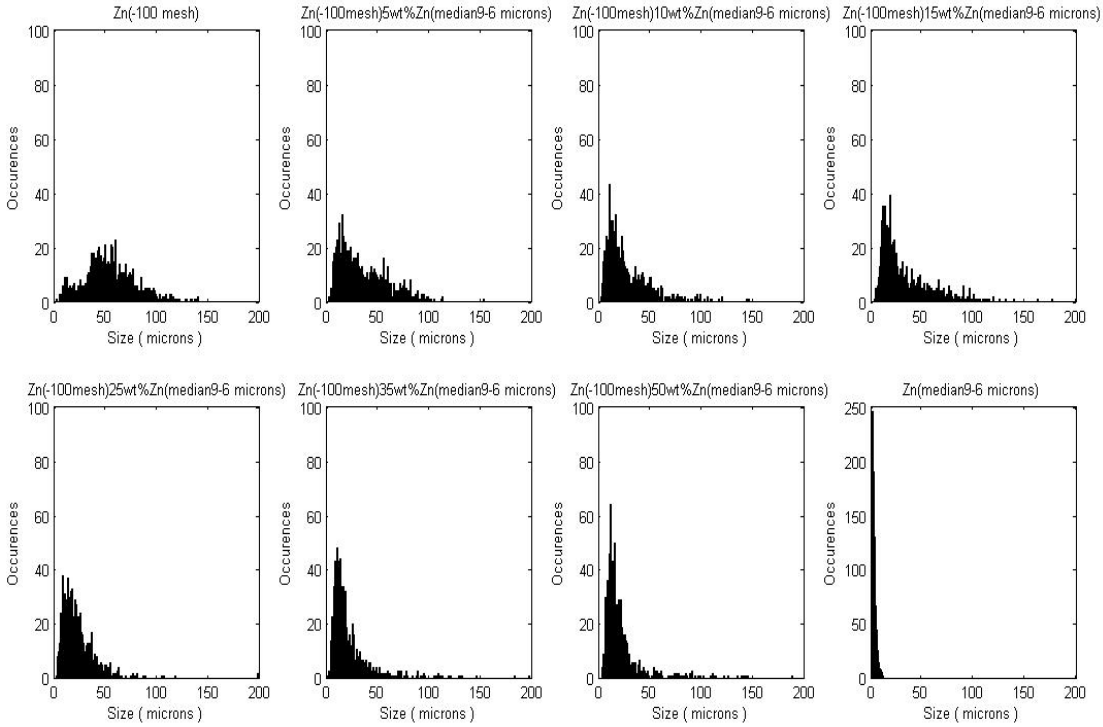

Fig. 3-7: Particle Size Distributions for Zinc Powder Mixtures Listed in Table 3-

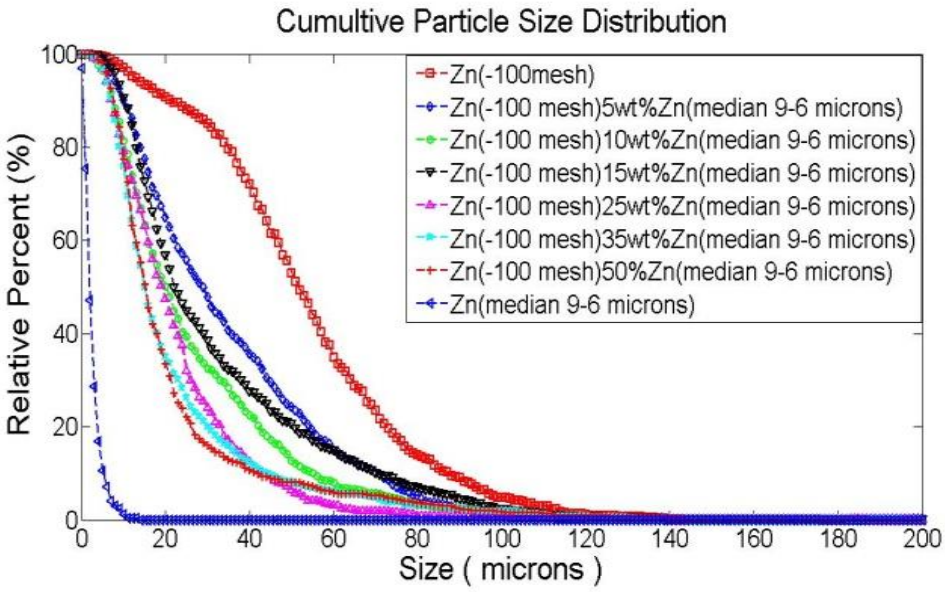

Fig.3-8: Cumulative Particle size

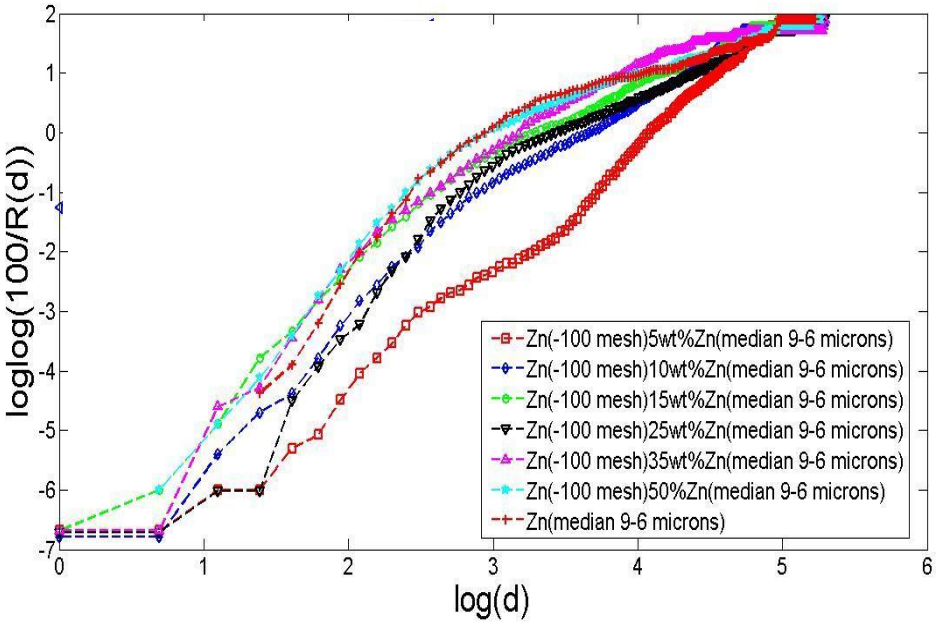

Fig. 3-9: log{log(100/R(d))} vs. log(d)

Sample	η	D (μm)	D(mean from data,μm)	r^2
1. Zn (-100 mesh)	2.421	60.59	54.87	0.9997
2. Zn (-100 mesh)10wt% Zn (median 9-6 μm)	1.439	38.30	36	0.9996
3. Zn (-100 mesh)10wt% Zn (median 9-6 μm)	1.287	28.51	28.14	0.9990
4. Zn (-100 mesh)15wt% Zn (median 9-6 μm)	1.275	33.96	33.72	0.9978
5. Zn (-100 mesh)25wt% Zn (median 9-6 μm)	1.566	24.50	24.24	0.9994
6. Zn (-100 mesh)35wt% Zn (median 9-6 μm)	1.326	21.75	23.38	0.9964
7. Zn (-100 mesh)50wt% Zn (median 9-6 μm)	1.494	20.70	22.83	0.9949
8. Zn (median 9-6 μm)	1.240	2.57	3.43	0.9997

Table 3-2: Fitting Data, MATLAB® nonlinear equation fitting routine (lsqcurvefit function)

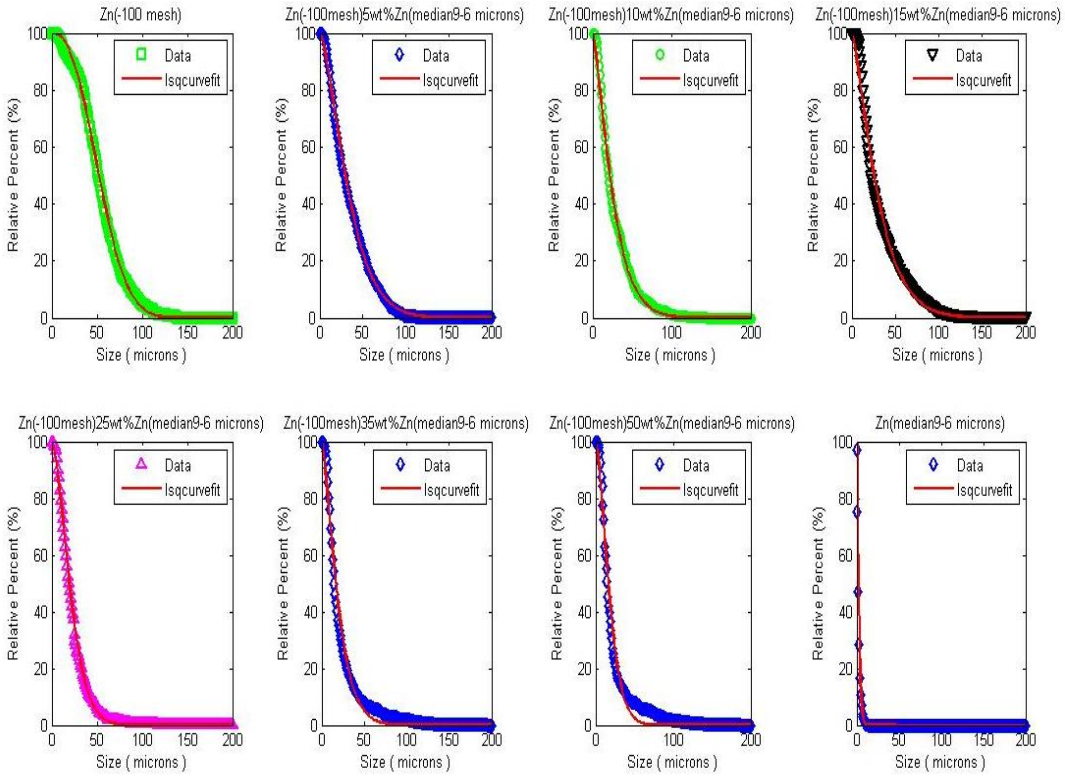

Fig. 3-10: Fitting Data vs. Experimental

3.3 Effects of particle size and morphology on densification behavior and tablet strength

As the weight percentage of Zn (median 9-6 μm) is increased there is a general trend for tap and tablet density to decrease (Fig. 3-3 – 3-4). Some of the natural consequences of ball milling a ductile material such as zinc are: cold welding which increases particle size, and cold working of zinc particles which increases strength [37]. However, as the zinc particles undergo excessive cold working, eventual fracture occurs and larger zinc agglomerates break into smaller ones. Fig. 3-11- 3-12 show SEM micrographs of Zn (-100 mesh) 25wt%Zn (median 9-6 μm) and Zn (-100 mesh) 50wt%Zn (median 9-6 μm). From these figures we see that zinc particles were first flattened under impact of ceramic balls forming flakes, these flakes then started to cold weld together forming larger zinc agglomerates. The lower tablet and tap densities in figure 4 can be attributed to an increase in particle irregularity and deviation from idealized spheres. The lower tablet densities as weight percent of Zn (median 9-6 μm) increases manifests itself in SEM micrographs of tablet surfaces (Fig. 3-13 - 3-16), where again, the increase in irregularity and dispersion of zinc granules increases surface porosity (dark spots in figures).

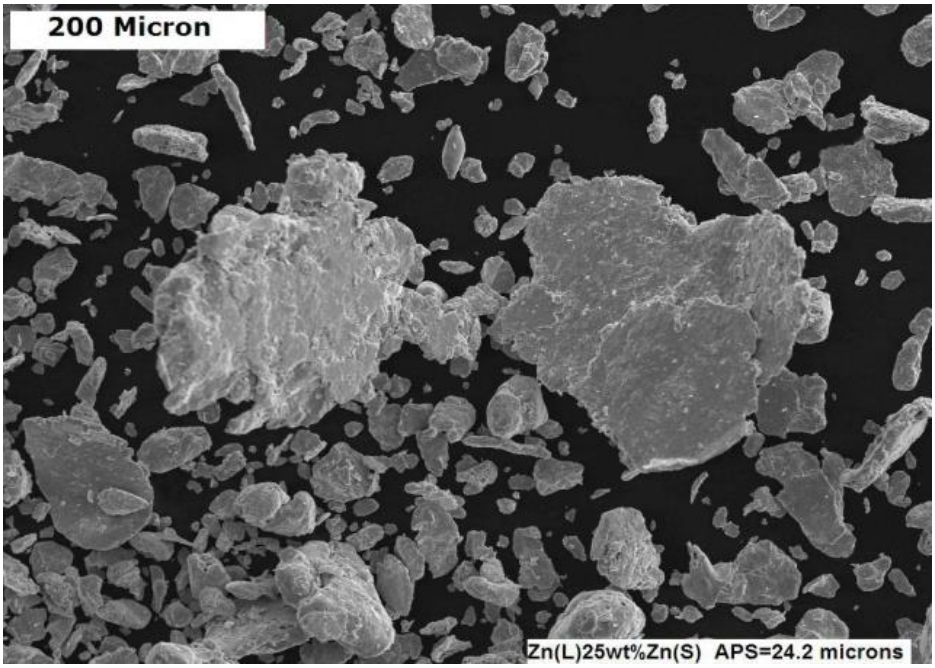

Fig.3-11: Zn (-100 mesh) 25wt%Zn(median 9-6 µm)

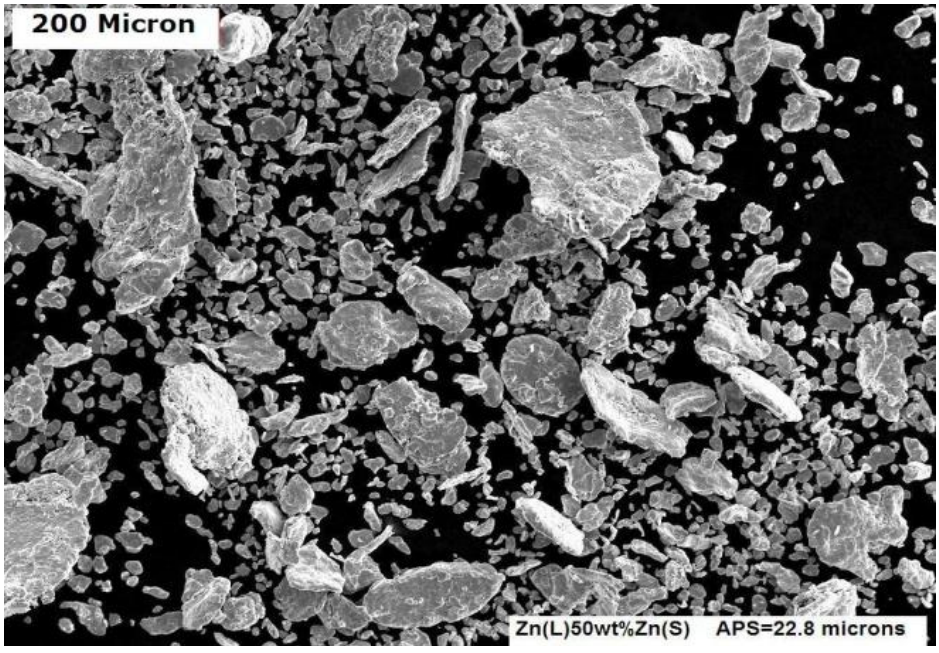

Fig.3-12: Zn (-100 mesh)50wt%Zn(median 9-6 µm)

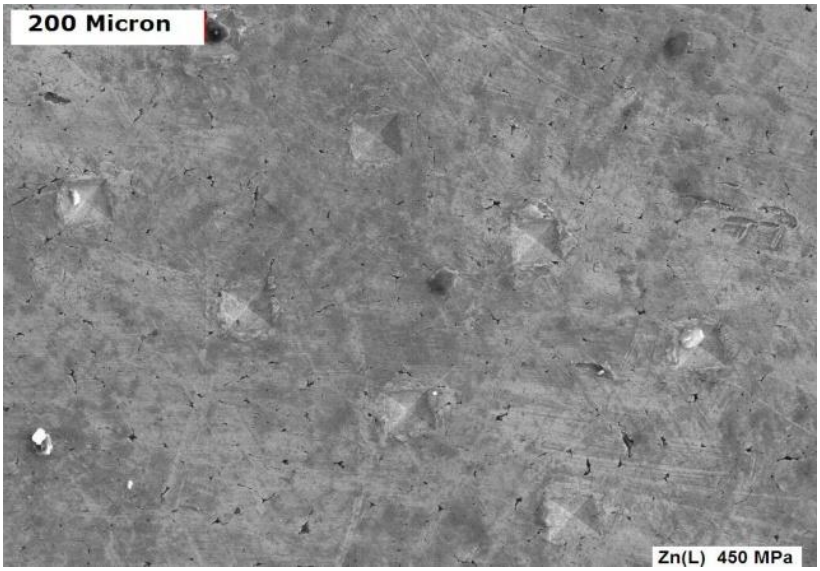

Fig.3-13: Zn (-100 mesh), 450 MPa.

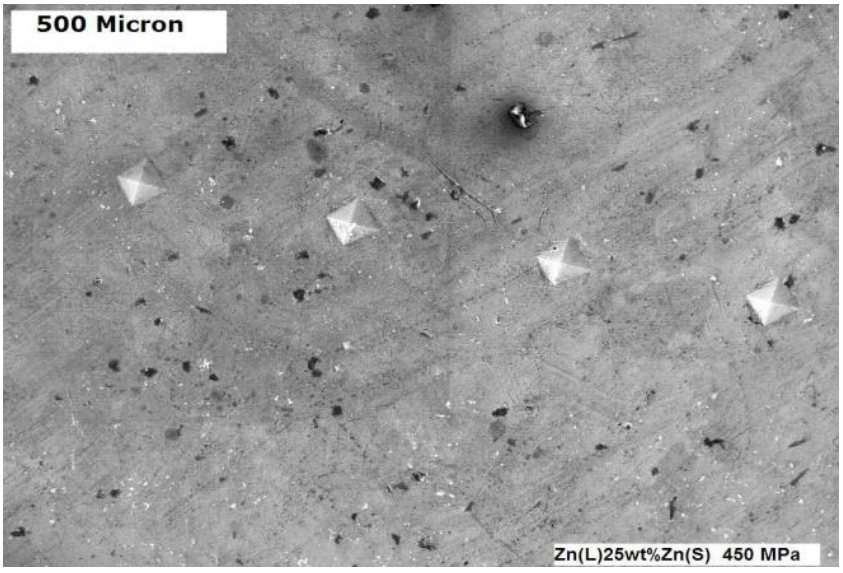

Fig.3-14: Zn (-100 mesh)25wt%Zn(median 9-6 µm) 450 MPa

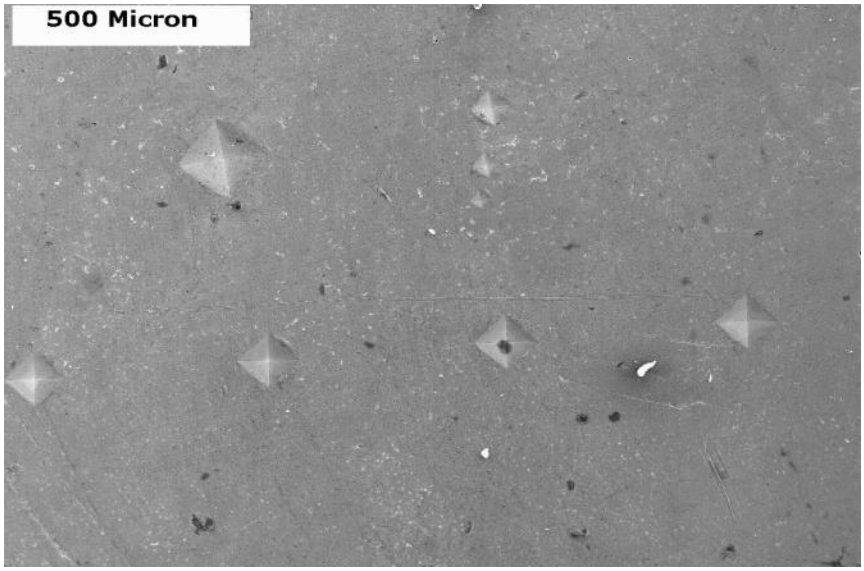

Fig.3-15: Zn (-100 mesh)35wt%Zn(median 9-6 µm) 450 MPa

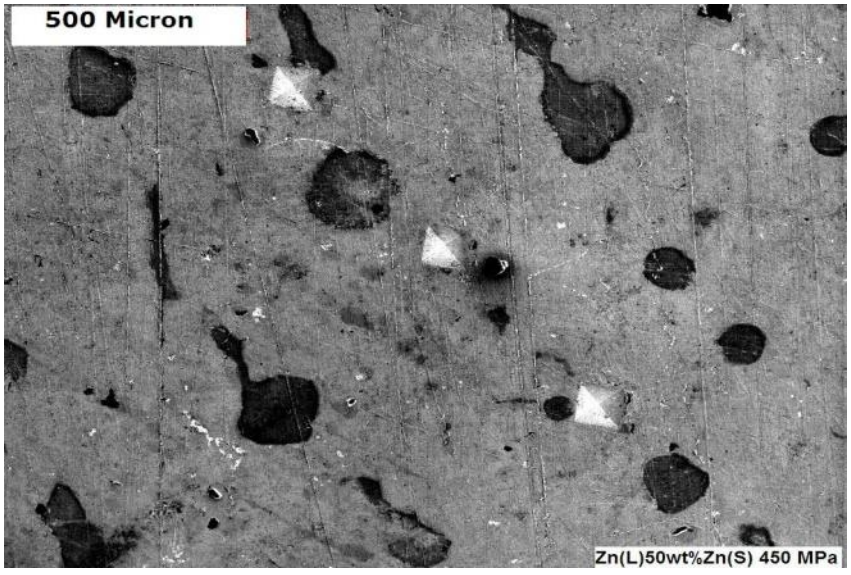

Fig. 3-16: Zn (-100 mesh)50wt%Zn(median 9-6 µm) 450 MPa

Compared to the commercially prepared zinc powders (Fig. 3-1 – 3-2), which exhibit a high degree of spherical symmetry in the 9-6 μm range and low degree of dispersion in the -100 mesh size ,the highly irregular zinc particles in Fig. 3-11 – 3-12 result in inefficient powder packing.

This study has shown a general trend for microhardness to increase as the weight percentage of Zn (median 9-6 μm) increases (Fig.3-6). This increase in hardness can be attributed to the disparity in size between the two zinc powders used in this experiment (Fig. 3-1 – 3-2); the total surface area per unit volume of zinc particles increases as the weight percent of Zn (median 9-6 μm) increases. This total increase in surface area per unit volume in turn creates more grain boundaries per unit volume in compacted specimens. These affects make penetrating the tablet surface with an indenter more difficult. The increase of grain boundaries per unit volume in zinc tablets, combined with cold working of zinc particles during the ball milling process, tend to mitigate the negative effects of porosity on hardness measurements.

The determination of Rosin-Rammler parameters through MATLAB® nonlinear equation fitting routine closely match the actual experimental data (Fig.3-10), this is further evident with high correlation coefficients in Table 3-2. Fig.3-10 also indicates that the Rosin-Rammler distribution function is adequate for describing metal powders that are not ball milled, as in the case with Zn (median 9-6 μm), which was produced by gas atomization (Fig.3-1).

The relationship between weight percent increase of Zn (median 9-6 μm) and Rosin-Rammler parameters (η, D) is shown in Fig.3-17 – 3-18. As weight percent of the

smaller zinc size increases the size distribution approaches that of commercially purchased Zn (median 9-6 µm) used in this experiment. The data for values of D in Table 2 in conjunction with Fig. 3-17 show that as the weight percentage of Zn (median 9-6 µm) is increasing APS exhibits the general trend of decreasing. Finally, Rosin-Rammler parameters vs. HV values for zinc mixture compacts are shown in Fig.3-19.

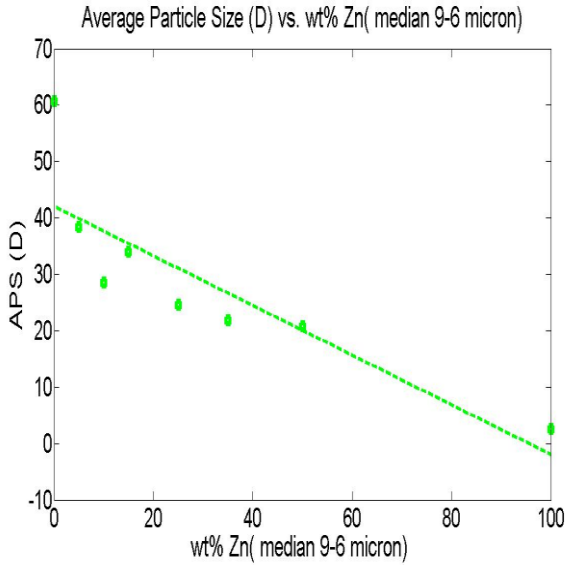

Fig.3-17: APS (D) vs. wt% Zn (median 9-6)

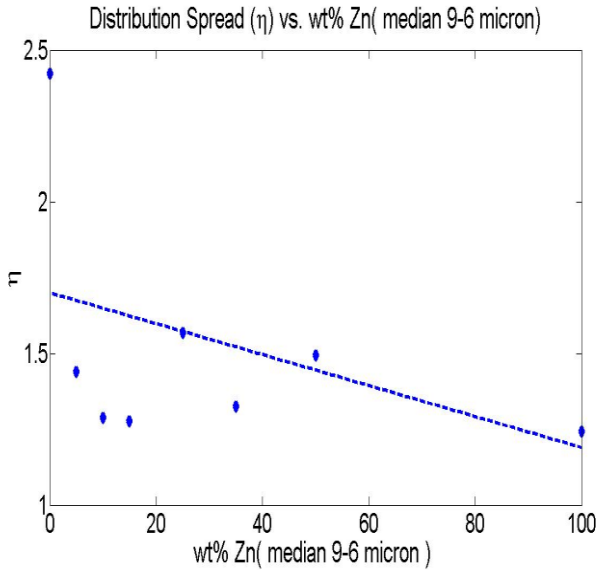

Fig.3-18: η vs. wt% Zn (median 9-6 µm)

As average particle size of distributions decreases hardness increases, this is due to the cold working brought about by ball milling and increase of grain boundaries per unit volume in zinc compacts. Microhardness is less sensitive to distribution spread parameter (η) (figure 3-19), as this can be seen in the nonconformity to a decreasing trend in percent ranges of 25-50wt% (figure 3-18).

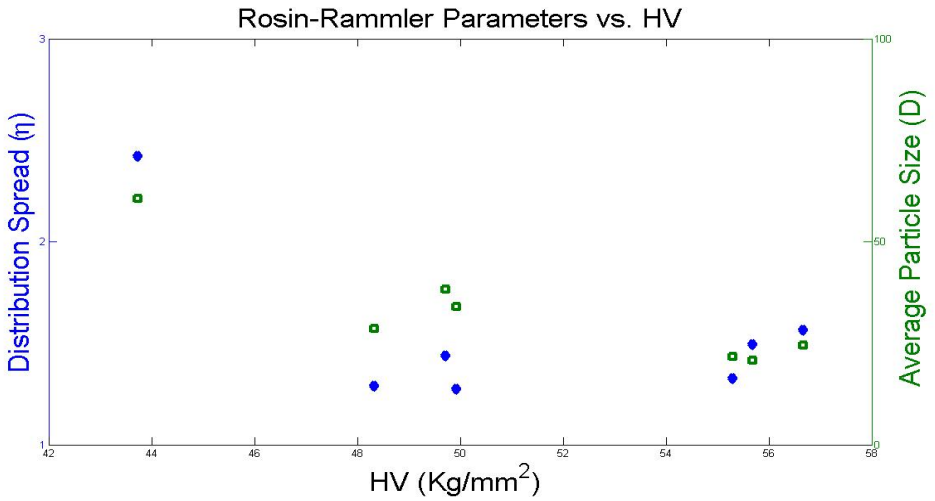

Fig.3-19: Rosin-Rammler Parameters vs. HV

3.4 Conclusions

The main conclusions derived from this study are summarized as follows:

1. Particle size distribution parameters play an important role in the overall densification behavior of zinc powders while undergoing the consolidation process. Particle morphology also plays an important role in maximizing packing efficiency in the tap and tablet densities. As average particle size decreases and

distribution spreads become narrower the hardness of zinc tablets increases. This study has also shown a decrease in tablet density as hardness increases, this can be due to excessive cold work experienced by zinc powders during the ball milling process. The amount of cold work experienced by zinc granules is shown to have a greater contribution to overall hardness than geometric hardening during the consolidation phase. This decrease of final "green" density will have deleterious effects during the sintering stage which will lead to components with poor strength and microstructure.

2. The ability to characterize skewed powder distributions has important industrial applications, as it is more cost effective to utilize metal powders which are highly irregular and have a wide range of particle size distributions [29, 32]. The Rosin-Rammler distribution has been shown to be an adequate mathematical function for describing zinc powders which have undergone morphological changes during a ball milling operation. This study has also established a relationship between the Rosin-Rammler function parameter (D) and HV. However, the relationship between η and HV has not been firmly established, as Fig.3-18 shows a clear departure from the decreasing linear trend in the 25-50wt% range. Thus, it is suggested that a modification of the Rosin-Rammler distribution be investigated which takes into account ball milling parameters and or particle irregularity.

3.5 Future Work

Sintering

Sinter specimens at 80% melting temperature for zinc under inert atmosphere. This will increase bonding between adjacent zinc granules creating a continuous matrix as opposed to an agglomerate of particles held together solely via mechanical interlocking. This will have the added benefit of creating zinc tablets that are structurally stable to withstand scale appropriate indentation testing, namely, superficial Rockwell.

Mechanical Testing, Superficial Rockwell

Employ superficial Rockwell testing as a more reliable/appropriate means of determining tablet strength. This will give a clearer indication of the dependence of tablet strength on Rosin-Rammler functional parameters and particle morphology. The utilization of Vickers micro-hardness testing in this study can be considered "scale" insensitive to bulk material properties. From table 3-2, for various bimodal powder compositions average particle size varies between 36-22 μm. From figures 3-13 through 3-16 it can be seen that the diagonals of the indents in the SEM micrographs are on the order of ~ 50 μm. Therefore, micro-indentation testing is inadequate in determining the negative effects resultant particle morphology of ball milled bimodal powder distributions have on bulk material properties of zinc compacts. Although useful, Vickers testing with its characteristically small indentation loads is indicative of the amount of strain hardening experienced by individual zinc particles during the ball milling process. At despairingly higher loads encountered in superficial Rockwell testing should impart an indentation "foot print" encompassing a significantly higher number of milled particles. These larger indentation foot prints will also encompass surface pores which should provide further insight into the contribution of residual porosity in overall hardness of tablet specimens.

Density Determination and Characterizing Porosity

Experimentally determining relative density is a poor descriptor. More useful descriptors are needed to describe porosity content and morphology as weight percentage of Zn (median 9-6 µm) particles increase. As noted in chapter 2, due to tolerances between the moving discs and die (figure 3-3), during the compaction process material is pushed into this area creating tablets with an "elephant foot" shape around their perimeter. This effect leads to zinc tablets that deviate from perfect cylinders making experimental determination of density unreliable using conventional Vernier calipers and electronic balance. More precise means to determine density can be carried out using a combination of SEM analysis and imaging techniques. Characterization of surface porosity, its descriptors, and tablet density will be carried out using ImageJ, which is an open source imaging software. The strategy used here is twofold:

1.SEM micrographs (in the form of TIFF images) of surfaces of zinc tablets are imported into ImageJ, manually thresholding is applied, and finally converted to 8-bit binary images (figure 3-20).

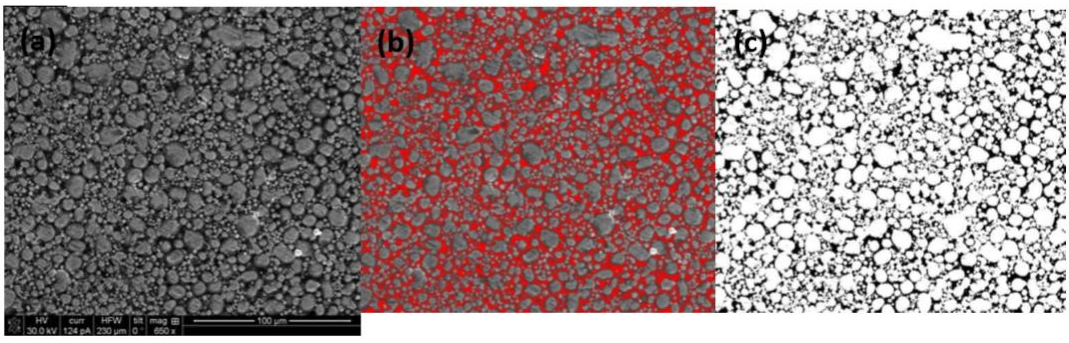

Figure 3-20: (a) SEM image of zinc tablet surface; (b) threshold image; (c) binary 8-bit image.

Thresholding is the simplest method of image segmentation. During the thresholding process, individual pixels in an image are marked as "object" pixels if their value is greater than some threshold value (assuming an object to be brighter than the background) and as "background" pixels otherwise. In this study the “object” pixels correspond to regions of surface porosity and the “background” pixels to regions of material (Zn). The “histogram” feature in ImageJ then gives a count of object pixels. With the scale bar annotation on the SEM micrographs, one can easily determine pixel size, and total area. Porosity percentage is then determined by the following equation:

$$Porosity = \frac{\#object\ pixels * pixel\ size^2}{total\ area} * 100 \qquad (3\text{-}3)$$

2. To characterize porosity as a function of Zn (median 9-6 μm) weight percentage, 8-bit binary images will be evaluated using the ImageJ “particle analyze” module. Most particle analysis software, including ImageJ, map the actual particle to an equivalent ellipse so that both area and perimeter matches. ImageJ has a built-in option for analyzing particles, which produces such output parameters as number of particles, areas, perimeters, circularity, orientation angle, and major and minor axes. In this study the “particles” being analyzed are individual surface pores.

Effects of Ball Milling Parameters on Tablet Microstructure

During the ball milling process there are two competing processes: cold welding of particles which leads to an increase in average particle size; excessive strain hardening of ductile metal particles which leads to eventual particle fracture and decrease of average particle size. For bimodal powder mixtures in this study, as weight percentage of Zn (median 9-6 μm) particles is increased the dominating effect of either particle welding or fracturing is unknown. The resultant particle size distribution will be adversely affected by either process which will in turn affect resultant tablet microstructure. In order to investigate this phenomena, Zn (-100 mesh) and Zn (median 9-6 μm) will be ball milled separately for a pre-determined period of time. Milled powders will then be consolidated (at varying increments along the ball milling period), following procedures as outlined in section 3.2, with tablet material properties determined as a function of milling time. More specifically, the following data curves will be produced: hardness vs. milling time, and relative density vs. milling time. This process will then be repeated for bimodal Zn powder mixtures (items 3-8 in table 3-1) and a comparison of resultant material properties will be made.

Chapter 4

Review: Fabrication and Mechanical Characterization of CNT/MMCs Fabricated via PM Techniques

4.1 Introduction

This review outlines recent developments carried out by researchers in the fabrication of CNT/MMCs and their resulting material properties. More specifically, this review focuses on various CNT dispersal mechanisms in the fabrication of CNT/MMCs via the powder metallurgy method (PM). Powder processing techniques have been employed to successfully synthesize a wide range of particulate reinforced composite materials utilized in transportation industries and as structural materials. Recently, PM techniques have emerged as an attractive fabrication route for composite mixtures with constituents on the sub-micron to nano scale. Of central importance in the PM technique is optimal blending and mixing of constituent phases. This is especially critical when mixing high aspect ratio nano particles such as CNTs with micron sized metal granules. The state and quality of CNT dispersion in the starting composite powder mixture is crucial to gain full advantage of subsequent consolidation/thermal processing phases in the PM fabrication route. Current review shows comprehensive approaches undertaken globally in obtaining optimal CNT dispersions in metal matrix systems utilizing a variety of techniques. The present review brings into focus the critical issues which affect the mechanical performances of CNT reinforced MMCs that include: CNT dispersal route, state and quality of nanotube dispersion, and the importance of the CNT/metal transition

layer as an effective stress transfer medium. Also elucidated in this review are nanotube dispersal mechanism, resultant material properties of CNT/MMCs, compatibility of CNTs in different metal systems, and CNT strengthening mechanisms.

Metals and their alloys have been widely used as structural components in a wide variety of transportation industries such as aerospace design [41]. This is due to its good strength to weight ratio, relative ease of formability, and its ability to withstand fatigue cracking due to stresses that occur during operation. However, as demand increases for higher performance materials, metals and their alloys are inadequate in providing both good strength and high stiffness. The challenge of next-generation transportation design is to incorporate composite materials with strength and stiffness that exceed those of standard metals and alloys while reducing weight. With global oil prices increasing, the ability to increase structural integrity while increasing fuel efficiency has become highly desirable in a multitude of transportation industries. These demands have spurred the development of MMCs with constituents on the sub-micron to nano scale which offer the benefits of increased strength while maintaining percent elongation. Today MMCs are used in various aerospace and automobile industries [42-44]. CNT/MMCs are unique as they can exhibit enhanced mechanical, thermal, and or electrical properties simultaneously making them highly functional materials. These properties make CNT/MMCs highly desirable in aerospace,
automobile, and electronics packaging applications where materials must fulfill multiple design criteria.

Since their discovery in 1991 [45], CNTs have revolutionized composite industries with their extraordinary mechanical properties; tensile strengths of single walled carbon

nanotubes (SWCNTs) as high as 22 GPa [46], and an average Young's modulus of 1.25 TPa [47]. These physical properties make CNTs ideal candidates as reinforcement phases for a wide range of structural materials used in transportation design. CNT/MMCs have the requirements to reduce the cost of transportation while increasing safety, strength, reliability, and functionality. Within the past decade much work has been carried out using CNTs as an exotic reinforcement phase in a host of different materials (fig.4-1).

The majority of the research has been carried out in regards to reinforcing polymer matrices. This can be due to the relative ease of polymer processing, which does not require extreme processing environments such as metals or ceramics. As well, CNTs have a low chemical compatibility with most metal systems and strengthening mechanisms are largely not yet well understood. Studies on the reinforcement of MMCs with CNTs have risen steadily throughout the years due to the development of novel nanotube dispersal mechanisms and the success of PM.

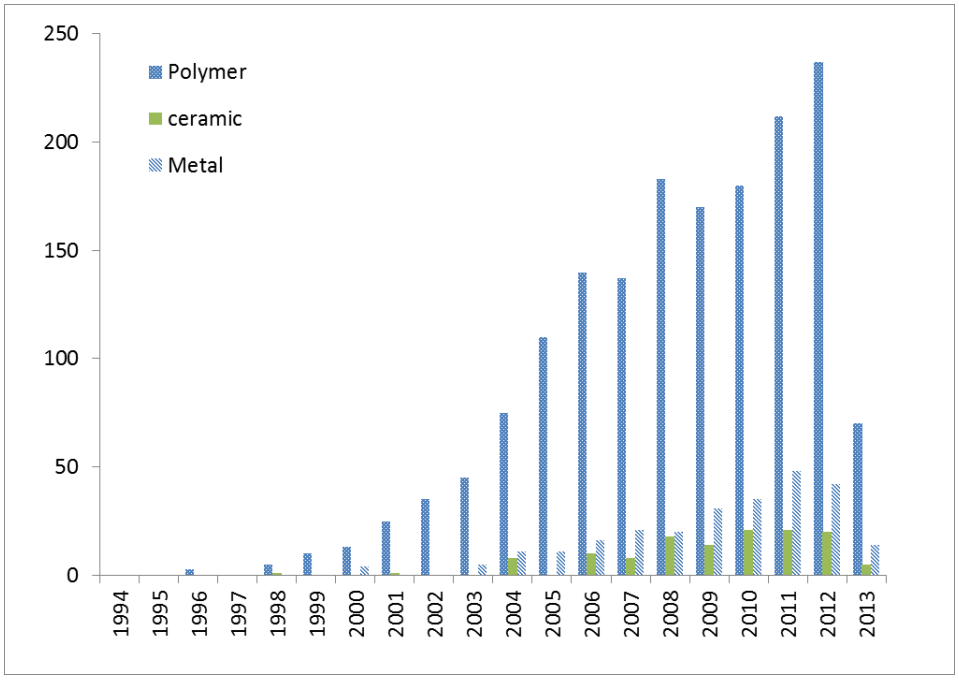

Figure 4-1. Number of publications on polymer/ceramic/metal- matrix composites during 1998-2013 (source: www.webofknowledge.com)

The majority of the research has been carried out in regards to reinforcing polymer matrices. This can be due to the relative ease of polymer processing, which does not require extreme processing environments such as metals or ceramics. As well, CNTs have a low chemical compatibility with most metal systems and strengthening mechanisms are largely not yet well understood. Studies on the reinforcement of MMCs with CNTs have risen steadily throughout the years due to the development of novel nanotube dispersal mechanisms and the success of PM as a viable fabrication route [48]. Although a number of review papers exist on CNT reinforced ceramic and polymer matrices [49-53], there exists limited information concerning CNT reinforced MMCs fabricated solely via PM techniques (fig.4-2) [54].

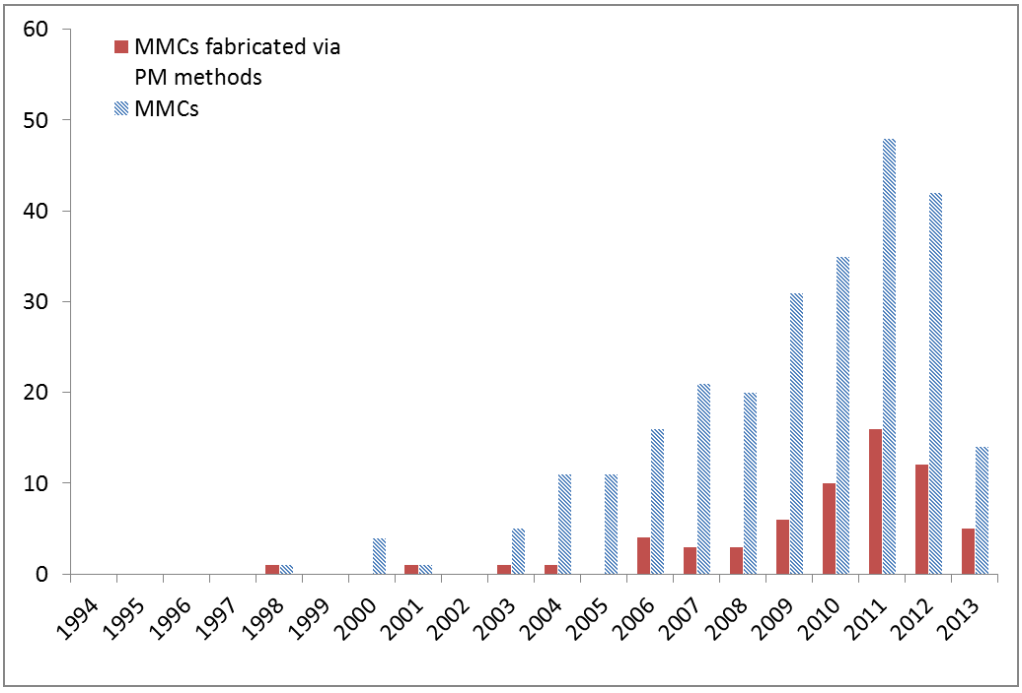

Figure 4-2. Number of publications on MMCs and MMCs fabricated via PM methods during 1998-2013 (source: www.webofknowledge.com)

There is not a single review article which deals with CNT reinforced MMCs fabricated via the powder metallurgy method. Therefore a systematic review of studies carried out on the fabrication and mechanical characterization of CNT/MMCs was found necessary for the following reasons. First, it will provide a summary of recent developments by researchers in the dispersion of CNTs in metal powder systems, and subsequent material properties of CNT/MMCs using dispersion-PM techniques. Second, it will serve as a guideline for future researchers who may not be familiar with this subject. The purpose of this article is to review studies carried out globally in the fabrication and mechanical characterization of CNT/MMCs fabricated using PM methods in order to obtain a clear picture of the state of the art of this emerging field.

4.2 Powder Metallurgy Route

There are many fabrication methods to obtain CNT reinforced aluminum matrix composites, amongst which, the PM technique could be considered the most effective and economic one [48,54]. Powder metallurgy is a very attractive forming and fabrication technique due to its

relatively low costs and the ability to form complex near net shapes with little secondary machining steps required. The PM fabrication route is characterized by: (i) blending and mixing of constituent phases, (ii) consolidation and sintering, (iii) post machining. For composite materials fabricated utilizing PM methods, stable and long-standing dispersion of particulate substances within the host matrix can be of high significance. The importance of a homogeneous, stable and long-standing particulate dispersion is of a

particular importance when the particulates are of a very small size (i.e., sub-micron or nano particulates), such as high aspect ratio carbon nanotubes. As outlined in the next section, CNTs form bundles, which can be difficult to isolate into individual tubes among metal powders. A variety of CNT dispersal techniques (and or combinations of) has been employed in conjunction with PM processing methods by researchers with varying levels of success. These CNT dispersal modes are but not limited to: mechanical mixing, ultrasonication, mechanical/magnetic stirring, in-situ chemical vapor deposition (CVD), surfactant assisted dispersion (wet-process), and other novel techniques. These CNT dispersal modes are discussed in further detail in the following sections. In all the works reviewed in this study, once CNT/metal powder composite mixtures are obtained, they are consolidated at room or elevated temperatures followed by sintering in inert gas environments. Spark plasma sintering (SPS) has emerged as a popular consolidation/sintering technique among researchers as the heat is supplied internally which facilitates fast cooling/heating rates which in turn aides the densification process. In most of these works, PM compacts are then subjected to further post sintering deformation processes such as: hot/cold extrusion, equal angular channel pressing, rolling, etc. These processes further densify the matrix surrounding while aligning CNTs in preferred directions.

4.3 Carbon Nanotube Aggregation

The nano-sized dimensions of CNTs (i.e., inner and outer diameters) cause them to have high surface areas [55]. These surface areas are usually positively or negatively

charged [56]. Large surface areas possessing electrical charges result in the existence of Van der Waal forces/energies, which in turn cause the CNTs to aggregate. High aspect ratio along with high flexibility of CNTs, are other factors that cause CNTs to aggregate together. CNTs tend to aggregate into rope-like structures, an example of a rope-like aggregation is shown in Fig.4-3. Such rope-like bundles may contain hundreds of close-packed SWCNTs that are tightly bound via Van der Waals attraction energies of approximately 500 eV/μm of SWCNT-SWCNT contact [57]. The addition of small Van der Waals energies existing along the large surface areas of the SWCNTs produces a high affinity between the SWCNTs. This leads to rope-like SWCNT aggregates that are highly entangled as seen in fig.4-3.

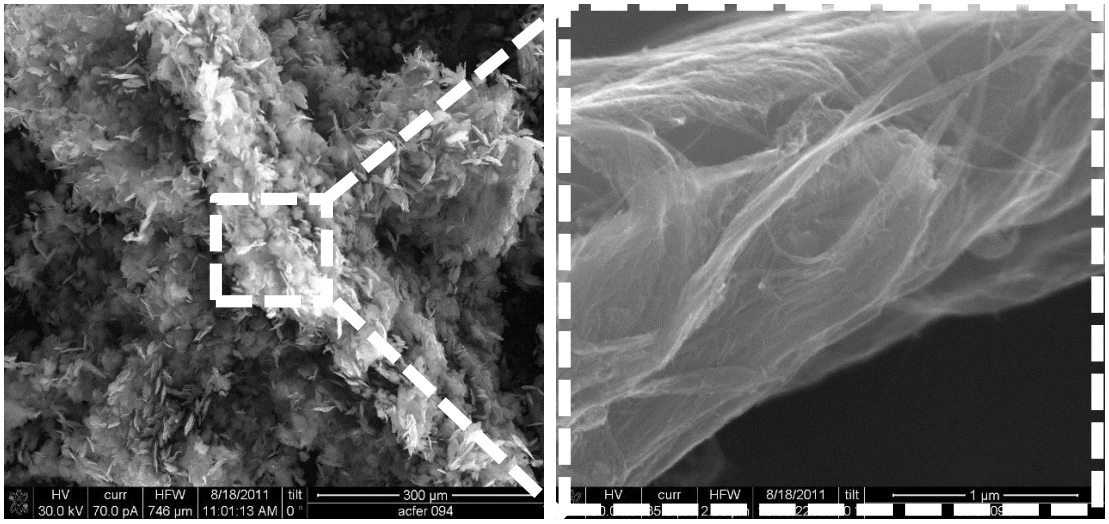

Figure 4-3: SEM images of SWNT ropelike and bundle aggregates

CNTs are widely used as a means to increase or decrease: thermal, electrical, and mechanical properties of the host material [57]. However, the fact that CNTs tend to aggregate within the host material inhibits the full harvest of these specific properties

within the host material. In the case of polymer matrices, this aggregation results in composites with physical properties and performances far below theoretical expectations [58]. The composites mechanical properties such as its modulus of elasticity are reduced as a direct result of the aggregation of the CNTs [58]. CNTs are also proven to function as locations of high stress concentration and consequently perfect sites for the initiation of a surface or internal crack [58]. The high aspect ratio of the CNTs as well as their alignment in a preferred direction, are other features that are highly utilized in achieving a desired mechanical properties within the composite material. To guarantee a maximum effectiveness of these features it is essential to have a homogenous and fiber-like distribution of CNTs [58].

In order to partially address the issue of good dispersion, it should be realized that the solubility of the CNTs within the matrix play a major role [59]. The more soluble the CNTs are within the host material, the better CNT dispersion patterns are observable. Another important factor with regards to the extraction of the full potentials of CNTs physical properties is the proper interfacial interactions between the CNTs and the host metal. Proper interfacial bonding between the CNTs and the metal matrix is the key to reliable interaction between these two chemically dissimilar materials.

Based on the sensitivity and inconsistency of the above mentioned factors, a diverse set of mechanical properties have been measured and reported by different research teams for the same metal composite materials incorporating CNTs. To obtain consistent mechanical responses in statistical materials such as these CNT composites, it is a prerequisite to satisfy the following criteria. The first and foremost criterion that needs to be satisfied is the presence of a homogeneous, stable and long-standing CNT dispersion

within the host material. The second requirement is the proper maintenance of the structural integrity of the CNTs. Finally, the interfacial bonding between the surfaces of the CNTs and the matrix must be maximized.

4.4 CNT dispersal modes

In the following section are discussed various CNT dispersal mechanisms employed by researcher groups reviewed in this study. Typical CNT dispersal mechanisms in the fabrication of CNT/MMCs via PM methods are: wet-process (surfactant assisted), mechanical milling, hand grinding, mechanical stirring, ultrasonication, electroless deposition (plating), in-situ chemical vapor deposition, molecular-level mixing, and other novel dispersal mechanisms. Some of these novel dispersal mechanisms are improvisations of ones previously outlined or new developments all together. It should also be noted that some researchers used combinations of dispersal mechanisms listed above in conjunction with each other to achieve homogeneous distribution of CNTs.

Surfactants

Some researchers have explored the use of surfactants (wet-process) to exfoliate CNT bundles into individual tubes. A surfactant is a surface tension reducing agent that has the ability of accumulation at both hydrophobic and hydrophilic surfaces [60]. Surfactants are amphiphilic compounds, meaning they possess both a polar and non-polar head-groups. The duality of the surfactants bestows them with the ability to insert themselves between the interfaces existing between immiscible media. Examples of such immiscible media are oil and water, oil and air, air and water or in the case of the works

reviewed in this study hydrophobic CNTs within the predominantly aqueous solutions. The charge of the surfactants head groups ranks them in different classifications. The classification can be reduced to nonionic, anionic, cationic or zwitter-ionic [60]. With regards to their use in the dispersion of CNTs within a matrix medium, two important qualities of surfactants are useful. First is their ability to be adsorbed at hydrophobic or hydrophilic interfaces. The driving forces for the adsorption behavior are caused by Van der Waals and Columbic attractions between the opposite charges of the surfactants and the CNTs or the host material [60]. Second is their ability to assemble themselves into 3D spherical structures called micelles. At and beyond a certain surfactant concentration, surfactants are thermodynamically driven to group themselves into micelles and self-assemble on CNT surfaces forming self-absorbed monolayers. Absorbed surfactant molecules then cause a repulsive barrier between CNTs hindering re-agglomeration into bundles in aqueous environments.

MMC/CNT composite powder mixtures prepared using this technique are Al/CNT[61], Al_{6063}/CNT[62], Mg/CNT[63-64], Mg_{AZ31B}/CNT[63], Mg_{AZ61}/CNT[64-65], and Ti/CNT[66-67]. In most studies, CNT bundles are first exfoliated in aqueous surfactant solutions and then combined with metal powders. With individual CNTs coating metal powder surfaces, residual surfactants are then easily removed in high temperature furnaces, and finally composite mixtures are consolidated via a variant of the PM process. Unlike other highly energetic dispersal modes such as mechanical milling, surfactant assisted dispersion preserves the unique electronic and spatial structure of CNTs. As some of these studies have shown [62-63,66-67], this method is effective at coating metal powders with individual CNTs. However, CNT bundles are never

exfoliated completely and as in the case of most studies reviewed, secondary ultrasonication steps must be taken to further exfoliate nanotube bundles

Mechanical Milling

Mechanical milling has been used for many years as a robust powder processing technique in the preparation of ceramic based metal composites or fine powders. Mechanical milling is also used for controlling fine scale microstructure and alloying materials that are incompatible. In the mechanical milling process, powders are placed in an energetic mill with a suitable grinding medium (typically in the form of ceramic or hardened steel marbles). Mills typically fall into three categories: attrition mill (vertical ball mill), vibratory mill, or planetary ball mill (horizontal ball mill). In the first type, attrition mills are characterized by stationary vertical tanks in which powders and grinding medium in the form of steel balls are agitated via impellers radiating from a central rotating shaft. Attrition mills are typically used for moderate amounts of powders in moderate milling times. Typically on the order of hours. In the second configuration, the vibratory mill (or commonly referred to as the shaker mill), in this system the powders and grinding balls are placed in a vial and agitated at high frequency in a complex cycle which can involve motion in three orthogonal directions. Vibratory mills can produce small amounts of alloyed powder in short milling times (~ 1 hr). The third and most commonly used type of mill employed by researchers is the planetary ball mill. In this type of mill, the powders (and grinding balls) are placed in ceramic or steel capsules, which are rotated about a central vertical axis at a speed below critical speed which would pin the grinding balls to the internal wall of the capsules. Planetary ball

mills can produce relatively large amounts of powder at the expense of long milling durations. Regardless of the type of mill used there are generally two competing processes. First, kinetic energy is transferred from the grinding medium to the ductile metal powders, which can undergo severe plastic deformation. As the process continues, the metal powders eventually become strain hardened which leads to brittle failure and eventual fracture. If adjacent powder particles are trapped between colliding balls (and have atomically clean surfaces) coalescence (cold welding) can occur. These competing processes continue throughout the milling process with an eventual steady-state powder size distribution met. For the cases of MMC/CNT powder mixtures prepared by mechanical milling, this dispersion technique has the advantage of impregnating CNTs within the soft metal matrix over long milling durations [68]. Which promotes mechanical adhesion of chemically dissimilar metal matrices and CNTs. However, this energetic process leads to excessive cold working and morphological changes in ductile metal powders. This can adversely affect certain PM process parameters (such as consolidation pressure) which can result in CNT/MMCs with poor microstructures. In this processing method, damage to CNTs during this energetic process should be avoided by careful determination of ball milling process parameters (ball-to-powder ratio, milling time, rotational speed). The majority of the works reviewed in this study used mechanical milling as the primary dispersal route, or in conjunction with other dispersal modes discussed in this section. MMC/CNT composite powder mixtures prepared solely using this technique are Al/CNT [68-78], Al_{2024}/CNT [79-83], Al_{6061}/CNT [84], Cu/CNT [85-88], Mg/CNT [89-92], Mg_{AZ91D}/CNT [93], and Ti/CNT [94-96].

Ultrasonication

During ultrasonication, mechanical energy is delivered to the liquid medium via ultrasonic waves of high frequency (>20 kHz) which generate local shear stresses that are ultimately responsible for dispersing CNT aggregates. The irradiation of a liquid containing aggregates with ultrasonic sound results in agitation of the colloid. These sound waves traveling through the liquid medium result in rarefaction cycles which create small voids or bubbles. During rarefaction and above a high enough ultrasonication frequency cavitation will occur. Once cavitation has occurred, the bubbles collapse in an explosive manner and create high strain rates ($10^9 s^{-1}$) in the vicinity of bubble implosion [97]. When this occurs local shear stresses for low viscosity fluids can be as high as 100 MPa [97]. In a proposed mechanism by Strano et al. [60], shear stresses produced by cavitation are imparted to CNT bundles which creates a pulling force "fraying" the ends of bundles. This fraying effect acts to expose surfaces of individual CNTs to the surrounding medium, which become sights for the absorption of interfacial molecules from the surrounding medium. As the process continues individual CNTs are slowly "unzipped" from bundles. CNT exfoliation states achieved by the ultrasonication process however are only temporary, therefore, some researchers find it necessary to ultrasonicate CNTs in the presence of a stabilizing agent. Typical stabilizing agents that can be used for CNT suspensions are but not limited to: ethanol, alcohol, toluene, and surfactants. For the cases reviewed in this study ultrasonication is typically used in conjunction with or as a precursor to another dispersal route. Most commonly, as a precursor to mechanical milling [81-83, 98-103] or electroless plating [64-66]. In some cases ultrasonication is the stand alone dispersal mode [107-108] or used to enhance

surfactant assisted dispersion [63]. MMC/CNT composite powder mixtures prepared solely using this technique are Al/CNT [107] and Al_{A5083}/CNT [108].

Electroless plating

Electroless plating is a deposition technique employed by research teams to overcome the poor wettability between CNTs and metals [105-106,109-111]. By improving wettability between these two incompatible materials, better CNT dispersion can be obtained along with an effective stress transfer medium between CNT and metal matrix. The basic electroless plating technique may be outlined as follows. First, CNTs are washed in acid to remove impurities and or metal catalyst particles. Due to the difficulty of metal atoms adhering to CNT surfaces, CNTs are then subjected to a pretreatment of weak acids to form hydroxlic, carbonylic, and carboxylic functional groups on CNT surfaces [112]. These functional groups act as nucleation sights for metal atoms. Pre-treated CNTs are then put in a nickel/copper electroless bath. As it is commonly known, electroless baths contains a metal salt (source of metal) and a reducing agent. These electroless baths also contain buffers and complexing agents. These compounds help to maintain the pH of the bath and availability of metal ions [113]. Finally, CNTs are washed using distilled water and subsequently dried. The morphology of the resultant nickel/copper coatings are largely dictated by process parameters such as pH and temperature of the solution [113]. Electroless nickel/copper deposition (plating) technique is advantageous in that metal ions are deposited directly onto surfaces of individually functionalized CNTs forming metal layers nanometer to submicron in thickness. Ni and Cu are more chemically compatible with most metal systems than

carbon, which can further facilitates the mechanical mixing/dispersion of nickel/copper plated CNTs with metal powders. For the majority of works reviewed in this study that utilized the electroless nickel/copper deposition technique to disperse CNTs, nickel/copper plated CNTs were then mechanically milled to further enhance CNT dispersion [106,109-110,114]. Electroless deposition technique can however be complex, plus, some of the acids used in this process can be hazardous to humans and the environment. MMC/CNT composite powder mixtures prepared using this technique are Cu/CNT [105-106,109], Cu-Sn/CNT [110] and Ti/CNT [111].

In-situ Synthesis of CNTs

As a means to overcome the limits of traditional mixing methods some researchers have grown CNTs in-situ on the surfaces of metal powders via chemical vapor deposition (CVD) techniques [114-117]. This process produces individual homogenously dispersed CNTs on metal powder surfaces. For Al/CNT composites fabricated using this method a catalyst precursor is first prepared [115-117]. Catalyst precursors are then reduced depositing Ni/Co nanoparticles on Al powder surfaces. Ni/Co nano particles then act as nucleation sites for CNTs which are “grown” on Al powder surfaces using conventional CVD methods. The CVD method, has been extensively employed to mass produce CNTs by the decomposition of a hydrocarbon at temperatures of 500-1000 ˚C in a quartz tube reactor. Using similar techniques, Sun et al. [114] successfully used Mg powders as catalyst carriers in the CVD method in the fabrication of Mg/CNT composite. Although this method overcomes issues of CNT dispersion, it can be a complex fabrication route that requires precise temperature control during the in-situ CVD process. The melting

temperatures of most metals lie in the regime of 500-1000 ˚C; metal catalysts can react with the metal surrounding at these elevated temperatures [114]. Great care must be taken to insure that during the reduction of catalyst precursors oxidation of metal powders does not occur. Formation of tough metal-oxides can severely degrade mechanical performances of CNT/MMCs.

Molecular Level Mixing

In the fabrication of Cu/CNT composites several works reviewed in this study employed a novel process called "molecular-level mixing." In this process Cu ions are attached on a molecular scale to CNT surfaces via functional groups [118-119]. In this method individual CNTs are homogeneously implanted within Cu powders [118-120]. This novel process for fabricating Cu/CNT composites first involves dispersing individual CNTs in aqueous environment via functionalization [119]. Once CNTs are functionalized, electro-repulsive energies are large enough to overcome Van Der Waal's energies binding CNTs together [119]. Cu ions are then provided to the CNT solution from an ion rich source such as copper acetate. Subsequent ultrasonication of the suspension assists the deposition of Cu ions and their bonding to functional groups on CNT surfaces [119]. The remaining steps involve calcination and reduction processes to obtain Cu/CNT composite powders [119]. Molecular level mixing homogeneously disperses intact CNTs within the Cu matrix [118-120]. In a study carried out by Cha et al. [119] it was revealed through transmission electron microscopy that CNTs formed a network within Cu grains, with Cu grains showing a lowered dislocation density.

MMC/CNT composite powder mixtures prepared using this technique are Cu/CNT [118-120].

Mechanical Stirring, Hand Grinding/Mixing

In the fabrication of CNT/MMCs some researchers chose to disperse CNTs following more traditional/conventional methods. Some of these processes are but not limited to: hand mixing, hand grinding, and magnetic stirring. Hang [121] and Feng [122] chose conventional hand grinding techniques (using a mortar and pestle) in the fabrication of Al/CNT and Ag/CNT composites respectively. Feng et al. reported CNT clustering above 10 vol % CNT addition. In both instances a type of process control agent is typically used to help avoid oxidation of metal powders during the grinding process. Kuzumaki et al. [123] stirred Al powder with CNTs in ethanol, however, this group also reported CNT clustering in the 5-10 vol % range. MMC/CNT composite powder mixtures prepared using this technique are Al/CNT [121,123] and Ag/CNT [122].

Novel CNT Dispersion Techniques

Some of the studies in this review chose to develop unique CNT dispersal mechanisms. Some of these novel dispersal mechanisms are improvisations of ones previously outlined [122,124-126] or are original developments [127-128]. Kurita et al. [124] used hetero-agglomeration principals to prepare Al/MWCNT- MMC with uniform MWCNT dispersion. In this process pristine MWCNTs are first dispersed in mild acid via ultrasonication and to attach oxygen functional groups. Al powders along with treated MWCNTs are than further mixed and ultrasonicated in ethanol. Due to the hetero-

agglomeration of oppositely charged Al particles and MWCNTs, Al particles coated with individual MWCNTs were obtained. Jiang et al. [125] developed a "flake powder metallurgy" to obtain uniform CNT distributions in Al/CNT composites. In this process spherically shaped Al powders are energetically milled to obtain nano-flakes with high surface areas and subsequently functionalized in polyvinyl alcohol. These steps aid in accommodating the 1-D nature of CNTs and making Al particles more compatible with carboxyl functionalized MWCNTs. In a study carried out by Feng et al. [122] CNTs are surface modified and dispersed via oxidization treatments in sulfuric/nitric acids. Treated CNTs are then hand ground with Ag powders. While Trinh et al. [126] used a chemical functionalization technique in conjunction with mechanical milling to disperse CNTs among CuSn powders. Kwon et al. [127] explored the feasibility of using natural rubber in a "nano-scale dispersion" process to homogeneously disperse individual CNTs among Al powder. However, this process did show condensation of CNTs on Al powder surfaces as revealed by scanning electron micrographs [127]. Cao et al. [128] proposed the in-situ synthesis of CNTs in Al powders via catalytic pyrolysis methods as a means to achieve homogeneous dispersion of undamaged CNTs. In this study, individual CNTs were homogeneously grown and decorated on surfaces of Al nano-flake powder.

4.5 Importance of CNT/Metal Interface

To unlock the full potential of CNTs as mechanical reinforcement phase in metal matrices a clear understanding of interfacial reactions between the metal matrix and CNTs is necessary. Good interfacial reactions between matrix and CNT provide for an

effective stress transfer medium and enhancement of composite performance. CNTs which consist of rolled layers of graphitic basal planes are thermodynamically stable in most metals at elevated temperatures [129]. However, most CNTs are produced via chemical vapor deposition (CVD) techniques as a means to produce them cheaply and in bulk. Unlike arc-discharge method for producing CNTs, CVD produces CNTs with defects along their outer walls. Graphitic prism planes, as these 'defects' are commonly referred to, are exposed to the surrounding metal matrix [129]. During CVD processes amorphous carbon layers have also been reported to form on outer walls of CNTs. In Al/C composites a typical precipitate that forms during thermal processing is aluminum carbide (Al_4C_3) due to a relatively low energy of formation [129]. Graphitic prism planes have a lower surface free energy than basal planes. As a result, Al_4C_3 tends to form at graphitic prism planes along CNT surfaces and ends [129]. Al4C3 has also been reported to form on amorphous carbon layers [129]. In their study, Ci et al. reported the formation of nano sized Al4C3 particles is most likely to occur at defect sites, and on amorphous carbon layers [89]. The authors of this study reported a high significance to the formation of Al_4C_3 at CNT ends, which tightly adheres the CNTs to the Al matrix [129]. Interestingly, Ci et al. also reported that for poorly graphitized CNTs carbide formation completely destroys the CNT structure leaving nano-sized Al_4C_3 dispersoids which may result in unfavorable mechanical properties of the composite. For Cu/CNT composites, effective transition layers are typically formed via deposition techniques (molecular-level mixing, functionalization, and nickel/copper plating) where metal atoms are deposited on CNTs that have been functionalized. Typical oxygen containing functional groups are oxygen (-O), hydroxyl (-OH), and carboxyl (-COOH) [104-106, 118-120]. Oxygen in

these CNT surface functional groups form bonds with Cu atoms either directly or via electron exchange forming “glue” between the CNT and Cu interfaces [130]. For Mg/CNT composites, the bonding between CNT/Mg is expected to be purely mechanical, as no chemical reaction takes place according to the C-Mg phase diagram [89]. However, by reinforcing Mg/Al alloys with CNTs, references [64-65, 92] reported the formation of ternary carbides (Al_2MgC_2) during processing which provided for an effective load transfer medium. Reference [65] reported needle-like protrusions of Al_2MgC_2 protruding form Mg/CNT interfaces, which can also promote mechanical adhesion. For Ti/CNT composites the formation of titanium carbide (TiC) during thermal processing is reported to act as the effective stress transfer medium [131].

4.6 Strengthening Mechanisms

Taking into consideration the physical properties and structure of CNTs, there exist various strengthening mechanisms which may act synergistically to enhance material properties of CNT/MMCs. Several strengthening mechanisms are considered for CNT/MMCs and discussed briefly below: Orowan looping (dispersion strengthening), shear lag theory, thermal mismatch, and grain refinement.

Orowan Looping/Dispersion Strengthening

It is reasonable to suspect that CNTs play a role in inhibiting dislocation motion when used as reinforcement phase in polycrystalline metals. In this strengthening phenomena precipitates or as in the case of MMCs, nano meter sized objects act as pinning points for dislocations or lead to bowing of dislocations between CNTs. This bowing effect can lead to the formation of dislocation loops and or back stresses which inhibit further dislocation

motion. As dislocations subsequently pass dislocation loops, dense tangles of dislocations can form leading to a high rate

of strain hardening. This phenomena acts to drive up the yield stress of the matrix, which leads to a strengthening effect. The Orowan stress required to drive a dislocation past a nanometer inclusion such as a CNT [99],

$$\Delta\tau = C * \frac{\mu b A^{\frac{1}{2}}}{r} * \ln(\frac{2r}{r_o}) \quad (4\text{-}1)$$

where *A* is the CNT volume fraction, *r* is the volume equivalent radius for CNT, r_o is the core radius of dislocation, *b* is Burgers vector, μ is the modulus of rigidity of the matrix.

Shear Lag Theory

For ductile metal matrices reinforced with rigid high aspect ratio cylindrical inclusions, knowledge of complex stress/strain states in constituents is essential in predicting composite strength. The shear lag theory takes into account interfacial shear stresses as a mode of stress transfer between CNT/metal interfaces. This model assumes good bonding at the metal/fiber interface for effective load transfer. However, it is commonly known that due to the irreconcilable differences in surface tension of CNTs and metals (~200 mN/m for CNTs, ~800 mN/m for metals) the two materials exhibit poor wettability [99]. This is of great concern for most metal/CNT composites. From shear lag theory the Young's modulus of fiber reinforced composite [78],

$$E_c = fE_f\left(1 - \frac{\tanh(ns)}{ns}\right) + (1-f)E_m\ ,\ n = \sqrt{\frac{2E_m}{E_f(1+\gamma_m)\ln(\frac{1}{f})}} \quad (4\text{-}2)$$

where n is a dimensionless parameter, γ_m is the Poisson's ration of the matrix, f is the volume fraction of reinforcement, and s is the aspect ratio of fiber. E_c, E_f, and Em are the Youngs moduli of the composite, fiber, and matrix. In their work, Kashayap et al. used shear lag model with experimental data of Al/MWCNT composite to estimate Young's modulus of a MWCNT (E_f) to within a couple % of the theoretically excepted value of 1 TPa [78].

Thermal Mismatch

The coefficient of thermal expansion (CTE) for most metals is $8*10^{-6}/^{\circ}C$ - $26*10^{-6}/^{\circ}C$, for CNTs it is considered to be equivalent to graphene ~ $1*10^{-6}/^{\circ}C$. Thus, for CNT/metal composites there exists a CTE mismatch between constituents which upon during thermal processing lead to prismatic punching of dislocations at the CNT/metal interface. This prismatic punching leads to an increase in dislocation density at CNT/metal interface and eventual work hardening of the metal matrix which in turn leads to strengthening of CNT/MMCs. The incremental strength [59],

$$\Delta\sigma=\alpha\mu\rho^{1/2}b, \qquad \rho=\frac{10A\epsilon}{bt(1-A)} \tag{4-3}$$

where A is the reinforcement volume fraction, ϵ is the thermal strain, μ is the modulus of rigidity, ρ is the dislocation density, b is Burger's vector, and t is the dimension of reinforcement.

Grain Size Refinement

In solid state powder metallurgy, thermal processing of CNTs with metals occurs during the sintering stage where diffusion processes act to weld adjacent metal granules

together creating a continuous matrix with CNT inclusions. During thermal processing of these CNT/MMCs, metal matrix region can experience grain growth which can be hindered by CNTs positioned at grain boundaries. It has been shown by Wilson et al. that as CNT concentration increased there exhibited a corresponding monotonic decrease in average grain size of Ti/SWCNT composite. Since strengthening is a function of grain size (Hall-Petch relation) in metals,

$$\sigma_y = \sigma_\infty + kd^{-1/2} \quad (4\text{-}4)$$

where d is grain size, σ_∞ and k are constants. An increase of CNTs at grain boundaries restricts grain growth, which leads to smaller grains and hence less motion of dislocation movement. This physical phenomenon strengthens the composite.

4.7 Mechanical Properties of Various CNT/MMC Systems

The state and quality of CNT dispersion in metal matrices has direct implications on the mechanical performances of CNT/MMCs. Of equal importance are interfacial bonding between CNT and matrix, PM process parameters, and CNT strengthening mechanisms. In the following section mechanical properties of various CNT/MMC systems are reported with emphasis on the corresponding CNT dispersal mechanism used and state/quality of CNT suspension in metal matrix. Also elucidated are CNT/metal interfacial bonding and strengthening mechanisms.

Aluminum/CNT and Aluminum-Alloy/CNT Composites

Ref.	CNT Type	CNT vol%/ wt %	CNT-geometry: Length (l)- µm Diameter (d)- nm	Metal powder	Powder size	CNT dispersal mechanism	Consolidation procedure	Composite material properties	Reference material properties	% increase material properties
[61]	MWCNT	0.5 wt%	l: 5-15 d: 60-100	Al	5 µm	Wet process, Mechanical milling	Spark plasma sintering/ hot extrusion	Wet Process- TS: 165 MPa Hv: 48 Mechanical Milling- TS: 206 MPa Hv: 58	Wet Process- TS*: 132 MPa Hv*: 40 Mechanical Milling- TS*: 166 MPa Hv*: 48	Wet Process- TS: 25% Hv: 20% Mechanical Milling- TS: 24% Hv: 21%
[62]	MWCNTs	1.22 vol%	l: 1.5 d: 9.5	Al - A6063	-	Wet process	Spark plasma sintering/ hot extrusion	Hv0.05: 55.2 YS: +5.6 MPa TS: +11.5 MPa		
[68]	MWCNT	2 wt%	l: 3-4 d: 140	Al	75 µm	Mechanical milling	-	Particle size increases upon long milling times		
[69]	MWCNT	4.5 vol%	l: 5 d: 2	Al	< 150 µm	Mechanical milling	Hot Rolled	YS: Δ100 MPa over reference material		
[70]	SWCNT	3.5 vol %	l: 5 d: 2	Al	< 150 µm	Mechanical milling	Cold compaction/ hot extrusion	YS: 500 MPa	YS*: 200 MPa	YS:150%
[71]	MWCNT	15 vol%	l: 30 d: 20	Al	63 µm	Mechanical milling	Hot-pressing	Hv20: 260.3 Hv0.02: 258.1	Hv20*: 36.8 Hv0.02*: 33.2	Hv20: 607% Hv0.02: 677%
[72]	MWCNT	2.5 wt%	l: 10-20 d: 30-50	Al	45 µm	Mechanical milling	Spark plasma extrusion	Hv5: 99.1 CYS: 415.3 MPa	Hv5*: 74.7 CYS*: 373.8 MPa	Hv5: 33% CYS: 11%
[73]	MWCNT	2.5 wt%	l: 3-4 d: 140	Al	75 µm	Mechanical milling	-	Mechanical milling time and CNT content can effect Composite particle size/morphology		

[74]	MWCNT	1.75 wt%	l: 10 d: 40-100	Al	325 mesh	Mechanical milling	Cold compaction/ hot extrusion	YS: 189 MPa TS: 243 MPa Hv: 73	YS*: 105 MPa TS*: 228 MPa Hv*: 68	YS: 80% TS: 7% Hv: 7%
[75]	MWCNT	2 wt%	l: 10-20 d: 30-50	Al	10-40 µm	Mechanical mixing	Spark plasma sintering	Hv: 88 Nano hardnes*: 1.42 GPa CYS: 280 MPa E: 84 GPa	Hv*: 36 Nano hardness*: 0.95 GPa CYS*: 80 MPa E*: 65 GPa	Hv: 144% Nano hardnes*: 49% CYS: 250% E: 29%
[76]	MWCNT	0.5 wt%	l: 3-4 d: 140	Al	75 µm	Mechanical milling	Hot Rolling	TS: ~ 140 MPa, YS: ~ 100 MPa, E: ~ 60 GPa		TS: 10% YS: 42.9% E: 20 %
[77]	SWCNT	3.5 vol%	l: 5 d: 2	Al	<150 µm	Mechanical milling	Pre (cold) compaction in Cu container/ hot extrusion	CYS: ~ 500 MPa YS: ~450 MPa	CYS*: ~ 200 MPa YS*: ~200 MPa	CYS: 150% YS: 125%
[78]	MWCNT	1.5 wt%	-	Al	-	Mechanical milling	Cold Compaction/ hot extrusion	E: 82.77 GPa, indirectly calculated using shear lag theory	E*: 70 GPa	E: 18%
[79]	MWCNT	0,0.5,1,2,3 ,4,5 wt%	l: - d: 80	Al-2024	Al -200 mesh, Mg -325 mesh, Cu -325 mesh, Mn -325 mesh, Ti -325 mesh, Zn -100 mesh	Mechanical milling	-	-Smallest particle size was obtained after 20 h milling time for all CNT contents. Different response for a given milling time was observed for all CNT concentrations		
[80]	MWCNT	5wt%	l: - d: 80	Al-2024	-	Mechanical milling	Cold compaction	Hv: 290.9	Hv*: ~75	Hv: 287%

[81] [82] [83]	MWCNT	1.0 wt%	l: - d: 20	Al-2024	50 µm	Ultrasonication/ mechanical milling	Cold compaction/ Hot extrusion	E: 102.2 GPa TS: 521.7 MPa Hv: 136 MPa	E*: 59.9 GPa TS*: 335.5 MPa Hv*: 94.2 MPa	E: 71% TS: 55% Hv: 44%
[84]	MWCNT	1 wt%	l: 5-20 d: 20-50	Al-6061	13.8 µm	Mechanical milling	Semi-solid powder processing	Hv: 83.3	Hv: ~45	Hv: 85%
[98]	SWCNT, DWCNT, MWCNT	2.0 wt%	l: 10,10,10 d: 1-2,5-20,1-2	Al	30 µm	Ultrasonication/ Mechanical milling	Plasma activated sintering	DWCNT Hv: ~78	Hv*: ~ 30	Hv: 160%
[99]	MWCNT, SWCNT	2 vol%	-	Al	200 mesh	Ultrasonication/ Mechanical milling	Cold compaction/ hot extrusion	MWCNT- E: 85.85 GPa YS: 99 MPa TS: 138 MPa SWCNT- E: 79.3 GPa YS 90.8 MPa TS: 134 MPa	MWCNT- E***: 87 GPa YS***: 197 MPa TS***: 101 MPa SWCNT- E***: 88 GPa YS*** 636 MPa TS***: 227 MPa	MWCNT- E:-1.75% YS: -50% TS: 36.5 % SWCNT- E: -10.25% YS: -85.7% TS: -41.1%
[100]	MWCNT	0.75 wt%	l: 10 d: <100	Al	325 mesh	Ultrasonication/ Mechanical milling	Cold compaction	YS: 23 MPa TS: 33 MPa Hv: 77	YS*: 6 MPa TS*: 9 MPa Hv*: 30	YS: 283% TS: 266% Hv: 156%
[101]	MWCNT	2 wt%	l: few ten of µm's d: 20-30	Al	< 25 µm	Ultrasonication/ Mechanical milling	Cold compaction	Microhardness: 64 kg/mm^2	Microhardness: 31 kg/mm^2	Microhardn ess: 106%
[102]	MWCNT	2wt%	l: 5 d: 20	Al	30 µm	Mechancal stirring-ultrasonication/ mechanical milling	Plasma activated sintering	Hv: 182.8	Hv*: 60.1	Hv: 204%

[103]	MWCNT	1.5 wt%	l: 3-4 d: 140	Al	25 µm	Ultrasonication/ Mechanical milling	Cold compaction	Micro hardness: 300 kg/mm^2 CYS: 270 MPa FS: 450 MPa	-	
[107]	SWCNT	5 wt%	-	Al	0.5 µm	Ultrasonication	Cold compaction/ hot compaction	Micro-hardness: 2.89 GPa	Micro-hardness*: 1.62 GPa	Micro-hardness: 78%
[108]	MWCNT	1.5 wt%	l: 1-10 d: 10-15	AA5083 Al	25 µm	Ultrasonication	Hot isostatic pressing/ extrusion	E: 76 GPa YS: 328 MPa TS: 427 MPa Hv0.5: 133	E*: 73.7 GPa YS*: 239 MPa TS*: 350 MPa Hv0.5*: 111	E: 3 % YS: 37% TS: 22% Hv0.5: 19%
[115]	MWCNT	5 wt%	l: 1.5-2.5 d: 5-25	Al	≤ 5 µm	Insitu chemical vapor deposition on Al powders	Cold compaction/cold compaction after sintering	Hardness: 0.65 GPa TS: 398 MPa	Hardness*: 0.15 GPa TS*: 140 MPa	Hardness: 333% TS: 184%
[116]	MWCNT	2.5 wt%	l: 2-5 d: 10	Al	50-80 µm	In-situ chemical vapor deposition in Al powders/ mechanical milling	Cold compaction/ hot extrusion	YS: 276 MPa TS: 160 MPa	YS*: 63 MPa TS*: 123 MPa	YS: 338% TS: 30%
[117]	MWCNT	1.5 wt%	l: 1-2 d: 10-20	Al	1.5 µm	In-situ chemical vapor deposition in Al powder	Cold compaction/ hot extrusion	CYS: 222 MPa	CYS: ~100 MPa	CYS: 122%
[121]	MWCNT	2 wt%	-	Al	70 µm	Hand Mixing	Cold compaction	Hv: 54.0	Hv: 29.9	Hv: 80%
[123]	MWCNT	10 vol%	-	Al	40 µm	Mechanical stirring	Hot pressing/ extrusion	TS: ~ 80 MPa	TS*: ~ 40 MPa	TS: 100%

[124]	MWCNT	1 vol%	l: 10 d: 50	Al	6 µm	Hetero-agglomeration / ultrasonication	Spark plasma sintering/ hot extrusion	TS: 160 MPa	TS*: 115 MPa	TS: 39%
[125]	MWCNT	2 vol%	l: 2.5 d: 50	Al	10 µm	Mechanical milling/Surface modification of Al nano-flake/slurry blending	Cold compaction/ hot extrusion	E: 89 GPa TS: 435 Mpa	E*: 70 GPa TS*: ~255 Mpa	E: 27% TS: 70%
[127]	MWCNT	5 vol%	l: 15-50 d: 20	Al	14.82 µm	Nano Scale Dispersion	Spark plasma sintering/ hot extrusion	Hv: 32 TS: 194 MPa	Hv*: 22 TS*: 85 MPa	Hv: 45 % TS: 128 %
[133]	MWCNT	0.5 wt%	l: 20-30 d: 20-30	Al	325 mesh	Ultrasonication/ magnetic stirring	Spark Plasma Sintering	Hv1: 38 TS: 116 MPa	Hv1*: 33 TS*: 81 MPa	Hv1: 15% TS: 43%
[134]	MWCNT	15 vol%	l: 30 d: 20	Al	63 µm	Mechanical milling	Hot pressing	Hv20: 260.3	Hv20: 36.8	Hv20: 607%

Table 4-1. *Denotes comparison to unreinforced metal powders, ** comparison to bulk metal, ***comparison to theoretical value

In studies performed by Yang [116] and Perez-Bustamante [100], yield stress (YS) of Al/CNT composites was improved remarkably with 2.5 and 0.75 wt% MWCNT addition. Experimental YS values reported by these research teams are 276 MPa [116] and 23 MPa [100], which show 338 % and 283% improvements over unreinforced Al powders. In the former study it was reported that in-situ CVD process combined with a short ball milling time led to individual MWCNTs being homogeneously dispersed on powder surfaces as well as impregnating in the Al matrix [116]. It was also reported in their study the CNT dispersal route along with a hot extrusion step (post consolidation) led to good interface bonding between Al matrix and MWCNTs [116]. Perez-Bustamante et al. [100] reported that the formation of an amorphous transition layer (formed between Al and CNT) and the thermal mismatch during sintering both increased adhesion between CNTs and Al matrix, thus increasing strength. The smallest improvement in YS was reported by Esawi et al. [76] to be 42.9% over unreinforced Al powder for 0.5 wt% MWCNT addition. To disperse MWCNTs Esawi et al. used two different types of mechanical mills: planetary and vibrational. It was found that higher rotational speeds obtained by the planetary ball mill (300 rpm compared to 46 rpm for vibrational mill) led to better MWCNT dispersions. CNT clustering was however reported for MWCNT additions above 1 wt%. George et al. [99] used ultrasonication in conjunction with mechanical milling to produce SWCNT/ and MWCNT/MMCs with YS that fell considerably below theoretically predicted values. The strengthening mechanism considered in this study was believed to be a synergistic effect of Orowan looping and thermal mismatch between CNTs and Al matrix. However, no evidence was found for Orowan strengthening mechanism during

TEM analysis. For aluminum-alloy CNT composites no appreciable improvements in YS were reported. To prepare Al_{A5083}/1.5 wt%-MWCNT and Al_{A6063}/1.22 vol%-MWCNT composites the research teams in these studies resorted to mechanical milling [108] and wet-process [62] to disperse MWCNTs. For AlA5083/1.5wt%-MWCNT fabricated by Stein et al. [108] CNT clusters tens of μm in size were reported for small milling times and speeds. Only after relatively long milling times at 600 rpm were individual CNTs found to be adequately dispersed and imbedded in Al_{A5083} powder. The authors of this study proposed CNT/matrix load transfer and Orowan strengthening to be the responsible agents for improvements in YS.

For the compressive yield stress (CYS) researchers reported a wide range of values using a variety of CNT dispersal routes and process methods [72, 75, 77, 103, 117, 128]. Yadav et al. reported a 250% increase in CYS of Al/2wt%-MWCNT composite over unreinforced Al powder [75]. Processing of Al/MWCNT composite mixture took place in a high speed vibration mill in the presence of poly acrylic acid dispersion agent [75]. The authors of this report attribute this

increase in CYS to homogenous MWCNT distribution in the starting powder, which is important to gain the full advantage of SPS processing method [75]. The authors of this study also believe dispersion strengthening phenomena to be a responsible strengthening agent [75]. References [77, 117] also reported appreciable increased (150% and 122%) in CYS, these works employed in-situ CVD method and mechanical milling as their prospective CNT dispersal mechanisms. The lowest improvements in CYS were reported by Morsi et al. who used conventional ball milling techniques to disperse 2.5wt% MWCNTs in pristine Al powder [72]. The authors of this study could not conclusively

attribute improvements in strength to strengthening mechanisms discussed in literature (thermal mismatch, Orowan looping, shear lag theory); but instead propose the likelihood of strengthening mechanisms associated with metal/CNT composites that have yet to discovered by researchers.

In the case of Young's Modulus (E) of Al/CNT composites, no substantial gains were reported above 30% of the reference material [78, 75-76, 78, 125]. Yadav et al. [45] increased E by 29% in the fabrication of Al/2wt% -MWCNT composite by conventional vibration milling route. In their study, the authors were unable to delineate dispersion strengthening and grain boundary strengthening as the responsible strengthening agent for Al/MWCNT composite. The authors of this study did not report finding any interfacial phase between MWCNTs and Al matrix as a possible stress transfer medium. Kashyap et al. [48] reported the lowest improvement in E, reporting an 18% improvement over unreinforced Al powder for 1.5 wt% CNT addition. Although quality or state of CNT dispersion was not elucidated in their work, it shed light on possible strengthening mechanism of MWCNTs in Al matrix [78]. In their work, experimental value for E of Al/2wt%-MWCNT was determined. With this value Young's Modulus of an individual MWCNT was back calculated using "shear lag model." This yielded a value of 0.887 TPa, which is close to the theoretically accepted value of 0.9 TPa [75] for an individual tube. For aluminum alloy/CNT composites only one research group reported fairly substantial gains in E [81-83]. Deng et. al [81] reported a 71% increase in E of Al_{2024}/1.0 wt%-MWCNT composite over unreinforced Al powder by first ultrasonicating CNTs in alcohol then ball milling with Al powder . The authors of this study attributed uniform CNT dispersion on Al powder surfaces to differences of specific

surface area of powders and CNTs in alcohol. Good interfacial bonding as seen by SEM analysis, and “bridging" and "pulling out" observed at fracture surfaces indicates stress transfer by shearing between CNT and matrix. However, no interfacial reactions between Al and CNTs during sintering processes were observed in this study. Stein et al. reported relatively little improvement (3% over unreinforced Al powder) in E of Al_{A5083}/1.5 wt%-MWCNT composite [108]. The authors of this ruled out carbide formation as a possible stress transfer medium, as shown in XRD analysis and by low processing temperatures (350˚C).

Throughout the works reviewed in this study, tensile strength (TS) of Al/CNT composites was widely reported. Due to the statistical nature of these materials and the conditions they are processed under, a wide range of values are reported for TS [61,76, 99-100,115-116,123-125,127]. In their studies, He and Kown et al. employed in-situ CVD [115] and nano scale dispersion [127] to homogeneously disperse MWCNTs in Al matrix on a molecular scale. At 5 wt% and 5 vol% MWCNT addition, both groups reported 184% [115] and 128% [127] increases in TS respectively. He et al. showed through TEM analysis that MWCNTs encapsulated by Ni nano particles are dispersed homogeneously within Al matrix [115]. Kwon et al. reported good uniform dispersion of MWCNTs on Al particles. However, some regions existed where MWCNTs were not well dispersed [127]. Only He et al. reported the formation of aluminum carbide during processing conditions, as this provided an effective stress transfer medium between Al matrix and MWCNT [115]. Interestingly, the highest improvement in TS of Al/CNT composite were achieved by dispersing MWCNTs via ultrasonication and mechanical milling steps [100]. Perez-Bustamante et al. achieved 266% increase of Al/MWCNT composite with 0.75 wt%

MWCNT addition [100]. TEM analysis shows that MWCNTs are dispersed homogeneously in Al matrix, and the existence of an amorphous transition layer formed between Al and MWCNTs [100]. Thermal mismatch and hence increased mechanical adhesion are supposed to be the strengthening mechanism [100]. However, as reported in this study, the control Al powder samples did not undergo a milling procedure before consolidation. In two different studies carried out by Perez-Bustamante and Morsi et al. it was found that mechanical milling time and CNT content can affect composite particle size and morphology [100,73]. The lowest improvements in TS values for Al/CNT composites were reported in reference [76], which used mechanical milling as their primary CNT dispersal mechanism. Only 10% improvements in strength were reported for 0.5 wt% MWCNT addition [76]. Esawi et al. reported CNT clustering for loading percentages greater than 0.5 wt%, which lead to an increase in composite porosity and corresponding decrease in material properties [76]. Deng et al. reported 55% increase in TS of Al2024/1.0 wt% -MWCNT composite [81]. It was reported in their study that MWCNTs were homogeneously distributed on powder surfaces, which was attributed to the ultrasonication-mechanical milling process. FSEM analysis also indicated stress transfer by shearing between matrix and MWCNT as a possible strengthening mechanism. Fukuda et al. reported only an incremental improvement of +11.5 MPa in TS for 1.22 vol% MWCNT addition in Al_{A6063} matrix. This research team resorted to surfactant assisted wet-process to disperse MWCNTs with zwitterions [62]. It was reported that further aging of Al alloy composite resulted in Mg consumption around MWCNTs, which led to incomplete matrix strengthening and a decrease of -6.1 MPa in TS [62].

Hardness as it is well known, is not an intrinsic material property but is an empirical parameter determined experimentally, and through a scaling transformation is an indicator of a materials strength (resistance to plastic deformation). It is a relatively quick and reliable testing procedure to implement and generally considered non-destructive. The majority of researchers who investigated the material responses of Al/CNT composite systems in this review reported either nano, micro, or macro hardness results. As in the case of the material properties discussed above, a wide spectrum of hardness values are reported, which is reflective of state/quality of CNT dispersion and hardness testing procedures. It is important to note that indentation (hardness) testing is very sensitive to structural inhomogeneities and scale effects (arising from disparity between indenter size and powder particle size). The largest micro hardness results were reported by Kwon et al. [71] in the fabrication of Al/15vol%-MWCNT composite via mechanical milling process. For 20 and 0.02 kgf loads the authors recorded 607% and 677% improvements in Vickers hardness [71]. At such high volume percentages it can be reasonable to associate dramatic improvements in hardness to dispersion strengthening mechanism. However, the authors of this study attributed improvements in hardness to MWCNTs being embedded in the soft Al matrix and a finer composite average particle size achieved by mechanical milling

[71]. It was proposed in another study that during the ball milling procedure CNTs act as lubricants making for more energetic collisions which resulted in increase of particle fracturing (and hence decrease of average composite particle size) [115]. Also reported in this study was the formation of a nano-sized layer of aluminum carbide which resulted in an effective stress transfer medium [71]. Interestingly, Chunnian et al. compared two

different dispersal mechanisms (mechanical milling and in-situ CVD) and their effects on resultant material properties in the fabrication of Al/5wt%-MWCNT composite [115]. This study reported 103% and 333% increase in micro hardness through mechanical milling and in-situ CVD techniques respectively. Although the authors attribute the increase in strength to homogeneously dispersed CNTs (dispersion strengthening), it was found that the in-situ CVD method helped to further improve gains in hardness to 333% by improving interfacial strength and maintenance of CNT structure [115]. Three research teams were able to achieve >100% improvements in micro hardness (for MWCNT additions < 2 wt%) through a combination of ultrasonication and mechanical milling CNT dispersion techniques [100-102]. All three research teams reported homogenous distribution of CNTs [100-102], whereas, all but one reported amorphous transition layers being formed between Al and CNTs [100-101]. The lowest improvement in micro hardness was reported in reference [74], in this study was reported only a 7% gain in micro hardness. Although the authors reported good CNT dispersion and the precipitation of aluminum carbide (during processing), the thermo-mechanical (hot extrusion) treatment is thought to be responsible for low hardness of composite [74]. Nano indentation testing is important because the hardness is greatly influenced by features in a very small volume of test material. Unlike micro or macro indentation testing where the bulk material response of the CNT/MMC composite is recorded. In a study performed by Yadav et al., nano indentation results showed a 144% increase in nano hardness by 2wt%-MWCNT addition [75]. They believe this increase is indicative of the strengthening and stiffening effects of reinforcing the Al matrix with MWCNTs. For aluminum alloys reinforced with CNTs, researchers also reported a spectrum of

hardness results owing to the different conditions these composites were processed under [62,80-81,84,108]. A 287% increase in micro hardness was reported in reference [80], the authors of this study fabricated Al2024/5wt%-MWCNT composite via mechanical milling. In this study, XRD analysis revealed the formation of aluminum carbide (between CNT and Al) during thermal processing, and good mechanical bonds (identified by fractographies) to result in an effective stress transfer medium. Along with good CNT distribution, the authors considered Oorwan looping mechanism as the main strengthening agent [80]. The smallest improvement in micro hardness was reported by Stein et al. to be 19% for Al_{A5083}/1.5wt%-MWCNT composite fabricated via mechanical milling [108]. The authors of this study reported CNT clustering on Al_{A5083} powder surfaces which ultimately decreased the composites mechanical performance.

Copper/CNT and Copper-Alloy/CNT Composites

Ref.	CNT Type	CNT vol%/ wt %	CNT-geometry: Length (l)- µm Diameter (d)- nm	Metal powder	Powder size	CNT dispersal mechanism	Consolidation procedure	Composite material properties	Reference material properties	% increase material properties
[85]	MWCNT	3 vol%	l: 1-10 d: 5-20	Cu	< 45 µm	Mechanical milling	Cold compaction/high pressure torsion	Hv0.5: 2.31 GPa	Hv0.5*: 1.73 GPa	Hv0.5: 34%
[86]	MWCNT	10 vol%	l:- d:40	Cu	0.2-0.3 µm	Mechanical milling	Cold compaction/ spark plasma sintering/ cold rolling	TS: 281 MPa E: 137 GPa YS: 197 MPa	TS*: 175 MPa E: 70 GPa YS: 135 MPa	TS: 61% E: 96% YS: 46%
[87]	MWCNT	1 wt%	l:- d: -	Cu	0.5-1.5 µm	Mechanical Milling	Cold compaction/ high pressure torsion	YS: 1125 MPa E: 117 GPa	YS*: 73 MPa E*: 91 GPa	YS: 52% E: 29%
[88]	MWCNT	0.1 wt%	l: 0.5-2 d: 10-20	Cu	3 µm	Mechanical milling	Hot-press sintering	Hardness: HRB 83.5	Hardness*: HRB 35.0	Hardness: 139%
[104]	SWCNT	0.08 wt%	l:1 d:0.7-1.3	Cu	-	Ultrasonication/ nickel electroless plating	Hot Pressed	Displacement rate increased during small-punch creep tests. Improved tribological properties.		
[105]	SWCNT	0.5 vol %	l:- d: 20-40	Cu	10-15 µm	Ultrasonication/ nickel electroless plating	Hot pressing	Displacement rate increased during small-punch creep tests and rupture time was longer than that of pure Cu specimen		
[106]	MWCNTSWCNT	1-6 wt%	l:- d: -	Cu	1-5 µm	Ultrasonication/ nickel electroless plating /mechanical milling	Cold compaction/ hot extrusion	Hv0.05,Hv0.1, Hv0.2, Hv0.3, Hv0.5: Hardness improved linearly up to 4 wt% over monolithic Cu		

[109]	MWCNT	12 vol% 2 wt%	l: 2-10 d: 15-20	Cu	70 µm	Nickel electroless plating / mechanical milling	Cold compaction	Hardness: HRB 21.5	Hardness*: HRB 10.2	Hardness: 111%
[110]	MWCNT	2 wt%	l: - d: 30-50	CuSn	100-200 µm	Copper electroless plating / mechanical milling	Cold compaction	Hv0.1: 490 RCS: 318.3 MPa	Hv0.1*: 231 RCS*: 212.2 MPa	Hv0.1: 112% RCS: 50%
[118]	MWCNT	10 vol%	l:- d:-	Cu	-	Molecular level mixing	Spark plasma sintering	Hv: 110 E: 136 GPa YS: 485 MPa	Hv**: 61 E**: 81 GPa YS**: 242 MPa	Hv: 80% E: 68% YS: 100 %
[119]	MWCNT	10 vol%	l:- d:10-40	Cu	-	Functionalization/molecular level mixing	Spark plasma sintering	YS: 455 MPa	YS**: 227 MPa	YS: 100%
[120]	MWCNT	1 wt%	l:- d: 20-40	Cu	1.5 µm 4.2 µm	Modified molecular level mixing process	Cold compaction/ spark plasma sintering	1.5 µm: YS: 460 MPa 4.2 µm: YS: 360 MPa	1.5 µm: YS*: 195 MPa 4.2 µm: YS*: 150 MPa	1.5 µm: YS: 135% 4.2 µm: YS: 140%
[126]	MWCNT	0- 3 wt%	l: 50 d: 50	Cu	2-3 µm	Chemical functionalization/ mechanical milling	Cold compaction	Coefficient of friction decreases with increasing mass fraction of CNTs		

Table 2. *Denotes comparison to unreinforced metal powders, ** comparison to bulk metal, ***comparison to theoretical value

Kim et al. were able to enhance the YS of unreinforced Cu by 2.3 times (140% improvement) using 5vol% MWCNT addition, this was achieved through a modified molecular level mixing process [120]. Owing to the molecular level mixing process, TEM analysis revealed that CNTs are embedded in Cu grains with a strong interface existing between the constituents [120]. In their study, the authors concluded that strengthening arises from homogeneously dispersed CNTs within the Cu matrix, strong interfacial bonds, and the synergistic effects of grain size refinement [120]. In two separate studies, Lim and Cha et al. [118-119] achieved 100% improvements in YS over unreinforced Cu powder both by using molecular level mixing process to disperse MWCNTs. Both research groups reported that MWCNTs were homogeneously implanted within Cu powders and attribute remarkable strengthening due to high-load transfer efficiency caused by strong bonding between CNTs and metal ions during molecular level mixing process [118-119]. The lowest improvements in YS were reported by two research teams who resorted to

mechanical milling as their primary CNT dispersal mode [86,87]. In reference [86] Cu/10vol%-MWCNT composite exhibited 46% improvements in YS, where in reference [87] Cu/1wt%-MWCNT composite showed 52% improvement in YS over their unreinforced Cu counterparts. Ki et al. through SEM analysis showed characteristic dispersion of MWCNTs in Cu matrix; dispersed regions in pure matrix and regions void of MWCNTs [86]. Ki et al. also reported a two-step yielding behavior which was attributed to Cu matrix regions rich and void of CNTs. Li et al. reported homogeneous

MWCNT distribution on both a micro/macro scale and grain refinement (during processing) as likely strengthening agents [87].

For Cu/CNT composites only three research teams experimentally measured and reported Young's Modulus [86-87,118]. Almost a 100% gain in E (compared to monolithic Cu) was reported by Kim et al. for Cu/10vol%-MWCNT composite [86]. As previously mentioned above, these authors reported inhomogeneous CNT distribution which led to a two phase composite, improvements in E are attributed to the energetic processing route (mechanical milling-cold compaction-SPS-rolling) [86]. Whereas Li et al. reported only a 29% increase in stiffness dispersing 1wt% MWCNTs in Cu matrix via mechanical milling process [87].

Lim et al. reported 80% gain in micro hardness for Cu/10vol%-MWCNT composite fabricated via molecular level mixing CNT dispersal route [118]. Which again as mentioned above in the case of measured YS, improvements in micro hardness (strength) are attributed to high-load transfer efficiency caused by strong bonding between CNTs and metal ions during molecular level mixing process [118]. Jenei et al. [85] only reported a 34% gain in micro hardness for Cu/3vol%-MWCNT addition fabricated via mechanical milling CNT dispersal route. In their study, it was found that the energetic milling of composite powders coupled with a high pressure torsion consolidation step led to CNT damage and fragmentation. It was reported that these CNT fragments do not strengthen composite through dispersion strengthening, but rather indirectly via an increase in dislocation density. The authors of this study therefore attribute strengthening to Orowan Looping mechanism and increased dislocation density as brought about by process methods [85]. In their study, Patil et al. investigated the effects of indentation

load and CNT concentration on micro hardness results [106]. For both Cu/MWCNT and Cu/SWCNT composites it was found that hardness improved linearly up to 4 wt% CNT addition, this trend was also reported for increasing indentation load [106]. The authors of this report attribute this increase in hardness to good interfacial bonding, uniform CNT distribution, and increased relative density. However, an increase in CNT wt% led to CNT clustering, which in turn increased porosity (decreased hardness) of Cu/CNT composite [106]. For Cu-Sn/2wt%-MWCNT prepared via electroless deposition methods by Jun et al., a 112% increase in micro hardness is reported [110]. References [88,109] reported substantial improvements in Brinnell hardness results for Cu/MWCNT composites over their unreinforced counterparts. For Cu/12vol%-MWCNT and Cu/0.1wt%-MWCNT the reported improvements in macro hardness are 111% [109] and 139% [88] respectively. Reference [109] reported that CNTs are homogeneously dispersed and good bonding between Cu and in-situ Ni atoms, which was attributed to nickel electroless plating process. However, for a much lower CNT concentration of 0.1 wt%, reference [88] reported a 139% increase in hardness via simple mechanical milling process. The authors of this study reported a two-phase composite through SEM analysis: 1)one

of which is void of CNTs, this phase is formed due to shifting of nanotubes towards the grain boundaries. 2) CNT/Cu Phase. High interface due to reduced particle size of Cu during mechanical milling of composite powders, and more homogeneous distribution of CNTs surrounding the dendritic arms of Cu particles provide higher interfacial strength with higher relative densities [88]. This helps to distribute the external load from matrix to CNTs during indentation testing by good interfacial strength at CNT/matrix [88].

Improvements in tensile stress were reported to increase by 61% by introducing 10 vol% MWCNT to Cu matrix [86]. Jun et al. measured the radial crushing strength (RCS) of Cu-Sn/2wt%-MWCNT composite and reported a 50% improvement over unreinforced Cu-Sn powder [110]. The authors of this study reported CNT agglomeration when CNT > 1wt%. Also reported in this study, limited interfacial interaction of electroless plated CNTs and Cu matrix. However, copper layers on CNTs interact with Sn melt flow creating α-CuSn. This intermediary phase improved adhesion between Cu matrix and CNTs, providing for an effective load transfer medium [110]. Lim and Trinh et al. both reported improved tribological properties in the testing of Cu/SWCNT [105] and Cu/MWCNT [126] composites. Lim et al. reported CNT clustering on fracture surfaces. However, due to CNT-Nickel plating process, interfacial load strength greatly improved [105]. Whereas Trinh et al., on the other hand attributed tribological improvements to homogenous dispersion of CNTs [126].

Magnesium/CNT and Magnesium-Alloy/CNT Composites

Ref.	CNT Type	CNT vol%/ wt %	CNT-geometry: Length (l)- µm Diameter (d)- nm	Metal powder	Powder size	CNT dispersal mechanism	Consolidation procedure	Composite material properties	Reference material properties	% increase material properties
[63]	MWCNT	1.14 vol%	l: 0.5-1 d: 15	Mg, Mg AZ31B	117 µm, 82 µm	Wet process/ ultrasonication	Spark plasma sintering/ hot extrusion	Mg/CNT YS: 253 MPa Mg AZ31B/CNT YS: 355 MPa	Mg/CNT YS*: 178 MPa Mg AZ31B/CNT YS*: 279 MPa	Mg/CNT YS: 42% Mg AZ31B/CNT YS: 27%
[64]	MWCNT	1.10 vol%	l: 1.5 d: 950	Mg, Mg AZ61	-	Wet process	Spark plasma sintering/ hot extrusion	Mg/CNT YS: 253 MPa Hv: 42.4 Mg AZ61/CNT YS: Δ 11.05 MPa TS: Δ 7.86	Mg YS: 178 MPa Hv: 43.5 Mg AZ61 - -	Mg/CNT YS: 42% Hv: -3%
[65]	MWCNT	1.56 vol%	l: 8 d: 150	AZ61 Mg	-	Wet process	Spark plasma sintering/ hot extrusion	YS: Δ 28.5 MPa		
[89]	MWCNT	0.3 wt%	l: - d: 20	Mg	-	Mechanical milling	Cold compaction/ hot extrusion	Hardness: 44.1 HR15T YS: 146 MPa TS: 209 MPa WOF: 15.8 MJ/m^3	Hardness*: 45.0 HR15T YS*: 127 MPa TS*: 205 MPa WOF*: 18.9 MJ/m3	Hardness: -2% YS: 15% TS: 2% WOF: -16%

[90]	MWCNT	1 wt%	l: - d: 40-70	Mg	60-300 µm	Mechanical milling	Cold compaction/ hot extrusion	Hv0.25: 43 YS: 117 MPa TS: 153.8 MPa	Hv0.25*: 41 YS*: 111.9 MPa TS*: 155.8 MPa	Hv0.25: 5% YS: 5% TS: -1%
[91]	MWCNT	2 wt%	l: - d:-	Mg	38 µm	Mechanical milling	Hot pressing/ hot isostatic pressing	E: 38.6 GPa	E*: 35.1 GPa	E: 10%
[92]	MWCNT	0.3 wt%	l: - d: 40 -70	Mg	60-300 µm	Mechanical milling	Cold compaction/ hot extrusion	Hv0.25: 60 YS: 160 MPa CYS: 148 MPa TS: 227 MPa CS: 424 MPa	Hv0.25*: 40 YS*: 93 MPa CYS*: 91 MPa TS*: 153 MPa CS*: 239 MPa	Hv0.25: 50% YS: 72% CYS: 63% TS: 48% CS: 77%
[93]	MWCNT	1vol%	l: 5 d:-	AZ91D Mg	< 100 µm	Mechanical milling	Hot pressed/ hot extrusion	E: 49 GPa TS: 388 MPa PS: 295 MPa	E*: 40 GPa TS*: 315 MPa PS*: 232 MPa	E: 23 % TS: 23% PS: 27%
[96]	MWCNT	2.4 wt%	l: - d: -	Mg	-	In-situ synthesis of CNTs/ mechanical milling	Cold compaction/ hot extrusion	TS: 284.6 MPa	TS*: 219.8 MPa	TS: 29%

Table 4-3. *Denotes comparison to unreinforced metal powders, ** comparison to bulk metal, ***comparison to theoretical value

For Mg/CNT composites the largest gains in YS were reported by Habibi et al. for 0.3wt% MWCNT addition utilizing a mechanical milling dispersal route [92]. Due to the poor solubility of C in Mg, it is expected that the bonding between Mg and CNT is supposed to be purely mechanical [89]. In their study small amounts of Al powder and MWCNTs are milled in the presence of stearic acid, then marbles are added with the mixture milled further. Finally, pure Mg powder is blended with Al-CNT mixture in same mechanical alloying machine. This addition of Al served as a bonding agent improving interfacial strength between Mg and CNTs [92]. Habibi et al. also reported uniform distribution of CNTs; attributed to adequate blending parameters and high extrusion ratio in fabrication step. However, some CNT clustering was observed [92]. Two other research teams reported YS for Mg/CNT composites fabricated via mechanical milling and the same consolidation route (cold compaction-hot extrusion) with significantly lower improvements in YS [89-90]. In the fabrication of Mg/0.3wt%-MWCNT composite Goh et al. reported 15% improvements in YS [89], whereas Thakur et al. reported 5% improvements in YS for Mg/1.0wt%-MWCNT composite [90]. Goh et al. reported the presence of CNT clusters and a higher level of porosity than pure Mg powder processed under the same conditions [89]. Residual porosity in PM compacts can be known to reduce the load bearing area and hence reduce mechanical performances of these composite materials. Thakur et al. concluded that poor interfacial adhesion lead to ineffective load transfer between Mg and CNT [90]. For Mg-alloy/CNT composites, one research team in three different studies achieved relatively small gains in YS. In all of their studies, Kondah and Fukuda et al. incorporated surfactant assisted CNT dispersion mechanism in their fabrication process [63-65]. All three studies followed a CNT

dispersal route developed by a Japanese research team where a zwitterion class of surfactant is used to disperse CNT bundles through dipole/dipole electrostatic interactions [132]. Mg-alloy/CNT composites prepared using this method are Mg_{AZ31B}/1.14vol%-MWCNT [63], Mg_{AZ61}/1.10vol%-MWCNT [64], and Mg_{AZ61}/1.56vol%-MWCNT [65]. Their reported improvements in YS are Δ76.0 MPa, Δ11.05 MPa, and Δ28.5 MPa respectively. In reference [63] the surfactant assisted wet process was effective at dispersing individual MWCNTs (l=0.5-1 μm, d=15 nm) on powder surfaces. However, when the MWCNT morphology was changed (l=3-10 μm, d=40 nm) 1-2 micron bundles were observed on powder surfaces. Strong interaction between CNT with MgO thin layers due to solid state diffusion was effective for tensile load transfer, authors also reported good metallurgical bonding between

MWCNTs and matrix. In a subsequent study by this research group in the fabrication of Mg_{AZ61}/1.10vol%-MWCNT composite it was reported that during processing, naturally formed MgO was not sufficient to strengthen interfacial bonding between CNTs and Mg matrix [64]. Furthermore, during tensile testing, free CNTs provided by the destruction of interfacial MgO provided for in-situ lubrication inhibiting mechanical performance [64]. For Mg_{AZ61}/1.56vol%-MWCNT composite fabricated by Fukuda et al. it was determined that the formation of secondary ternary carbides (Al_2MgC_2) during thermal processing acted to strengthen the interface between matrix and CNT, but also reduced the strength of the composites [65]. As it was reported that at 1.56 vol% CNT addition, percent elongation decreased to 5.4% compared to 14.7% for pristine MgAZ61 [65].

For tensile strength the greatest improvements were reported in reference [92] for Mg/0.3wt%-MWCNT composite prepared using conventional mechanical milling technique. As in the case of YS, as noted above, the addition of small amounts of Al powder during the milling process greatly increased interfacial strength [92]. In an opposite trend Thakur et al. reported no apparent change in TS for Mg/1.0wt%-MWCNT composite also using mechanical milling methods in the composite fabrication process [90]. The authors attributed this to poor interfacial adhesion between CNTs and Mg matrix and thus ineffective load transfer. For Mg_{AZ91D}/1vol%-MWCNT composite fabricated via mechanical milling route 23% improvement in TS is reported [93]. In their work, electron micro-probe analysis revealed that CNTs are homogeneously dispersed in the vicinity of Mg grain boundaries. As a result, the strengthened near-surface of Mg domains by a coverage of CNTs is highly resistant to deformation, which contributed to enhancement of mechanical properties.

For the case of reported micro hardness measurements in this study, both research groups reported slight decreases in hardness compared to their Mg counterparts fabricated via same processes [64,89]. Goh et al. elucidated that the 2% decrease in hardness for Mg/0.3wt%-MWCNT composite is indicative that CNTs have little contribution to the prevention of localized plastic deformation of the Mg matrix [89]. Whereas the authors of reference [64] attributed the decrease in hardness to the in-situ lubrication effects of free CNTs in the Mg_{AZ61} matrix.

Habibi et al. reported significant improvements in tensile and compressive behavior of Mg/0.3wt%-MWCNT composite fabricated via mechanical milling route [92]. CYS and compressive stress (CS) of Mg/CNT composite in this study improved by 63% and

77% respectively. The authors of this study proposed the effect of three strengthening mechanisms (or synergetic coupling between the three) underpinning mechanical improvements: grain size refinement, Orowan dislocation strengthening, crystallographic texture, and geometrically necessary dislocations arising from thermo-elasto-plastic mismatch between CNTs and Mg matrix [92]. Goh et al. reported a decrease in work until fracture (WOF) of Mg/0.3wt%-MWCNT composite compared to pristine Mg powder processed under the same conditions [89]. A possible explanation could be due to the effect of CNT clustering which drives up porosity. It was reported in this study that up to 0.18 wt% CNT addition, WOF increased [89].

Silver/CNT Composites

Ref.	CNT Type	CNT vol%/ wt %	CNT-geometry: Length (l)- µm Diameter (d)- nm	Metal powder	Powder size	CNT dispersal mechanism	Consolidation procedure	Composite material properties	Reference material properties	% increase material properties
[82]	MWCNT	8,9 vol%	l: 30-50 d: 0.5-50	Ag	30	Oxidation treatment/ hand grinding	Cold compaction	Hv: 84 (9 vol% CNT addition) BS: 465 MPa (8 vol%)	Hv*: 66 BS*: 427 MPa	Hv: 27% BS: 9%

Table 4- 4. *Denotes comparison to unreinforced metal powders, ** comparison to bulk metal, ***comparison to theoretical value

Feng et al. increased the micro hardness and bend strength (BS) of Ag/9vol%-MWCNT composite fabricated via oxidation treatment-hand grinding CNT dispersal route [122]. The authors of this study reported homogenous distribution of CNTs for weight percentages less than 9 vol% CNT addition. Beyond this amount, CNT clustering was observed which led to a decrease in relative density and consequently micro hardness. It was reported that the only plausible strengthening mechanism had to be mechanical interlocking as CNTs and Ag were reported to exhibit an extremely weak interface as inferred by SEM micrographs of fractured surfaces.

Titanium/CNT Composites

Ref.	CNT Type	CNT vol%/ wt. %	CNT-geometry: Length (l)- µm Diameter (d)- nm	Metal powder	Powder size	CNT dispersal mechanism	Consolidation procedure	Composite material properties	Reference material properties	% increase material properties
[66]	MWCNT	0.35 wt%	l: 0.5-1 d: 20	Ti	30 µm	Wet process (surfactant)	Spark plasma sintering/ hot extrusion	Hv (0.05 N): 285 YS: 697 MPa TS: 754 MPa	Hv (0.05 N)*: 261 YS*: 591 MPa TS*: 472 MPa	Hv (0.05 N): 9% YS:18% TS: 60%
[67]	MWCNT	0.35 wt%	l: 0.5-1 d: 10	Ti	30 µm	Wet process (surfactant)	Spark plasma sintering/ hot extrusion	TS: 742 MPa YS: 592 MPa	TS*: 585 MPa YS*: 423 MPa	TS: 27% YS: 40%
[94]	MWCNT	-	l: 2-3 d: 5-50	Ti	-	Mechanical milling	Hot pressing	Hv: 1216 E: 198 GPa	Hv*: 221 E*: 120 GPa	Hv: 450% E: 65%
[95]	MWCNT	1.8 vol%	l: >1 d: 5-20	Ti	13.75 µm	Mechanical milling	Hot pressed	Hv10: 425 FS: 947 MPa	Hv10*: 270 FS*: 400 MPa	Hv10: 57% FS: 136%
[96]	MWCNT	0.4 wt%	l: 8 d: 150	Ti	150 µm	Mechanical milling	Spark plasma sintering/ hot extrusion	YS: 542.2 MPa	YS*: 386.7 MPa	YS: 40%
[111]	SWCNT	4.5 wt%	l: - d: 1.4	Ti	144 µm	Nickel electroless plating/ mechanical milling	Cold compaction/ induction melting method	Hv: 885	Hv*: 307	Hv: 188%

Table 4- 5. *Denotes comparison to unreinforced metal powders, ** comparison to bulk metal, ***comparison to theoretical value

In an attempt to increase YS of Titanium (Ti) matrix using MWCNTs three research teams achieved this goal utilizing a variety of CNT dispersal mechanisms. Interestingly two research teams reported the same improvements in YS (40%) using conventional mechanical milling techniques [96] and surfactant assisted dispersion [67]. Kondoh et al. investigated the dispersion of MWCNT bundles using a zwitterionic class of surfactant in the fabrication of Ti/MWCNT composites [66-67]. This is the same dispersal route developed by Fugetsu et al [132]. In their study it was revealed that CNTs are dispersed homogeneously as seen on powder and fracture surfaces, although some bundles existed [67]. It is believed that dispersion strengthening due to both CNTs and in-situ formed titanium carbide (TiC) are responsible agents for improvements in material properties. It was discovered through SEM and EDS analysis that TiC dispersoids formed during thermal processing exhibited two types of morphologies: elongated and spherical. Elongated TiC particles (<10 μm in length) were found to be aligned in the extrusion direction (due to gross plastic deformation of Ti matrix during extrusion) with good interfacial reaction with matrix [67]. On the other hand, spherical TiC particles indicate incompletely exfoliated CNT bundles [67]. Reference [96] likewise reports a 40% increase in YS following a more conventional mechanical milling route coupled with the same consolidation route reported by reference [67]. In their work it was determined that the in-situ formation of TiC dispersoids contributed to dispersion strengthening effects achieved by CNTs. In a subsequent study performed by Kondoh et al. [66] the same fabrication route was followed using CNTs of bigger diameter (20 nm as opposed to 10 nm) which resulted in just 18% improvements in YS. The same CNT weight percentages

were adhered to as well. The authors of this work [66] did not elucidate as to why there exists such a discrepancy in YS from previous work [67], but did, however, attribute improvements in YS to the same strengthening mechanisms. The authors of this study did suggest that another plausible strengthening mechanism could be that CNTs are effective at disrupting grain growth during thermal processing [66].

Kondoh et al. in their study showed 60% improvements in TS for Ti/0.35wt%-MWCNT [66]. These improvement in TS was attributed to the effectiveness of zwitterions in dispersing individual CNTs on powder surfaces and the strengthening mechanisms mentioned above [66]. Remarkably, Kondoh et al. showed that as CNT content increased and in spite of the strength improvements in TS, the elongation until failure remained constant 34-36%.

Particularly noteworthy are the relatively large improvements in micro hardness (450%) and Young's modulus (65%) of Ti/MWCNT composite fabricated by mechanical milling techniques by Kuzumaki et al. [94]. These considerable increases in strength are attributed to: dispersion strengthening, formation of tough TiC particles, and suppression of grain growth by CNTs.

4.8 Summary and Future Scope

MMC composites reinforced with CNTs have garnered much attention in the past decade, as witnessed by the increased number of publications on the subject. This can be attributed to the high commercial availability of CNTs with different morphologies, and varying levels of purity. Interest in PM as a viable fabrication route for CNT/MMCs has also drawn considerable interest among researchers due to its low power requirements,

relative ease of implementation, and capabilities to homogeneously disperse nano particles among metal powders. Most engineering metals which are used in a wide variety of transportation, building, and consumer industries can greatly benefit from enhanced mechanical properties. CNT/MMCs are also considered highly functional materials, not only can material properties be enhanced, but thermal and electrical properties simultaneously. Improvements in mechanical strength have been observed by addition of CNTs in Al-,Cu-, Mg-, Ag-, and Ti-based composites. However, due to their nano-scale structure and intrinsic electrical properties CNTs form large micron sized bundles which can be difficult to exfoliate into long lasting stable dispersions. It has been observed that material properties and performances of CNT/MMCs for large weight (volume) fractions of CNTs can be severely diminished due to the inclusion of CNT bundles (defects). As shown, numerous studies have tried to overcome this obstacle with varying levels of success. Some of the conventional (and non-conventional) routes taken by researchers to disperse CNTs are mechanical milling/mixing, hand grinding, wet-process (surfactant assisted dispersion), molecular-level mixing, electroless deposition (plating), ultrasonication, and in-situ CVD. Some researchers have also developed novel CNT dispersal techniques, improvised existing ones, or used combinations of different techniques to achieve stable dispersions.

Good interfacial bonding at the CNT/metal interface is crucial for effective stress transfer and hence strengthening of the composite. Due to the poor solubility of carbon in most metal systems, poor interfacial bonding has been reported. This leads to ineffective load transfer between the metal matrix and CNT, which acts to diminish bulk material properties of composite. It has been shown that for a given metal system with CNT

inclusions the material properties can vary and in some cases drastically. This can be due to quality of CNT/metal interface, effective load transfer, and CNT clustering. Furthermore, due to the above mentioned phenomena experimentally measured material properties fall below theoretical expectations.

There still remains many hurdles for researchers in the fabrication of CNT/MMCs. Some of these are the homogeneous dispersion of CNTs in metal matrices in the context of a bulk manufacturing process. CNT strengthening mechanisms are still not well understood and need to be studied in further detail. Improvements in material properties of composites due to CNT strengthening mechanisms need to be clearly delineated from other strengthening mechanisms related to the fabrication process. There needs to be a way to compare various CNT dispersal techniques through a "universal" parameter that takes into account state and quality of CNT dispersion in a matrix medium. The dependency of material properties on the formation of intermediary phases (such as carbides) at the CNT/metal interface during thermal processing need to be better understood. Process parameters and techniques need to be optimized to

achieve better CNT/metal interfaces, as this will lead to effective load transfer and improved utilization of the outstanding intrinsic material properties of CNTs themselves.

Characterization techniques need to be developed at different scales given the hierarchy of microstructures that exist in these composite materials. Importantly, a bridge between bulk material properties and material properties on the nano-scale needs to be developed and well understood, as there may not be a one-to-one correspondence between the two phenomena. Newer models must be developed that take into account CNT curvature, morphology, and bundling in order to adequately predict material

properties. Most importantly, CNT toxicity in humans, chemically-affected by a surrounding matrix, needs to be well understood.

Chapter 5

Optimizing powder metallurgy methods: Effects of carbon nanotube dispersal mechanisms on mechanical properties of aluminum/carbon nanotube composites

5.1 Introduction

The influence of carbon nanotube (CNT) dispersion techniques (surfactant-assisted dispersion, ultrasonication, and magnetic stirring) and surface functionalization of CNTs on mechanical properties of nanocomposites fabricated via powder metallurgy (PM) techniques is characterized. Functionalized multi-walled carbon nanotubes (f-MWCNTs) dispersed using a combination of techniques results in Al/f-MWCNT composites with excellent microstructure and enhanced mechanical properties. Non-functionalized CNTs dispersed using zwitterionic surfactants show good dispersion patterns on Al powder surfaces and results in composites with good strength and relative densities are also obtained. CNTs dispersed solely via shear mixing techniques resulted in highly embrittled composites with poor microstructure. Also discussed in this study is the usefulness of scanning electron microscopy (SEM) in conjunction with image analysis techniques in characterizing porosity in Al/CNT composites.

Aluminum and its alloys have been widely used as structural components in a wide variety of transportation industries such as aerospace design. This is due to its good strength to weight ratio, relative ease of formability, and its ability to withstand fatigue cracking due to stresses that occur during operation. However, as demand increases for

higher performance materials, aluminum and its alloys are inadequate in providing both good strength and high stiffness. The challenge of next-generation transportation design is to incorporate composite materials with strength and stiffness that exceed those of standard aluminum and its alloys while reducing weight. Additionally, with global oil prices increasing, the ability to increase structural integrity while increasing fuel efficiency has become highly desirable in a multitude of transportation industries. These demands have spurred the development of metal-matrix composites (MMCs) with constituents on the sub-micron to nano scale which offer the benefits of increased specific strength while maintaining percent elongation. Today, MMCs are used in various transportation industries [135-137]. Carbon nanotube /metal-matrix composites (CNT/MMCs) are unique as they can simultaneously exhibit enhanced mechanical, thermal, and/or electrical properties making them highly functional materials for diverse applications. These properties make CNT/MMCs highly desirable not only in transportation industries, but also electronics packaging applications. In electronics packaging industries, as electrical components become increasingly miniaturized, efficient heat dissipation becomes critical as to not affect performance.

Since their discovery in 1991 [138], CNTs have emerged as the "darlings" of the materials science disciplines and hold the promise to revolutionize composite industries with their extraordinary mechanical properties; tensile strengths of single walled carbon nanotubes (SWCNTs) as high as 22 GPa [139], and an average Young's modulus of 1.25 TPa [140]. These extraordinary mechanical properties make CNTs ideal candidates as reinforcement phases for a wide range of structural materials used in transportation design. Studies on the reinforcement of MMCs with CNTs have risen steadily

throughout the years due to the development of novel nanotube dispersal mechanisms and the success of PM as a viable fabrication route [141]. However, in a comprehensive review previously carried out by the authors of this study, research carried out in the fabrication (via PM methods) and mechanical characterization of CNT/MMCs within the past couple decades, a broad range of mechanical properties are reported using various nanotube dispersion techniques [142]. Furthermore, researchers report different mechanical properties using the same nanotube dispersion technique in reinforcing the same metal system [142]. Therefore, the authors of this study find it necessary to investigate the synergetic effect of CNT surface functionalization and combinations of nanotube dispersion techniques in optimizing mechanical performances and microstructure of Al/CNT nanocomposites.

Since their discovery, synthesis of CNTs has been achieved on an industrial scale. Researchers now have the ability to acquire CNTs of varying purity, geometry (aspect ratio, single/multi/double-walled), and electrical character from a multitude of manufacturers. However, commercially available CNTs are routinely purchased in powder form with individual tubes highly entangled. The nano-sized dimensions of CNTs (i.e., inner and outer diameters) cause them to have high surface areas [143]. Large surface areas possessing electrical charges result in the existence of Van der Waal forces/energies, which in turn cause the CNTs to aggregate. High aspect ratio along with high flexibility of CNTs, are other factors that cause CNTs to aggregate together into structures of varying morphologies and hierarchy (Fig.5-1). Such bundles may contain hundreds of close-packed SWCNTs that are tightly bound via Van der Waals attraction energies of approximately 500 eV/μm of SWCNT-SWCNT contact [144].

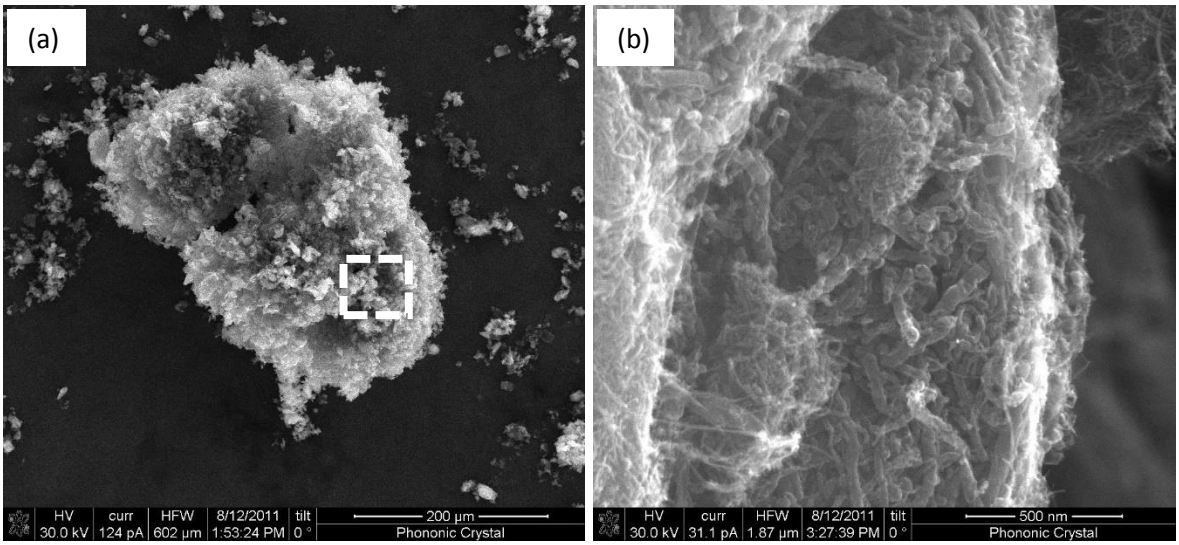

Figure 5-1: (a) SEM micrographs of MWCNT aggregates, (b) magnified image of marked rectangle in (a).

A diverse set of mechanical properties have been measured and reported by different research teams for the same metal composite materials incorporating CNTs [142]. Typical CNT dispersal mechanisms in the fabrication of CNT/MMCs via PM methods are: wet-process (surfactant assisted), mechanical milling, hand grinding, mechanical stirring, ultrasonication, electroless deposition (plating), in-situ chemical vapor deposition, molecular-level mixing, and other novel dispersal mechanisms [142]. Some researchers have explored the use of surfactants (wet-process) to exfoliate CNT bundles into individual tubes. With regards to their use in the dispersion of CNTs within a matrix medium, two important qualities of surfactants are useful. First is their ability to be adsorbed at hydrophobic or hydrophilic interfaces. Second is their ability to assemble themselves into 3D spherical structures called micelles. Absorbed surfactant molecules cause a repulsive barrier between CNTs hindering re-agglomeration into bundles in aqueous environments. During ultrasonication, mechanical energy is delivered to the

liquid medium via ultrasonic waves of high frequency (>20 kHz) which generate local shear stresses that are ultimately responsible for dispersing CNT aggregates [145]. In a proposed mechanism by Strano et al., shear stresses produced by cavitation are imparted to CNT bundles, which create a pulling force, "fraying" the ends of bundles [146]. This fraying effect acts to expose surfaces of individual CNTs to the surrounding medium, which become sites for the absorption of interfacial molecules from the surrounding medium, in the case of surfactant assisted dispersion. As the process continues, individual CNTs are slowly "unzipped" from bundles. CNT exfoliation states achieved by the ultrasonication process however are only temporary; therefore, some researchers find it necessary to ultrasonicate CNTs in the presence of a stabilizing agent.

In the present study, aluminum based composites containing MWCNTs, f-MWCNTs, and SWCNTs of various geometries are synthesized using a combination of and or standalone CNT dispersion techniques in an attempt to achieve homogeneous distribution of CNTs in the surrounding Al matrix. By implementing combinations of different CNT dispersion techniques, nanotube distribution patterns (individual tubes, CNT micro/nano bundles, CNT webs) will vary accordingly, which will have direct influence on composite microstructure and mechanical performances. Nanotube dispersion techniques used in this study are: surfactant assisted dispersion, ultrasonication, and magnetic stirring. Additionally, multi-walled CNTs used in this study are functionalized in order to increase their solubility in surfactant solutions. Composite powders are then uniaxialy compacted at room temperature followed by sintering in inert environment. To characterize mechanical performances of composites fabricated incorporating different

CNT dispersal techniques, indentation testing, x-ray microanalysis, SEM analysis, and image analysis techniques are used in this study.

5.2 Experimental procedure

The following materials listed in Table 5-1 were used in this study to fabricate Al/CNT composites.

Metal Powder:	***Aluminum (Al)***	***APS: ~ 45 µm***	
CNT Type	**Outer Diameter (nm)**	**Length (µm)**	**Descriptor**
Multi-walled	*10-20*	*10-30*	*$MWCNT_L$*
Functionalized Multi-walled	*10-20*	*10-30*	*$f\text{-}MWCNT_L$*
Multi-walled	*< 8*	*0.5-2*	*$MWCNT_S$*
Functionalized Multi-walled	*< 8*	*0.5-2*	*$f\text{-}MWCNT_S$*
Single-Walled	*1-4*	*5-30*	*SWCNT*

Table 5-1: Materials used in this study.

Al/$MWCNT_L$, Al/f-$MWCNT_L$, Al/$MWCNT_S$, Al/f-$MWCNT_S$ and Al/SWCNT composites were fabricated with 1 wt% CNT loading. Many applications involving MWCNTs require chemical modification of the nanotube surface to make them more amendable to physical manipulation using surfactants. In order to increase the solubility of MWCNTs in surfactant solutions carboxylic acid functional groups (-COOH) were grafted onto the nanotube surface (Fig.5-2).

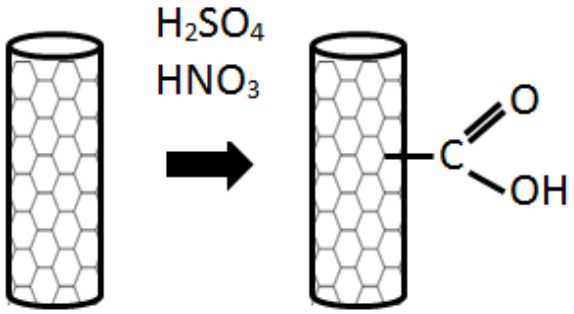

Figure 5-2: Schematic diagram of the functionalization process.

These oxygen containing functional groups promote hydrogen bonding between MWCNTs and hydrophobic tails of zwitterionic surfactants used in this study. An increase in absorption sites on outer walls of MWCNTs is hypothesized to improve dispersion efficiency of zwitterions used in this study.

Zwitterionic surfactant gels with CNTs are prepared according to a dispersal route outlined by Fugetsu et al. 3-(N,N-dimethylstearylammonio) propanesulfonate, a typical linear zwitterionic surfactant is characterized by a hydrophobic C18-alkyl tail, and a hydrophilic sulfonate/quaternary-ammonium head group [132]. Electrostatic interactions occurring at the hydrophilic head group (due to localized positive and negative charge) are the driving force in overcoming intertube Vander Walls forces which are responsible for CNT agglomerations [132]. With CNT/surfactant gels adequately prepared, colloidal suspensions are prepared by ultrasonicating gels in sodium iodide (NaI) solution using a VibraCell® ultrasonication machine. NaI solution acts to further stabilize CNT/surfactant molecules and prevent the re-agglomeration of individual CNTs into clusters. The ultrasonicator used in this study utilizes a 5mm micro-tip that is inserted directly into the aqueous CNT/surfactant suspension. The power setting of the

ultrasonicator was set at 260W, with sonication times of 0, 1, 3, and 5 minutes. Optimizing sonication times is critical to ascertain its effectiveness at further exfoliating CNT clusters and allowing individual free surfactants in colloidal suspensions to assemble on surfaces of CNTs. Al powders are then added to sonicated/unsonicated aqueous CNT suspensions and magnetically stirred for 1 hr forming smooth slurries. In order to remove excess moisture content and residual surfactants, the slurry is subjected to a two-step curing process: 1) excess moisture is first removed in a high temperature furnace at 100 ^{0}C for 1hr; 2) residual surfactants are then removed at 500 ^{0}C for 1 hr. Once residual surfactants have been removed, composite Al/CNT powders are uniaxially compressed using an Instron 4400R tensile/compression machine, at room temperature under 400 MPa of pressure in an A2- air hardened cylindrical die producing half-inch (12.7 mm) nominal diameter tablets.

Approximately 1 gram of Al/CNT composite powder was weighed to manufacture each tablet. Details of the compaction procedure were reported in a previous study by the authors [148]. Al/CNT tablets in the green state were then sintered in a high temperature furnace at 580°C for 2hr under Argon gas.

Processing routes for CNT types (Table 5-1) are listed in Table 5-2. Case M1C, M2C, S1C, where raw CNTs are first ultrasonicated in NaI solution for periods of 0, 1, 3, 5 minutes. CNT/NaI colloidal suspensions are then magnetically stirred with Al powders forming composite slurry which is then subjected to a one-step curing process for moisture removal.

Case	CNT Type	CNT Dispersal Route		
M1C	*$MWCNT_L$*		*Ultrasonication (0, 1, 3, 5 mn)→*	*Magnetic Stirring*
M1	*$MWCNT_L$*	*Surfactant Assisted→*	*Ultrasonication (0, 1, 3, 5 mn) →*	*Magnetic Stirring*
M1f	*f-$MWCNT_L$*	*Surfactant Assisted→*	*Ultrasonication (0, 1, 3, 5 mn) →*	*Magnetic Stirring*
M2C	*$MWCNT_S$*		*Ultrasonication (0, 1, 3, 5 mn) →*	*Magnetic Stirring*
M2	*$MWCNT_S$*	*Surfactant Assisted→*	*Ultrasonication (0, 1, 3, 5 mn) →*	*Magnetic Stirring*
M2f	*f-$MWCNT_S$*	*Surfactant Assisted→*	*Ultrasonication (0, 1, 3, 5 mn) →*	*Magnetic Stirring*
S1C	*SWCNT*		*Ultrasonication (0, 1, 3, 5 mn) →*	*Magnetic Stirring*
S1	*SWCNT*	*Surfactant Assisted→*	*Ultrasonication (0, 1, 3, 5 mn) →*	*Magnetic Stirring*

Table 5-2: Al/CNT fabrication routes used in this study.

Case M1, M2, S1, where viscous CNT gels are first prepared using surfactant assisted dispersion route developed by Fugetsu et al. and previously discussed. CNT gels prepared via wet-process and subjected to ultrasonication in NaI solution are then magnetically stirred with Al powders, and finally subjected to a two-step curing process as previously described [132]. For the case of M1f, M2f, absorption sites for surfactants are created on MWCNT outer walls using a functionalization procedure previously outlined. Functionalized CNT gels are then prepared using the same surfactant wet-process developed by Fugetsu et al., ultrasonicated in NaI solution, magnetically stirred with Al powders, and finally the composite slurry is subjected to two-step curing process for moisture and surfactant removal [132]. In this study, SWCNTs are not subjected to a

functionalization procedure, as previous studies have shown the process to be too aggressive completely destroying their tubular motif [143].

SEM analysis was carried out using a FEI Quanta 3D Field Emission Gun SEM/Focused ion beam instrument. Energy dispersive spectroscopy (EDS) analysis was also carried out using this SEM instrument, as this gives a qualitative picture of aluminum oxide growth formed during curing of composite powders. Characteristic x-ray spectra were taken using an accelerating voltage of 10 keV and beam current of 1.19 nA. X-ray spectra were acquired at magnifications of 1,200X and 10,000X respectively. Experimental determination of composite tablet density was determined using two approaches: (1) by conventional means using Vernier calipers and a digital scale with a resolution in the micro-gram range; (2) using a combination of SEM and imaging analysis techniques. Due to tolerances between the moving discs and die, during the compaction process material is pushed into this area creating tablets with an "elephant foot" shape around their perimeter [148]. This effect leads to composite tablets that deviate from perfect cylinders making determination of density using conventional Vernier calipers and electronic balance uncertain. Perhaps a more precise means to determine density can be carried out using a combination of SEM analysis and imaging techniques. Determination of tablet density will be carried out using ImageJ, which is an open source imaging software and SEM micrographs of composite tablet surfaces. The strategy used here is twofold:

1. SEM micrographs (in the form of TIFF images) of composite tablet surfaces are imported into ImageJ, converted to 8-bit binary images, and finally manual thresholding is applied. During the thresholding process, individual pixels in an image are marked as "object" pixels if their value is greater than some threshold value (assuming an object to be brighter than the background) and as "background" pixels otherwise. In this study the "object" pixels correspond to regions of surface porosity and the "background" pixels to regions of material. The "histogram" feature in ImageJ then gives a count of object pixels. With the scale bar annotation on the SEM micrographs one can easily determine pixel size, and total area. Porosity percentage is then determined by the following equation:

$$Porosity\ \% = \frac{\#\ Object\ Pixels * (pixel\ size)^2}{total\ area} * 100 \qquad (5\text{-}1)$$

2. With thresholding applied, 8-bit binary images of SEM micrographs are evaluated using the ImageJ "particle analyze" plug-in. Most particle analysis software, including ImageJ, map the actual object of interest to an equivalent ellipse so that both area and perimeter matches as closely as possible. ImageJ produces such output parameters as number of particles, areas, perimeters, circularity, orientation angle, and major and minor axes. In this study the "particles" being analyzed are individual surface pores. For both these imaging techniques discussed above SEM micrographs are acquired at magnifications of 1,200X and 10,000X. Experimentally determined tablet densities using conventional means and image analysis techniques of SEM micrographs are normalized by bulk density for pure (99.9999%) cast aluminum respectively.

Indentation testing is utilized extensively in this study to investigate states of CNT dispersion on the material response of Al/CNT composites. Macro-hardness testing is employed using a Buehler© Macromet II Rockwell/Superficial type hardness tester. First, a 1/16 inch ball tip indenter is applied to the tablet surface with a 3 kg minor load, and then a major load of 15 kg is applied and held for 10s. Three tablets are tested for each data set with an average of 10 indentations performed per tablet.

5.3 Results and Discussion

Fig. 5-3 shows CNT morphologies of composite mixtures prepared according to Table 5-2. SEM micrographs for cases M1C (Fig.5-3(a)), M2C (Fig.5-3(d)), and S1C (Fig.5-3(g)) show Al particles fully engulfed within large CNT clusters or blanked with dense CNT "sheets." For these cases ultrasonication was not energetic enough to fully exfoliate CNT clusters into individual tubes. In a study carried out by Stein et al. it was reported that in the preparation of 1.5wt%MWCNT/ AA5083 composite, MWCNTs were ultrasonicated with AA5083 powders in isopropanol for 1hr [149]. The authors of this study reported that prolonged sonication times were not adequate to overcome Van der Waal forces and clusters as large as 100 μm were observed.[16] However, Zhong et al. reported good nanotube dispersion ultrasonicating nanotubes in the presence of Al powder for 30 minutes in alcohol [150]. The authors of this study attributed good dispersion to the nano-sized Al particles which had an average size of 50 nm [150]. Whereas, the average particle size of Al powder used in this current work has an average particle size of 45μm.

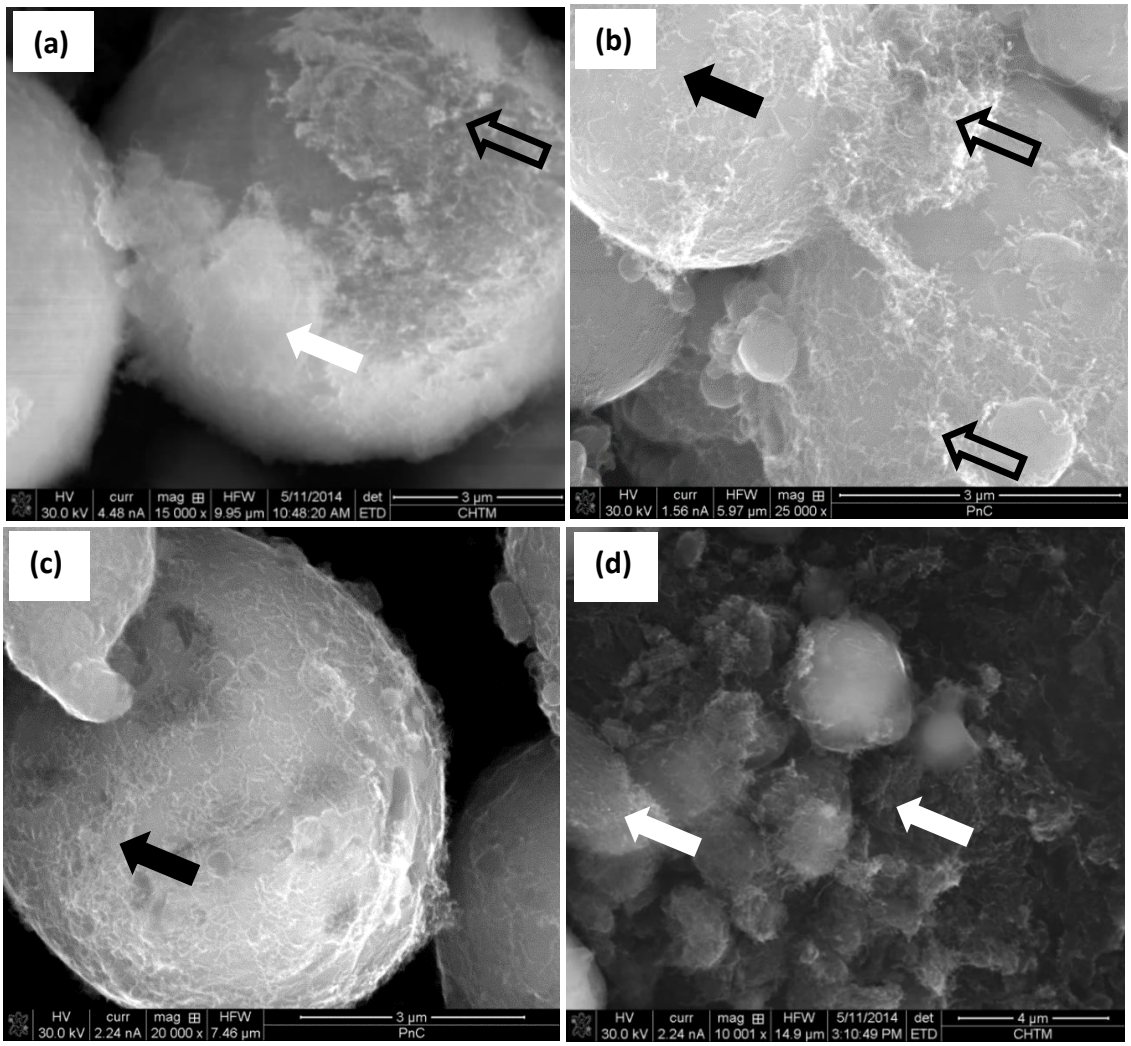

Figure 5-3: SEM micrographs of composite powder surfaces subject to 5-minute sonication time (a) M1C, (b) M1, (c) M1f, (d) M2C. Where individual MWNTs are marked by black arrows, MWCNT clusters/sheets by white arrows, and MWCNT webs by outlined black arrows.

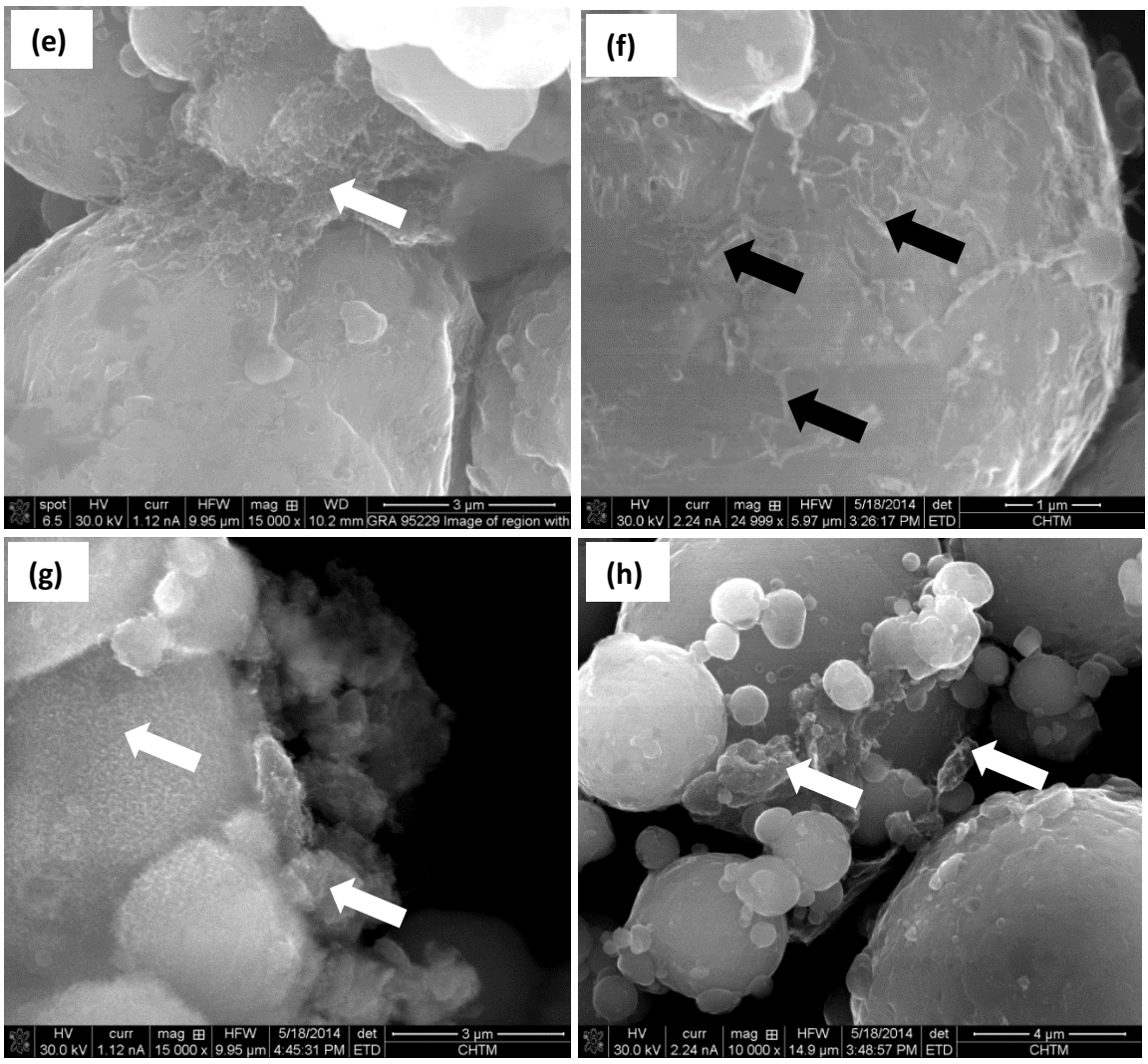

Figure 5-3: SEM micrographs of composite powder surfaces 5 minute sonication time: (e) M2, (f) M2f, (g) S1C, (h) S1. Where individual CNTs are marked by black arrows and CNT clusters/sheets by white arrows.

The poor dispersion patterns observed in the M1C, M2C, and S1C cases can be explained by CNTs reconfiguring to a new equilibrium state of low energy, forming clusters, upon completion of the sonication process. This is especially likely to occur in the absence of surfactants absorbed onto outer CNT walls providing necessary static charge repulsion to stabilize CNTs after sonication. In this study, upon completion of the ultrasonication, CNT colloidal suspensions were immediately magnetically stirred with Al powders

which subsequently formed thick composite "sludges." In a theoretical analysis to guide/explain CNT dispersion processes using ultrasonication techniques, Huang et al. concluded that in the absence of surfactants, CNT re-agglomeration is driven by inter-tube Van Der Waal forces [151]. Additionally, it was shown that subsequent shear mixing (magnetic stirring as in the case of this study) after obtaining a well dispersed CNT suspension can accelerate the re-agglomeration process [151]. Comparing cases M1 (Fig. 5-3(b)), M2 (Fig. 5-3(e)), and S1 (Fig.5-3(h)) to the previous cases discussed, slightly better dispersion patterns are observed using surfactant assisted dispersion technique. In Fig. 5-3(b) is observed an interconnected $MWCNT_L$ web and smaller clusters coating Al particle surfaces. For Fig. 5-3(e) and Fig. 5-3 (h), Al particle surfaces show two distinct dispersion patterns: (1) regions free of CNTs, (2) regions populated with sub-micron CNT aggregates. Previous studies have shown this surfactant-assisted dispersion technique to be effective at coating metal powders with individual CNTs [152-155]. However, some of these same studies have shown that CNT bundles are never exfoliated completely into individual tubes using surfactant assisted dispersion and CNT clusters are introduced into metal matrices[152-155] . Therefore it is necessary to compliment surfactant assisted dispersion with ultrasonication steps to further exfoliate CNT aggregates. During the sonication process, rapid cavitation of air bubbles in the aqueous suspension produce shear stresses which creates a pulling force "fraying" the ends of CNT bundles. As described by Strano et al. this fraying effect acts to expose surfaces of individual MWCNTLs, which become sites for the absorption of zwitterionic surfactant molecules from the surrounding medium [60]. As the process continues, individual CNTs are slowly "unzipped" from larger clusters. For cases M1f (Fig. 5-3(c))

and M2f (Fig. 5-3(f)) CNT dispersion patterns are characterized by individual tubes coating Al particle surfaces. For these cases the functionalization process is effective at attaching oxygen containing functional groups on outer shells of MWCNTs used in this study. These oxygen containing functional groups act as absorption sites for zwitterions further promoting dispersion and ultimately stability in colloidal suspensions.

Fig. 5-4 show density data determined experimentally and by image analysis of SEM micrographs of composite tablet surfaces.

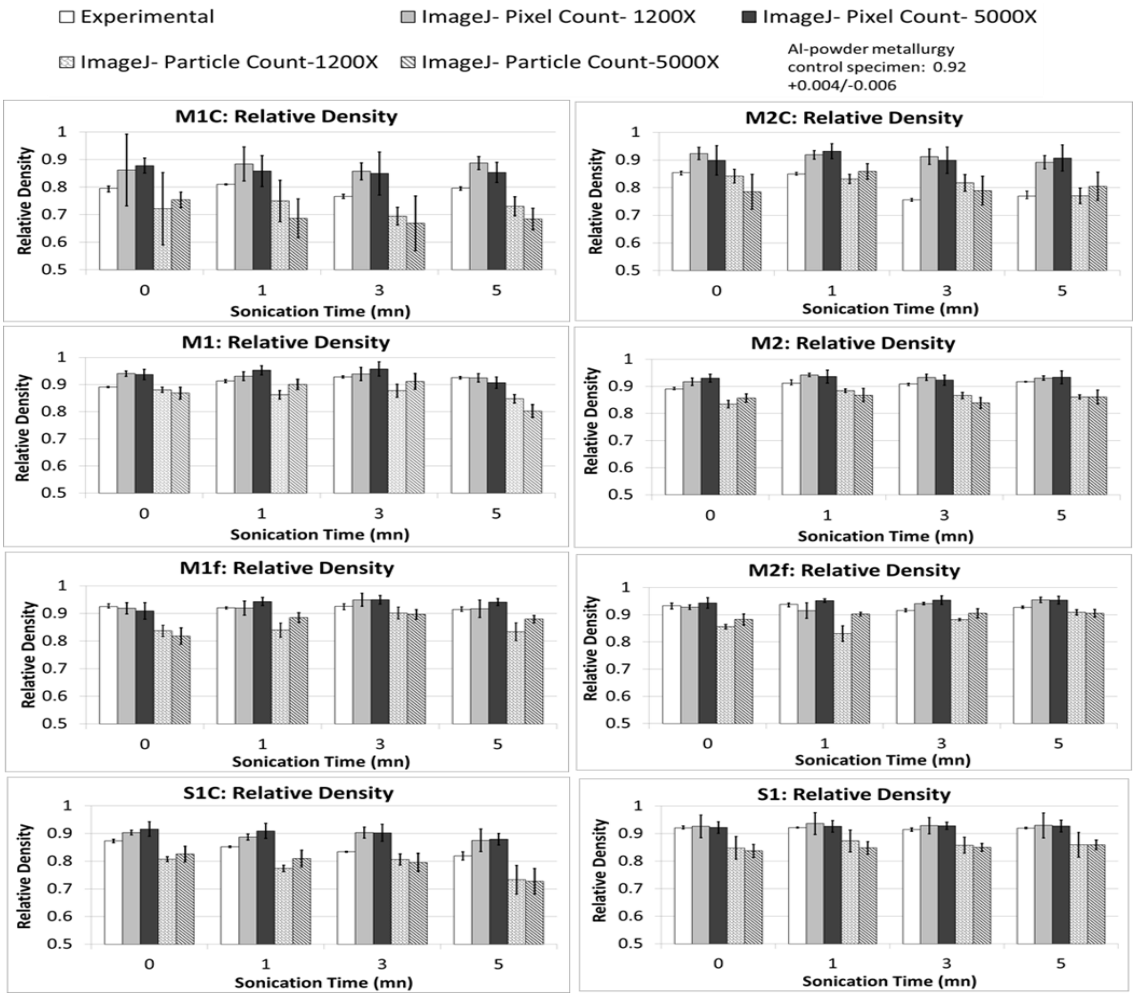

Figure 5-4: Relative density data determined experimentally and using image analysis. Densities are normalized by density (2.71 g/cm^3) for pure (99.9999%) cast aluminum.

For the M1C, M2C, and S1C cases there exist noticeable deviations between experimentally determined density and that determined using ImageJ particle analyze plug-in. In these cases, the particle analyze technique tends to underestimate experimentally determined density. In the ImageJ particle analyzing process, surface pores are modeled as ellipses with equivalent area and perimeter of the pores (Fig. 5-4(c,f)). In a study carried out by Igathinathane et al., the authors used the ImageJ particle analyze to determine the size distribution of food grains and biomass [156]. The authors of this study reported dimension representation anomalies using major and minor axes to represent length and width produced significant overestimation/underestimation of highly non-circular objects such as rectangles and triangles [156].[23] For the M1C, M2C, and S1C cases with high surface porosity, size and areas of individual surface pores on composite tablet surfaces are inefficiently fitted using ellipses (Fig. 5-5(f)). For the remaining cases (M1, M2, S1 M1f, M2f) this effect becomes less pronounced as CNT clusters are further exfoliated and composite porosity decreases (Fig. 5-5(c)).

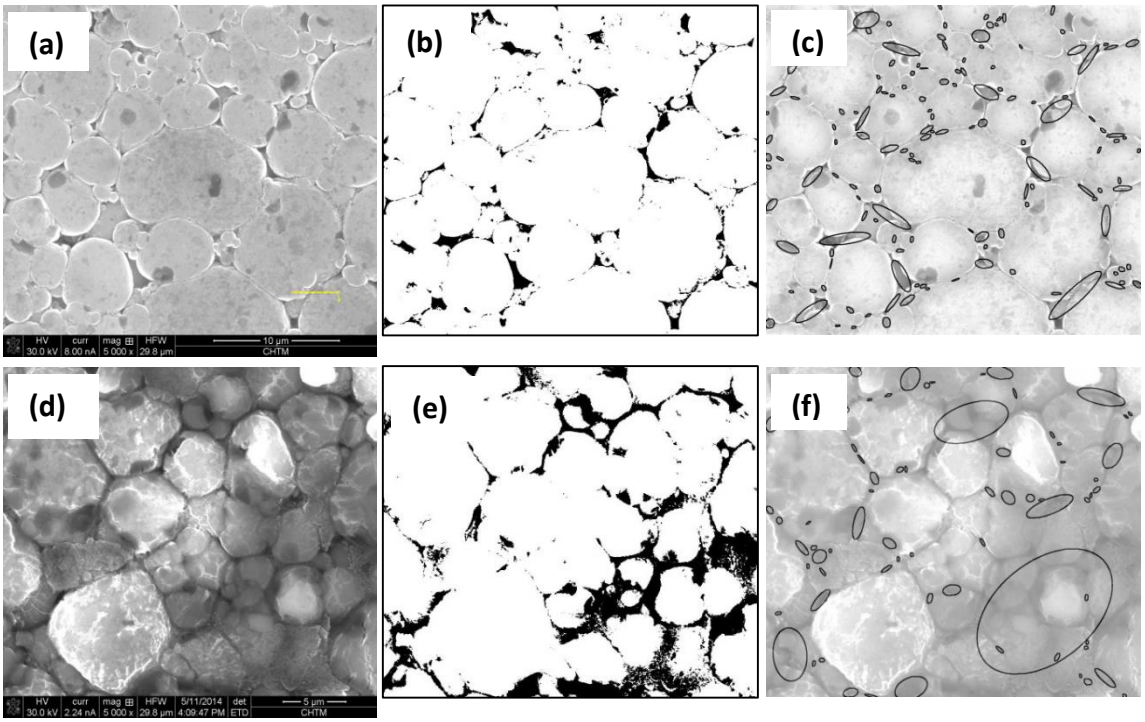

Figure 5-5:(a) SEM image of M1f composite tablet surface, (b) threshold image of (a), (c) fitted ellipses to surface pores in (a), (d) SEM image of M1C composite tablet surface, (e) threshold image of (d), (e) fitted ellipses to surface pores in (d).

It is recommend by the authors of this study that for powder compacts, surface porosity analysis using ImageJ particle analyze plug-in be applied in conjunction with the development of shape correction factor which takes into account porosity shape. The CNTs used in this study consist of a mixture of metallic and semi-conducting type, as a result, for poor dispersion patterns observed in the cases where the primary CNT dispersion routes consist of shear mixing (ultrasonication, magnetic stirring), SEM imaging of composite tablets and mixtures becomes problematic. During SEM analysis, large CNT clusters in Fig. 5-3(a, d, g) are unable to efficiently disperse charge buildup. As a result, local electric fields are produced which interfere with the incident electron beam, this effect results in imaging artifacts and poor quality of SEM micrographs (Fig.

5-5(d)). For M1C, M2C, and S1C cases poor quality of SEM micrographs of tablet surfaces, differentiation between objects of interest (surface pores) and foreground objects becomes difficult during the manual thresholding process (Fig. 5-5(d-e)). In these cases ImageJ pixel counting process overestimates experimentally determined density. For the remaining cases (S1, M1, M2, M1f, M2f) where shear mixing is preceded by surfactant assisted dispersion, ImageJ pixel counting technique more closely approximates experimentally determined density. For these cases there exists a general trend for density to be slightly overestimated using this technique. In an earlier study carried out by these authors it was shown that for uniaxial one-sided compaction, for the compacted side of the tablets, compressive stresses are the highest and there is a loss of compaction efficiency along the depth of the tablet towards the non-compacted side [148]. For mico-hardness (HV) values measured along the tablet depth, highest HV values were measured at the compacted surface of the tablet [148]. In this study, SEM micrographs are obtained from compacted tablet surfaces and then analyzed using image analysis techniques. Planar densities determined using both image analysis techniques at the compacted surfaces are taken as constant throughout the depth of the tablet arriving at a bulk tablet density. As shown in the author's previous study double-sided compaction aids in further densification and homogenization of powder compacts [148]. Therefore, for Al/CNT composites that have undergone a homogenization procedure, it is expected that image analysis techniques utilizing the "pixel-counting" method will more closely approximate experimentally determined density.

Figure 6 compares the Superficial Rockwell hardness and experimentally determined density for all cases. The hardness and densities are measured against sonication time of

CNTs in aqueous suspensions. For cases M1 and M2 the hardness is gradually increased above the hardness of pure Al powder metallurgy sample for increased sonication times. It demonstrates the effectiveness of ultrasonication to expose absorption sites on outer MWCNT walls to free surfactants in aqueous suspensions. As the sonication process continues, MWCNTs are "unzipped" from larger clusters with absorbed free surfactants providing the necessary static repulsion in NaI stabilizing solution.

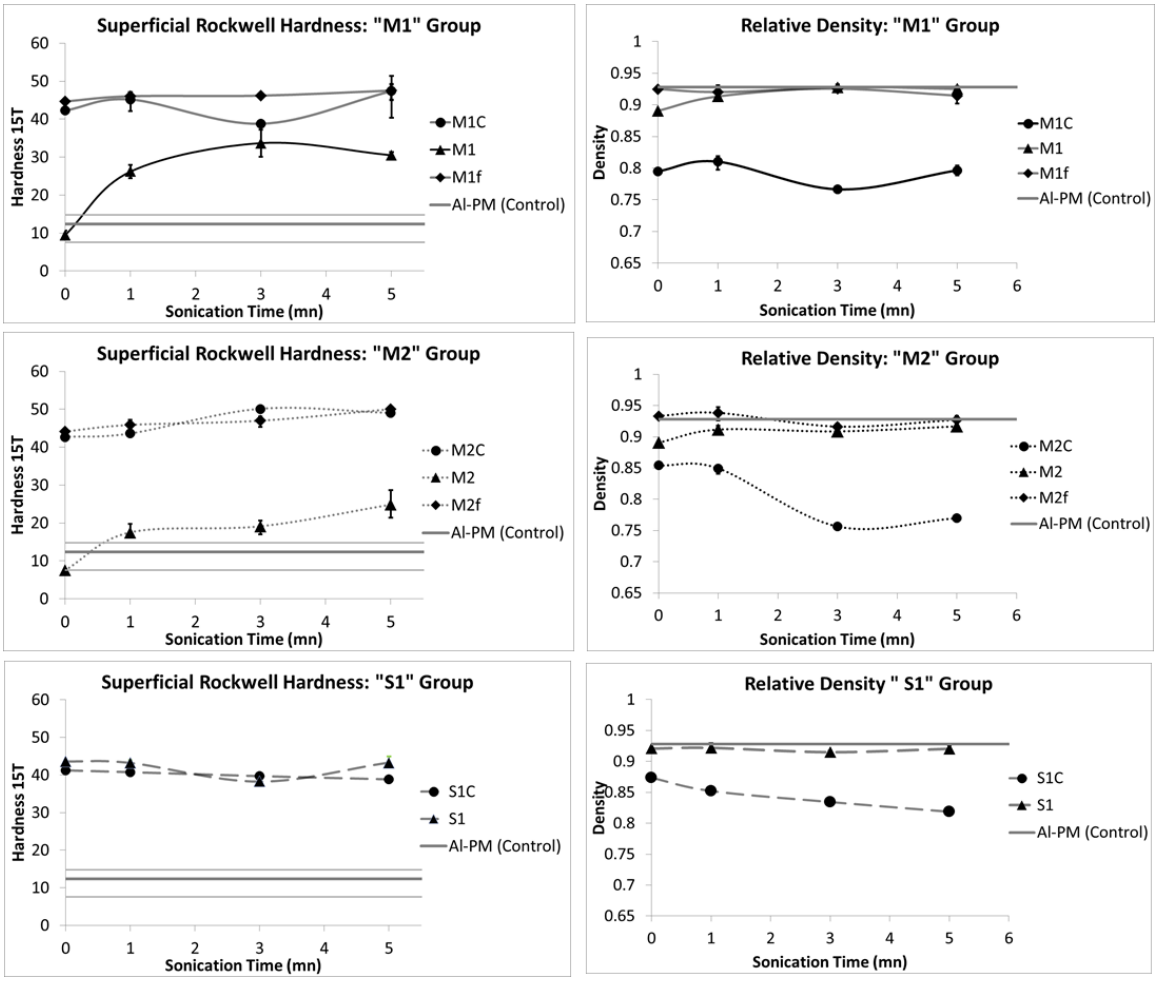

Figure 5-6: Superficial Rockwell and experimentally determined density data. Densities are normalized by density (2.71 g/cm3) for pure (99.9999%) cast aluminum.

For M1and M2 cases, as sonication time increases, MWCNT clusters are further exfoliated and composite tablet densities approach that of Al-PM control specimen (Fig. 5-6). Therefore, dramatic increases in hardness are primarily attributed to efficient dispersion of MWCNTs with superior mechanical properties and to a lesser extent a decrease in porosity. For the case of SWCNTs dispersed under the same conditions, case S1 shows a remarkable improvement in hardness over pure Al powder consolidated and sintered under the same conditions. However, experimentally measured hardness and density are insensitive to sonication procedure for case S1. For the cases of S1C and M2C, upon completion of sonication, magnetic stirring of SWCNTs with Al powder promotes reagglomeration of nanotubes which leads to increased porosity of formed tablets. This increase in porosity becomes more pronounced as sonication time increases. Interestingly, in this study cases M1C, M2C, and S1C show a noticeable deviation in trend to M1, M2, and S1 groups. Namely, as porosity increases there exists a corresponding increase in observed hardness. For cases M1C, M2C, and S1C poor relative density achieved by the fabrication processes result in hardness values that rival other cases in this study. For no ultrasonication time (0mn), MWCNT functionalization and surfactant assisted dispersion results in increased composite density (Fig. 5-6). However, higher hardness values are reported for Al/MWCNT composites containing MWCNTs dispersed solely via magnetic stirring (no ultrasonication). It is well known in literature and shown in a previous study that as porosity of powder compacts increases there is a corresponding decrease in tablet strength [148]. This non trivial material behavior (increase in porosity, high hardness) can be attributed to the mechanical responses of CNT bundles under compression during indentation processes and tough

oxide particles being formed during composite fabrication. During the densification of Al/CNT composite mixtures and subsequent sintering, large CNT clusters become trapped in tablet pores (Fig. 5-7). Under an applied indentation load these CNT clusters offer resistance to the spherical indenter tip being driven into the tablet surface.

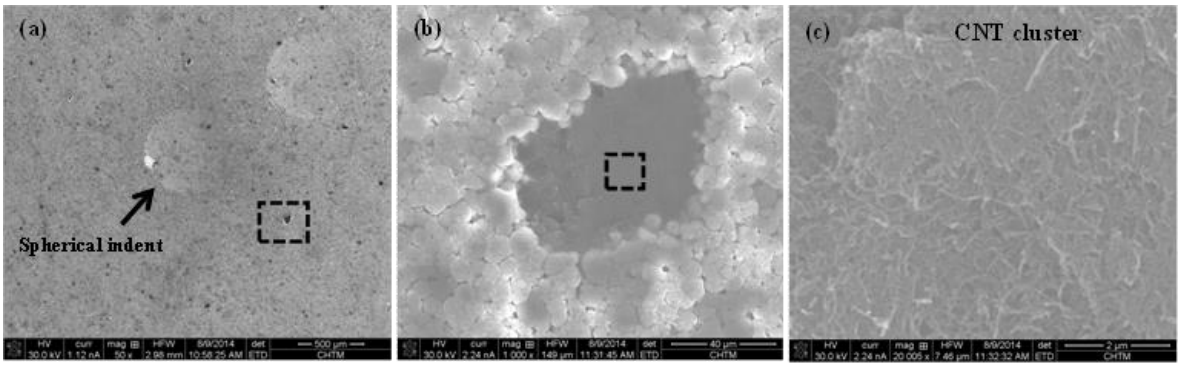

Figure 5-7: (a) SEM micrograph of case M1C tablet surface (0-minute sonication), (b) magnified image of marked rectangle in (a), (c) magnified image of marked rectangle in

In molecular dynamics simulations carried out by Liew et al., it was found that critical buckling loads of SWCNT clusters was much higher (5X) than that of individual SWCNTs [157]. The authors of this study attributed this increase in buckling load to long range Van Der Waals interactions which improved the overall rigidity of CNT clusters [157]. Liu et al. used molecular mechanics simulations to investigate the buckling behavior of MWCNT and SWCNT clusters under nanoindentation [158]. Similarly, their study showed that MWCNT and SWCNT clusters were found to be sturdier than their sub unit components in withstanding buckling under simulated nanoindentation loads [158]. Although difficult to quantify the contribution of CNT bundle buckling resistance to increases of composite hardness, experimental density data reveals porosity levels as high as ~ 20% in M1C, M2C, and S1C cases. As seen in Fig. 5-7 , where shear mixing is used as the stand- alone CNT dispersion route (M1C, M2C,

S1C), spherical Superficial Rockwell indents can encompass multiple surface pores containing CNT clusters which can be tens of microns across. It is believed that addition of stiff material (CNT clusters) into composite pores provides resistance to applied indentation loads increasing hardness. Formation of oxide layers during curing phases of M1C, M2C, and S1C composite mixtures are believed to also contribute to increases in composite hardness and inhibit diffusion processes during sintering. Fig.5-8 and Fig.5-9 show EDS spectra for all cases in this study, spectra are acquired at 1200X magnification in order to encompass many particles. For M1C, M2C, and S1C cases the presence of high oxygen peaks are indicative of oxide growth during curing phases of composite powders.

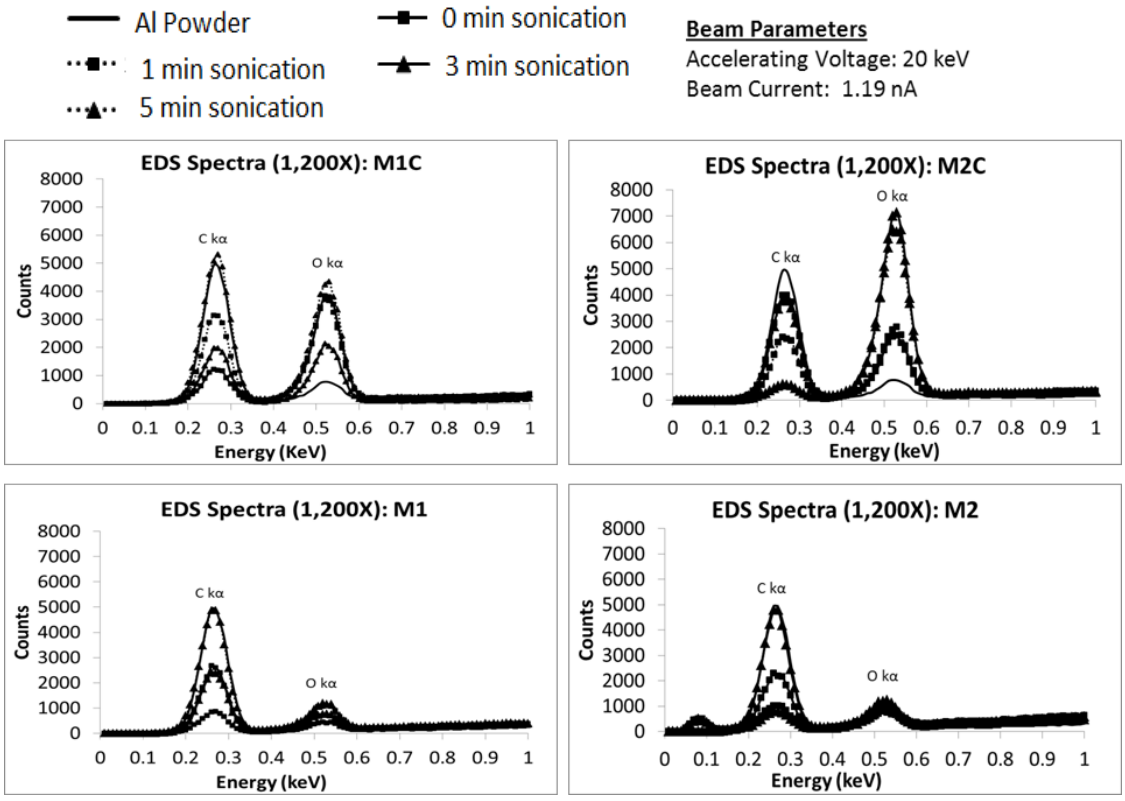

Figure 5-8: EDS spectra of M1C, M1, M2C, and M2 composite powders acquired at 1200X magnification.

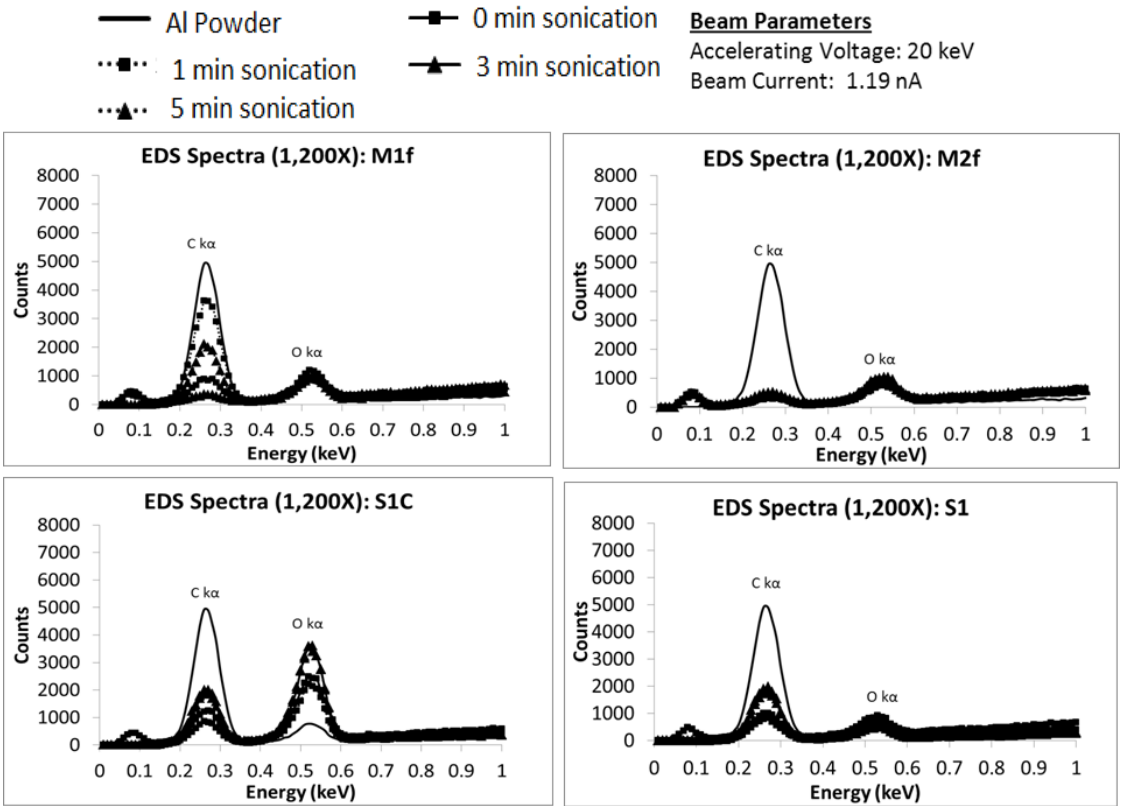

Figure 5-9: EDS spectra of M1f, S1C, M2f, and S1 composite powders acquired at 1200X magnification.

Thick oxide layers can impede neighboring particle diffusion during the sintering process and prevent a continuous Al network from being formed with noticeable particle boundaries present (Fig. 5-10(a)). These particle boundaries can severely limit dislocation mean free path in the sintered Al matrix which acts to increase hardness. Additionally, oxides which are in the form of very small particles dispersed throughout the composite can act as dislocation barriers which cause the composite to become embrittled.

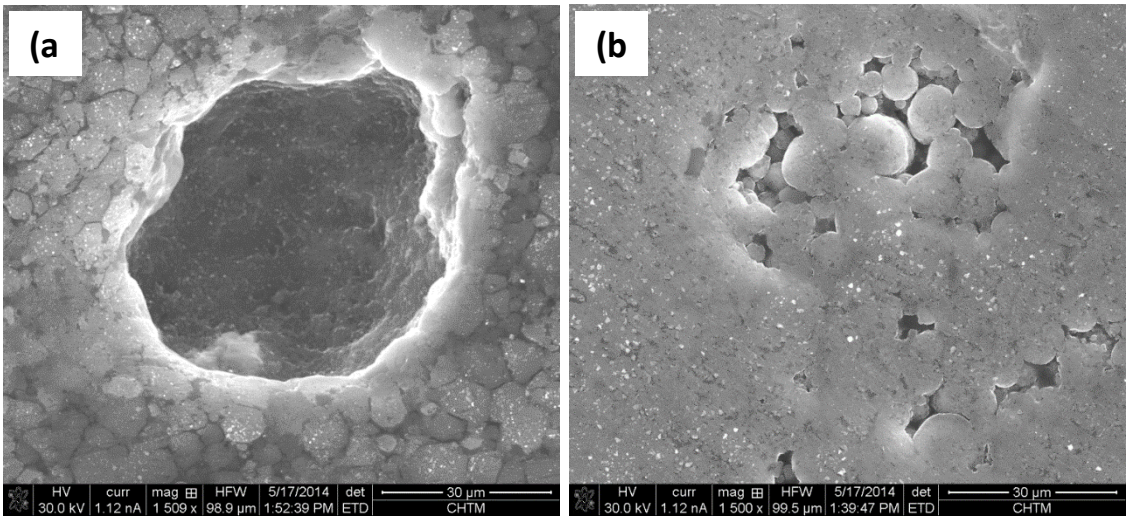

Figure 5-10: SEM micrographs of ground tablet surfaces: (a) M1C (5min sonication), (b) M1f (5min sonication).

In order to obtain better nanotube dispersion patterns in this study and good relative density it was necessary to modify MWCNT surfaces with oxygen containing functional groups. As seen in Figure 6, hardness values for cases M1f and M2f are higher than the cases where functionalization was not employed. Improvements in hardness in these cases can be attributed to good MWCNT dispersion, and high relative density achieved by the exclusion of CNT clusters (Fig. 5-10(b), Fig. 5-11(c)). Additionally, for the case of functionalized nanotubes (f- MWCNTs), this study shows that secondary ultrasonication steps have little effect at further dispersing the f- MWCNTs. Fig. 5-11 shows SEM micrographs of pore interiors and MWCNT morphology present. For the M2C case Fig. 5-11(a) shows that MWCNT bundles are not completely exfoliated and greatly impede the densification process preventing particle contact among Al granules. For the cases of M2 and M2f, Fig. 5-11(b,c) provides evidence that dispersion routes used in this study are effective and exfoliating MWCNT clusters into individual tubes. In the M2f case, CNT clusters are not visible in SEM micrographs which indicate

homogenous dispersion of f-MWCNTs. The presence of large CNT clusters in the composite mixtures can act to disrupt this complex densification process. Additionally, oxide layers present on Al particle surfaces may remain intact due to CNT clusters disrupting the formation of particle contact and subsequent cleavage of oxide layers. Good mechanical performance of M1 and M2 cases is attributed to the effectiveness of surfactant assisted dispersion in impregnating soft Al matrix with individual tubes. For increased sonication times, this study has shown that MWCNT clusters are further exfoliated which increases hardness and density in the M1 and M2 cases. For the S1 case surfactant assisted dispersion and ultrasonication is ineffective at exfoliating SWCNT clusters compared to a stand-alone sonication procedure (S1C).

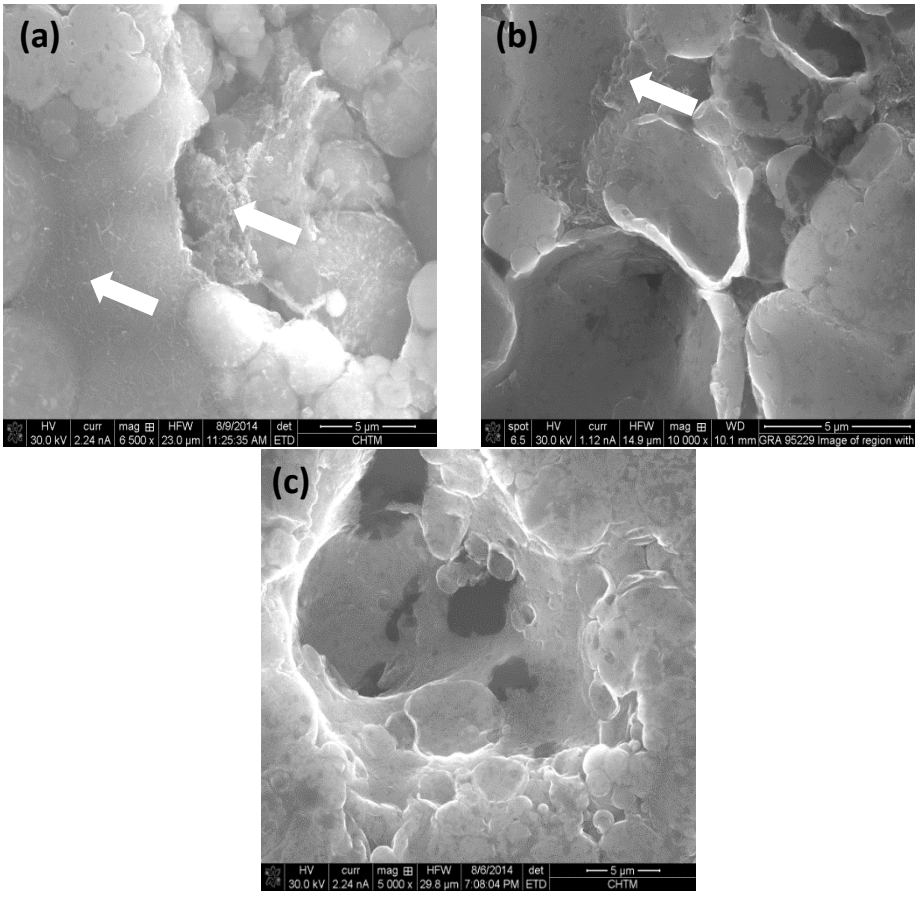

Fig. 5-11: SEM micrographs of pore interiors: (a) M2C, (b) M2, (c) M2f. MWCNT clusters are marked by white arrows.

5.4 Conclusion

The f-MWCNT dispersion route which consists of a synergistic effect of dispersion techniques discussed above (M1f, M2f) produces Al/f-MWCNT composites with superior mechanical properties and low presence of oxide particles. This increase in mechanical performance is attributed to uniform dispersion of individual f-MWCNTs on Al powder surfaces. This study has shown that in some cases surface modification of nanotube surfaces with oxygen containing functional groups is necessary to promote surfactant absorption, further exfoliating CNT clusters. Additionally, this study has shown that subsequent ultrasonication steps are not necessary to further disperse f-MWCNTs in NaI solution. For MWCNTs and SWCNTs that aren't functionalized, surfactant-assisted dispersion is effective at exfoliating CNT clusters. However, subsequent ultrasonication steps are required to further expose CNT surfaces to surfactant molecules in aqueous suspensions. This nanotube dispersion route produced composites (M1, M2, S1) with good strength and low porosity compared to the Al control group. It should be noted that in these cases sonication times > 3 minutes is necessary to minimize inclusion of CNT clusters into Al matrix. For the cases (M1C, M2C, S1C) where shear mixing (ultrasonication and magnetic stirring) is the stand-alone dispersion route, poor nanotube dispersion patterns are observed. For these cases high hardness and porosity content is reported compared to the Al control group. This counter intuitive mechanical response given poor nanotube dispersion can be explained by high oxide formation during composite processing. Oxide layers on Al powder surfaces disrupt diffusion process and prevent adjacent al particles from forming a continuous and stable network. Fine oxide particulates dispersed throughout the Al matrix can also act as dislocation

barriers, in this study embrittling Al/CNT composites. It was also determined that the inclusion of CNT clusters into pores offer buckling resistance to applied indentation loads which act to drive up tablet hardness. Addition of CNT clusters into Al matrix also act to impede densification of the composite powder compact, interrupting Al particle contact among nearest neighbors, and ultimately preventing the formation of a continuous network during sintering. Of all the cases investigated in this study, functionalized MWCNTs have been shown to be the superior Al reinforcing agent when dispersed using zwitterionic surfactants and shear mixing. This is due to homogenous dispersion as brought about by the fabrication route used in this study and geometry of MWCNTs. The Van Der Waal attractions between concentric MWCNT shells and geometry offer superior mechanical performances over their SWCNT counterparts.

Chapter 6

Optimizing powder metallurgy methods: Effects of carbon nanotube dispersal mechanisms on elastic/thermal properties of aluminum/carbon nanotube composites

6.1 Materials and Composite Processing

The following materials listed in Table 6-1 were used in this study to fabricate aluminum/carbon nanotube (Al/CNT) composites.

Metal Powder:	***Aluminum (Al)***	***APS: ~ 45 µm***		
CNT Type	**Outer Diameter (nm)**	**Length (µm)**	**Density (g/cm^3)**	**Descriptor**
Multi-walled	*10-20*	*10-30*	*2.1704±0.1032*	*$MWCNT_L$*
Functionalized Multi-walled	*10-20*	*10-30*	*-*	*$f\text{-}MWCNT_L$*
Multi-walled	*< 8*	*0.5-2*	*2.2405±0.0075*	*$MWCNT_S$*
Functionalized Multi-walled	*< 8*	*0.5-2*	*-*	*$f\text{-}MWCNT_S$*
Single-Walled	*1-4*	*5-30*	*2.2735±0.1106*	*SWCNT*

Table 6-1: Materials used in this study.

Density determination of $MWCNT_L$, $MWCNT_S$, and SWCNT powders were carried out using helium gas pyconometry methods at Sandia National Laboratories (Electronic, Optic and Nanomaterials Department) under the direction of Dr. Pin Yang. The values reported in table 1 for each type of nanotube are the average of four measurements. Densities were not determined for functionalized multi-walled nanotubes (f-MWCNTs) due to experimental difficulties in producing the minimum amount (1 gram) of raw powder for helium gas pyconometry measurements.

CNT dispersion routes designed specifically for this study are listed in Table 6-2 below.

Case	CNT Type	CNT Dispersal Route		
M1C	*$MWCNT_L$*	-	*Ultrasonication (0, 1, 3, 5 mn)→*	*Magnetic Stirring*
M1	*$MWCNT_L$*	*Surfactant Assisted→*	*Ultrasonication (0, 1, 3, 5 mn) →*	*Magnetic Stirring*
M1f	*f-$MWCNT_L$*	*Surfactant Assisted→*	*Ultrasonication (0, 1, 3, 5 mn) →*	*Magnetic Stirring*
M2C	*$MWCNT_S$*	-	*Ultrasonication (0, 1, 3, 5 mn) →*	*Magnetic Stirring*
M2	*$MWCNT_S$*	*Surfactant Assisted→*	*Ultrasonication (0, 1, 3, 5 mn) →*	*Magnetic Stirring*
M2f	*f-$MWCNT_S$*	*Surfactant Assisted→*	*Ultrasonication (0, 1, 3, 5 mn) →*	*Magnetic Stirring*
S1C	*SWCNT*	-	*Ultrasonication (0, 1, 3, 5 mn) →*	*Magnetic Stirring*
S1	*SWCNT*	*Surfactant Assisted→*	*Ultrasonication (0, 1, 3, 5 mn) →*	*Magnetic Stirring*

Table 6-2: Al/CNT fabrication routes used in this study.

Details of CNT dispersion routes and composite fabrication procedure are reported in a previous study by the authors [159]. Once composite Al/CNT are adequately prepared, powders are uniaxially compressed (one-sided) using an Instron 4400R tensile/compression machine, at room temperature under 400 MPa of pressure in an A2-air hardened cylindrical die producing half-inch (12.7 mm) nominal diameter tablets. Approximately 1 gram of Al/CNT composite powder was weighed to manufacture each tablet. Al/CNT tablets in the green state were then sintered in a high temperature furnace at 580°C for 2hr under Argon gas.

6.2 Composite Porosity Determination

Experimental determination of composite tablet porosity was determined using two approaches: (1) by conventional means using Vernier calipers, digital scale with a resolution in the micro-gram range, and detailed knowledge of composite solid phase material properties; (2) using a combination of SEM and imaging analysis techniques (pixel counting and particle analyze methods using ImageJ software). Details concerning composite porosity determination via SEM and image analysis techniques are discussed in a previous study by the authors [159]. The porosity % (P) is determined knowing the theoretical (true) composite density (ρ_{TH}) and experimentally determined composite density (ρ_{EXP}):

$$P = 100\ x\ \frac{\rho_{TH} - \rho_{EXP}}{\rho_{TH}}. \quad (6\text{-}1)$$

Where ρ_{TH} assumes a fully dense composite and is calculated using a simple rule of mixtures:

$$\rho_{TH} = f_{Al}\rho_{Al} + f_{CNT}\rho_{CNT}. \quad (6\text{-}2)$$

In Equation 6-2 "f_{Al}" and "f_{CNT}" are the weight fractions of CNTs and Al powder. "ρ_{Al}" and "ρ_{CNT}" are the densities of CNTs and Al powder. The density of *f-MWCNT$_L$* / *f-MWCNT$_S$* are taken to be that of *MWCNT$_L$* / *MWCNT$_S$* . Fig. 6-1 show porosity data determined experimentally and by image analysis of SEM micrographs of composite tablet surfaces. For the M1C, M2C, and S1C cases there exist noticeable deviations between experimentally determined porosity and that determined using ImageJ particle

analyze plug-in. In these cases, the particle analyze technique tends to overestimate experimentally determined porosity. In the ImageJ particle analyzing process, surface pores are modeled as ellipses with equivalent area and perimeter of the pores (Fig. 6-2(c,f)). Dimension representation anomalies using major and minor axes to represent length and width produce significant overestimation/underestimation of highly non-circular objects such as surface pores in Fig. 6-2(c,f). For all cases with high surface porosity, size and areas of individual surface pores on composite tablet surfaces are inefficiently fitted using ellipses (Fig. 6-2(f)). For the remaining cases (M1, M2, S1 M1f, M2f) this effect becomes less pronounced as CNT clusters are further exfoliated and composite porosity decreases (Fig. 6- 2(c)). It is recommend by the authors of this study that for powder compacts, surface porosity analysis using ImageJ particle analyze plug-in be applied in conjunction with the development of shape correction factor which takes into account porosity shape. It should be noted that the CNTs used in this study consist of a mixture of metallic and semi-conducting type, as a result, for poor dispersion patterns observed in the cases (M1C,M2C,and S1C) where the primary CNT dispersion routes consist of shear mixing (ultrasonication, magnetic stirring), SEM imaging of composite tablets and mixtures becomes problematic. During SEM analysis, large CNT clusters in Fig. 6-2(a) and Fig. 6-4 are unable to efficiently disperse charge buildup. As a result, local electric fields are produced which interfere with the incident electron beam, this effect results in imaging artifacts and poor quality of SEM micrographs (Fig. 6-2(d)).

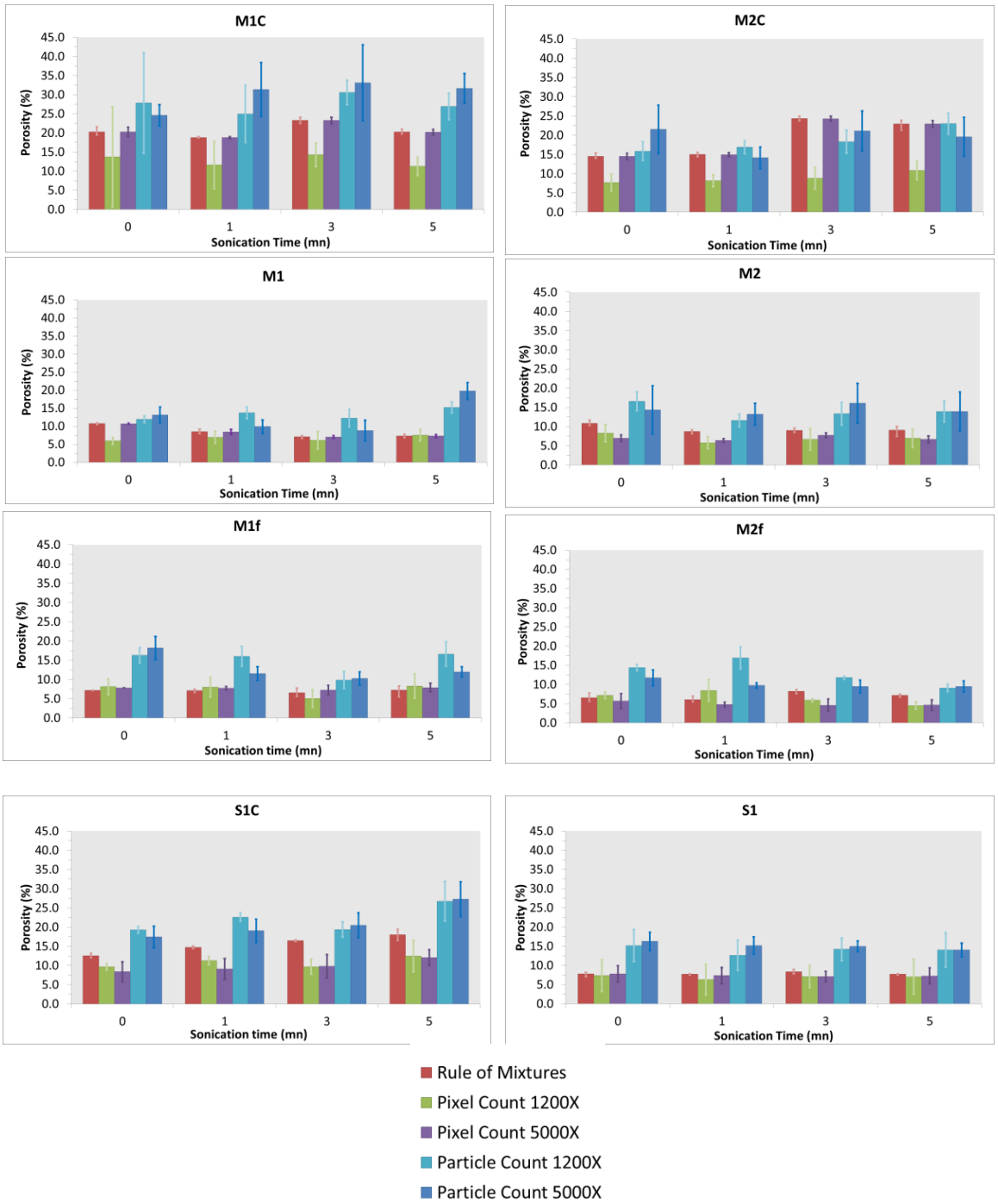

Figure 6-1: Porosity data determined experimentally and using image analysis techniques.

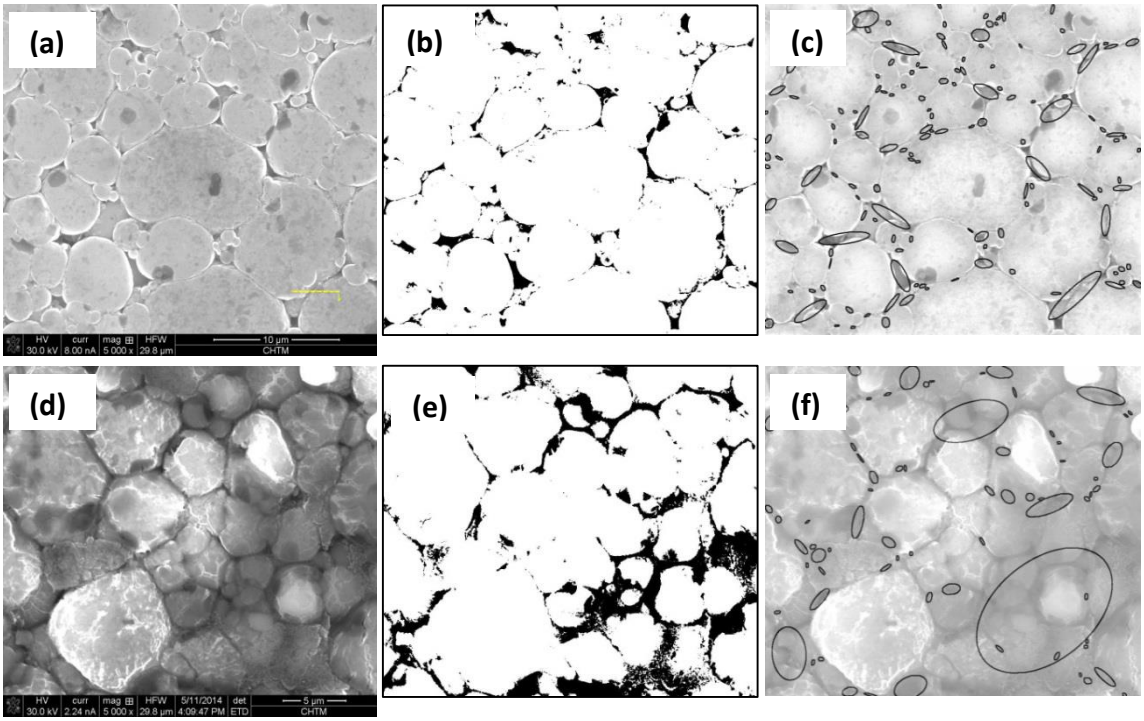

Figure 6-2: (a) SEM image of M1f composite tablet surface, (b) threshold image of (a), (c) fitted ellipses to surface pores in (a), (d) SEM image of M1C composite tablet surface, (e) threshold image of (d), (e) fitted ellipses to surface pores in (d).

For M1C, M2C, and S1C cases poor quality of SEM micrographs of tablet surfaces, differentiation between objects of interest (surface pores) and foreground objects becomes difficult during the manual thresholding process (Fig.6-2(d-e)). In these cases ImageJ pixel counting process can underestimate experimentally determined porosity. For the remaining cases (S1, M1, M2, M1f, M2f) where shear mixing is preceded by surfactant assisted dispersion, ImageJ pixel counting technique more closely approximates experimentally determined porosity. For some of these cases there exists a general trend for porosity to be slightly underestimated using this technique. In an earlier study carried out by these authors it was shown that for uniaxial one-sided compaction, for the compacted side of the tablets, compressive stresses are the highest and there is a loss of compaction efficiency along the depth of the tablet towards the non-compacted side [160]. For mico-hardness (HV) values measured along the tablet depth, highest HV values were measured at the compacted surface of the tablet [160]. In this study, SEM micrographs are obtained from compacted tablet surfaces and then analyzed using image analysis techniques. Planar densities determined using both image analysis techniques at the compacted surfaces are taken as constant throughout the depth of the tablet arriving at a bulk tablet porosity. As shown in the author's previous study double-sided compaction aids in further densification and homogenization of powder compacts [160]. Therefore, for Al/CNT composites that have undergone a homogenization procedure, it is expected that image analysis techniques utilizing the "pixel-counting" method will more closely approximate experimentally determined density.

6.3 Qualitative X-ray Microanalysis

Several researchers have reported the absorption of water and O_2 in hollow CNTs at room temperature [187]. Absorbed O_2 can experience deapsorbtion at temperatures > 200 ^{0} C. The released O_2 and water during sintering can oxidize the surrounding Al matrix material [187]. The formation of tough nano meter sized aluminum oxide (Al_2O_3) particles can act as strengthening agents if well dispersed in metal matrices significantly affecting material properties. In order to gain insight to the formation of Al_2O_3 during composite fabrication x-ray microanalysis qualitative was performed using an FEI Quanta 3D Field Emission Gun scanning electron microscope. Fig.6-3 through Fig.6-5 show EDS spectra for all cases in this study, spectra were acquired at a magnification of 1200X with accelerating voltage of 5 keV and beam current of 852 pA.

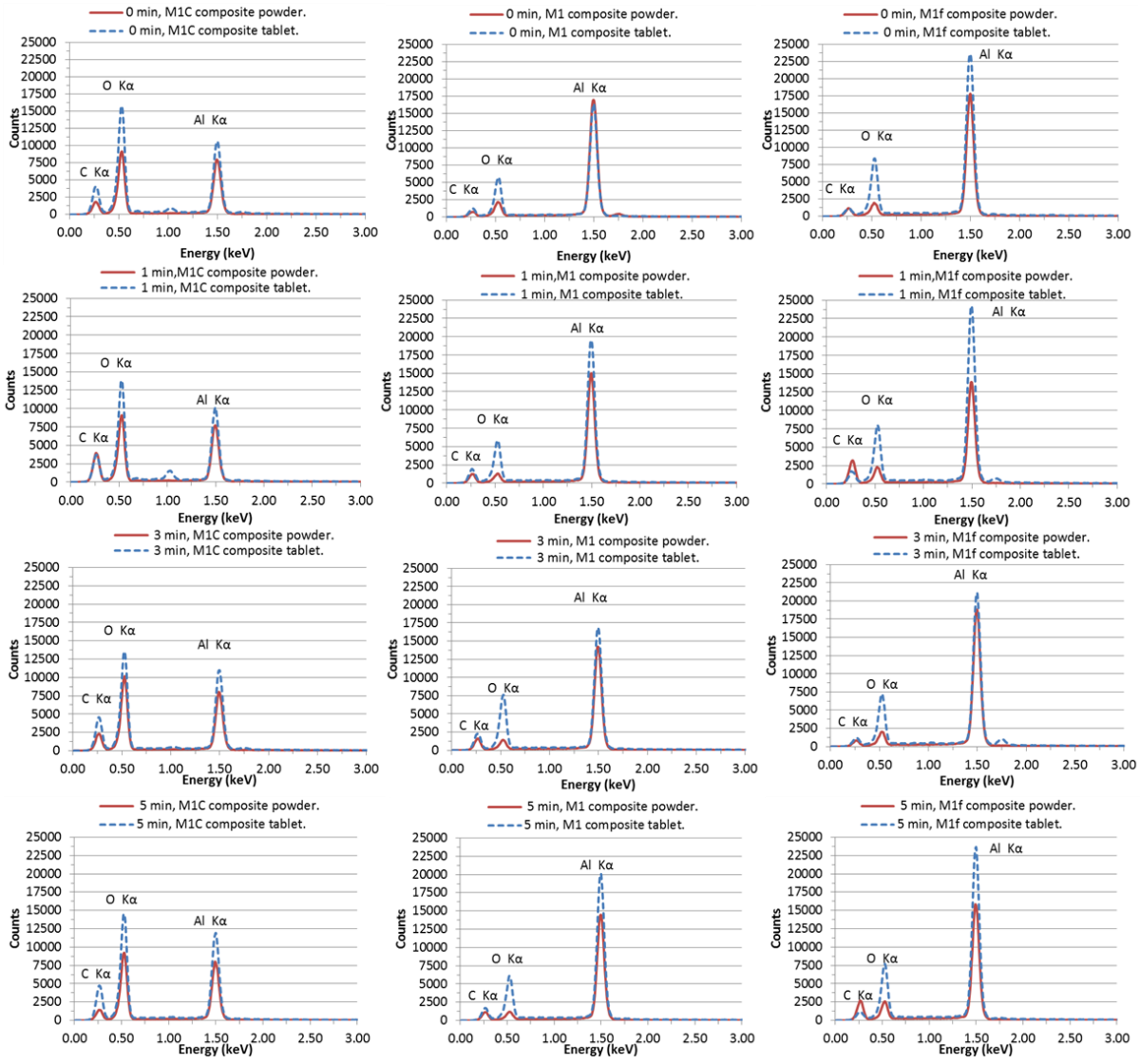

Figure 6-3: EDS spectra of composite mixtures (upon completion of surfactant removal) and tablets (after sintering) for M1 groups. Spectra are acquired at a magnification of 1200X with accelerating voltage of 5 keV and beam current of 852

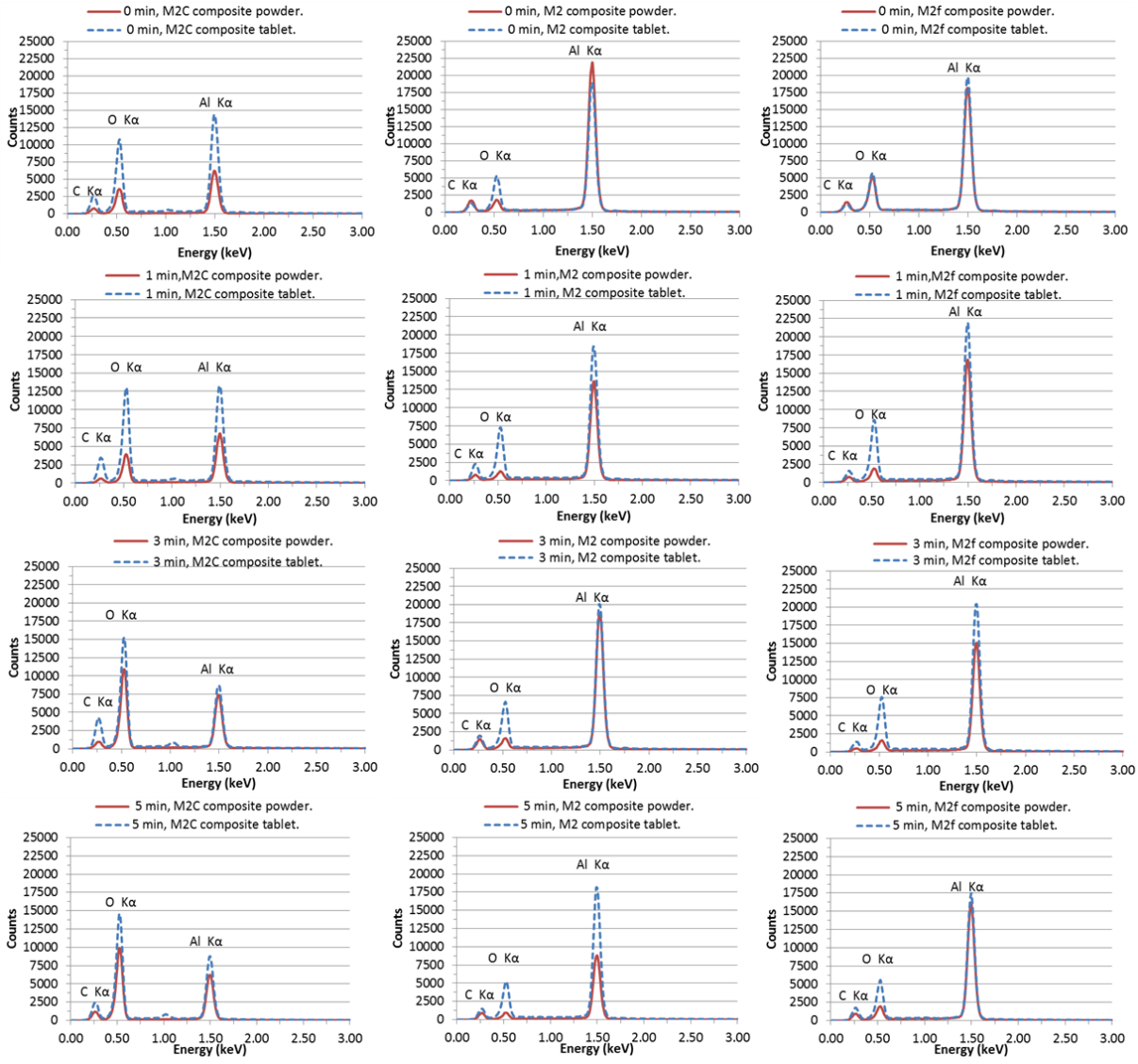

Figure 6-4: EDS spectra of composite mixtures (upon completion of surfactant removal) and tablets (after sintering) for M2 groups. Spectra are acquired at a magnification of 1200X with accelerating voltage of 5 keV and beam current of 852 pA.

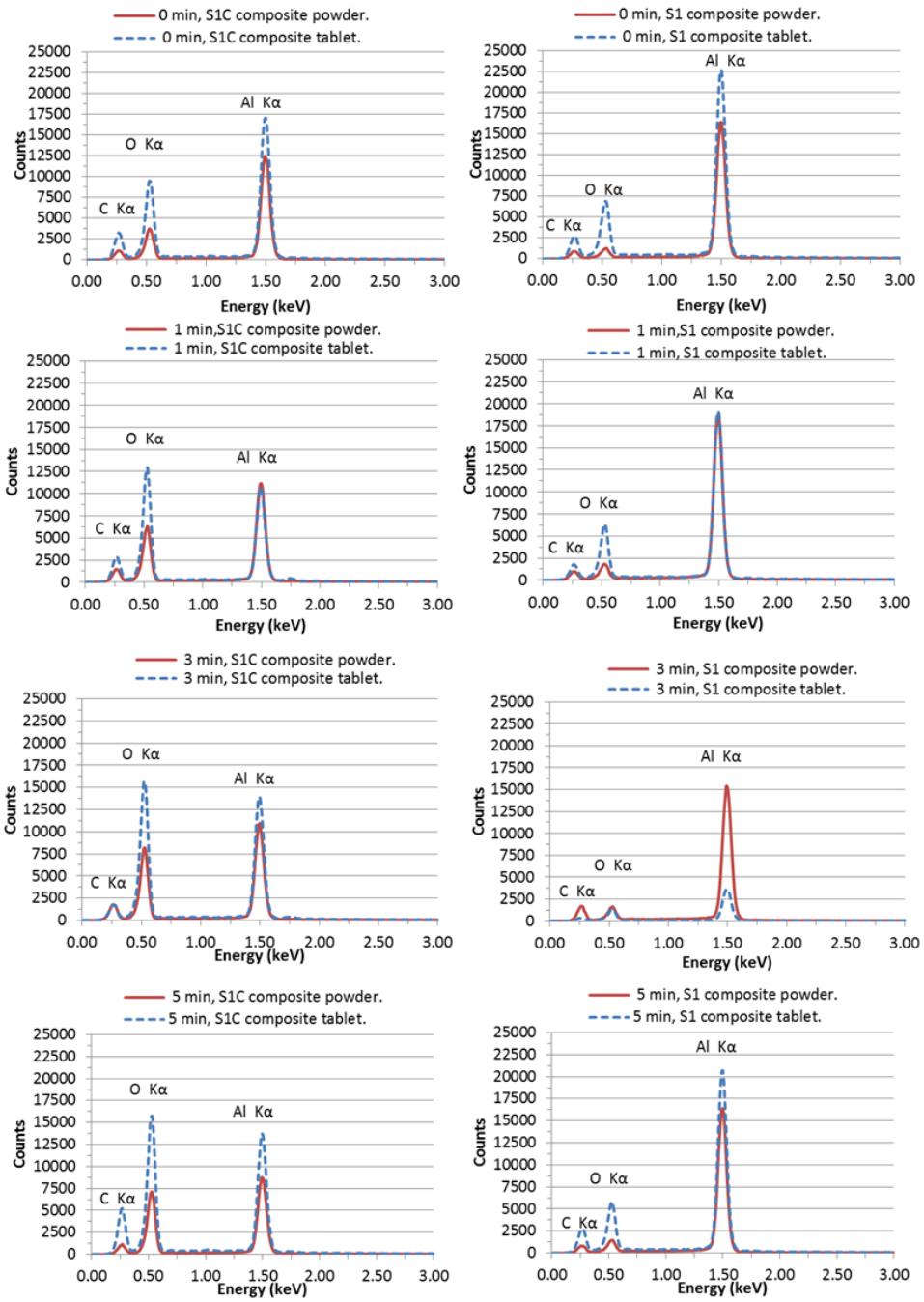

Figure 6-5: EDS spectra of composite mixtures (upon completion of surfactant removal) and tablets (after sintering) for S1 groups. Spectra are acquired at a magnification of 1200X with accelerating voltage of 5 keV and beam current of

during curing phases of composite powders and sintering of composite tablets. Thick oxide layers can impede neighboring particle diffusion during the sintering process and prevent a continuous Al network from being formed with noticeable particle boundaries present (Fig.6-6 through Fig.6-8). These particle boundaries can severely limit dislocation mean free path in the sintered Al matrix which acts to increase hardness. Additionally, oxides which are in the form of very small particles dispersed throughout the composite can cause the composite to become embrittled (Fig.6-6 through Fig.6-8).

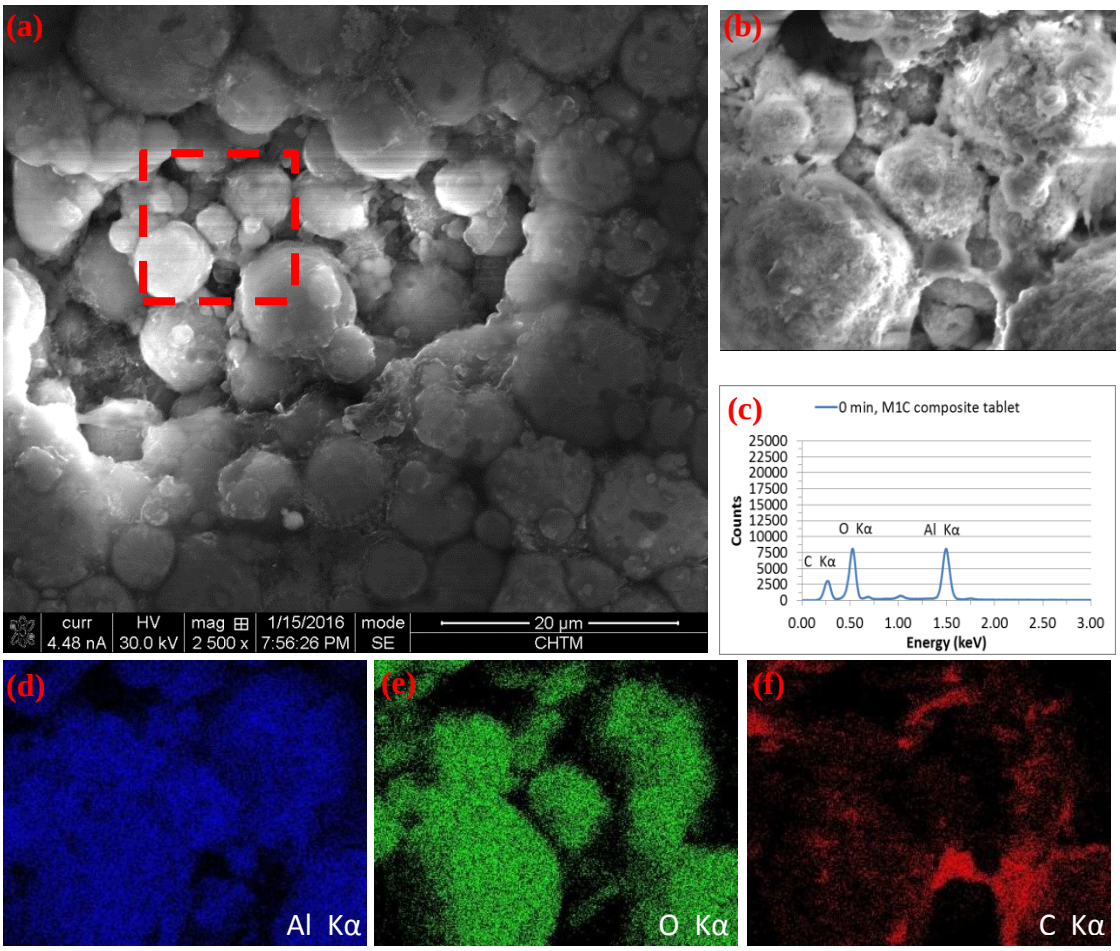

Figure 6-6: (a) SEM micrograph of M1C composite surface showing surface pore and noticeable Al particle boundaries. (b) Magnified image region of marked rectangle in (a) and x-ray map capture region. Magnification is 12000X, accelerating voltage is 5 keV and beam current is 852 pA. (c) X-ray spectra generated by capture region in (b).

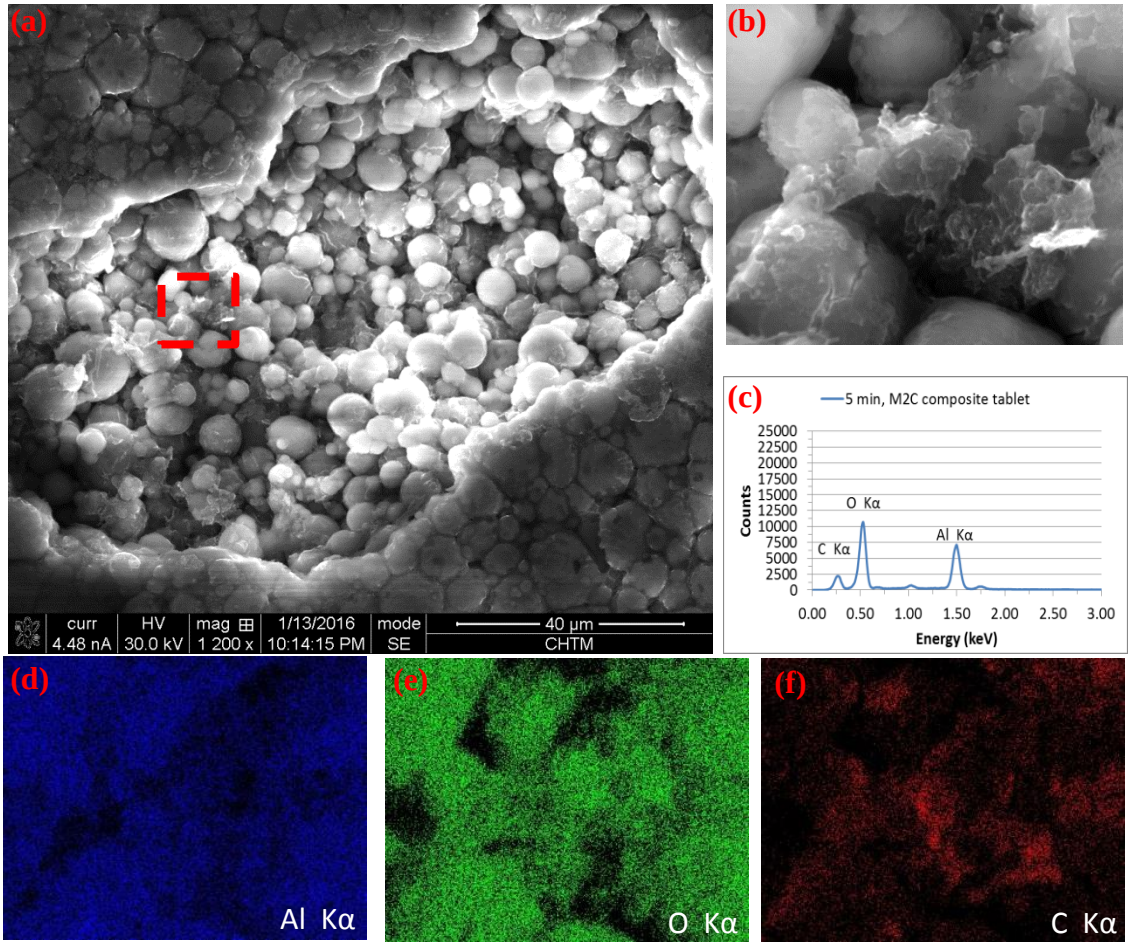

Figure 6-7: (a) SEM micrograph of M2C composite surface showing surface pore and noticeable Al particle boundaries. (b) Magnified image region of marked rectangle in (a) and x-ray map capture region. Magnification is 12000X, accelerating voltage is 5 keV and beam current is 852 pA. (c) X-ray spectra generated by capture region in (b).

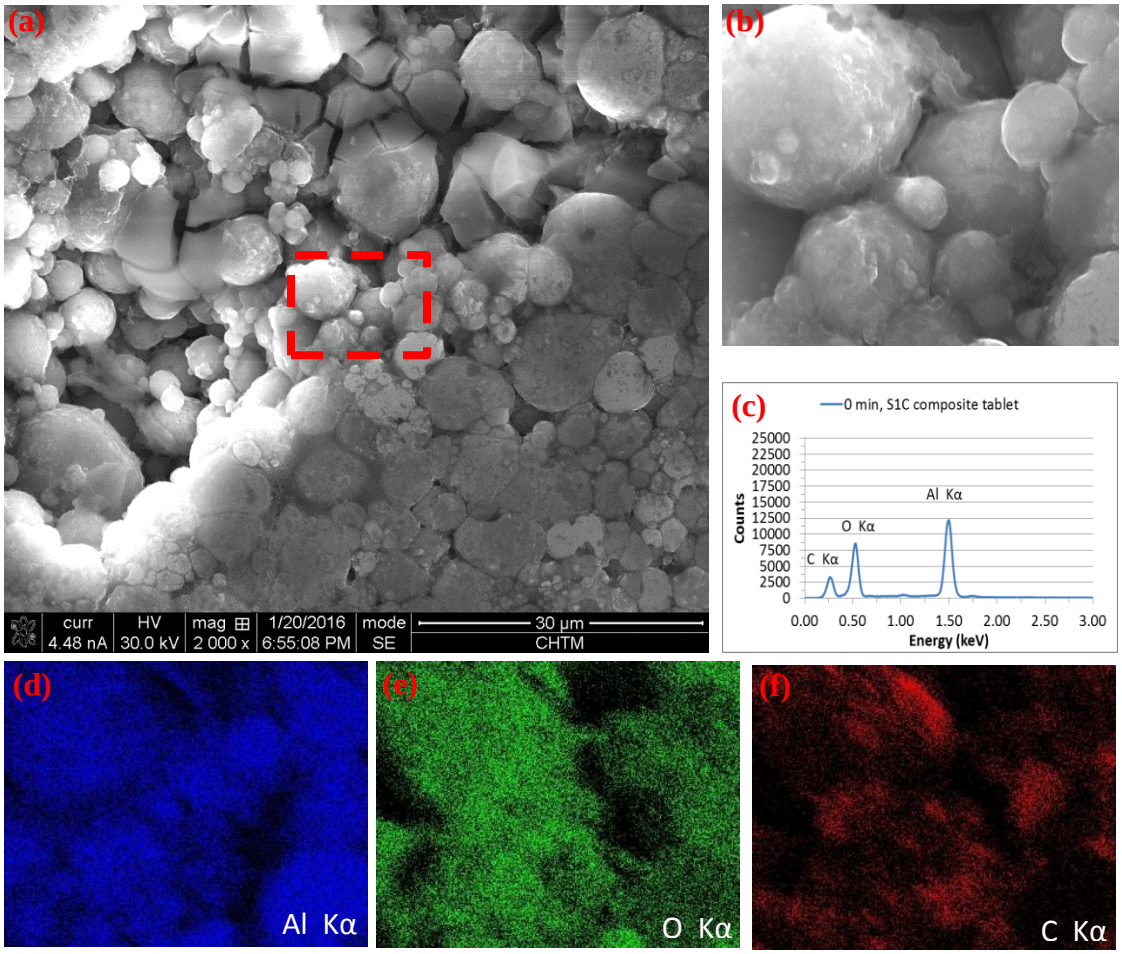

Figure 6-8: (a) SEM micrograph of S1C composite surface showing surface pore and noticeable Al particle boundaries. (b) Magnified image region of marked rectangle in (a) and x-ray map capture region. Magnification is 12000X, accelerating voltage is 5 keV and beam current is 852 pA. (c) X-ray spectra generated by capture region in (b).

6.4 Composite Elastic Properties Determination

Determining elastic constants (Young's modulus and Poisson's ratio) via mechanical testing techniques requires specimens that have been carefully machined (and or fabricated) to fit the specifications of the tensile testing apparatus while adhering to ASTM standards. Mechanical testing, such as tension or compression, is considered a highly destructive testing technique which requires significant investment in equipment and training. Powder metallurgy (PM) compacts are inherently porous materials with characteristic density gradients which make fabricating components to ASTM standards very difficult. Typically PM components are relatively small in nature and cylindrical in shape to minimize density gradients and maximize ease of fabrication. Taking the above into account and do the geometry of samples evaluated in this study, elastic properties of Al/CNT composites are determined using contact ultrasonic techniques. This non-destructive ultrasonic technique has been widely used in industry for the detection of flaws or cracks in structural components, is inexpensive and highly portable [163]. Ultrasonic techniques have also been used by a wide range of researchers to assess the microstructure and material properties of PM compacts under various conditions [164-170]. To the authors knowledge this testing technique has not been reported in literature in the determination of elastic moduli of CNT-metallic composites fabricated via powder metallurgy techniques. Acoustic measurements of Al/CNT composites were performed at Sandia National Laboratories (Electronic, Optic and Nanomaterials Department) under the direction of Dr. Pin Yang. Elastic properties of Al/CNT composites was carried out using the 'pulse-echo" method with ultrasonic pulses provided by Olympus© piezoelectric 5 MHz normal and shear wave transducers. During testing the

piezoelectric transducers produce ultrasonic pulses which propagate through the sintered PM compact as longitudinal/transverse elastic waves (Fig. 6-9). The transducers are also capable of detecting echoes generated off the front and back of Al/CNT composite tablet surfaces. After propagation through the composite tablets, output signals from the transducers are displayed on a PC using a custom oscilloscope/data analysis LabView virtual instrument (VI). For these measurements common table honey was chosen as the viscous couplant.

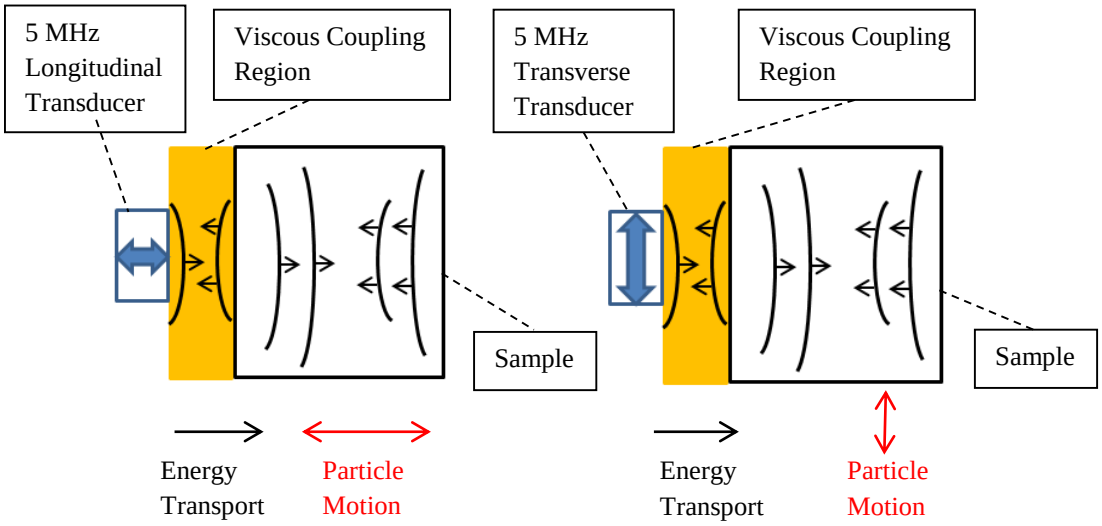

Figure 6-9: Diagram of ultrasonic testing setups. Ultrasonic wave fronts schematically illustrated. Note: for illustrative purposes viscous coupling region is exaggerated.

The first pulse recorded is the echo generated off the viscous coupling/tablet interface. The second pulse, which corresponds to the echo generated off the back free surface of the tablet, arrives later in time than the first pulse. The difference, Δt, between the arrival time of the first and second pulse is the ultrasonic time of flight through the composite tablet. Fig. 6-10 shows an actual trace take from a measurement.

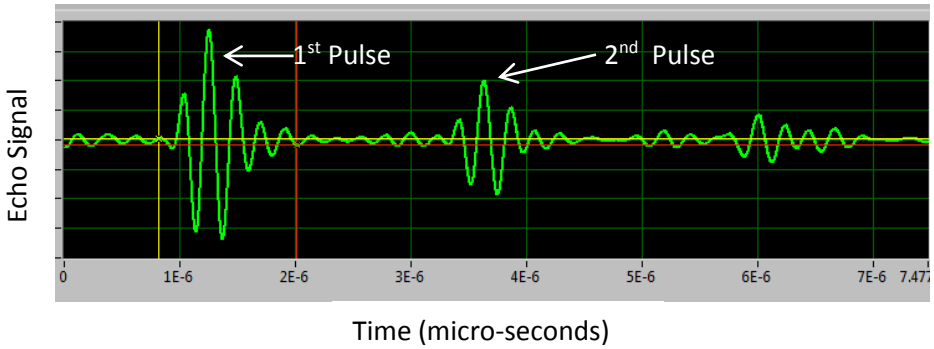

Figure 6-10: Ultrasonic trace recorded during testing.

Knowledge of transit times along the cylindrical tablet axis (energy transport direction) and tablet height allow the determination of longitudinal/transverse velocities by the following equations:

$$V_L = \frac{2x}{(\Delta t)_l}, V_T = \frac{2x}{(\Delta t)_t} \tag{6-3}$$

Where x is the tablet height, V_L is the longitudinal velocity, V_T is the transverse velocity, and Δt is the time of flight. The subscripts on Δt denote time of flights measured using either longitudinal (l) or transverse (t) transducers. With precise knowledge of transverse and longitudinal velocities longitudinal Poisson's ratio is calculated using:

$$\nu = \frac{1-2(\frac{V_T}{V_L})^2}{2-2(\frac{V_T}{V_L})^2}. \tag{6-4}$$

Knowing the tablet density (ρ) one can now calculate Young's (E) and Shear (G) moduli using the following sets of equations:

$$E = \frac{V_L^2 \rho(1+\upsilon)(1-2\upsilon)}{(1-\upsilon)}, \; G = V_T^2 \rho. \tag{6-5}$$

Bulk modulus (B) is then calculated using:

$$B = (V_L^2\rho - 2G) + \frac{2}{3}G. \quad (6\text{-}6)$$

To determine room temperature elastic moduli three samples at each composition were measured with averages reported. Pure cast aluminum and aluminum powder- PM samples were are also measured and reported for comparative purposes.

For the nanocomposites fabricated in this study, bulk elastic properties will be largely dictated by: resultant composite microstructure due to processing, state/quality of carbon nanotube (CNT) dispersion, and solid phase material properties. Nanotubes of varying geometry (Table 6-1) are used to investigate their effectiveness as reinforcing agents in soft Al matrix and their susceptibility to CNT dispersion routes designed in this study. The elastic properties of single/multi- walled CNTs (SWCNT/MWCNTs) are reported to depend on: chirality, tube diameter, number of shells, length, and inter-shell distance [171-172]. In their investigation into the buckling behavior of MWCNTs using molecular dynamics simulations, Zhang et al. showed that MWCNTs with large differences between the diameters of the inner and outermost tubes, the tubes do not buckle simultaneously. Conversely, if there is a relatively small difference between the diameters of the inner and outermost tubes, the tubes will buckle simultaneously [171]. This is because at relatively small differences between outer/inner most tube diameters, Van der Waal interactions become important. In their study it was also shown that given a constant inner/outer tube diameter and the number of shells present elastic moduli and buckling strain can vary appreciably [171]. In the evaluation of the elastic properties of CNT composites using finite element techniques, Joshi et. al showed that MWCNT composites provide better values of stiffness in compressive loading as compared to tensile loading [172]. Under tensile loading, slippage occurs between adjacent walls of

MWCNTs and inter-layer Van Der Waal forces are not strong enough to transfer load efficiently to inner tubes [172]. Under compressive loading MWCNTs are superior to their SWCNTs counterparts, load is transferred through buckling and bent sections of the nanotubes [172]. Sizes of nanotubes also play an important role in their strengthening capabilities as CNTs with larger aspect ratio will assist greater load transfer and hence efficient utilization of reinforcement.

Residual porosity which is inherent in powder metallurgy (PM) compacts, if not properly controlled, can have detrimental effects on resultant microstructure and mechanical performances upon completion of processing. One method researchers use to control resultant porosity is by carefully choosing metal particle size, microstructure, and morphology [173]. In the case of metal-CNT composites, fabricated via PM techniques, if not adequately exfoliated, large CNT clusters can impede densification processes resulting in porous compacts. It has been well documented in literature that for porous powder compacts porosity content, pore morphology, pore distribution and degree of interconnectedness all act to affect bulk elastic properties [165,175-176]. In one study it was shown that low/high porosity regimes in powder metallurgy compacts exhibit different elastic behavior [174]. This was attributed to low porosity compacts characterized by small spherical and isolated pores; whereas, high porosity compacts are characterized by clustered, irregular pores with a high degree of interconnectedness [174]. Variations in pore structure can cause anisotropy in elastic properties of powder compacts. The aforementioned porosity characteristics can also have profound effects on elastic waves propagating through the composite material which affects precise determination of bulk composite elastic properties [165]. As discussed above, a common

method for the determination of elastic properties of solids is via acoustic measurements. Using this measurement technique, a piezoelectric transducer produces ultrasonic waves which propagate elastically through the solid material of interest. Its energy is absorbed in the material by solid and gaseous phases present. Two relevant modes by which this can happen are by: ultrasonic waves displacing air between connected pores, thermal elastic damping and direct mechanical damping in the material itself. In their study, Asamani et al. concluded that connected pores can induce dispersion phenomena of ultrasonic waves requiring a more complex treatment of acoustic data [164]. In their study they also showed that ultrasonic waves transmitted along the pressing direction (longitudinal) are more sensitive to porosity than transverse waves. For the cases of nanocomposites reinforced with CNTs, as CNT clusters become exfoliated porosity content decreases; this acts to increase ultrasonic wave velocities and hence elastic properties. It is reasonable to conceive that CNT clusters trapped in pores can act as porous absorbers due to their low density and tubular structures. Improvements in Poisson's ratio (ν) for Al/CNT composites are uncertain at this time as ν of SWCNTs/MWCNTs reported in literature is quite scattered (Fig.6-11).

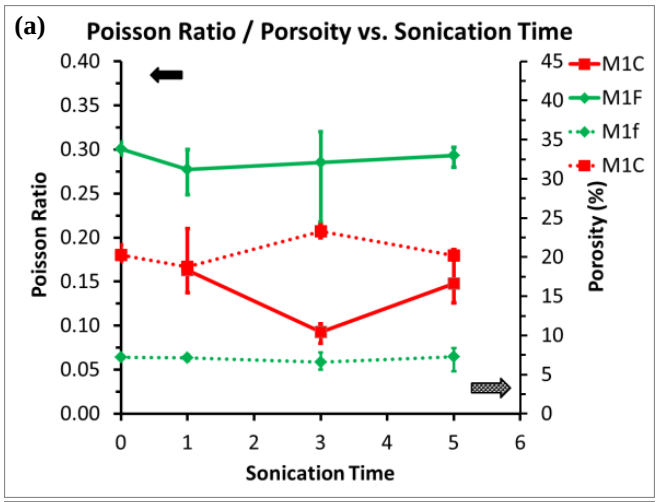

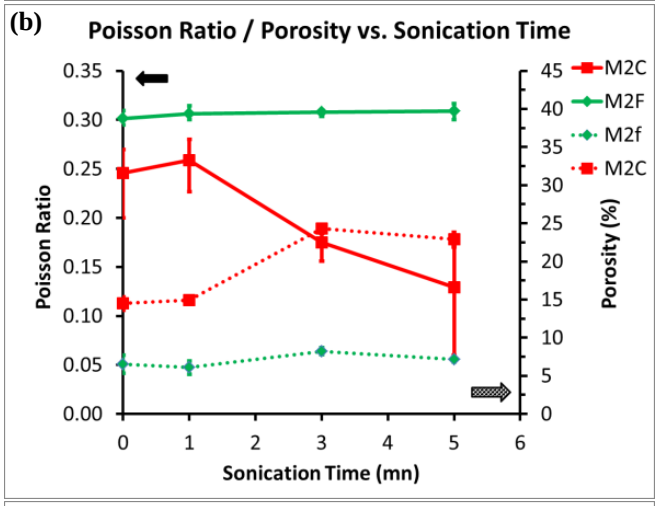

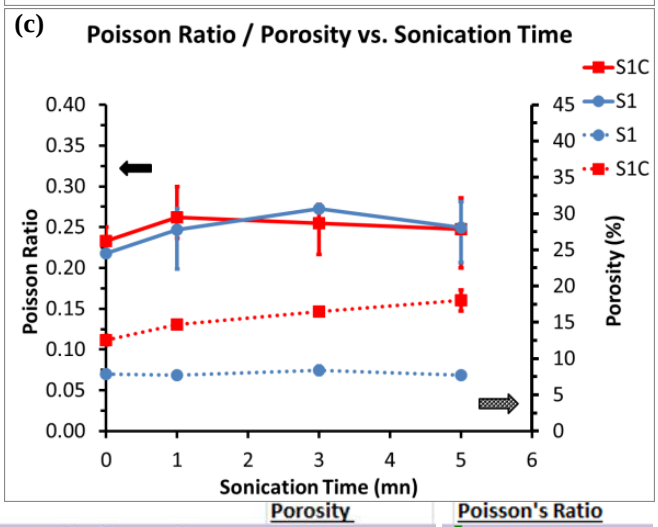

	Porosity	Poisson's Ratio
Pure Aluminum - Literature	*NA*	*0.35*
Pure Aluminum - Cast	*0*	*0.31 ± 0.05/0.05*
Pure Aluminum - PM	*7.33 ± 0.44/0.63*	*0.34 ± 0.01/0.01*

Figure 6-11: Poisson ratio/porosity vs. sonication time. (a) M1C, M1f. (b) M2C, M2f . (c) S1C, S1. Note: Left y-axis corresponds to Poisson's ratio values (solid data lines) and right y-axis corresponds to porosity values (dotted data lines).

Using an improved molecular structural model Zhao et al. computed ν for SWCNTs of varying morphology and compared with other published data [170]. The authors of this study reported values ranging from 0.18-0.23 for SWCNTs; compared to values in literature ranging from 0.06-0.55 using various experimental/computational analysis approaches. Likewise, for MWCNTs, using molecular dynamics simulations Zhang et al. reported values ranging from 0.17- 0.37 [171]. What are the correct values of ν for SWCNTs/MWCNTs of varying geometry and chirality? It seems as if these questions have not been fully addressed yet.

For most Al/CNT fabrication routes implemented in this study, ν of nanocomposites follows the same qualitative pattern, as porosity content increases/decreases ν decreases/increases (Fig. 6-11). Quantitatively, ν can vary drastically depending on type of dispersion technique implemented and nanotube character. Together the data in Fig. 6-11 for nanocomposites reinforced with CNTs dispersed using shear mixing techniques (S1C, M1C, M2C) suggest ν at high porosity is attributable to pore character and insensitive to solid phase material properties. It is suggested that the bulk elastic response is due to localized Poisson effects and poor deformation transfer throughout the composite. For high porosity cases (S1C, M1C, M2C) inter particle contact regions are relatively small and well separated. Under these conditions lateral strains (resulting from local normal strains) in the Al matrix have a greater likelihood of intruding into pore space. Therefore residual pores act to attenuate lateral strains thus preventing adjacent solid phase material from being strained and efficient deformation transfer through the bulk. These localized Poisson effects due to high porosity content act to suppress the solid phase material properties and or CNT strengthening effects. For the cases of Al

reinforced with functionalized CNTs (M1f, M2f) composite porosity is insensitive to increased ultrasonication and ν remains constant (Fig. 6-11(a-b)). Compared to the previously discussed cases, the available pore space to 'absorb' lateral local deformation is greatly reduced as MWCNT clusters become increasingly exfoliated. With decreased porosity, greater inter particle contact regions are formed and relatively close together; this enables more of the Al matrix material to be involved in the strain transfer process throughout the bulk of the composite. In these cases improved structural connections are achieved throughout the Al matrix as MWCNT clusters are further exfoliated increasing strain transfer processes, and, as this occurs solid phase elastic properties take on a more dominant role in composite strengthening. For both M1f/M2f cases ν remains constant for increased sonication durations and is equivalent to pure cast aluminum tested in this study (Fig. 6-11). For nanocomposites prepared with SWCNTs that have been dispersed via surfactants followed by shear mixing (S1) low relative porosities are obtained compared to S1C, however, no apparent increase in ν is reported. In order to gain insight into this departure in material behavior form the previous cases (M1C, M1f, M2C, and M2f) it is helpful to observe the axial/radial (longitudinal/transverse) velocities of elastic wave propagation in the nanocomposites for all cases (Fig. 6-12).

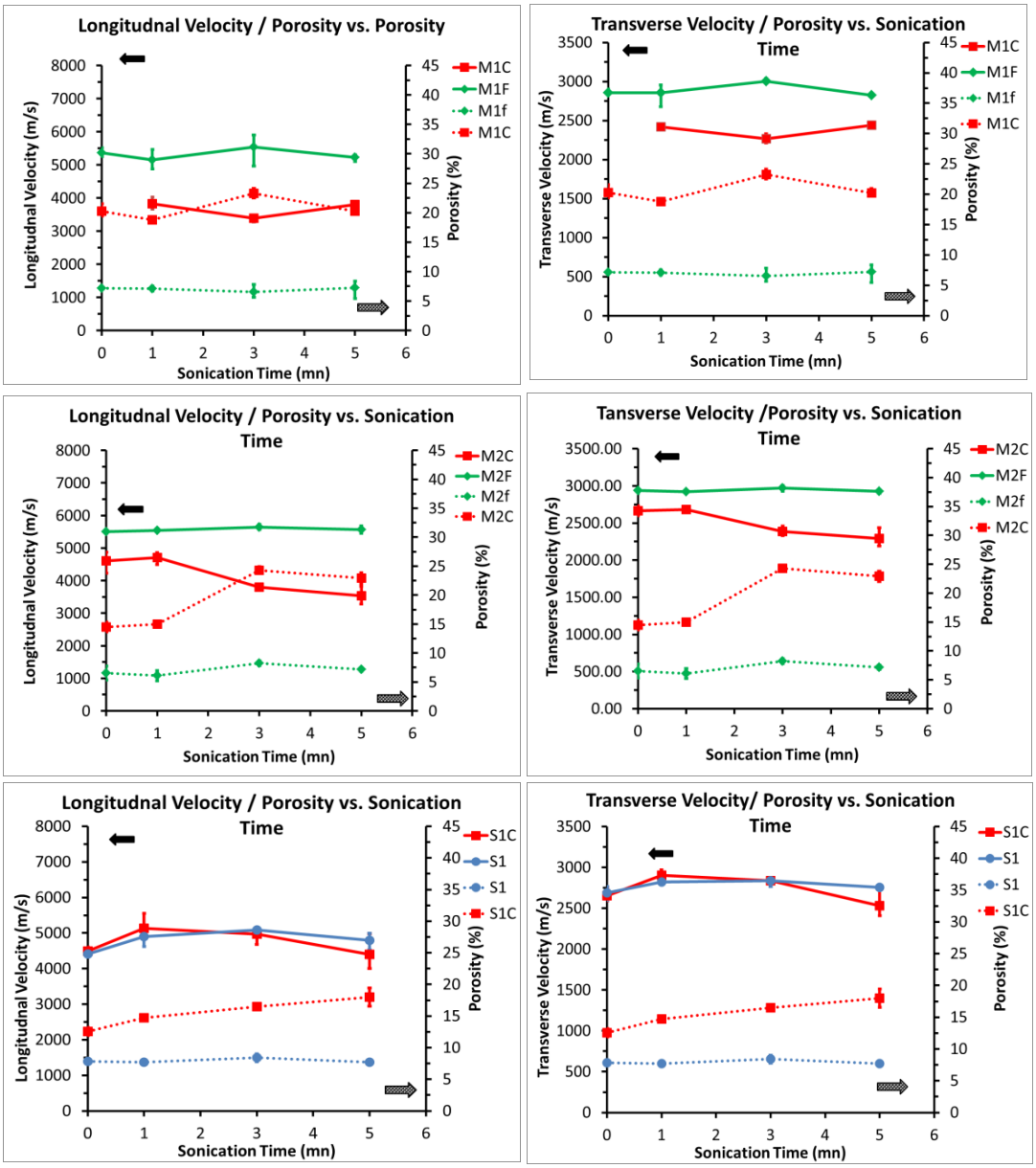

	Porosity	Longitudnal Velocity (m/s)	Transverse Velocity (m/s)
Pure Aluminum - Literature	*NA*	*NA*	*NA*
Pure Aluminum - Cast	*0*	*6774.54*	*3187.82*
Pure Aluminum - PM	*7.33 ± 0.44/0.63*	*6380.28 ± 4.49/2.25*	*3159.55 ± 6.06/5.51*

Figure 6-12: Longitudinal (axial) and transverse (radial) elastic wave velocities for nanocomposites. Note: Left y-axis corresponds to velocity values (solid data lines) and right y-axis corresponds to porosity values (dotted data lines).

For all cases in this study the longitudinal velocities are typically ~ 2X that of the transverse velocities. This can be due to inherent pore anisotropy in the powder metallurgy compacts and has been reported in literature [165]. Pores in planes parallel to the cylindrical sample axis are elongated compared to pores in planes that are orthogonal to the axis (Fig. 6-13). Qualitatively, for nanocomposites reinforced with MWCNTs, as porosity content increases there is a corresponding drop in transverse/longitudinal velocities. Interestingly, for the cases of nanocomposites containing SWCNTs there exist no quantitative differences in longitudinal/transverse velocities between S1C and S1 groups given appreciable differences in porosity content. This leads to the hypothesis that the observed phenomenon is due to differences in pore morphology, distribution and or connectivity for S1C/S1 cases. For S1C shear mixing is not sufficient enough to exfoliate SWCNT clusters; this acts to greatly inhibit the densification process during consolidation phase and can result in relatively large pores with good connectivity. As opposed to closed pores, connected pores allow movement of air which results in viscous loss and thermal damping effects which help to dissipate ultrasonic waves. This can affect composite mechanical properties and their determination via acoustic measurements.

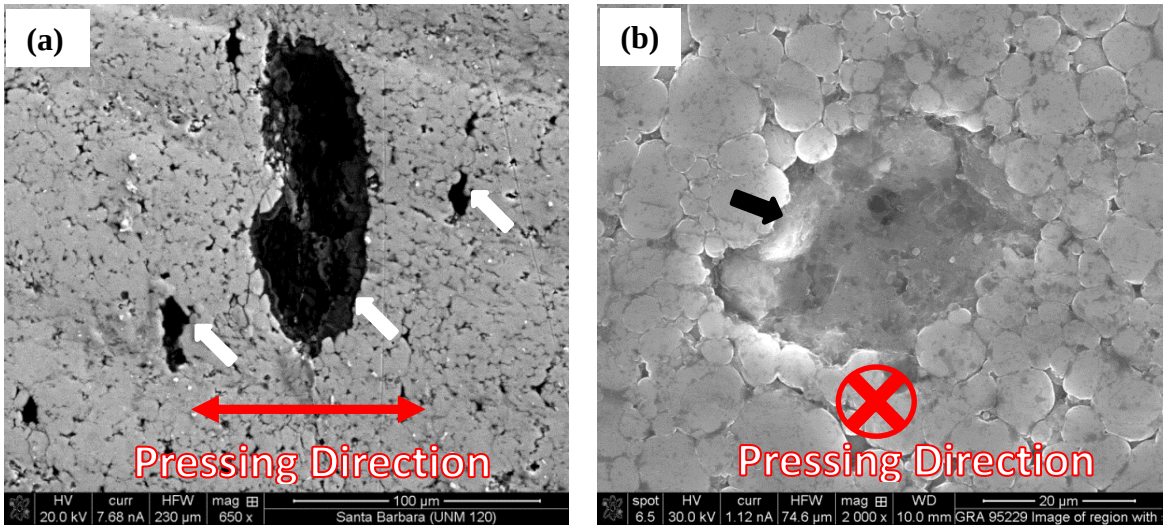

Figure 6-13: Composite tablet, M1- 5 min sonication time. (a) Polished cross section parallel to tablet axis. White arrows indicate elongated pores in planes parallel to tablet axis (pressing direction). (b) Surface perpendicular to tablet axis. Black arrows indicate circular pores in planes perpendicular to tablet axis.

It should be noted that in this study elastic properties for M1-group, M2-group, and M1C (0 min ultrasonication) were not attainable upon multiple measurements for multiple samples of the same composition. This is due to delamination cracks in the nanocomposites as brought about by fabrication processes (Fig. 6-14). As discussed above, these long cracks (elongated pores), which are sub – millimeters in dimension act to severely attenuate ultrasonic waves and thus prevent measurements of elastic properties. In Fig. 6-14 it is believed that these large delamination cracks may also behave as free surfaces which can distort transit time and velocity measurements of ultrasonic waves propagating through the bulk composites.

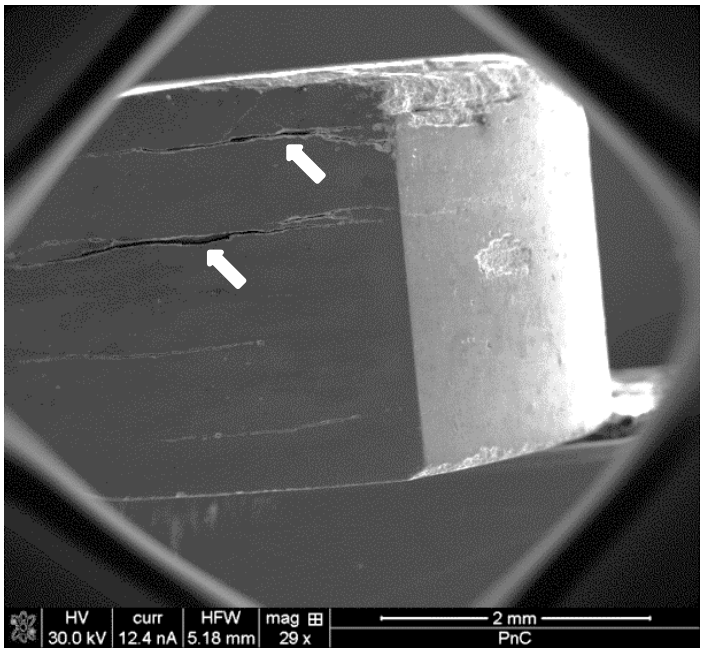

Figure 6-14: SEM micrograph of ground cross section parallel to cylindrical tablet axis, M1 (5 min sonication). White arrows indicate delamination

Reported in an earlier study by the authors, the state and quality of CNT dispersion in the starting composite mixture is crucial to take advantage of subsequent consolidation/thermal processing procedures in the PM route [159]. Young's modulus (E) ,shear modulus (G), and bulk modulus (B) values reported in this study (Fig. 6-15) for nanocomposites fall below solid phase material and control sample values. However, the reported data trends show that CNT dispersion routes can have profound effects on the resultant nanocomposite microstructure and bulk elastic properties. For no ultrasonication time (0 min), S1C exhibits a 60.4 % increase in porosity content over S1 while elastic moduli remains relatively unchanged for both groups (Fig. 6-15 (g-h)). In a study by Huang et al. it was shown that subsequent shear mixing (magnetic stirring as in the case of this study) after obtaining a well dispersed CNT suspension can accelerate the re-agglomeration process in the absence of a stabilizing agent [178].

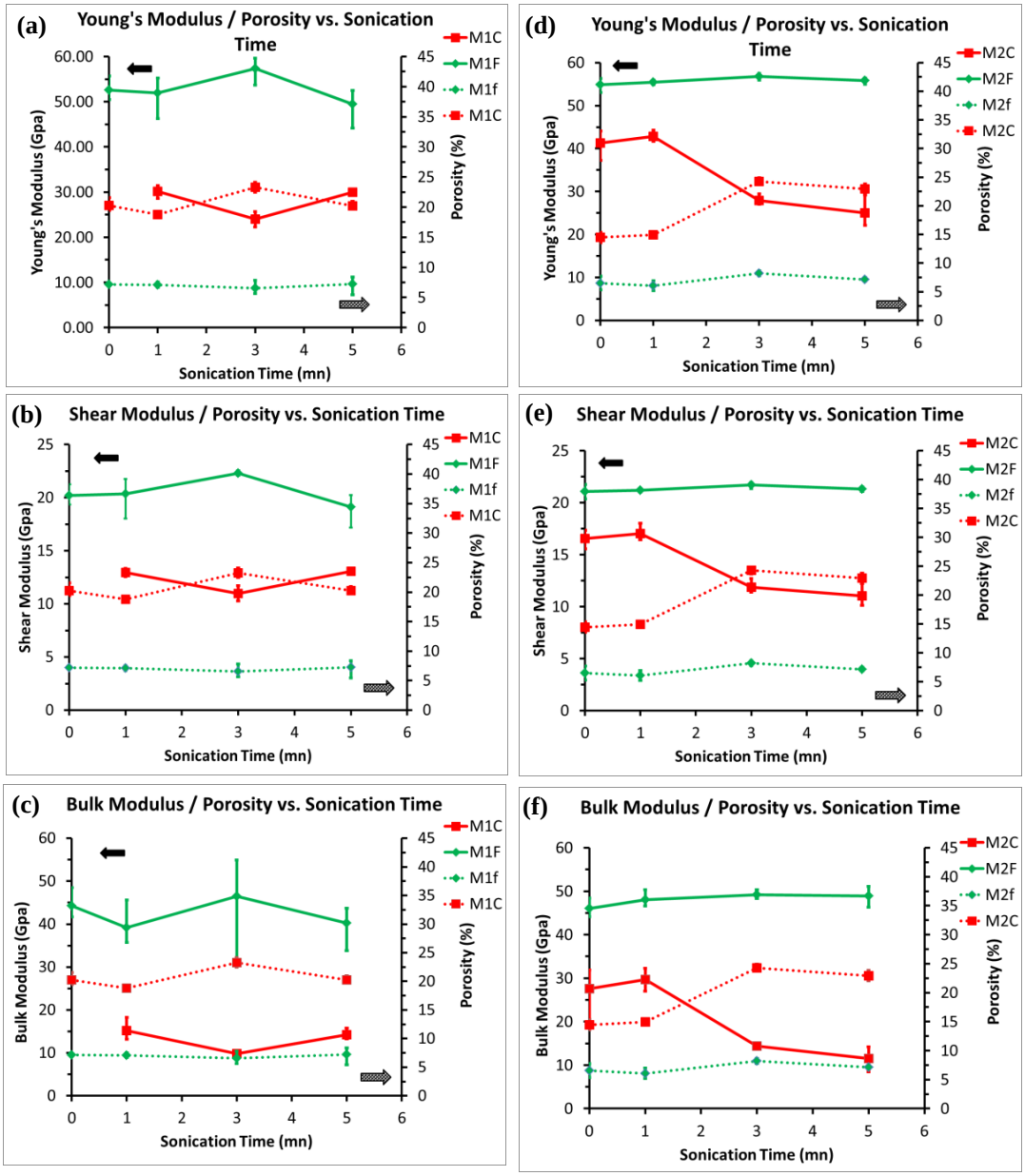

	Porosity	Hardness	Poisson's Ratio
Pure Aluminum - Literature	NA	NA	0.35
Pure Aluminum - Cast	0	NA	0.31 ± 0.05/0.05
Pure Aluminum - PM	7.33 ± 0.44/0.63	12.4 ± 2.4	0.34 ± 0.01/0.01

	Young's Modulus (Gpa)	Shear Modulus (Gpa)	Bulk Modulus (Gpa)
Pure Aluminum - Literature	70	26	76
Pure Aluminum - Cast	71.23 ± 1.71/1.71	25.6 ± 1.60/1.60	81.48 ± 1 4.78/14.78
Pure Aluminum - PM	64.55 ± 2.92/3.51	23.97 ± 0.10/0.09	70.03 ± 0.26/0.20

Figure 6-15: Elastic moduli (E,G,B): (a-c) M1 group and (d-f) M2 group. Note: Left y-axis corresponds to elastic moduli values (solid data lines) and right y-axis corresponds to porosity values (dotted data lines).

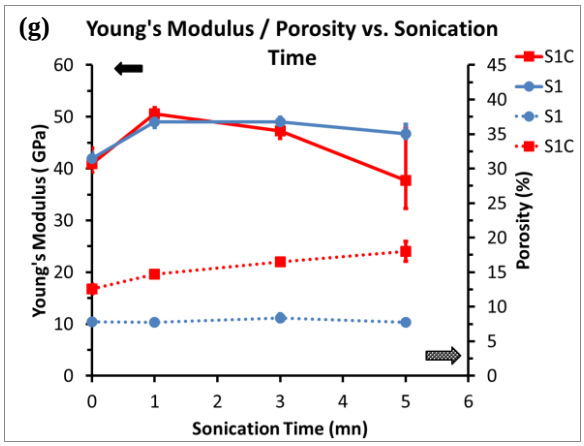

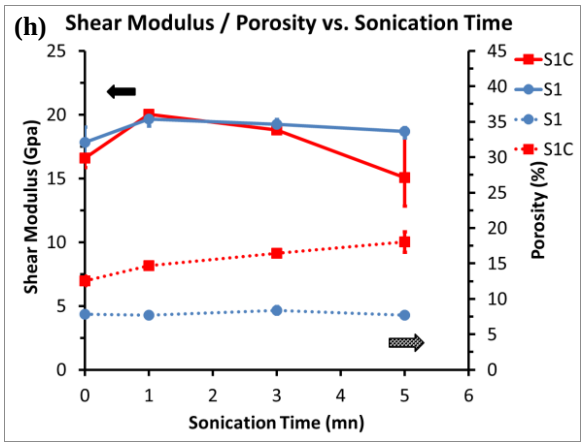

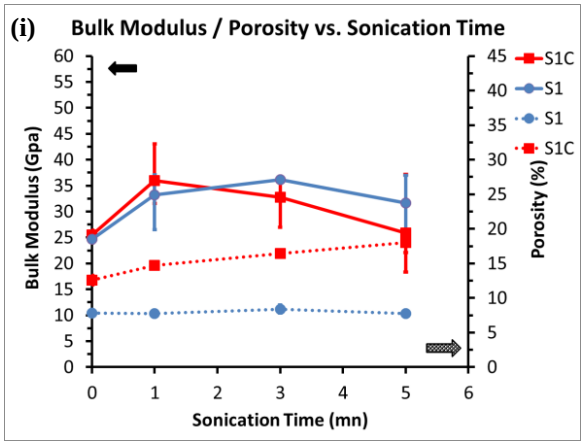

	Porosity	Hardness	Poisson's Ratio
Pure Aluminum - Literature	NA	NA	0.35
Pure Aluminum - Cast	0	NA	0.31 ± 0.05/0.05
Pure Aluminum - PM	7.33 ± 0.44/0.63	12.4 ± 2.4	0.34 ± 0.01/0.01

	Young's Modulus (Gpa)	Shear Modulus (Gpa)	Bulk Modulus (Gpa)
Pure Aluminum - Literature	70	26	76
Pure Aluminum - Cast	71.23 ± 1.71/1.71	25.6 ± 1.60/1.60	81.48 ± 1 4.78/14.78
Pure Aluminum - PM	64.55 ± 2.92/3.51	23.97 ± 0.10/0.09	70.03 ± 0.26/0.20

Figure 6-15: Elastic moduli (E,G,B): (g-i) S1 group. Note: Left y-axis corresponds to elastic moduli values (solid data lines) and right y-axis corresponds to porosity values (dotted data lines).

In this study surfactant assisted dispersion plays an important role in preventing isolated SWCNTs from re-agglomerating into larger clusters during subsequent magnetic stirring (shear mixing) with Al powders. This was discussed in an earlier published study and is attributed to dipole-dipole electrostatic interactions occurring at surfactant head groups which are able to overcome Vander Waals interactions responsible for CNT agglomeration [159]. For S1group 1 minute sonication duration is beneficial at breaking up large SWCNT clusters while reducing porosity content in the nanocomposite remains constant. The accompanying increase in elastic moduli is attributed to SWCNT strengthening and to a much lesser extent geometric hardening. For S1 group as sonication time increases there is no change in porosity content and elastic moduli remain constant. The sonication power (240 W) used in this study maybe not be energetic enough to exfoliate the unique SWCNT aggregates; SWCNTs tend to form tightly packed parallel bundles, whereas thicker MWCNTs form cross meshed bundles [178]. In powder form, raw SWCNTs are composed of a hierarchal structure of different morphologies as seen in Fig.6-15(a). Large micron sized clusters are composed of smaller sub-micron sized clusters (Fig. 6-16(a)). The S1 dispersion route is effective at exfoliating larger clusters into smaller ones (Fig. 6-16(b)) and into individual tubes. However, sub-micron tightly packed SWCNT bundles are not exfoliated completely and can become easily imbedded in large pores of the resulting Al/SWCNT composite (Fig. 6-16(c-d)). Individual SWCNTs which are highly entangled in these sub-micron clusters, which in turn are located in pores, do not contribute to strengthening of the Al matrix.

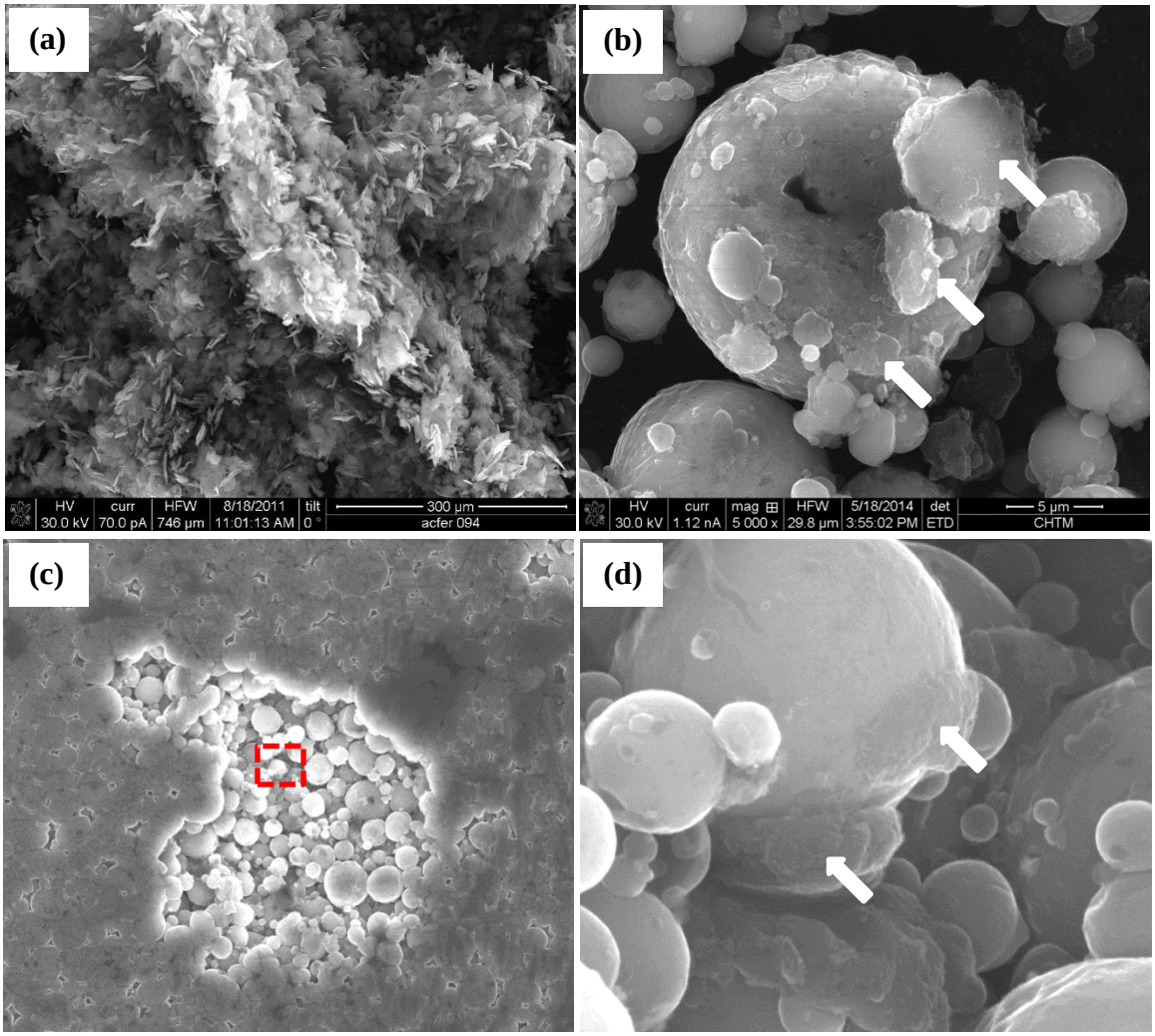

Figure 6-16: (a) SWCNTs in powder form showing hierarchal structure. (b) Al/SWCNT composite mixture. (c) Surface pore Al/SWCNT composite tablet. (d) Magnified rectangular region in (c). White arrows indicate sub-micron sized SWCNT clusters.

In the case of 1 minute sonication time for S1C group there exists an initial increase in elastic moduli, comparable to S1, while porosity content has increased. As porosity content is increased one should expect a reduction in elastic properties of the nanocomposite, this is contrary to the observed data for S1C/M1C/M2C. This counterintuitive material behavior can be explained by the presence of aluminum oxide (Al_2O_3) growth on Al powder particle surfaces (Fig.6-17 through Fig. 6-19) during

nanocomposite processing which subsequently act as dispersion strengthening agents in processed composite tablets.

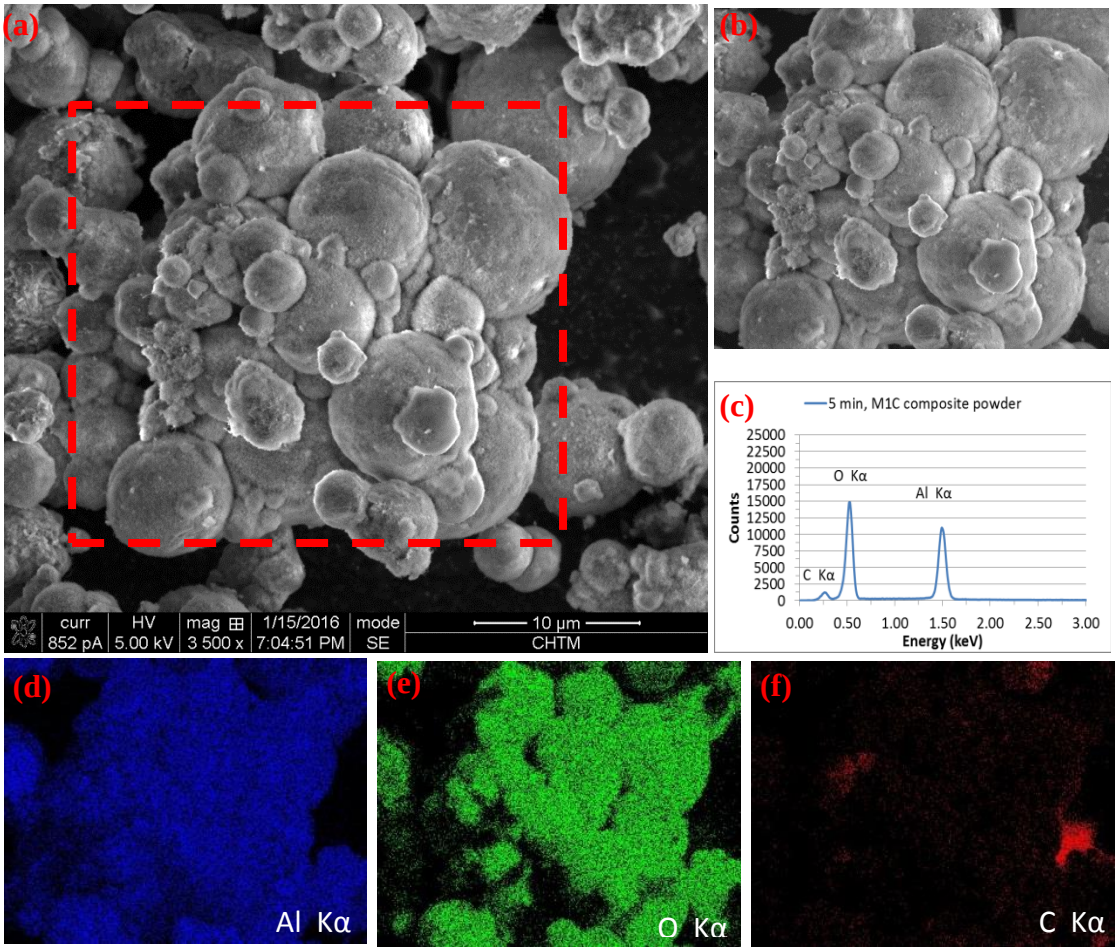

Figure 6-17: (a) SEM micrograph of M1C composite powder showing heavy oxidation. (b) Magnified image region of marked rectangle in (a) and x-ray map capture region. Magnification is 5000X, accelerating voltage is 5 keV and beam current is 852 pA. (c) X-ray spectra generated by capture region in (b). (d-f) Corresponding aluminum, oxygen, and carbon x-ray maps of region (b).

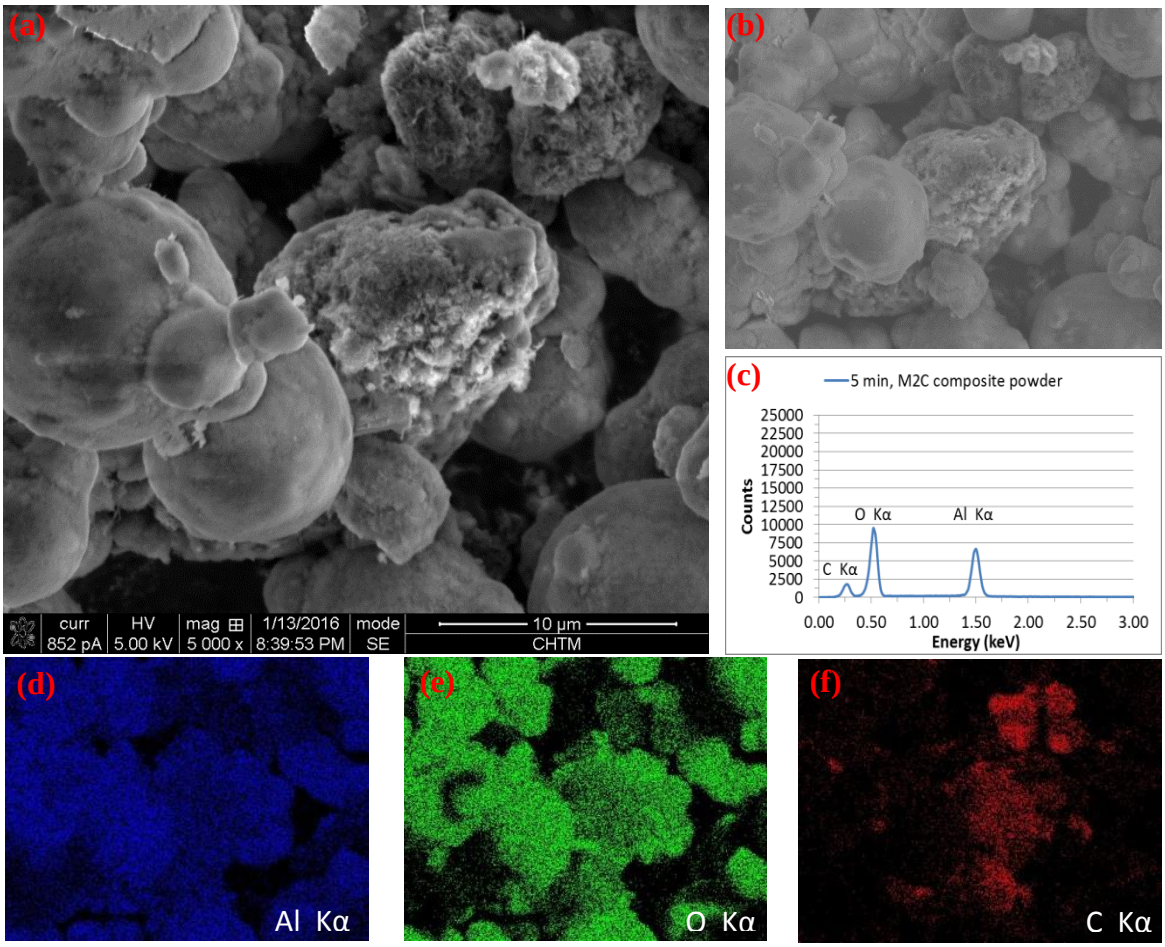

Figure 6-18: (a) SEM micrograph of M2C composite powder showing heavy oxidation. (b)X-ray map capture region. Magnification is 5000X, accelerating voltage is 5 keV and beam current is 852 pA. (c) X-ray spectra generated by capture region in (b). (d-f) Corresponding aluminum, oxygen, and carbon x-ray maps of region (b).

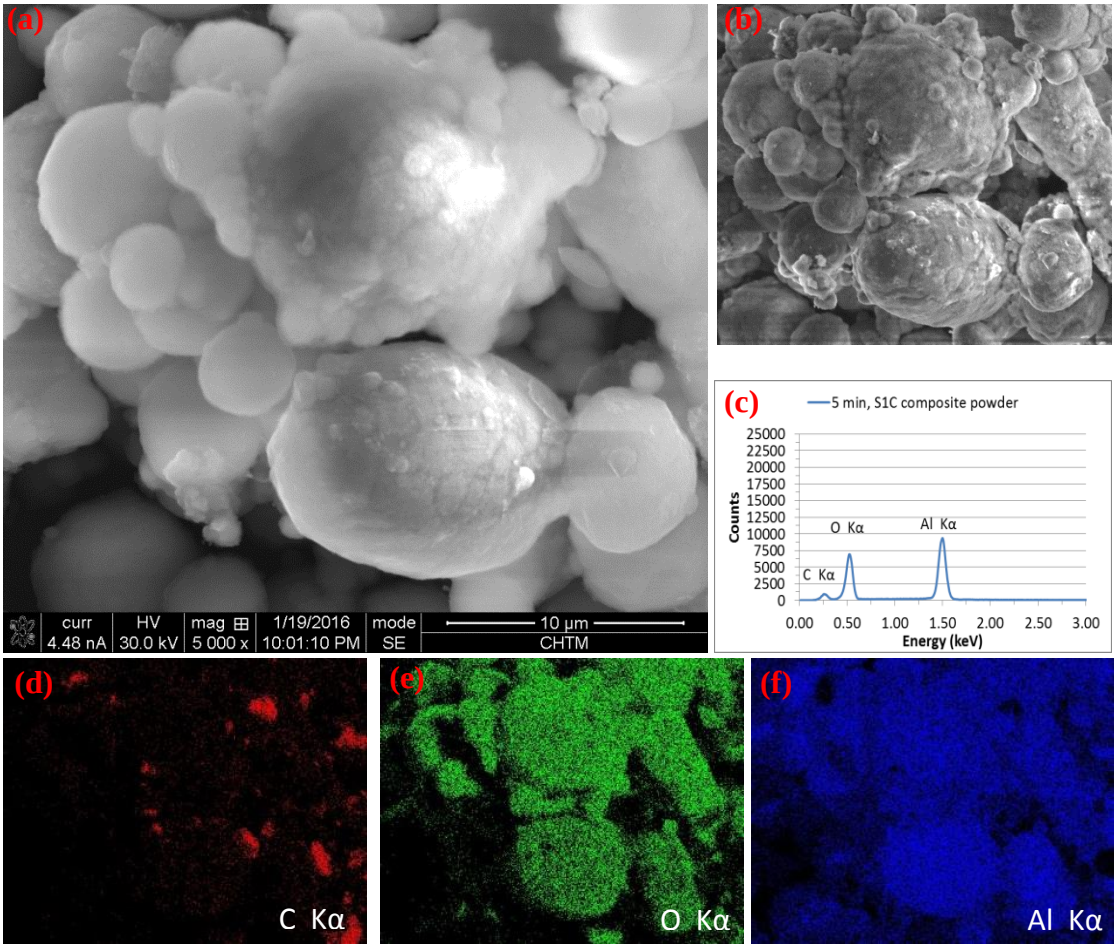

Figure 6-19: (a) SEM micrograph of S1C composite powder showing heavy oxidation. (b) X-ray map capture region. Magnification is 5000X, accelerating voltage is 5 keV and beam current is 852 pA. (c) X-ray spectra generated by capture region in (b). (d-f) Corresponding aluminum, oxygen, and carbon x-ray maps of region (b).

During compaction and thermal processing, fine particulates of Al_2O_3 present on Al powder surfaces can become embedded in inter particle contact regions. These very fine and tough Al_2O_3 particles if well dispersed can inhibit dislocation motion between adjacently welded Al granules increasing geometric stiffness of the bulk composite. Al_2O_3 dispersion strengthening in polycrystalline metals is a well-documented phenomena and in some studies it has been reported increases in E of sintered aluminum

powder due to Al_2O_3 dispersoids [179]. In this study, formation of oxide layers during curing phases of M1C, M2C, and S1C composite mixtures are believed to contribute to increases in mechanical properties. Fig. 6-3 through Fig.6-5 show EDS spectra for all cases in this study, spectra are acquired at 1200X magnification in order to encompass many particles. Spectra are acquired at an acceleration voltage of 5 keV and beam current of 0.85 nA. These parameters are chosen as such to limit the spatial resolution of the electron beam and to ensure x-rays are being generated from powder surfaces or within a minimal depth. For M1C, M2C, and S1C cases the presence of high oxygen peaks in x-ray spectra and maps (Fig.6-17 through Fig. 6-19) are indicative of oxide growth during curing phases of composite powders. For S1C/M1C/M2C it is believed that Al_2O_3 dispersoids embedded in inter-particle contact regions can act to increase stiffness of the bulk composite. For S1C it has already been shown that poor SWCNT dispersion patterns exist (Fig. 6-16) and SEM analysis did not reveal the existence of individual tubes on Al powder surfaces. Therefore, it is believed that Al_2O_3 particles are the main reinforcement agent. For S1C, as sonication time increases beyond 1 minute, there exists a monotonic increase in surface porosity and a steady decline in elastic properties (Fig. 6-15(g-h)). It is believed that in this regime, increases in porosity content acts to severely mitigate any gains from Al_2O_3 dispersion strengthening. For small inter particle contact regions at high porosity content, Al_2O_3 dispersoids can be detrimental to mechanical response of the bulk composite. Under applied stresses, fine Al_2O_3 particles trapped in inter particle contact regions can lead to stress intensification and plastic decohesion. In the case of S1 group, 1 minute ultrasonication duration is effective at further aiding surfactant assisted dispersion and there exists a 17%/10% increase in E/G

from 0 min- ultrasonication. As ultrasonication time increases porosity content and elastic moduli remain constant, this may indicate a lack of absorption sites on outer walls of SWCNTs and poor dispersion capability. For the S1 group it is believed by the authors that to some extent geometric hardening and individual SWCNTs are the main reinforcement agents as Fig. 6-20 exhibits a low presence of oxide growth Al powder particle surfaces.

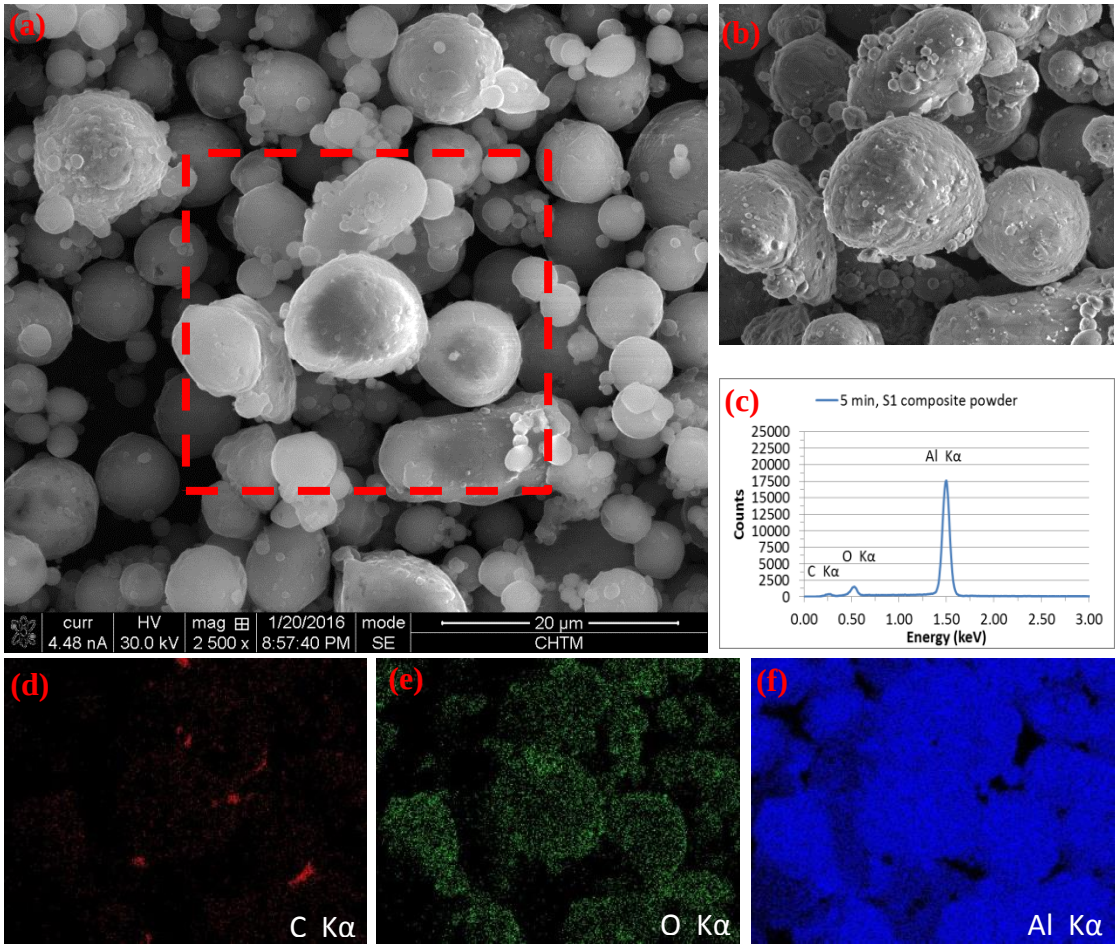

Figure 6-20: (a) SEM micrograph of S1 composite powder showing slight oxidation. (b) Magnified image region of marked rectangle in (a) and x-ray map capture region. Magnification is 5000X, accelerating voltage is 5 keV and beam current is 852 pA. (c) X-ray spectra generated by capture region in (b). (d-f) Corresponding aluminum, oxygen, and carbon x-ray maps of region (b).

The data in Fig. 6-15 (g-h) shows that sonication duration of 1 minute is the optimal, for both S1C and S1 cases; sonication times greater than 1 minute have no effect on increasing elastic properties. For the M1C group, the data is incomplete, as previously discussed, due to poor microstructure and delamination cracking elastic data for M1C – 0 minute ultrasonication time was unattainable. Fig. 6-15 (a-c) exhibits a concave character in elastic moduli with an accompanying convex character in porosity as sonication time increases. Given their high aspect ratio, $MWCNT_L$s dispersed solely using shear mixing techniques have a higher likelihood of re agglomerating compared to their smaller $MWCNT_S$s counterparts. It is believed by the authors of this study that the concave/convex nature of the elastic moduli/sonication time data in Fig. 6-15 (a-c) is attributed to magnetic stirring with Al powders. As previously discussed, combining Al powder with ultrasonicated aqueous surfactant MWCNT solutions via magnetic stirring, re agglomeration of individual MWCNTs is promoted with an associated decline in composite mechanical properties. In the case of M1f, when functionalization procedure is first applied followed by wet process, subsequent sonication does further promote dispersion of f-$MWCNT_L$s with an increase in elastic moduli. During the ultrasonication process individual f-$MWCNT_L$s are "unzipped" from larger clusters exposing absorption sites to free surfactants, which promote further dispersion and isolation of individual tubes. In the case of (M1f- 3 min ultrasonication time) porosity content is below that of PM-Al control sample by 10.3% with a corresponding drop of 14.0%/10.4% in E/G. SEM microscopy reveal the presence of individual tubes coating Al powder surfaces (Fig. 6-21), however, 6.6% residual porosity content in this case conceals any improvements in composite stiffness due to inclusion of individual MWCNTs. The

relatively high uncertainties in E values for M1f are due to regions in the nanocomposite void of MWCNTs and regions populated with individual tubes. For ultrasonication times > 3 minutes, porosity increases slightly with a corresponding decrease in elastic properties. Differences in elastic moduli between M1C/M1f groups are mainly attributed to differences in pore morphology, content, and its spatial distribution in the nanocomposites (Fig. 6-22(a-b)); which is directly related to state and quality of $MWCNT_L$ dispersion on Al powder surfaces in starting composite mixtures.

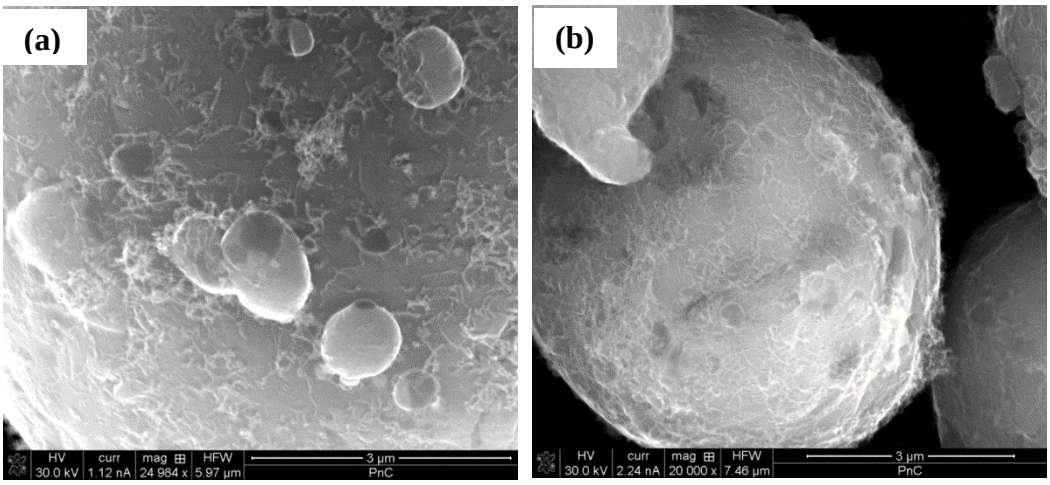

Figure 6-21: (a) M1f- 0 min sonication composite mixture. (b) M1f- 5 min sonication composite mixture.

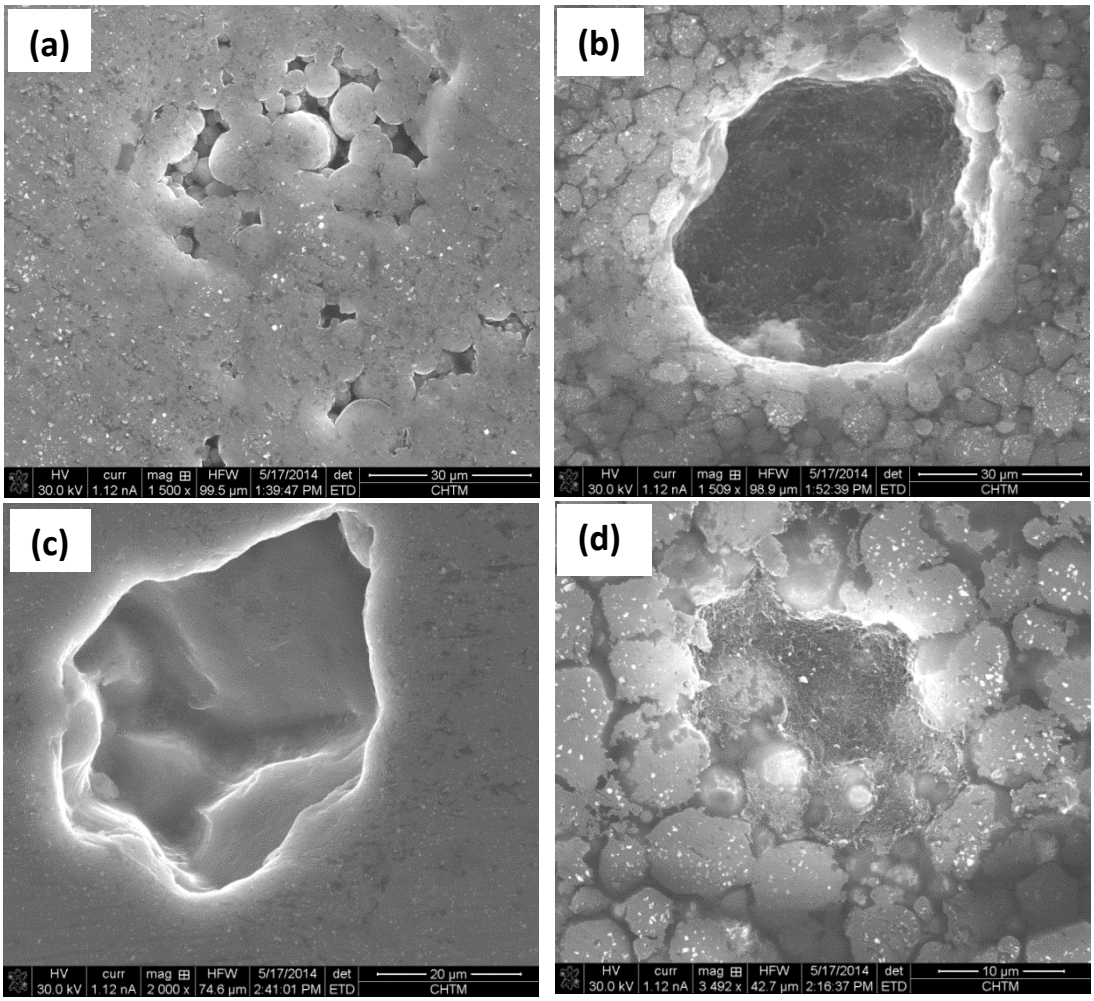

Figure 6-22: SEM micrographs of ground tablet surfaces: (a) M1f (5min sonication), (b) M1C (5min sonication), (c) M2f (5min sonication), (d) M2C (5min sonication).

As seen in Fig. 6-22, for ground composite surfaces, large MWCNT clusters severely inhibit densification of the composite mixture leading to poor microstructure, high porosity content, and a relatively high degree of pore connectivity in the sintered compact. While porosity content dictates the strength of a powder metallurgy compact, microscopic ductility can be influenced by the size distribution, orientation, interconnectedness, and degree of clustering of pores. In a study carried out by Hentschel et al. in the elastic properties (determined via acoustic techniques) of metal powders

during compaction it was found that pore morphology and connectivity can significantly modify surrounding mechanical fields [175]. In their study it was found that for a given porosity content, spherical isolated pores provided the stiffest bulk mechanical response whereas irregular shaped connected pores act to reduce bulk stiffness. In another study it was shown through microstructure-based FEM modeling of PM compacts that for porosity contents > 5% pores tend to be interconnected and highly clustered, resulting in significant strain localization in regions (ligaments) between pores . It was also shown that pore clusters can initiate plastic deformation due to localized stress intensity. Thus, a small section of the microstructure becomes plastically deformed, so that a large portion of the material remains un-deformed. For clustered pores, strain intensification at the sintered ligaments between pores can also serve as regions for crack initiation [175]. This can lead to the onset of crack initiation linking pores, which reduce the effective load bearing area locally, resulting in fracture. At higher densities, the pores were more spherical and more homogeneously distributed, resulting in a more homogeneous distribution of plastic strain over a larger fraction of material [181]. The reduction in bulk stiffness of M1C/M2C cases can be rationalized by considering the equivalent plastic-strain evolution in the microstructures shown in Fig. 6-22 and Fig. 6-23. In Fig. 6-23 SEM micrographs comparing tablet surfaces for M2C (0 minute sonication time) and M2f (1 minute sonication time) large surface pores (filled with MWCNT clusters) are unhomogeneously dispersed in Fig. 6-23 (a) which can lead to strain localization as discussed above. Whereas in the case of M2f (Fig. 6-23 (b)) large pores are not present on tablet surfaces which indicates good exfoliation of MWCNT clusters, resulting in more uniform plastic flow and an effective strain transfer medium.

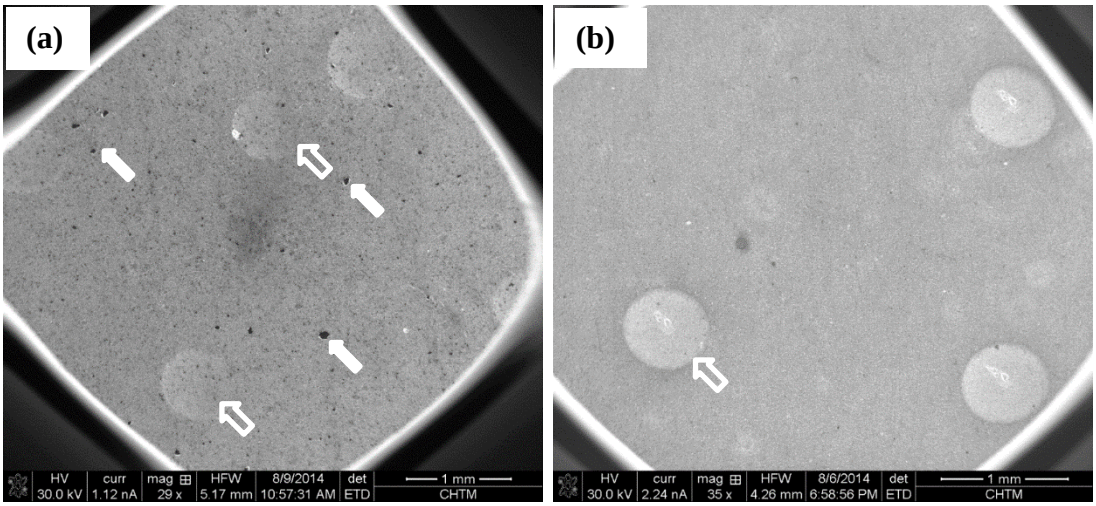

Figure 6-23: (a) M2C (0 min sonication) tablet surface. (b) M2f (1 min sonication) tablet surface. Solid white arrows indicate pores/MWCNT clusters and outlined white arrows indicate Rockwell hardness indentations.

These relatively large and connected pores (Fig. 22(b,d)) not only reduce geometric stiffness and structural integrity of the nanocomposite, but also induce dispersion phenomena of elastic waves necessitating a more robust interpretation of acoustic data. Whereas in Fig. 22 (a,c) the pores are small, irregular in shape, and well isolated. When the size of the pores is smaller than the wavelength of the propagating ultrasonic wave and pores are well isolated from one another, the damping capabilities are severely diminished. The low porosity content, pore morphology, and spatial distribution of pores in M1f/M2f composites all create an efficient strain transfer medium in the bulk composite increasing stiffness. Propagation of ultrasonic waves in PM compacts is also governed by the bonding between metal particles [166]. The quality of this bonding determines the degree to which ultrasound is delayed and attenuated in traversing inter-particle interfaces. Good bonding leads to high velocities and low attenuations, while poor bonding leads to low velocities and high attenuations [166].

For the M2C and M2f groups ultrasonication has no effects on further dispersing MWCNTs or its effectiveness is severely mitigated by subsequent magnetic stirring with Al powders. For initial sonication durations of less than 1 minute, no apparent change in porosity content is reported and elastic moduli remain unchanged in the case of M2C. For times greater than 1 minute the effectiveness of longer ultrasonication durations promotes re-agglomeration of MWCNTs into clusters as brought about by magnetic stirring. As in the case of M1C, the inclusion of MWCNTS clusters into the Al matrix severely degrade bulk elastic properties and result in poor microstructure (Fig. 6-22(c)). For M2f porosity content and elastic moduli remain unchanged for all ultrasonication times. This is attributed to the effectiveness of surface functionalization of MWCNTs combined with ultrasonication at coating individual Al particles with individual tubes. For M2f, uncertainties in elastic moduli are small which indicates smooth homogeneous distribution of individual tubes in the soft Al matrix. For M1f and M2f groups, no significant distinction in nanocomposite elastic moduli was observed given the different geometries of MWCNTs used in this study and similar composite porosity content. This can be due to multiple factors: inefficient bonding of MWCNTs to Al matrix, inability of CNT dispersion route (M1F) to exfoliate highly entangled MWCNTL clusters, and or spatial distribution of pores.

In this study, experimental results for bulk modulus (B) are disappointing. For all cases B has dropped by as much as 44-69% below control sample values used in this study (Fig. 6-15(c,f,i). These results show that high porosity contents in the cases of S1C/M1C/M2C result in a more open physical structure that is easier to compress uniformly and absorb deformation. In the case of Al reinforced with SWCNTs, as

before, surfactant assisted dispersion followed by ultrasonication is effective at further exfoliating SWCNT aggregates. For ultrasonication times less than 3 minutes there exists a gradual rise in B as porosity content remains unchanged. As large SWCNT clusters become exfoliated into smaller submicron clusters, it is expected that inter-particle contact regions will increase leading to geometric stiffening and a more stable inter-particle network throughout the bulk composite.

In the case of S1C there exists an initial increase in B for ultrasonication duration of 1 minute, this is believed to be due to Al_2O_3 dispersion strengthening; as previously discussed, porosity playing a more dominant role as ultrasonication time increases with a corresponding degradation in material properties. X-ray microanalysis has also shown an increase in oxide signature as porosity content increases (Fig. 6-5). Thick oxide layers initially present on Al particle surfaces (Fig. 6-19) can act to disrupt densification processes resulting in poor inter-particle interfaces and a highly disordered and discontinuous Al network upon completion of sintering (Fig. 6-6).

For M1C and M2C cases porosity contents as high as 20% is attributed to the highly compressible nature of the composites and there exists a good correlation between increasing/decreasing porosity content and decreasing/increasing bulk modulus. At these high porosities, any contribution from solid phase material properties to effective bulk modulus is suppressed. Interestingly, for M1f and M2f cases as ultrasonication time increases porosity content remains constant towards that of pure Al powder processed under similar conditions (consolidation pressure and sintering conditions). Given similar porosity content as the Al-PM control sample, M1f and M2f exhibit on average 33% and 29% reduction in bulk modulus. Fig. 6-12 shows a slight reduction in transverse

velocities for M1f/M2f groups from Al-PM control sample, however, the drop in longitudinal velocity from Al-PM control samples for these groups is more significant. These differences in bulk moduli are believed to be due in part to pore morphology, anisotropy, and spatial distribution in the bulk composite. Due to the spatial "mesh-like" configuration of f-MWCNTs on Al powder particle surfaces (Fig. 6-21) it is believed that there exists no contribution to bulk composite properties. During loading, it is believed that deformation of Al matrix will cause f-MWCNTs to re-orientate; as opposed to tubes which are mutually self-aligned in a preferred direction and provide stiffening affect.

6.5 Composite Thermal Properties Determination

Carbon nanotubes have emerged as a promising conducting reinforcing agent with axial thermal conductivities of individual MWCNTs reported to be ~ 3000 W/m K at room temperature [182]. Berber et al., through molecular dynamics simulations, predicted the thermal conductivity of an individual SWCNT to be 6600 W/m K at room temperature [183]. In their study was also reported the reduction in thermal conductivity, due to inter-layer interactions, when graphene layers are stacked and CNTs are brought into contact with one another [183]. The conduction reinforcement capabilities of CNTs will depend largely on homogeneous dispersion in the host matrix, retention of their unique tubular structure, and good bonding with the matrix material. Of equal importance are the type, geometry, defects, and purity of CNTs used as thermal reinforcement agent. An intrinsic property of CNTs, chirality, will dictate whether CNTs are of semiconducting or metallic type; chirality has direct implications on their

electrical/thermal characters. Amorphous carbon and or inherent defects on outer walls of CNTs due to synthesis can also act as scattering sites reducing phonon mean free path and thermal conductivity. In this study it was believed that the networked f-$MWCNT_{L}$s/f-$MWCNT_{S}$s/SWCNTs homogeneously dispersed on Al powder surfaces could perform as a channel for electron or phonon transport thus improving the thermal performance Al powder metallurgy components . In order to investigate the thermal properties of Al/CNT composites a TA Instruments© Discovery/Xenon Flash (DXF) EM-200 instrument was utilized. Using the following fundamental relationship the thermal conductivity (λ) of a specimen can be easily determined:

$$\alpha = \frac{\lambda}{\rho C_p}. \tag{6-7}$$

In the equation above "ρ" is the density of the material being analyzed, α is it's thermal diffusivity, and finally C_p is the specific heat capacity. For this test the specific heat capacity and thermal diffusivity are measured directly with the thermal conductivity derived using equation 7. In its most basic operation a light source (laser) heats the sample from one side with a detector on the opposite side monitoring the time dependent temperature rise (Fig. 6-24).

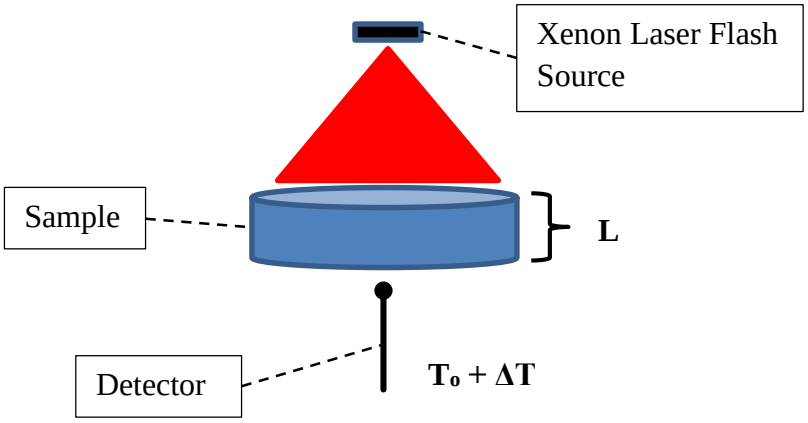

Figure 6-24: Laser flash analysis measurement principle.

By measuring the temperature rise and the time taken for the back side to reach half of its maximum value the thermal diffusivity can be determined using Parker's relation:

$$\alpha = \frac{0.1388L^2}{t_{1/2}}. \qquad (6\text{-}8)$$

In the above equation "L" is the sample thickness and "$t_{1/2}$" is the time to reach half max. By direct knowledge of the specimen parameters and directly measuring the thermal diffusivity/specific heat capacity one can determine the thermal conductivity.

Preliminary measurements were carried out on representative samples in order to access the feasibility of conducting a full set of measurements on all groups. Results are shown in the table below.

Sample	Conductivity [W/(m*K)]	Specific Heat [J/(Kg*K)]	Diffusivity [cm^2/S]	Porosity [%]
Pure Cast Al-Literature	237	896	0.8418	NA
Pure Cast Al	232.98	895.2	0.9638	NA
PM- Al	204.28	951.6	0.8586	7.33±2.92/3.51
M1f (5 min ultrasonication)	127.27	988.1	0.5194	7.25±0.44/0.40
S1 (5 min ultrasonication)	134.63	946.5	0.5761	7.72±0.14/3.51

Table 6-3. Preliminary thermal measurement results.

The experimentally measured value for pure (99.9999%) cast Al agrees well with value reported in literature. For Al PM control sample the presence of ~ 7% residual porosity content causes the thermal conductivity to drop by 12.3 %. This is should be expected as increasing the porosity in the Al powder compact decreases inter-particle contact surface area. This in turn causes an increase of thermal resistance at the interface which acts to increase the overall resistance of the powder compact. As this occurs the speed at which heat travels (diffusivity) in the material is attenuated and the conductivity drops. For the cases of Al powder reinforced with f-MWCNT$_{LS}$ and SWCNTs the thermal conductivity drops by as much as 35% given very similar porosity contents as the Al-PM control sample. For the M1f sample this can be attributed to the functionalization procedure and the resulting creation of defect sites on the outer walls of MWCNTs. These defect sites, which disrupt the periodic array of carbon atoms on outer MWCNT walls, purposely created for the absorption of zwitterionic surfactants can act to reduce the phonon mean free path. The presence of small nano-meter sized oxides if homogeneously on surfaces of Al powders and inter-particle contact regions may increase overall bulk resistance

reducing composite thermal conductivity. For Al reinforced with SWCNTs dispersed using surfactants followed by ultrasonification (S1), there exists slight improvements in thermal conductivity over M1f case. This may be due to the effective length of SWCNTs used in this study. In a study by Song et al., theoretical analysis supported by experimental results revealed that appropriate length distribution of CNTs could improve and more effectively enhance the conductive reinforcing capabilities of CNTs in glycerin composites [184]. In their study it was found that raw MWCNTs with an initial average length > 3 microns increased the thermal conductivity of a silicone elastomer by 105%. By modifying the length of the MWCNTs via mechanical milling to with an average of 1 micron, the thermal conductivity of silicone elastomer was improved further by 174% [184]. Their results showed that the raw (unmodified) MWCNTs were entangled and crooked which resulted in inefficient heat transfer in composites [161].

As reported earlier, elastic properties of Al/CNT composites fell below expectations and that of Al control samples investigated in this study. Taking into consideration the preliminary thermal results discussed above, and the lack of improvements in elastic properties of Al/CNT composites, it is believed that there may not exist an Al-CNT interface in the composites fabricated in this study and hence an efficient stress/heat transfer medium. The authors of this study acknowledge that detailed transmission electron microscopy (TEM) analysis and diffraction indexing of crystalline structures present in Al/CNT composites will need to be carried out in future work to determine whether an interfacial region exists. Lack of an Al-CNT interface is not the only barrier to improved thermal performances of Al/CNT composites, thermal/mechanical processing routes implemented, CNT type, and solid state material properties of

composite constituents can all have profound effects on thermal performances. As already discussed, residual porosity and CNT dispersion if not adequately controlled can severely mitigate thermal properties of Al/CNT composites. Intermediary Al phases as brought about by the composite fabrication process and resultant Al grain size can also affect thermal conductivity. It also important to note that the CNTs used in this study, synthesized by chemical vapor deposition (CVD) techniques, are a mixture of the metallic and semiconducting type. Due to the inability to control CNT chirality and diameter during the synthesis of CNTs it has been reported that synthesis via CVD techniques results in mixtures which 1/3 of the CNTs are of metallic type [186].

6.6 Discussion

The table below compares material properties and improvements as reported by various researchers in the fabrication of Al/CNT composites with results in this study. Also elucidated are consolidation procedure, CNT dispersion route, CNT geometry, and Al particle size. In the current study 250-300 % improvements in hardness are reported over pure Al powder processed under the same conditions. These dramatic increases in hardness are attributed to homogeneous dispersion of individual tubes on powder surfaces, their performance under compression, good densification of the composite powder compact, and to a lesser extent the existence of tough oxide particles. As already discussed, x-ray microanalysis did reveal the presence of oxides on tablet and Al particle surfaces, which if homogeneously dispersed and nano-meter in size can act as dislocation barriers and strengthening agents. Currently there exists no evidence for the formation of

an Al-CNT interface; however, it is believed that mechanical interlocking and adhesion due to CTE mismatch are mechanisms responsible for transferring load from the ductile Al matrix to rigid CNTs.

CNT Type	Ref.	CNT vol% / wt %	CNT-geometry : Length (l)- µm Diameter (d)- nm	Metal powder	Powder size	CNT dispersal mechanism	Consolidation procedure	Composite material properties	Reference material properties	% increase material properties
f-MWCNTs	Current Study	1.0 wt%	l: 10-30 d:10-20	Al	45 µm	Wet process/ Ultrasonication/ Magnetic Stirring	Cold Compaction	f-MWCNTs Rockwell: 47.55 E: 57.33 GPa	f-MWCNTs Rockwell*: 12.4 E*: 64.55	f-MWCNTs Rockwell: 283% E: -11%
f-MWCNTs			l: 0.5-2.0 d: < 8			Wet process/ Ultrasonication/ Magnetic Stirring		f-MWCNTs Rockwell: 50 E: 56.82 GPa	f-MWCNTs Rockwell*: 12.4 E*: 64.55	f-MWCNTs Rockwell: 303% E: -12%
SWCNT			l: 5-30 d:1-4			Wet process/ Ultrasonication/ Magnetic Stirring		SWCNT Rockwell: 43.60 E:49.04 GPa	SWCNT Rockwell*: 12.4 E*: 64.55	SWCNT Rockwell: 251% E: -24%
MWCNT	[61]	0.5 wt%	l: 5-15 d: 60-100	Al	5 µm	Wet process, Mechanical milling	Spark plasma sintering/ hot extrusion	Wet Process- Hv: 48 Mechanical Milling- Hv: 58	Wet Process- Hv*: 40 Mechanical Milling- Hv*: 48	Wet Process- Hv: 20% Mechanical Milling- Hv: 21%
MWCNTs	[62]	1.22 vol%	l: 1.5 d: 9.5	Al - A.60 63	-	Wet process	Spark plasma sintering/ hot extrusion	Hv0.05: 55.2		
MWCNT	[71]	15 vol%	l: 30 d: 20	Al	63 µm	Mechanical milling	Hot-pressing	Hv20: 260.3 Hv0.02: 258.1	Hv20*: 36.8 Hv0.02*: 33.2	Hv20: 607% Hv0.02: 677%

MWCNT	[72]	2.5 wt%	l: 10-20 d: 30-50	Al	45 µm	Mechanical milling	Spark plasma extrusion	Hv5: 99.1	Hv5*: 74.7	Hv5: 33%
MWCNT	[74]	1.75 wt%	l: 10 d: 40-100	Al	325 mesh	Mechanical milling	Cold compaction/ hot extrusion	Hv: 73	Hv*: 68	Hv: 7%
MWCNT	[75]	2 wt%	l: 10-20 d: 30-50	Al	10-40 µm	Mechanical mixing	Spark plasma sintering	Hv: 88 Nano hardnes*: 1.42 GPa E: 84 GPa	Hv*: 36 Nano hardness*: 0.95 GPa E*: 65 GPa	Hv: 144% Nano hardnes*: 49% E: 29%
MWCNT	[76]	0.5 wt%	l: 3-4 d: 140	Al	75 µm	Mechanical milling	Hot Rolling	E: ~ 60 GPa		E: 20 %
MWCNT	[78]	1.5 wt%	-	Al	-	Mechanical milling	Cold Compaction/ hot extrusion	E: 82.77 GPa, indirectly calculated using shear lag theory	E*: 70 GPa	E: 18%
MWCNT	[80]	5wt %	l: - d: 80	Al-2024	-	Mechanical milling	Cold compaction	Hv: 290.9	Hv*: ~75	Hv: 287%
MWCNT	[81] [82] [83]	1.0 wt%	l: - d: 20	Al-2024	50 µm	Ultrasonication/ mechanical milling	Cold compaction/ Hot extrusion	E: 102.2 GPa Hv: 136 MPa	E*: 59.9 GPa Hv*: 94.2 MPa	E: 71% Hv: 44%
MWCNT	[84]	1 wt%	l: 5-20 d: 20-50	Al-6061	13.8 µm	Mechanical milling	Semi-solid powder processing	Hv: 83.3	Hv: ~45	Hv: 85%
SWCNT, DWCNT, MWCNT	[98]	2.0 wt%	l: 10,10,10 d: 1-2,5-20,1-2	Al	30 µm	Ultrasonication/ Mechanical milling	Plasma activated sintering	DWCNT Hv: ~78	Hv*: ~ 30	Hv: 160%
MWCNT, SWCNT	[99]	2 vol%	-	Al	200 mesh	Ultrasonication/ Mechanical milling	Cold compaction/ hot extrusion	MWCNT- E: 85.85 GPa SWCNT- E: 79.3 GPa	MWCNT- E***: 87 GPa SWCNT- E***: 88 GPa	MWCNT- E: -1.75% SWCNT- E: -10.25%

MWCNT	[100]	0.75 wt%	1: 10 d: <100	Al	325 mesh	Ultrasonication/ Mechanical milling	Cold compaction	Hv: 77	Hv*: 30	Hv: 156%
MWCNT	[101]	2 wt%	1: few ten of µm's d: 20-30	Al	< 25 µm	Ultrasonication/ Mechanical milling	Cold compaction	Microhardness: 64 kg/mm^2	Microhardness: 31 kg/mm^2	Microhardness: 106%
MWCNT	[102]	2wt %	1: 5 d: 20	Al	30 µm	Mechanical stirring-ultrasonication/ mechanical milling	Plasma activated sintering	Hv: 182.8	Hv*: 60.1	Hv: 204%
SWCNT	[107]	5 wt%	-	Al	0.5 µm	Ultrasonication	Cold compaction/hot compaction	Micro-hardness: 2.89 GPa	Micro-hardness*: 1.62 GPa	Micro-hardness: 78%
MWCNT	[108]	1.5 wt%	1: 1-10 d: 10-15	AA 5083 Al	25 µm	Ultrasonication	Hot isostatic pressing/ extrusion	E: 76 GPa Hv0.5: 133	E*: 73.7 GPa Hv0.5*: 111	E: 3 % Hv0.5: 19%
MWCNT	[115]	5 wt%	1: 1.5-2.5 d: 5-25	Al	≤ 5 µm	Insitu chemical vapor deposition on Al powders	Cold compaction/cold compaction after sintering	Hardness: 0.65 GPa	Hardness*: 0.15 GPa	Hardness: 333%
MWCNT	[121]	2 wt%	-	Al	70 µm	Hand Mixing	Cold compaction	Hv: 54.0	Hv: 29.9	Hv: 80%
MWCNT	[125]	2 vol%	1: 2.5 d: 50	Al	10 µm	Mechanical milling/Surface modification of Al nano-flake/slurry blending	Cold compaction/hot extrusion	E: 89 GPa	E*: 70 GPa	E: 27%
MWCNT	[127]	5 vol%	1: 15-50 d: 20	Al	14.82 µm	Nano Scale Dispersion	Spark plasma sintering/ hot extrusion	Hv: 32	Hv*: 22	Hv: 45 %
MWCNT	[133]	0.5 wt%	1: 20-30 d: 20-30	Al	325 mesh	Ultrasonication/ magnetic stirring	Spark Plasma Sintering	Hv1: 38	Hv1*: 33	Hv1: 15%

Table 6-4: Table comparing material properties of Al/CNT composites by various researchers and this study. *Denotes comparison to unreinforced metal powders, ** comparison to bulk metal, ***comparison to theoretical value

In order to obtain homogeneous dispersion and imbed CNTs within Al matrix many researchers use mechanical milling [80-84,98-102,125] post CNT purification or as a compliment to prior CNT dispersion. One of the favorable outcomes of energetically milling nanotubes with metal powders is that physically imbeds nanotubes inside the ductile matrices. Mechanical milling was not chosen as a CNT dispersion route in this study for the following reasons:

1. Mechanical milling is considered a highly energetic dispersion route which can lead to defects and physical damage on the outer walls of MWCNTs as opposed to surfactant dispersion which retain the pristine tubular motif [61].
2. Mechanical milling can also lead to excessive strain hardening of metal powder particles and unfavorable changes in particle morphology (Fig. 6-25).
3. In most studies successful impregnation of CNTs in metal matrices is characterized by long milling conditions (>10 hours). Under these conditions there exist two competing phenomena, cold welding of particles and strain hardening of which leads to eventual particle fracture. If not properly controlled these two competing processes can lead to unwanted changes in particle size distribution.
4. Morphological changes in particle shape and or excessive cold working of metal powders necessitate higher consolidation pressures or more exotic compaction routes to avoid unfavorable powder packing characteristics.

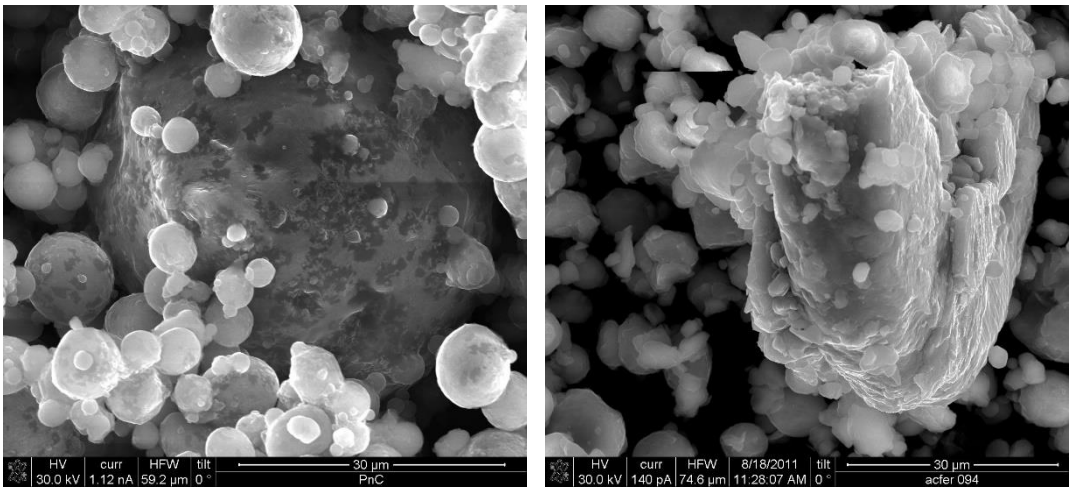

Figure 6-25: (a) Spherical aluminum powder used in this study as purchased from the manufacturer. (b) Aluminum powder in (b) mechanically milled for 1 hr at 350 rpm with a ball to powder ratio of 10:1.

Some researchers listed in the table above chose to compliment mechanical milling with post thermal/mechanical deformation procedures such as spark plasma sintering (SPS), hot consolidation, and or hot/cold extrusion. These consolidation routes are helpful as they are able to mitigate excessive strain hardening due to mechanical milling and or arrive at a desired grain size/shape. Extrusion uses compressive and shear stresses to create components of fixed cross-sectional shape by use of a die. The benefits of extrusion in regards to Al/CNT composites is that results in not only equiaxed grains but preferential alignment of nanotubes which may be useful for specific load bearing applications. If carried out at elevated temperatures, hot extrusion can result in increased densification of the composite due to strain rate sensitivity of metals to temperature. The main characteristics of SPS are that a very high current is pulsed through a graphitic compaction die, this current induces joule heating in the metal compact by induction. This process facilitates extremely fast heating/cooling rates and is typically carried out while a compaction force is applied to the powder compact.

One of the benefits of SPS is that temperatures just above the melting temperature of Al are attainable for incredibly short durations [187]. During this process the briefly present Al liquid is able to break Al_2O_3 layers, infiltrate into regions between Al particles, and coat individual CNTs if present [187]. Although it is generally acknowledged that CNTs are thermodynamically/chemically stable at high temperatures with Al and retain their pristine cylindrical structure consisting of concentric rolled up graphitic basal planes, formation of carbides is possible at processing temperatures below 700^0 C [29]. If sites of structural disorder, nano defects, amorphous carbon layers, and or open ends (dangling carbon bonds) of CNTs are present SPS which is characterized by high temperatures for short durations has been known to result in the formation of carbides [29,127].

The physical damage inflicted by mechanical milling can lead to the breaking of carbon bonds in prism planes in the outer shells of MWCNTs; if milled for long durations can result in the complete loss of their physical structure/unique properties and dissolution into amorphous carbon in metal matrices. Although beneficial in creating structural defects for the subsequent formation of aluminum carbide and hence an interfacial Al-CNT region, mechanical milling if not properly controlled can severely mitigate the advantages of post consolidation routes such as SPS. The formation of excessive amounts of carbides during SPS and their introduction into the Al matrix can work against any benefits from CNT strengthening. As in the case of the current study, the formation of excessive oxides during composite fabrication resulted in the imbrittlement of Al-CNT composites and poor microstructure.

Researchers achieved equally impressive if not higher increases in composite hardness using the more conventional CNT dispersion technique of mechanical milling with Al (Al alloy) powders for long durations [71,80]. Typically, due to powder particle morphological changes and strain hardening, higher compaction pressures are needed to achieve high relative density. Or as in the case of studies reported in table 4, hot pressing or extrusion is implemented to further densify the powder compact. However, using these techniques, it is important to carefully delineate strengthening mechanisms due to composite processing from those due to CNTs as reinforcements. Using a mechanical milling route followed by consolidation at room temperature, Bustamante et al. reported a 285% increase in composite hardness by 5 wt% MWCNT loading [80] . For long milling durations the authors of this study did report CNT damage and as a result an amorphous carbon layer on the outer MWCNT walls; the presence of amorphous carbon layers did favor the formation of aluminum carbide (Al_4C_3) which adheres the MWCNTs to the Al matrix forming an intermediary transition layer [80]. However, semi-quantitative x-ray analysis revealed the presence of as much as 9.2 wt% Al_4C_3 in the form of needle-like dispersoids in the aluminum alloy matrix [80]. These tough carbides can also act as barriers impeding dislocation motion increasing the yield behavior of the metal matrix. Kwon et al. reported dramatic increases in hardness (600-670%) over the reference material by dispersing 15 vol% MWCNTs using mechanical milling techniques followed by hot pressing. Such large improvements in hardness can be attributed to the relatively large quantity of stiff MWCNTs introduced into the Al matrix [71]. The authors of this study did report finding aluminum carbide which significantly affected hardness of Al/MWCNT composites providing an effective stress transfer medium. As

in the case of Bustamante et al., it is reasonable to conceive that at such a high CNT loading (15 vol%) Al_4C_3 may play a crucial role as a strengthening agent. However, the authors of this study did not elucidate on this possible strengthening mechanism. In another study, structural defects were detected on CNT surfaces due to the ball milling procedure; HTEM analysis revealed phases associated with Al such as: AlN, Al_2O_3 and Al_4C_3 [101] . The authors of this study attributed increased microhardness to the formation of these phases and good nanotube dispersion [101]. In order to avoid oxidation or formation of tough carbides He et al. developed a novel fabrication process where Ni nano particles were deposited evenly on Al powders followed by an insitu synthesis of CNTs via chemical vapor deposition (CVD) techniques [115]. The authors of this study reported homogenous dispersion of CNTs and good bonding with Al matrix; these factors increased composite microhardness by over 300 % and tensile strength more than two fold [115]. Xie et al. avoided oxidation of Al alloy powders by employing a semi-solid processing route [84]. Other researchers did not find evidence for the formation of intermediary phases and proposed the adhesion of CNTs to Al matrix promoted by CTE mismatch [74,100,102]. Choi et al. proposed that despite poor interfacial bonding between Al and CNTs, one possible stiffening/strengthening model is that CNTs behave as "latches" suppressing the deformation of Al matrix [98]. In another work by Bustamante et al. was reported a slight gain of 7% in microhardness using a combination of mechanical milling and hot extrusion [74]. However their pure Al reference sample did not follow the same fabrication route; it was only extruded and sintered in the same conditions [74]. Although the formation of Al_2O_3 was reported in

this study, the authors fail to delineate strengthening effects due to CNTs or composite processing (work hardening, carbide formation) [74].

Researchers also investigated the elastic properties of Al/CNT composites using mechanical testing techniques [75-76, 78, 81, 99,108,125]. In most cases this involved secondary thermal/mechanical deformation processes such as extrusion and hot pressing to arrive at the desired specimen geometry for tensile testing. Yadav et al. reported an increase of 29% in Young's modulus by consolidating Al/MWCNT composite mixtures via spark plasma sintering [75]. The authors of this study reported porosity content of nanocomposites as high as 4.4% which was attributed to MWCNT agglomeration. Strengthening mechanisms in their study was reported to be homogeneous distribution of CNTs which disrupted grain growth during processing. In their study, x-ray microanalysis did not detect the formation of carbides; however, the presence of aluminum oxide was detected [75]. Similarly, Deng et al. did not detect the presence of Al_2O_3 in Al/CNT composites but reported $CuAl_2$ phase in the form of 100 nm flakes uniformly dispersed in the composites [81]. These fine second phases and grain refinement strengthening by CNTs were reported to strengthen and increase composite material properties [81]. This study also reported the clustering of CNTs impeding densification and ultimately becoming defect sources in the metal matrix. The incompatibilities of Al with CNTs were overcome by producing Al nanoflakes and modifying the surfaces with polyvinyl alcohol (PVA) hydrosol [125]. This enabled the uniform distribution of CNTs powder surfaces and ultimate enhancement of material properties of composites.

George et al. prepared MWCNT and SWCNT composites with and without the aid of an Al-CNT wetting agent (K_2ZrF_6) in order to increase compatibility [99]. Comparing composite elastic moduli values determined experimentally and to theoretical expectations (shear lag model) the authors found that the use of a wetting agent produced minimal gains in Young's modulus [99]. Without a wetting agent decreases in elastic moduli were reported. In both cases no secondary aluminum phases were detected and slight improvements in strength were attributed to a synergestic effect of CNT strengthening mechanism [99]. It should also be noted that the authors of this study failed to report the effects of mechanical milling and strain hardening as a possible strengthening mechanism as elastic moduli for a control sample was not reported. Esawi et al. reported a modest gain (20%) in Young's modulus for CNTs dispersed via mechanical milling and subsequent consolidation via hot rolling for 0.5 wt% CNT loading [34]. Their study also reported a decrease in mechanical properties for CNT loadings of 2 wt% as clustering became more prevalent and acted to impede densification. Stein et al. attributed dismal improvements in elastic module of CNT composites to the hypothesis that CNTs were not sufficiently dispersed at the scale of metal grain size despite the presence of individual tubes on powder surfaces [108]. In their study secondary phases were not detected [108].

This study has shown that homogeneous dispersion of CNTs in the starting composite mixture is crucial to gain advantage of subsequent consolidation and thermal processing. If not well dispersed the introduction of CNT clusters among Al powders can impede densification leading to high porosity content in the sintered powder compact. As discussed in the previous section, high porosity content can result in pores with a high

degree of connectivity, irregular in shape, and can be clustered. As opposed to low porosity content cases where the pores are smaller, spherical, and tend to be well dispersed in the bulk compact. High residual porosity content can have profound effects on the resulting mechanical fields under loading conditions which can lead to localized strain intensification and degradation of elastic properties.

In order to gain full advantage and translate the unique physical properties of CNTs to a host matrix it is imperative to utilize a synergistic effect of CNT dispersion techniques. This study has shown that without subsequent ultrasonication procedures, surfactant assisted dispersion in many cases is not sufficient enough to fully exfoliate CNT clusters into individual tubes. Furthermore, if CNTs do not contain the requisite absorption sites on their outer walls for interfacial molecules, surfactant assisted dispersion and ultrasonication can be of little benefit or their dispersion capabilities weakened. Taking this into consideration, this study showed that functionalization of MWCNT surfaces maybe necessary to create absorption sites on outer walls in order for MWCNTs to become more soluble in aqueous surfactant solutions. If using a combination of CNT dispersion techniques it is also important to take into account how prior gains in CNT dispersion may be affected or mitigated by subsequent CNT exfoliation techniques. In this study it was learned that subsequent shear mixing of aqueous CNT suspensions with Al powder acted to facilitate re agglomeration of individual tubes into small aggregates. It is also important to take into account type CNTs and purity of CNT powder for a specific application. Although widely available in powder form, CNT powders typically have a distribution of lengths and diameters. The purity of CNT powders can also vary dramatically from manufacturers. CNT powders can have small quantities of amorphous

carbon on outer walls and or contain impurities. In order to be used as thermal or electrical reinforcements CNTs must be of the metallic type. Typically if synthesized via CVD techniques, CNTs powders will consist of tubes that are semiconducting and metallic. These can introduce complex and time consuming separation/purification steps to acquire pure CNT powders of a specific character. These processes can result in significant CNT mass loss and may be costly to implement.

As discussed in previous chapters, due to the similar electro negativities, carbon exhibits poor solubility in aluminum. Furthermore, due to large differences in surface tension CNTs exhibit poor wettability with aluminum making solid state processing routes such as powder metallurgy viable alternatives to casting. In order to gain full advantage of their unique mechanical/thermal/electrical proper creation and maintenance of a metal-CNT interface is imperative. Researchers have utilized a variety of different approaches to take advantage of structural defects already existing on the outer walls of CNTs and form intermediary phases between aluminum and carbon. Such as spark plasma sintering which is characterized by fast hot/cooling rates and high temperatures which are favorable for aluminum carbide formation. Some researchers have taken novel approaches to overcome this hurdle by growing CNTs on Al powder surfaces using in situ using CVD methods or coating CNTs with nickel atoms using deposition techniques.

Lastly, this research has shown that it is crucial for researchers to properly delineate Al/CNT composite strengthening due to individual CNTs or processing techniques. As already discussed in great detail, in an attempt to realize an interfacial region (and effective stress transfer region) through the synthesis of aluminum carbides, some researchers have inadvertently introduced secondary strengthening agents into the metal

matrix which can have unintended consequences on the physical performance of Al/CNT composites. In this study, for certain cases it was found that the formations of tough oxides were responsible for high composite hardness, poor microstructure, and poor elastic properties. Some researchers fail to take into account the effects of strain hardening of metal powders due to mechanical milling and its contribution to improvements in composite strength. Some researchers will implement thermo/mechanical consolidation post mechanical milling, however, it can be difficult to quantify the amount of recovery and matrix softening. As it is known that individually dispersed CNTs can act to pin grain growth during the recovery process leading to a Hall-Petch strengthening effect.

For future research it is recommended that a detailed analysis using transmission electron microscopy technique be carried out to infer the existence of an Al-CNT interface.

In order to improve composite densification, Al-CNT adhesion due to CTE mismatch, and mechanical interlocking of CNTs to Al particles a more robust consolidation protocol be implemented. This can be achieved by the following:

1. Utilize the MTS tensile tester located in the material testing lab, Mechanical Engineering department –UNM, to consolidate composite mixtures under higher pressures. The use of this machine will allow the consolidation of Al-CNT composite mixtures to be carried out under a controlled rate to pressures of 600 MPa or higher. This is due to the increased load capacity of the MTS machine over the Instron 4400R which provided a maximum compaction force of 400 MPa in this study.

2. With an increased consolidation pressure available it is also highly recommended that the die tooling setup be changed to that of stainless steel. As opposed to the current one which is made of A2 air hardened tool steel. Use of a stainless steel die setup will facilitate ease of ejection of composite tablets from the die and reduce frictional forces. Stainless steel dies can be purchased from a variety of companies whom specialize in fabricating custom die setups for powder compaction applications.
3. Use of a more robust lubrication protocol in the inter die wall during compaction will also help to reduce frictional forces encountered. It is recommended that the use of boron nitride paste be used as a lubricant as opposed to zinc stearate.
4. This study has shown that double sided compaction of composite tablets acts to further densify and homogenize Al-CNT green tablets. It is recommended that this technique be implemented in conjunction with post machining (if necessary) of the green tablet in order to re-insert back into the die (after the first compaction cycle).

In order to reduce oxidation of Al/CNT composite mixtures during curing phases it is recommended that this be carried out under an inert environment under carefully controlled conditions. To reduce slight oxidation during sintering of Al/CNT tablets under argon gas, the gas outlet can be immersed in a type of mineral oil as opposed to water. This will lessen the likelihood of water vapor returning into the quartz tube furnace (due to pressure differences) upon completion of sintering.

Due to recent advances in the bulk production of CNTs, it is strongly recommend by the authors of this study that functionalized CNTs be purchased if surfactant assisted is carried out to disperse CNTs. This will not require the necessity to functionalize CNTs by oneself. This process requires the use of dangerous acids at elevated temperatures and is extremely time consuming. During the functionalization process it is necessary to continuously wash/rinse treated CNTs, this can result in excessive mass loss of starting CNTs and can be costly. Purchasing CNT powders with a narrow size distribution, free of impurities, of either metallic or semiconducting type, will increase their thermal/electrical reinforcement capabilities.

For this study it is recommended that upon completion of intense ultrasonication of surfactant-CNT gels in sodium iodide stabilizing solution, this aqueous solution be stirred with Al powders while simultaneously being subjected to a “light” ultrasonic bath . This can lessen the likelihood of CNTs re agglomerating during the shear mixing process.

The importance of this work is that it adds to the preexisting knowledge base of research into applications of carbon nanotubes as exotic reinforcements in metal systems. This work can also serve as a roadmap for future researchers who are interested in exploring possible inroads to fabricating metal-CNT composites free of defects and with CNTs that are homogeneously distributed and well bonded to the metal interface. Of equal importance of this work is creating a stepping stone for future researchers to realize the bulk manufacturing of CNT-metal composites on an industrial scale and their applications in consumer products, defense, automotive, and aerospace industries.

However there remain substantial hurdles for researchers to clear before this can become a reality. Work needs to be carried out into characterizing the interfacial interactions between carbon nanotubes and metals to achieve an effective stress/electrical/thermal transfer interface. A better understanding of the creation of secondary metal-carbon phases during composite fabrication and how to mitigate their effects as strengthening agents needs to be carried out. Fabrication routes need to be developed that are cost effective and achievable on an industrial scale, not just in the laboratory. A lot of researchers must resort to exotic consolidation routes such as spark plasma sintering to achieve the required microstructure. For components of more complex geometry in mass production this may not be cost effective or highly impractical in an industrial setting. Likewise, very complex CNT dispersion techniques such as in situ CVD process may not be achievable on a large scale. Finally, CNTs need to be cheaply produced that are of high structural quality and purity, as this will increase their availability to researchers and or companies.

References

[1] Dale, R.J., 2011, "Powder Metallurgy- Intrinsically Sustainable," International Journal of Powder Metallurgy, Vol. 47, No. 1, pp.27-31

[2] Levina, D. A., Chernyshev, L. I., Mikhailovskaya, N. V., 2007, "CONTEMPORARY POWDER METALLURGY: ACHIEVEMENTS AND PROBLEMS," Powder Metallurgy and Metal Ceramics, Vol. 46, Nos. 3-4, pp. 202-205.

[3] Bulger, M., 2012, "State of the PM Industry in North America- 2012," International Journal of Powder Metallurgy, Vol. 48. No. 4, pp. 29-32.

[4] Iijima, S., 1991, "Helical microtubules of graphitic carbon," Nature, 354, pp 56-58.

[5] Li,F., Cheng, H.M., Bai, S., Su, G., Dresselhaus, M.S., 2000, "Tensile strength of single-walled carbon nanotubes directly measured from their macroscopic ropes," Applied Physics Letters, Vol. 77,No.20, pp.77-80.

[6] Krishnan, A., Dujardin, E., Ebbesen, T.W., Yianilos, P.N., Treacy, M.J., 1998,"Young's modulus of single-walled nanotubes," Physical Revies B, Vol. 58, No.20.[4] Vaisman, L., Wagner, H. D., and Marom, G., "The role of surfactants in dispersion of carbon nanotubes," Journal of Advances in Colloid and Interface Science, 2006, Vol. 128–130, pp.37–46.

[7] Pop, E., Mann, D., Wang, Q., Goodson, K., Dai, H., 2005, "Thermal Conductance of an Individual Single-Wall Carbon Nanotube above Room Temperature," Nano Letters, Vol. 6, No.1, pp.96–100.

[8] frank, S., Poncharal, P., Wang, Z.L., De Heer, W., 1998, "Carbon Nanotube Quantum Resistors," Science, Vol. 280, No.12

[9] Quadrini, F., Squeo, E., 2008, "Density Measurement of Powder Metallurgy Compacts by Means of Small Indentation," Journal of Manufacturing Science and Engineering, Vol. 130, No. 3, pp.0345031-0345034.

[10] Ludwig, R., Apelian, D., Leuenberger, G., 2005, "An NDE Methodology to Predict Density in Green-State Powder Metallurgy Compacts," Journal of Nondestructive Evaluation, Vol. 24, No. 3, pp.109-119.

[11] Dawson, A. L., Bussiere, J. F., 1998, "Ultrasonic Characterization of Iron Powder Metallurgy Compacts During and After Compaction," Advanced Performance Materials, Vol. 5, pp. 97-115.

[12] Fleck, N., Smith, R., 1981, "Effect of Density on Tensile Strength, Fracture Toughness, and Fatigue Crack Propagation behavior of Sintered Steel," Powder Metallurgy, Vol. 24, No. 3, pp.121 – 125.

[13] Carnavas, P., Page, N., 1998, "Elastic properties of compacted metal powders," Journal of Materials Science, Vol. 33, pp. 4647 – 4655.

[14] Kumar, P., Kumaran, S., 2010, "Comparison Study of Fly Ash Reinforced AA6061 Composites Using Press Sinter Extrusion and Press Extrusion," Powder Metallurgy, Vol.53, pp.163-168.

[15] Chapra, S., Canale, R., 1998, "Numerical Methods for Engineers, Third Edition," WCB/McGraw-Hill, Boston, pp.438-443.

[16] Al-Qureshi, H.A., Soares, M.R., Hotza, D., Alves, M.C., Klein, A.N., 2008, "Analyses of the Fundamental parameters of Cold Die Compaction of Powder Metallurgy," Journal of Mater Proc Tech, Vol. 199, pp.417-424.

[17] Kim, H., Estrin, Y., Gutmanas, E.Y., Rhee, C., 2001, "A Constitutive Model for Densification of Metal Compacts: The Case of Copper," Materials Science and Engineering, Vol.A307, pp.67-73.

[18] Martin, C.L., Bouvard, D., Shima, S., 2003, "Study of Particle Rearrangement During Powder Compaction by the Discrete Element Method," Mechanics and Physics of Solids, Vol.51, pp.667-693.

[19] Kim, H. S., Won, C. W., Chun, B. S., 1998, "Plastic Deformation of Porous Metal with an Initial Inhomogeneous Density Distribution," Journal of Materials Processing Technology, Vol. 74, pp. 213-217.

[20] Lee, D., Kim, H., 1992, "Plastic Yield Behavior of Porous Metals," Powder Metallurgy, Vol. 35, No. 4, pp. 275 – 279.

[21] Yoon, S.C., Kwak, E.J., Kim, T., Cheon, B.S., Kim, H.S., 2008, "Yield and Densification Behavior of Rapidly Solidified Magnesium Powders," Materials Transactions, Vol.49, No.5, pp.967-971.

[22] Alves, M.M., Martins, A.F., Rodrigues, M.C., 2006,"A New Yield Function for Porous Materials," Journal of Materials Processing Technology, Vol.179, pp.36-43.

[23] Narayanasamy, R., Ponalagusamy, R., Subramanian, K.R., 2001, "Generalized Yield Criteria of Porous Sintered Powder Metallurgy Metals," Journal of Materials Processing Technology, Vol.110, pp.182-185.

[24] Kandeil, A., Malherbe, M.C., Critchley, S., Dokainish, M., 1977,"The Use of Hardness in the Study of Compaction Behavior and Die Loading," Powder Technology, Vol. 17, pp. 253-257.

[25] Ponalagusamy, R., Narayanasamy, R., Subramanian, K.R., 2005, "Prediction of Limit Strains in Sheet Metals by Using New Generalized Yield Criteria," Materials and Design, Vol.28, pp.913-920.

[26] Narayan, S., Rajeshkannan, A., 2011, "Densification Behavior in Forming of Sintered Iron-0.35% Carbon Powder Metallurgy Preform During Cold Upsetting," Materials and Design, Vol.32, pp.1006-1013.

[27] Tszeng, C.T., 1998, "Considering Particle Morphology in a Constitutive Model for Metal Powders Compaction," Metall and Mater Trans, Vol. 30A, pp.1159-1162.

[28] Kalpakjian, S., and Schmid, S., 2006, "Manufacturing Engineering and Technology, Fifth Edition," pp. 483-512, Pearson-Prentice Hall, Upper Saddle River, New Jersey.

[29] Ramakrishnan, K N., 2000, "Modified Rosin Rammler Equation for Describing Particle Size Distribution of Milled Powders," Journal of Materials Science Letters, Vol.19, pp. 1903-1906.

[30] Lee, D.N., Kim, H.S., 1992,"Plastic Yield Behavior of Porous Metals," Powder Metallurgy, Vol.35, pp. 275-279.

[31] Sinka, I.C., 2007, “Modeling Powder Compaction,” Kona, Vol.25, pp.4-22.

[32] Tszeng, C.T., 1998, “Considering Particle Morphology in a Constitutive Model for Metal Powders Compaction,” Metallurgical and Materials Transactions, Vol.30A, pp.1159-1162.

[33] Wu, Chuan-Yu. Cocks, C.F., 2006, “Numerical and Experimental Investigations of the Flow of Powder into a Confined Space,” Mechanics of Materials, Vol.38, pp.304-324.

[34] Rosin, P., Rammler, E., 1993, “The laws Governing the Fineness of Powdered Coal,” Journal of the Institute of Fuel, pp.29-36.

[35] Quadrini, Fabrizio. Erica, Squeo A., 2008, “Density Measurement of Powder metallurgy Compacts by Means of Small Indentation,” Journal of Manufacturing Science and Engineering, Vol.130, pp.1-4.

[36] Kim, H.S., Won, C., Chun, B.S., 1998, “Plastic Deformation of Porous Metal With an Initial Inhomogeneous Density Distribution,” Journal of Material Science and Processing, Vol.74, pp.213-217.

[37] Esawi, A. Morsi, K., 2007,”Dispersion of Carbon Nanotubes (CNTs) in Aluminum Powder, “Composites, 38,646-650, (2007).

[38] Lee,Seung H. Kim, Hong J. Sakai, Etsuo. Daimon, Masaki, 2003, “Effect of Particle Size Distribution of Fly Ash-Cement System on the Fluidity of Cement Pastes,” Cement and Concrete Research, Vol.33, pp.763-768.

[39] Brezani, Ivan.Zelenak, Fridrich., 2010, “Improving the Effectivity of Work with Rosin-Rammler diagram by using MATLAB®GUI tool,”Acta Montanistica, Vol.15, pp.152-157.

[40] Mikli, Valdek.Kaerdi, Helmo.Kulu, Priit.Michal,Besterci., 2001, “Characterization of Powder Particle Morphology,” Estonian Academy of Science and Engineering, Vol.7, pp.22-34.

[41] Starke, E.A., Staley, J.T., 1996, “Application of modern aluminum alloys to aircraft,” Aerospace Sci. Vol. 32, pp. 131-172.

[42] Parsonage, T., 2000, “Beryllium metal matrix composites for aerospace and commercial applications,” Materials Science and Technology, Vol.16, pp.732-738.

[43] Vijayarangan, S., Rajamanickam, N., Sivananth, V., 2013, “Evaluation of metal matrix composite to replace spheroidal graphite iron for a critical component, steering knuckle,” Materials and Design, Vol.43, pp.532-541.

[44] Saito, T., 1995, “A cost-effective P/M titanium matrix composite for automobile use,” Advanced Performancae Materials, Vol.2, pp.121-144.

[45] Iijima, S.,1991,”Helical microtubules of graphitic carbon,” Nature, 354, pp 56-58.

[46] Li,F., Cheng, H.M., Bai,S., Su,G., Dresselhaus,M.S., 2000, “Tensile strength of single-walled carbon nanotubes directly measured from their macroscopic ropes,” Applied Physics Letters, Vol. 77,No.20, pp. 77-80.

[47] Krishnan, A., Dujardin, E., Ebbesen, T.W., Yianilos, P.N., Treacy, M.J., 1998, “Young’s modulus of single-walled nanotubes,” Physical Revies B, Vol. 58, No.20.

[48] Kipourus, G.J., Caley, W.F., Bishop, D.P., 2006, "On the advantages of using powder metallurgy in new light metal alloy design," Metallurgical and Materials Transactions A, Vol.37, pp.3429-3436.

[49] Cho, J., Boccaccini, A.R., Milo, S., Shaffer, S.P., 2009, "Ceramic matrix composites containing carbon nanotube," Journal of Material Science, Vol.44, pp.1934–1951.

[50] Xiea, X., Maia, Y., Zhoub, X., 2005, "Dispersion and alignment of carbon nanotubes in polymer matrix: A review," Materials Science and Engineering, Vol.49, pp.89–112.

[51] Bounix, C., Katz, E., Yerushami, R., 2012, "Conjugated polymers-carbon nanotubes –based functional materials for organic photovoltaics: a critical review," Polymers Advanced Technology, Vol. 23, pp.1129-1140.

[52] Breuer, O., Sundararaj, U., 2004, "Big returns from small fibers: A review of polymer/carbon nanotube composites," Polymer Composites, Vol.25, pp. 630-645.

[53] Coleman, J.N., Khan, U., Blau, W., Gun'ko, Y.K., 2006, "Small but strong: A review of the mechanical properties of carbon nanotube-polymer composites," Carbon, Vol.44, pp.1624-1652.

[54] Bakshi S. R., Lahiri, D., Agarwal, A., 2010, "Carbon nanotube reinforced metal matrix composites – a review," International Materials Reviews, Vol.55, No.1, pp.41-56.

[55] Wang, H., Zhou,W., Ho,D. L., Winey, K. I., Fischer, J. E., Glinka, C. J., Hobbie, E. K., 2004, "Dispersing Single-Walled Carbon Nanotubes with Surfactants: A Small Angle Neutron Scattering Study," Journal of Nano Letters, Vol. 4, No. 9, pp. 1789-1793.

[56] Matarredona, O., Rhoads, h., Li, Z., Harwell, J. H., Balzano, L., Resasco, D. E., 2003, "Dispersion of Single-Walled Carbon Nanotubes in Aqueous Solutions of the Anionic Surfactant NaDDBS," Journal of Physics and Chemistry, Vol. 107, pp. 13357-13367.

[57] Girifalco, L. A., Hodak, M., Lee, R. S., 2000, "Carbon nanotubes, buckyballs, ropes, and a universal graphitic potential," Journal of Physical Review B, Vol. 62, No. 19, pp. 13104-13110.

[58] Xie, X. L., Mai, Y. W., Zhou X. P., 2005, "Dispersion and alignment of carbon nanotubes in polymer matrix: A review," Journal of Material Science and Engineering R Reports, Vol. 49, No. 4, pp. 89–112.

[59] Ham, H. T., Choi, Y. S., Chung, I. J., 2005, "An explanation of dispersion states of single-walled carbon nanotubes in solvents and aqueous surfactant solutions using solubility parameters," Journal of Colloid and Interface Science, Vol. 286, No. 1, pp. 216-223.

[60] Strano, M. S., Moore, V. C., Miller, M. K., Allen, M. J., Haroz, E. H., Kittrell, C., Hauge, R. H.Smalley, R. E., 2003, "The role of surfactant adsorption during ultrasonication in the dispersion of single-walled carbon nanotubes," Journal of Nanoscience and Nanotechnology, Vol. 3, pp. 81-86.

[61] Liao, J., Tan, M., 2011, "Mixing of carbon Nanotubes (CNTs) and Aluminum Powder for Powder Metallurgy Use," Powder Technology, Vol.208. pp. 42-48.

[62] Fukuda, H., Kondoh, K., Umeda, J., Fugetsu, B., 2011, "Aging behavior of the matrix of aluminum-magnesium-silicon alloy including carbon nanotubes," Materials Letters, 6 Vol.5, pp. 1723-1725.

[63] Kondoh, K., Fukuda, H., Umeda J., Imai, H., Fugetsu, B., 2010, "Microstructural and mechanical analysis of carbon nanotube reinforced magnesium alloy powder composites," Material Science and Engineering A, Vol.527, pp. 4103-4108.

[64] Fukuda, H., Kondoh, K., Umeda, J., Fugetsu, B., 2011, "Fabrication of magnesium based composites reinforced with carbon nanotubes having superior mechanical properties," Materials Chemistry and Physics, Vol.127, pp. 451-458.

[65] Fukuda, H., Kondoh, K., Umeda, J., Fugetsu, B., 2011, "Interfacial analysis between Mg matrix and carbon nanotubes in Mg-6 wt% Al alloy matrix composites reinforced with carbon nanotubes," Composites Science & Technology, Vol.7, pp. 705-709.

[66] Kondoh, K., Threrujirapapong, T., Imai, H., Umeda, J., Fugetsu, B., 2009, "Characteristics of powder metallurgy pure titanium matrix composite reinforced with multi-walled carbon nanotubes," Composites Science and Technology, Vol.69, pp. 1077-108.

[67] Kondoh, K., Threrujirapapong, T., Imai, H., Umeda,J., Fugetsu, B., 2008, "CNTs/TiC reinforced titanium matrix nanocomposites via powder metallurgy and its microstructural and mechanical properties" Journal of Nanomaterials, Vol.2008, 4 pages.

[68] Esawi, A., Morsi, K., 2006, "Dispersion of carbon nanotubes (CNTs) in aluminum powder," Composites, Vol.38, Part A, pp. 646-650.

[69] Choi, H.J.,Shin, J.H., Bae, D.H., 2011, "The enhancement of warm temperature mechanical properties of ultrafine-grained aluminum by carbon nanotubes," Materials Science and Engineering A, Vol.528, pp. 6134-6139.

[70] Choi, H.J., Bae, D.H., 2011, "Strengthening and toughening of aluminum by single-walled carbon nanotubes," Materials Science and Engineering A, Vol.528, pp. 2412-2417.

[71] Kwon, H., Bradbury, C.R., Leparoux, M., 2011, "Fabrication of functionally graded carbon nanotube-reinforced aluminum matrix composite," Advanced Engineering Materials, Vol.13, pp. 325- 329.

[72] Morsi, K., Esawi, A.M.K., lanka, S., Sayed, A., Taher, M., 2010, "Spark Plasma Extrusion (SPE) of ball-milled aluminum and carbon nanotube reinforced aluminum composite powders," Composites Part A, Vol.41, pp. 322-326.

[73] Morsi, K., Esawi, A., 2007, "Effect of Mechanical Alloying Time and Carbon Nanotube (CNT) Content on the evolution of Aluminum (Al) - CNT Composite," Journal of Material Science, Vol.42, pp. 4954-4959.

[74] Perez-Bustamante, R., Gomez-Esparza, C.D., Estrada-Guel, M., Miki-Yoshida, M., Licea-jimenez, L., perez-Garcia, S.A., Martinez-Sanchez, R., 2009, "Microstructural and mechanical characterization of Al-MWCNT composites produced by mechanical milling," Materials Science and Engineering A, Vol.502, pp. 159-163.

[75] Yadav, V., Harimkar, S., 2011, "Microstructure and properties of spark plasma sintered carbon nanotube reinforced aluminum composites," Advanced Engineering Materials, Vol.13, No.12, pp.1128-1134.

[76] Esawi, M.K., El Borady, M.A., 2008, "Carbon nanotube-reinforced aluminum strips," Composites Science and Technology, Vol.68, pp. 486-492.

[77] Choi, H.J., Bae, D.H., 2011, "Strengthening and toughening of aluminum by single-walled carbon nanotubes," Materials Science and Engineering A, Vol.528, pp. 2412-2417.

[78] Kashyap, K.T., Koppad, P., Puneeth, K.B., Ram, H.R., Mallikarjuna., 2011, "Elastic Modulus of multi-walled carbon nanotubes reinforced aluminum matrix nanocomposite-A theoretical approach," Computational Materials Science, Vol.50, pp. 2493-2495.

[79] Perez-Bustamante, R., Perez-Bustamante, F., Estrada-Guel, I., Sahtillan-Rodriguez, C.R., Matutes-Aguino, J.A., Herrara-Ramirez, J.A., Miki-Yoshida, M., Martinez-Sanchez, R., 2011, "Characteristics of Al2024-CNTs composites produced by mechanical alloying," Powder Technology, Vol.212, pp. 390-396.

[80] Perez-Bustamante, R., Perez-Bustamante, F., Strada-Guel, I., Licea-Jimene, L., Miki-Yoshida, M., Martinez-Sanchez, R., 2013, Vol.75, pp. 13-19.

[81] Deng, C., Zhang, X., Ma, Y., Wano, D., 2007, "Fabrication of Aluminum matrix composite reinforced with carbon nanotube," Rare Metals, Vol.26, No.5.

[82] Deng, C.F., Wang, D.Z., Zhang, X.X., Li, A.B., 2007, "Processing and properties of carbon nanotube reinforced aluminum composites," Materials Science and Engineering A, Vol.444, pp. 138-145.

[83] Deng, C., Zhang, X., Wang, D., Lin, Q., Li,A., 2006, "Preperation and characterization of carbon nanotube/aluminum matrix composites," Material Letters, Vol.61, pp. 1725-1728.

[84] Wu, Y., Kim, G.Y., 2011, "Carbon nanotube reinforced aluminum composite fabricated by semi-solid powder processing," Journal of Materials Processing Technology, Vol.211, pp. 1341-1347.

[85] Jenei, P., Yoon, E.Y. Gubicza, J., Kim, H.S., Labar, J.L., 2011, "Microstructure and hardness of copper-carbon nanotube composites consolidated by high pressure torsion," Materials Science and Engineering A, Vol.528, pp. 4690-4695.

[86] Kim, K.T., Cha, S.I., Hong, S.H., Hong, S., 2006, "Microstructures and tensile behavior of carbon nanotube reinforced Cu matrix nanocomposites," Material Science and Engineering A, Vol.430, pp. 27-33.

[87] Li, H., Misra, A., Horita, Z., Koch, C., Mara, N.A., Dickerson, P.O., 2009, "Strong and ductile nanostructured Cu-carbon nanotube composite," Applied Physics Letters, Vol.95, pp. 071907.

[88] Uddin, S.M., Mahmad, T., wolf, C., Glanz, C., Kolaric, I., Volkmer, C., Holler, H., Wienecke, U., Roth, S., Fecht, H., 2010, "Effect of size and shape of metal particles to

improve hardness and electrical properties of carbon nanotube reinforced copper and copper alloy composites," Composites and Science Technology, Vol.70, pp. 2253-2257.

[89] Goh, C.S., Wei, J., Lee, L.C., Gupta, M., 2005, "Development of novel carbon nanotube reinforced magnesium nanocomposites using the powder metallurgy technique," Nanotechnology, Vol.17, pp.7-12.

[90] Thakur, S.K., Kwee G.T., Gupta, M., 2007, "Development and characterization of magnesium composites containing nano-sized silicon carbide and carbon nanotubes as hybrid reinforcements," Journal of Material Science, Vol.42, pp. 10040-10046.

[91] Carreno, M.E., Yang, J., Couteau, E., Hernandi, K., Seo, J.W., Bonjour, C., Forro, L., Scheller, R., 2004, "Carbon nanotube/magnesium composites," Physica Status Solidi, Vol.201, No.8, pp. R53-R55.

[92] Habibi, M.K., Hamouda, A.M.S., Gupta, M., 2012, "Enhancing tensile and compressive strength of magnesium using ball milled Al-CNT reinforcement," Composites Science and Technology, Vol.72, pp. 290-298.

[93] Shimizu, T., Sakaki, K., Hayashi, T., Kim, Y.A., Endo, M., Morimoto, S., Koide, A., "Multi-walled carbon nanotube-reinforced magnesium alloy composites," Scripta Materialia, Vol.58, pp. 267-270.

[94] Kuzumaki, T., Ujiie, O., Ichinose, H., Ito, K., 2000, "Mechanical characteristics and preparation of carbon nanotube fiber-reinforced Ti composite," Advanced Engineering Materials, Vol.2, No.7, pp. 416-418.

[95] Melendez, M., Neubauer, E., Angerer, P., Danninger, H., Torralba, J.M., 2011, "Influence of nano-reinforcements on the mechanical properties and microstructure of titanium matrix composites," Composites Science and Technology, Vol.71, pp. 1154-1162.

[96] Li, S., Sun, B., Imai, H., Mimoto, T., Kondoh, K., 2013, "Powder metallurgy titanium metal matrix composites reinforced with carbon nanotubes and graphite," Composites: Part A, Vol.48, pp. 57-66.

[97] Huang, Y.Y., Terentjev, E., 2012, "Dispersion of Carbon Nanotubes: Mixing, Sonication, Stabilization, and Composite Properties," Polymers, Vol. 4, pp. 275-295.

[98] Choi, H., Wang,L.,Cheon, D., Lee, W., 2013, "Preparation by mechanical alloying of Al powders with single-,double-,and muti-walled carbon nanotubes for carbon/metal nanocomposites," Composite Science and Technology, Vol.74, pp. 91-98.

[99] George, R., Kashyup, K.T., Rahul, R., Yamdagni, S., 2005, "Strengthening in carbon nanotube/aluminum (CNT/Al) composites," Scripta Materialia, Vol.53, pp. 1153-1163.

[100] Perez-Bustamante, R., Estrada-Guel, I., Antunez-flores, W., Miki-Yoshida, M., Ferreira, P.J., Martinez-Sanchez, R., 2008, "Novel Al-matrix nanocomposite reinforced with multi-wallled carbon nanotubes," Journal of Alloys and Compounds, Vol.450, pp.323-326.

[101] Singhal, S.K., Pasricha, R., Teotia, S., Kumar, G., Mathur, R.B., 2011, "Fabrication and characterization of Al-matrix composites reinforced with Amino-functionalized carbon nanotubes," Composite Science and Technology, Vol.72, pp. 103-111.

[102] Wang, L., Choi, H., Myoung, J., Lee, W., 2009, "Mechanical alloying of multi-walled carbon nanotubes and aluminum powders for the preparation of carbon/metal composites," Carbon, Vol.47, pp. 3427-3433.

[103] Singhal, S.K., Pasricha, R., Jangra, M., Chahal, R., Teotia, S., Mathur, R.B., 2012, "Carbon nanotubes: Amino functionalization and its application in the fabrication of Al-matrix composites," Powder Technology, pp. 254-263.

[104] Kim, C., Lim, B., Kim, B., Shim, U., Oh, S., Sung, B., Choi, J., Ki, J., Baik, S., 2009, "Strengthening of copper matrix composites by nickel-coated single-walled carbon nanotube reinforcement," Synthetic Metals, Vol.159, pp. 424-429.

[105] Lim, B., Kim, C., Kim, B., Shim, V., Oh, S., Sung, B., Choi, J., Baik, S., 2006, "The effects of interfacial bonding on mechanical properties of single-walled Carbon nanotube reinforced copper matrix nanocomposite," Nanotechnology, Vol.17, pp. 5759-5764.

[106] Patil, R.G., Chatpalli, V., Kannan, K.R., 2010, "Study on Young's modulus and microhardness of carbon nanotubes reinforced copper nanocomposites," Materials Science and Technology, Vol.26, No.4, pp. 478-481.

[107] Zhong, R., Cong, H., Hou, P., 2002, "Fabrication of nano-Al based composites reinforced by single-walled carbon-nanotubes," Carbon, Vol.41, pp. 848-851.

[108] Stein J., Lenczowski, B., Frety, N., Anglaret,E., 2012, "Mechanical reinforcement of a high-performance aluminum alloy AA5083 with homogeneously dispersed multi-walled carbon nanotubes," Carbon, Vol.50, pp. 2264-2272.

[109] Tu, J.P., Yang, Y.Z., Wang, L.Y., Ma, X.C., Zhang, X.B, 2001, "Tribololgical properties of carbon-nanotube-reinforced copper composites," Tribology Letters, Vol.10, No.4, pp. 225-228.

[110] Jun, L., Ying, L., Lixian, L., Xuejuan., 2012, "Mechanical properties and oil content of CNT reinforced porous CuSn oil bearings," Composites: Part B, Vol.43, pp. 1681-1686.

[111] Wilson, K., Barrera, E.V., Bayazitoglu, Y., 2010, "Processing of titanium single-walled carbon nanotube metal-matrix composites by the induction melt method," Journal of Composite Materials, Vol.44, No.9, pp. 1037-1048.

[112] Xua, C., Wub, G., Liub, Z., Wub, D., Meeka, T., Hanc, Q., 2004, "Preparation of copper nanoparticles on carbon nanotubes by electroless plating method," Materials Research Bulletin, Vol.39, pp.1499–1505.

[113] Chen, X., Xia, J., Peng, J., Li, W., Xie, S., 1999, "Carbon-nanotube metal-matrix composites prepared by electroless plating," Composites Science and Technology, Vol.60, pp.301-306

[114] Sun, F., Shi, C., Rhee, K.Y., Zhao, N., 2013, "In situ synthesis of CNTs in Mg powder at low temperature for fabricating reinforced Mg composites," Journal of Alloys and Compounds, Vol.551, pp. 496-501.

[115] He, C., Zhao, N., Shi, C., Du, X.,Li, J., Li, H., Cui, Q., 2007, "An approach to obtaining homogeneously dispersed carbon nanotubes in Al powders for preparing reinforced Al-matrix composites," Advanced Materials, Vol.19, pp. 1128-1132.

[116] Yang, X., Liu, E., shi, C., He, C., Li, J., Zhao, N., Kondoh, K., 2011, "Fabrication of carbon nanotube reinforced Al composites with well-balanced strength and ductility," Journal of Alloys and Compunds, Vol.563, pp. 216-220.

[117] Yang, X., Shi, C., He, C., Liu, E., Li, J., Zhao, N., 2011, "Synthesis of uniformly dispersed carbon nanotube reinforcement in Al powder for preparing Al composites," Composites A, Vol.42, pp. 1833-1839.

[118] Lim, B.K., Hwang, J.W., Lee, D.J., Suh, S.H., Hong, S.H., 2011, "Fabrication process and multi-functional applications of carbon nanotube nanocomposites," Journal of Composites Materials, Vol.46, No.14, pp. 1731-1737.

[119] Cha, S.I., Kim, K.T., Arshad, S.N., Mo, C.B., Hong, S.H., 2005, "Extraordinary strengthening effect of carbon nanotubes in metal-matrix nano composites processed by molecular level mixing," Advanced Materials, Vol.17, pp. 1377-1381.

[120] Kim, K.T., Eckert, J., Menzel, S.B., Gemming, T., Hong, S.H., 2008, "Grain refinement assisted strengthening of carbon nanotube reinforced copper matrix nanocomposite," Vol.92, pp.121901-1.

[121] Jiang, J., Wang, H., Yang, H., Xu, J., 2007, "Fabrication and wear behavior of CNT/Al composites," Transactions of Nonferrous Metals Society of China, Vol.17, pp.s113-s116.

[122] Feng, Y., Yuan, H.L., Zhang, M., 2005, "Fabrication and properties of silver-matrix composites reinforced by carbon nanotubes," Materials Characterization, Vol.55, pp. 211-218.

[123] Kuzumaki, T., Miyazawa, K., Ichinose, H., Ito, K., 1998, "Processing of carbon nanotube reinforced aluminum composite," Materials Research Society, Vol.13, pp. 2445-2449.

[124] Kurita, H., kwon , H., Estili, M., Kawasaki, A., 2011, "Multi-walled carbon nanotube- aluminum matrix composites prepared by combination of hetero-agglomeration method, spark plasma sintering and hot extrusion," Metal Transactions, Vol.52, No.10, pp. 1960-1965.

[125] Jiang,L., Li, Z., Fan, G., Cao, L., Zhang,D., 2012, "The use of flake powder metallurgy to produce carbon nanotube (CNT)/aluminum composites with a homogeneous CNT distribution," Carbon, Vol.50, pp. 1993-1998.

[126] Trinh, P.V., Trung, T.B., Thang, N.B., Thang, B.H., Tinh, T.H., Quang, L.D., 2010, "Calculation of the friction coefficient of Cu matrix composite reinforced by carbon nanotubes," Computational Materials Science, Vol.49, pp. S239-S241.

[127] Kwon, H., Estilli, M., Takagi, K., Miyazaki, T., 2009, "Combination of hot extrusion and spark plasma sintering for producing carbon nanotube reinforced aluminum composites," Carbon, Vol.47, pp. 570-577.

[128] Cao. L., Li, Z., Fan, G., Jiang, L., Zhang, D., Moon, W.J., Kim, Y.S., 2012, "The growth of carbon nanotubes in aluminum powders by the catalytic pyrolis of polyethylene glycol," Carbon, Vol.50, pp.1057-1052.

[129] Ci, L., Ryu, Z., Jin-Phillipp, N.Y., Ruhle, M., 2006, "Investigation of the interfacial reaction between multi-walled carbon nanotubes and aluminum," Acta Materialia, Vol. 54, pp. 5367-5375.

[130] Park, M., Kim, B.H., Kim, S., Han, D.S., Kim, G., Lee, K., 2011, "Improved binding between copper and carbon nanotubes in a composite using oxygen-containing functional groups," Carbon, Vol.49, pp. 811-818.

[131] Felten, A., Suarez-Martinez, I., Ke, X., Tendeloo, G., Ghijsen, J., Pireaux, J., Drube, W., Bittencourt, C., Ewels, C., 2009, "The Interface between Titanium and Carbon Nanotubes," ChemPhysChem, Vol.10, pp. 1799-1804.

[132] Fugetsu,B., Han, W., Endo, N., Kamiya, Y., Okuhara, T., 2005, "Disassembling Single-walled Carbon Nanotube Bundles by Dipole/Dipole Electrostatic Interactions," Chemistry Letters, Vol.34, No.9,pp. 1218-1219.

[133] Nie, J., Jia, C., Shi, N., Zhang, Y., Jia, X., 2011, "Aluminum matrix composites reinforced by molybdenum-coated carbon nanotubes," Vol.18, No.6, pp. 695-701.

[134] Kwon, H., Bradbury, C.R., Leparoux, M., 2011, "Fabrication of functionally graded carbon nanotube-reinforced aluminum matrix composite," Advanced Engineering Materials, Vol.13, No.4m, pp. 325-329

[135] Parsonage T., 2000, "Beryllium metal matrix composites for aerospace and commercial applications." Mater Sci Tech Ser, Vol.16, pp.732-738.

[136] Vijayarangan S., Rajamanickam N., Sivananth V., 2013, "Evaluation of metal matrix composite to replace spheroidal graphite iron for a critical component, steering knuckle," Mater Design, Vol.43, pp.532-541.

[137] Saito T. A, 1995, "Cost-effective P/M titanium matrix composite for automobile use," Adv Perform Mater, Vol.2, pp.121-1324.

*[138] Iijima S., 1991, "Helical microtubules of graphitic carbon," Nature, Vol.354, pp.56-58.

[139] Li, F., Cheng, H.M., Bai, S., et al., 2000, "Tensile strength of single-walled carbon nanotubes directly measured from their macroscopic ropes," Appl Phys Lett, Vol.77, pp.77-80.

[140] Krishnan, A., Dujardin, E., Ebbesen, T.W., et al., "Young's modulus of single-walled nanotubes," Phys Rev B, Vol.58.

[141] Kipourus, G.J., Caley W.F., Bishop D.P., 2006 "On the advantages of using powder metallurgy in new light metal alloy design," Metall Mater Trans A, Vol. 37, pp.3429- 3436.

[142] Rael, B.J., Khraishi, T.A., 2013, "Review: carbon nanotube dispersal mechanisms in the fabrication of powder metallurgy metal matrix composites and effects on mechanical properties," Int J Appl Mult Mech, Vol.2, pp.323-360.

[143] Wang, H., Zhou, W., Ho, D.L., et al., 2004 "Dispersing single-walled carbon nanotubes with surfactants: a small angle neutron scattering study," Nano Lett, Vol. 44, pp.1789-1793.

[144] Girifalco, L.A., Hodak, M., Lee, R.S., 2000, "Carbon nanotubes, buckyballs, ropes, and a universal graphitic potential," Phys Rev B, Vol.62, pp.13104-13110.

[145] Huang, Y.Y., and Terentjev, E., 2012, "Dispersion of carbon nanotubes: mixing, sonication, stabilization, and composite properties," Polymers, Vol.4, pp.275-295.

[148] Rael, B.J., Dyck, C.L., Khraishi, T.A., et al., 2012, "Characterization of zinc powder compactions: factors affecting mechanical properties and analytical powder metallurgy models," J Eng Mater-T ASME, Vol. 134.

[149] Stein, J., Lenczowski, B., Frety, N., et al., 2012, "Mechanical reinforcement of a high-performance aluminum alloy AA5083 with homogeneously dispersed multi-walled carbon nanotubes," Carbon, Vol.50, pp.2264-2272.

[150] Zhong, R., Cong, H., Hou, P., 2002, "Fabrication of nano-Al based composites reinforced by single-walled carbon-nanotubes," Carbon, Vol.41, pp.848-851.

[151] Huang, Y.Y., Terentjev, E., 2012 "Dispersion of carbon nanotubes: mixing, sonication, stabilization, and composite properties" Polymers, Vol.4, pp.275-295.

[152] Fukuda, H,, Kondoh, K., Umeda, J., et al., "Aging behavior of the matrix of aluminum-magnesium-silicon alloy including carbon nanotubes," Mater Lett, Vol.65, pp. 1723-1725.

[153] Kondoh, K., Fukuda, H., Umeda, J., et al., 2010, "Microstructural and mechanical analysis of carbon nanotube reinforced magnesium alloy powder composites," Mater Sci Eng A, Vol.527, pp.4103-4108.

[154] Kondoh, K., Threrujirapapong, T., Imai, H., et al., "Characteristics of powder metallurgy pure titanium matrix composite reinforced with multi-walled carbon nanotubes," Compos Sci Technol, Vol.69, pp.1077-1080.

[155] Kondoh, K., Threrujirapapong, T., Imai, H., et al., 2008 "CNTs/TiC reinforced titanium matrix nanocomposites via powder metallurgy and its microstructural and mechanical properties," J Nanomater.

[156] Igathinathane, C., Pordesimo, L.O., Columbus, E.P., et al., 2008, "Shape identification and particle size distribution from basic shape parameters using ImageJ," Comput Electron Agr, Vol.63, pp.168-182.

[157] Liew, K.M., Wong, C.H., Tan, M.J., 2005, "Buckling properties of carbon nanotube bundles," Appl Phys Lett, Vol.87.

[158] Liu, L., Cao, G., Chen, X., 2008, "Mechanisms of nanoindentation on multi-walled carbon nanotube and nanotube cluster," J Nanomater.

[159] Rael, B.J., Khraishi, T.A., Jiang, Y., Yaquin, F., 2016, "Optimizing Powder Metallurgy Methods: Effects of Carbon Nanotube (CNT) Dispersal Mechanisms on Mechanical Properties of Aluminum-CNT Composites," Journal of Composite Materials, Vol. 50, No. 4.

[160] Rael, B.J., Dyck, C.L., Khraishi, T.A., et al., 2012, "Characterization of zinc powder compactions: factors affecting mechanical properties and analytical powder metallurgy models," J Eng Mater-T ASME, Vol.134.

[161] Liew, K.M., Wong, C.H., Tan M.J., 2005, "Buckling properties of carbon nanotube bundles," Appl Phys Lett, Vol. 87.

[162] Liu, L., Cao, G., Chen, X., 2008, "Mechanisms of nanoindentation on multi-walled carbon nanotube and nanotube cluster," J Nanomater.

[163] Dawson, A.L., Bussiere, J.F, "Ultrasonic characterization of iron powder metallurgy compacts during and after compaction," 1998, Advanced Performance Materials, Vol.5, pp.97-115.

[164] Asami, M., Kermel, C., Leriche, A., Ourak, M., "Influence of porosity on Young's modulus and Poisson's ratio in alumina ceramics," 2000, Jornal of the European Ceramic Society, Vol.21, pp 1081-1086.

[165] Parthasarathi, S., Prucher, T., Yu, C.J., Jo, J., Henry, R.J., "Determination of dynamic elastic properties of powder metallurgy components," 1993, Review Of Progress in Quantitative Nondestructive Evaluation, Vol. 12, pp. 1631-1636.

[166] Dawson, A.L., Bussiere, J.F., 1998, "Ultrasonic characterization of iron powder metallurgy compacts during and after compaction," Advanced Performance Materials, Vol. 5, pp 97-115.

[167] Carnavas, P.C., Page, N.W., "Elastic properties of compacted metal powders," 1998, Journal of Material Science, Vol. 33, pp 4647-4655.

[168] Moon, J.R., "Elastic moduli of powder metallurgy steels," 1989, Powder Metallurgy, Vol. 32, No.2, pp 132-139.

[169] Hentschel, M.W., Page, N.W., 2006, "Elastic properties of powders during compaction. Part 1: Pseudo-isotropic moduli," Journal of Material Science

[170] Zhao, P., Shi, G., 2011, "Study of Poisson's ratios of graphene and single-walled carbon nanotubes based on an improved molecular structural mechanics model," Vol.5, No.1, pp 49-58.

[171] Zhang, Y.Y., Wang, C.M., Tan, V.B.C., 2008, "Examing the effects of wall numbers on buckling behavior and mechanical properties of multiwalled carbon nanotubes via molecular dynamics simulations," Journal of Applied Physics, Vol. 103.

[172] Joshi, P., Upadhyay, S.H., 2014, "Evaluation of elastic properties of multi walled carbon nanotube reinforced composite," Computational Materials Science, Vol. 81, pp 332-338.

[173] Carnavas, P.C., Page, N.W., 1998, "Elastic properties of compacted metal powders," Journal of Material Science, Vol. 33, pp 4647-4655.

[174] Moon, J.R., 1989, "Elastic moduli of powder metallurgy steels," Powder Metallurgy, Vol. 32, No.2, pp 132-139.

[175] Hentschel, M.W., Page, N.W., 2006, "Elastic properties of powders during compaction. Part 1: Pseudo-isotropic moduli," Journal of Material Science

[176] Asami, M., Kermel, C., Leriche, A., Ourak, M., 2000, "Influence of porosity on Young's modulus and Poisson's ratio in alumina ceramics," Jornal of the European Ceramic Society, Vol.21, pp 1081-1086

[177] Parthasarathi, S., Prucher, T., Yu, C.J., Jo, J., Henry, R.J., 1993, "Determination of dynamic elastic properties of powder metallurgy components," Review Of Progress in Quantitative Nondestructive Evaluation, Vol. 12, pp. 1631-1636.

[178] Huang Y.Y., Terentjev E.., 2012, "Dispersion of carbon nanotubes: mixing, sonication, stabilization, and composite properties," Polymers, Vol.4, pp. 275-295.

[179] Redsten, A.M., Klier, E.M., Brown, A.M., Dunand, D.C., 1995, "Mechanical properties and microstructure of cast oxide-dispersion-strengthened aluminum," Materials Science & Engineering A, Vol. 201, pp. 88-102.

[180] Tsukrov, I., Novak, J., 2002, "Effective elastic properties of solids with defects of irregular shape," The International journal of Solids and Structures, Vol. 39, pp. 1539-1555.

[181] Chawla, N., Williams, J.J., Deng, X., McClimon, C., Hunter, L., Lau, S.H., 2009, "Three-dimensional characterization and porosity modeling of porosity in PM steels," International Journal of Powder Metallurgy, Vol. 45, Issue 2, pp 19-29.

[182] Kim, P., Shi, L., Majumdar A, et al., 2001, "Thermal transport measurement of individual multi-walled nanotubes," Phys Rev Letter, Vol.87, 215502–1-4.

[183] Berber, S., Kwon, Y., Tomanek, D., 2000, "Unusually high thermal conductivity of carbon nanotubes," Physical Review Letters, Vol. 84, No. 20, pp.4613-1616.

[184] Song, P.C., Liu, C.H., Fan, S.S., 2006, "Improving the thermal conductivity of nanocomposites by increasing the length efficiency of loading carbon nanotubes," Applied Physics Letters, Vol. 88.

[185] Shin, S.E., Choi, H.J., Bae, D.H., “Electrical and thermal conductivities of aluminum-based composites containing multi-walled carbon nanotubes,” Journal of Composite Materials, Vol. 47, No. 18, pp.2250-2256.

[186] Dresselhaust, M.S., Eklund, P.C., “Phonons in carbon nanotubes,” 2000, Advances in Physics, Vol. 49, No.6, pp. 705-814.

[187] Zhou, W., Bang, S., Kurita, H., Mizazaki, Fan, Y., Kawasaki, A., “Interface and interfacial reactions in multi-walled carbon nanotube reinforced aluminum matrix composites,” 2016, Carbon, Vol.96, pp. 919-928.